Doctoral Dissertation

**Guidelines for Urban Land Use Planning in
the Central Business District of Bangkok
from the viewpoint of Urban Heat Island Mitigation**

**(バンコク CBD における都市ヒートアイランド
緩和のための土地利用計画ガイドラインに関する研究)**

2024 March

Tarnrawee Ngamsiriudom

Acknowledgment

Abstracts

Urban Heat Islands (UHIs), characterized by elevated temperatures in densely built areas, pose significant challenges to local climates, particularly in sprawling cities like Bangkok. This study investigates the UHI phenomenon in Bangkok using a **two-scale approach: mesoscale (regional and provincial)** and **microscale (urban district)**. By integrating field observations, numerical models, and empirical generalizations synthesized from developed **urban environmental climate maps (UECMs)**, this research aims to enhance urban planning by translating complex urban climate phenomena into spatial data, ultimately informing effective policy decisions. While previous research primarily focused on developed countries with temperate climates, **this study addresses the gap in tropical Southeast Asia**. It examines Bangkok, a megacity facing rapid urbanization, severe UHI effects, lack of urban climate study, situated in a unique plain basin with extensive water networks. Utilizing Thai government observation climate data and clarified spatial data, the study investigated the relationship between spatial variables and urban climate. Further, numerical models were employed to overcome resource limitations and analyze urban ventilation, air temperature, regional climate, and land use. This comprehensive approach aims to inform urban land-use planning and guide policymakers in addressing Bangkok's specific climatic challenges.

Three main objectives guided this research: 1) Apply diverse methodologies and scales of urban climate study to understand urban climate in tropical countries. 2) **Clarify the relationship** between Bangkok's climate and influencing spatial variables from a UHI mitigation perspective at two urban scales. 3) **Identify critical areas** affected by the UHI phenomenon at both scales. The study focused on supporting BMA land-use policies at both mesoscale (regional and provincial) and microscale (Central Business Districts, CBDs).

At the mesoscale level, the study extended its scope to the Bangkok Metropolitan Region (BMR) and employed two urban climate methodologies. Firstly, field observations incorporated 2019 **climate data from 68 stations** along with spatial variables (land cover, distance to coastline, distance to rivers/canals) to analyze the relationship between climate data and its spatial distribution. This revealed correlations between **nocturnal air temperature fluctuations and green cover, diurnal variations impacted by distance to coastline, and significant influence of both distance and building coverage on summer wind speed.** Consequently, a BMR UECM was constructed based on these three variables, identifying nine distinct zones with critical areas requiring intervention, particularly in central BMA. Secondly, numerical calculations and cluster analysis using **Weather Research and Forecasting (WRF)** models revealed spatiotemporal temperature and wind speed patterns, dividing BMA into six temperature and six ventilation zones. UECMs of BMA were developed based on these zonal maps and overlaid with high-density building coverage. While both mesoscale climate findings highlighted critical areas, comparing them emphasized **the limitations of relying solely on one method in data-scarce environments.** Although observation data offers real-world information, its scarcity can lead to inaccuracies. Notably, high-density coastal areas with strong sea breezes exhibited poor ventilation,

underlining the need for diverse data sources. Conversely, **inland areas with open spaces displayed potential for high wind speeds, highlighting the influence of local topography.**

Microscale Analysis of CBDs, the study investigated ventilation and temperature characteristics of two Bangkok CBDs (Yaowarat and Ratchadamri) using 2022 field measurements, spatial analysis, and computational fluid dynamics (CFD) simulations. The focus was on key factors influencing urban ventilation, particularly wind speed and open space ratio within a 100-meter radius. Comparative analysis revealed distinct ventilation characteristics between the areas due to their unique topography. However, both demonstrated suboptimal ventilation, requiring improvements in wind velocity. Microclimate analysis and UECM development for the Ratchadamri area, based on field measurements, numerical models, and correlation analysis, **identified areas with high building coverage and limited greenery as critical for high temperatures** (wet bulbed globe temperature) **and low wind speed.** These variables were used to create a district-scale UECM, dividing the area into six distinct zones based on thermal environment, ventilation, and urban characteristics. Notably, Zone 6 represented a critical area with the highest temperature and lowest wind speed.

The study's findings led to the development of design proposals for mitigating the UHI phenomenon. At the regional scale, a master plan for creating ***"The Urban Ventilation Corridor in the BMR"*** *– a continuous open space running north-south through collaboration with four provinces* – could improve ventilation and mitigate UHIs. Additionally, utilizing the existing water network as an urban humid ventilation corridor was proposed. At the district scale, ***adapting vernacular architectural characteristics to create horizontal open public spaces*** and connecting them with existing open areas could improve airflow and mitigate heat and air pollution. Additionally, shaded open spaces adapted to tropical activities and livelihoods were proposed.

This study demonstrates a **novel approach** to urban climate analysis by **integrating diverse methodologies and scales**. Applied to a tropical metropolis like Bangkok, it offers valuable insights for shaping governmental policies and urban planning across the BMA at various scales. Moreover, it underscores the critical role of urban climatology in Thailand, fostering stakeholder awareness and highlighting the synergy between field measurements and numerical modeling to inform evidence-based urban planning decisions. Notably, further community engagement through workshops could refine the developed Urban Environmental Climate Maps (UECMs) at both scales, ensuring long-term viability and alignment with local needs. Additionally, expanding the research methods beyond the specific context of summer climate analysis towards encompassing broader environmental issues and seasonal variations holds promise for future investigations.

Table of content

Chapter 1
Introduction

Contents

1.1   Background of the study and previous related research

1.1.1   Urban Heat Islands Phenomenon

Over half of the global population currently resides in urban areas (UNFPA, 2007), and projections indicate that by 2030, nearly 60% of the Earth's population will be urban dwellers (UN, 2008). The swift urbanization observed over the last five decades has not only facilitated the migration of new residents to urban locales but has also systematically transformed the physical landscape of urban environments (Ng et al., 2013)

Global warming is the long-term heating of the Earth's surface observed since 1850. Its pace has significantly increased in the last hundred years due to the human population (NOAA, 2023). Figure 1-1 shows the recent temperature trends in global average surface temperature between 1993 and 2022 and it shows that most of the planet is warming. The highest density of population is also situated in the urban area, especially the Megacity, with over 10 million people.

Among the formidable challenges affecting local climates, urban heat islands (UHIs) have emerged as a prominent concern. The term "UHI" refers to the phenomenon of altered temperatures in urban areas compared to their rural surroundings (Oke, 1982). Specifically, UHIs are characterized by temperature differentials between urban and rural areas, with various metrics available to quantify this disparity (Schwarz, 2012). The urban heat island phenomenon denotes higher temperatures in densely built-up areas relative to their surroundings. Causative agents of UHIs encompass population surges, urban and industrial expansion, impermeable surfaces, and anthropic activities (Hongsuk, 1992; Pakarnseree et al., 2018). The UHI effect adversely impacts the environment, residents' health (Walter et al., 2021; Zhendong et al., 2021), and energy consumption. Understanding the UHI mechanism in cities is imperative for proposing effective mitigation measures. This urgency has prompted a call to action for local planners and policymakers, compelling them to prioritize safeguarding local climates and environmental assets through climate change adaptations in urban construction.

Numerous studies have explored the relationship between UHI and the local environment. The research results underscore the significance of green infrastructure, as evidenced by its effectiveness in mitigating UHI effects, particularly in the city center (Kamma et al., 2020; Jing et al., 2021; Peng et al., 2021). Furthermore, effective strategies for mitigating the UHI effect include reducing anthropogenic heat and enhancing the porosity of urban areas (Tingzhen et al., 2021).
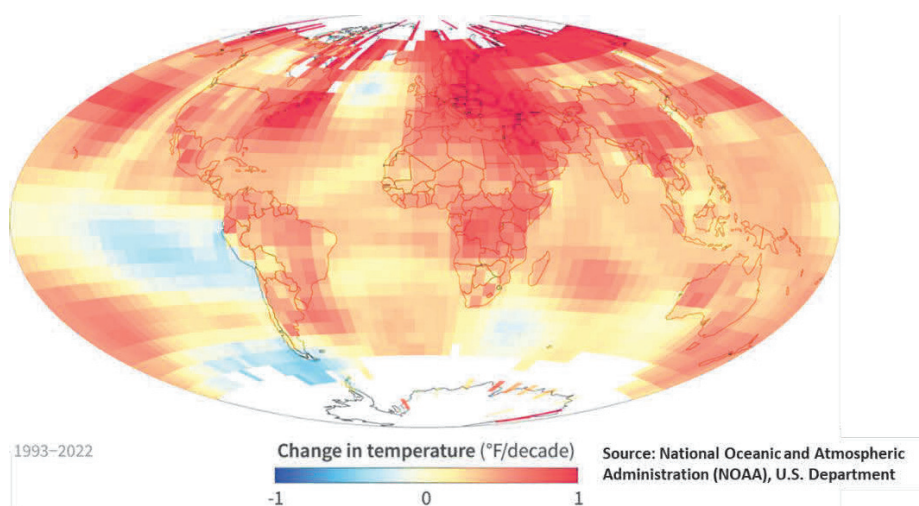
Figure 1-1 Trends in global average surface temperature between 1993 and 2022

(Source: National Oceanic and Atmospheric Administration (NOAA), U.S. Department)

1.1.2   Urban Climate Study

In addition to investigating the urban heat island effect, it is equally crucial to examine the characteristics of local climate and urban climate. This is imperative because each city possesses distinct geographic and physical attributes, leading to varied outcomes and management approaches for climate change issues. Previous related research has underscored the significance of delving into urban climate studies and applying the findings to local management plans (Moriyama and Tanaka, 2012; Matsuo and Tanaka, 2019)

Urban climate studies focus on understanding the impact of cities on local and regional climate, as well as the consequences of climate change on urban areas. These studies aim to improve our understanding of urban climate processes, such as heat and moisture fluxes, air pollution dispersion, and urban heat island effect, and their effects on energy balance and transport. Urban climate studies are characterized by a variety of methodological approaches and a variety of study scales.

1.1.2.1 Urban Study Scales and a Variety Methods of Urban Climate Study

Urban climate models can divide into three study scales: Macroscale— class of atmospheric phenomena with horizontal dimensions of hundreds to thousands of kilometers and a lifetime of weeks to decades. Includes continental to global features such as monsoons, weather systems, and global climate distribution: Mesoscale— class of atmospheric phenomena with horizontal dimensions of about 20 to 200 km such as urban heat islands, country breezes, sea breezes, and valley winds: Microscale— class of atmospheric phenomena with horizontal dimensions from the millimeters to 1 km with a lifetime of minutes to hours.

The UHI Phenomenon regarding to the mesoscale to the microscale. Therefore, from the viewpoint of UHI mitigation and adaptation, the necessity for a two-scale examination of urban climate is because each urban scale encounters different phenomena that are influenced by different urban variables. However, both urban climate scales influenced each other and affected the large scale of residents.

The meso-urban climate is related to geography, and land use classification, and could clarify the critical area for mitigating the urban heat island phenomenon that is related to the regional and provincial urban planning (Bangkok Metropolitan Region and Bangkok Metropolitan Area). On the other hand, the microclimate was influenced by urban elements such as buildings, streets, urban surface materials, green areas with tropical plants, urban topography, etc. Therefore, each urban scale had a different type of data, measurement, and methodologies to consider. Moreover, both led to the different scales and organization of urban management and urban planning with different stakeholders. Each urban climate scale encompasses different factors impacting residents with different phenomena, and identifying these factors can enhance the efficacy of mitigating the urban heat island effect, as both urban climate scales positively correlate with each other (Figure 1-2).
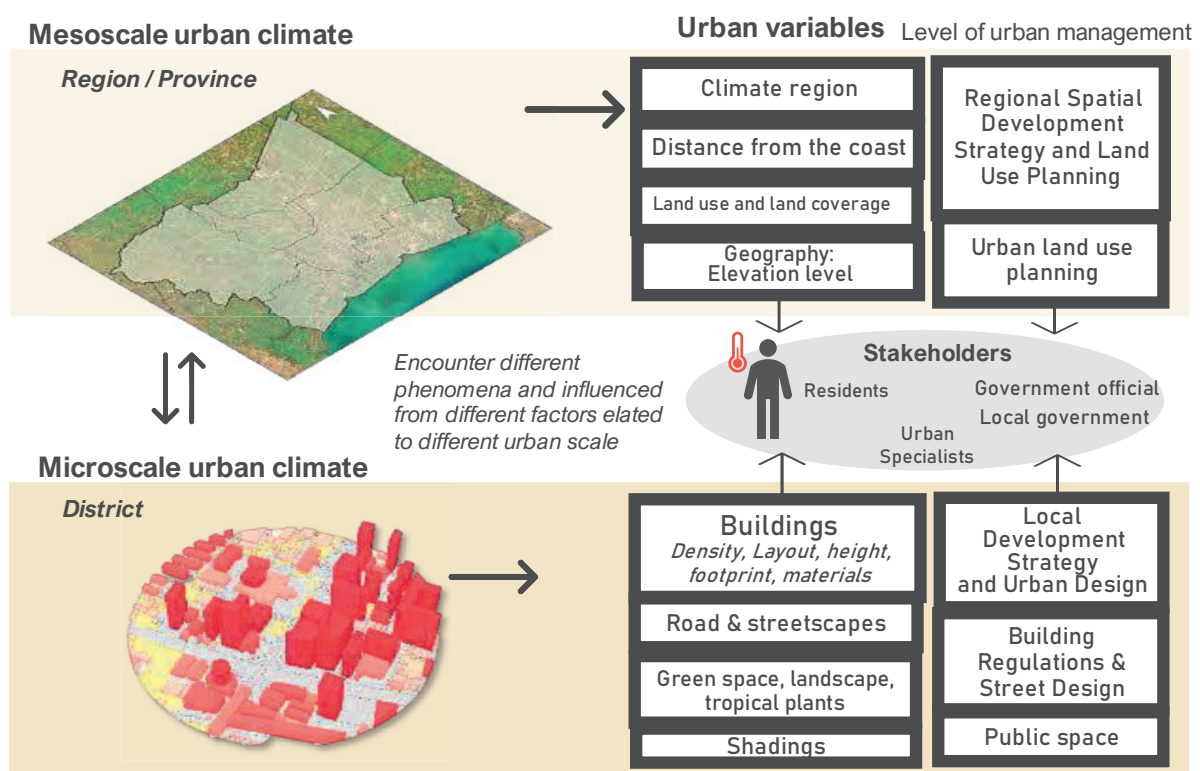
Fig. 1-2 The urban climate scales, urban variables, and urban management level

The study of Oke et al. (2017) scopes the urban climate studies by four methodologies used in urban climatology: field observation that relies on measurements of surface and atmospheric properties using sensors; physical modeling in which observations are made using scaled representation of the urban surface; numerical models that represent the urban surface and simulate atmospheric processes using mathematical equations; empirical generalization and synthesis, which establishes statistical relationships between parameters of the urban climate system using any, or a combination of, the previous approaches.

The first methodology is field measurements. It employed a traditional approach to analyzing urban microclimates using conventional meteorological measurement devices (Rizwan et al., 2008; Santamouris, 2007; Mill et al., 2014). Field observations began in the early nineteenth century with Luke Howard's work (Oke et al., 2017). Data was collected daily over 25 years, providing a significant knowledge base for the study of urban climates. This methodology is still popular and is a fundamental step in understanding the present climate situation in each area. Two main types of observations are deployed. The first is an instrumented station situated to provide long-term but routine urban meteorological information. Such stations are used by national weather service agencies or municipal authorities, for operational and regulatory purposes (Oke et al., 2017). The second is the field campaign established to evaluate some aspects of the urban climate.

The simplest way to sample an urban climate over time is to use a conventional weather station, designed for long-term use to observe climate properties (precipitation, wind, temperature, etc.) comparable to those gathered at other sites. Another way to sample urban climates over space is to move the sensors through the urban atmosphere. Traverse observations or mobile measurements are usually conducted while the measurement platform is in motion. However, traverses are not suited for wind observations. Until present, observations continue to play a leading role in evaluating urban climate effects and developing an understanding of the responsible processes. Given the growth in the number and size of cities, the relative paucity of urban meteorological stations, and the need for atmospheric observations in cities, it is more crucial than ever.

Since the early 2000s, the development of realistic urban climate models, advanced computational resources, and numerical simulation approaches has become increasingly popular (Souch and Grimmond, 2006; Arnfield, 2006; Blocken, 2015). A variety of models of varying sophistication have been employed to understand exchanges of energy, mass, and momentum within the urban boundary layer or at the urban surface.

Consequently, the state of the atmosphere is a boundary condition for a model of the urban surface provides the boundary conditions for a mesoscale atmospheric model. Increasingly, these two types of models are coupled in so-called urban climate models (UCMs), where the climates of the urban atmosphere and surface evolve together in response to exchange to/from the surface-atmosphere domain.

Numerical modeling is one of the fundamental tools, together with observations and physical modeling, to understand urban climates. As noted, the numerical models can be used to conduct laboratory-like experiments that allow the complexity of the real world to be simplified and to isolate and examine the effects of modifying one part of the system. Moreover, there are a great many different UCMs that could be categorized, many of which are functions of the size of the modeling domain and the degree of simplification that this entails (Oke et al., 2017). A simple twofold division into micro-scale UCMs and mesoscale UCMs.

The Weather Research and Forecasting (WRF) model stands out as a highly adaptable and extensively utilized Numerical Weather Prediction (NWP) system, serving both atmospheric research and operational forecasting purposes. This collaborative development involved institutions such as the National Center for Atmospheric Research (NCAR). For researchers, WRF can produce simulations based on actual atmospheric conditions or idealized conditions with a mesoscale numerical weather prediction system (NCAR, 2023). WRF offers operational forecasting as a flexible and computationally efficient platform while reflecting recent advances in physics, numerics, and data assimilation contributed by developers from the expansive research community. WRF is currently in operational use at the Thai Meteorological Department (TMD).

Moreover, on the micro/local scale, models able to simulate airflow around obstacles are usually classed as computational fluid dynamics (CFD) models. These models are usually performed on generic urban surfaces, such as building arrays, or around individual buildings where considerable attention is paid (Oke et al., 2017).

The evaluation of urban climate can help identify climate resource spaces, preservation spaces, sensitive spaces, and restoration spaces, and inform the development of climate optimization strategies, such as ventilation corridors. Additionally, urban climate studies explore the synergies and tensions between climate resiliency goals, economic development, equity, and social justice, aiming to empower local communities in climate adaptation and resiliency efforts (Mill et al., 2022).

However, the complexity of urban climatic phenomena poses significant challenges for stakeholders (Ren et al., 2013). Understanding the characteristics of the urban climate is pivotal for effective urban planning; hence, policymakers must take proactive measures to mitigate the temperature, which is rising steadily year by year (Pakarnseree et al., 2018; Rizwan et al., 2008). Moreover, citizens and politicians are less aware than urban planners, designers, and urban climate experts. Awareness raising should involve media campaigns and further education on good practices (Lenzholzer et al., 2020; Stella et al., 2020).

1.1.2.2 Urban Environmental Climate Maps

The complexity of urban climatic phenomena is one of the obstacles for urban planners and stakeholders to understand their situation and make policies to respond to these issues. Therefore, urban environmental climate maps (UECMs) have been devised and envisaged to augment urban planning from a climatic standpoint and inform decision-makers.

Initially, UECMs drew inspiration from the Klima-Atlas, a German climate atlas, defined as "maps designed to facilitate a profound comprehension of the regional climatic conditions" (Matsuo and Tanaka, 2019). This concept spread from Germany to other European cities and the Klima-Atlas production guideline was published, standardizing Verein Deutscher Ingenieure's method (1997) (Verein Deutscher Ingenieure, 1997). Recently, these maps have been updated to incorporate urban warming measurements and air pollution distribution (Ng and Ren, 2015). These maps provide information about the physical characteristics of urban areas that affect the local thermal environment.

The World Urban Database and Access Portal Tools (WUDAPT) project aims to develop a global database of cities that can be integrated with existing land cover databases to support environmental studies (Fredrik et al., 2018). These methodological frameworks can serve as guiding principles, addressing gaps in this dissertation, aligning with the prevailing conditions, and fostering sustainable urban development initiatives.

The UECMs comprise a "Climate Analysis Map" and a "Recommendation Map", created in two different scales based on the specific planning focus: urban scale and neighborhood scale (Matsuo and Tanaka, 2019). UECM is crafted by experts, drawing on observation data and numerical simulations. Advances in climate simulation techniques, GIS techniques, and remote sensing techniques have been noteworthy in recent years. GIS techniques facilitate easy data modification and overlay of various geographical data, while remote sensing techniques enable the creation of UHI evaluation maps, including vegetation distribution maps. The application of these techniques has streamlined the process of creating a "Climate Analysis Map".

In addition, the Local Climate Zone (LCZ) scheme is used to classify natural and urban landscapes based on climate-relevant surface properties, providing a culturally neutral framework for collecting information about the internal physical structure of cities (Benjamin et al., 2015). Remote sensing data can be used to map LCZs, but traditional land use/land cover map accuracy assessment approaches may not accurately depict the local thermal environment. A new accuracy assessment approach has been proposed to better understand the accuracy of LCZ maps in portraying the physical properties of the urban environment (Chao et al., 2011).

Therefore, the UECMs were purposed to fill these gaps and play a role in providing climate information from the urban climate expert to support the urban planners' decision-making. When stakeholders make decisions, they can use this map as a communication tool.

1.1.2.3 Urban Climate Study in Southeast Asia: Case Study of Bangkok, Thailand

The urban climate study has spread from developed countries e.g. Germany, England, the United States, and Japan. These countries studied the environmental issues related to their urban climate and led to urban planning and policies. However, different parts of the world have different climates, and most of these countries are located in similar global climate regions. Various regions across the globe exhibit distinct climatic conditions.

The widely accepted framework for classifying climates was introduced in 1900 by the Russian-German scientist Wladimir Köppen. Köppen's classification system is based on the correlation between the type of vegetation in a given area and its prevailing climate. Through a comprehensive analysis of vegetation, temperature, and precipitation data, Köppen, along with other scientists, formulated a systematic approach to designate climate regions. The Köppen climate classification system (Kottek et al., 2006) categorizes climates into five primary groups: tropical (A); arid/dry (B); mild temperature (C); continental temperate (D), and polar (E). Each of these climate groups is further subdivided into specific climate types, providing a comprehensive and nuanced understanding of the diverse climatic patterns observed worldwide. Each largest cities are concentrated in A, C, and D climates, where available water and temperature suitable for growing crops are relatively abundant (Oke et al, 2017).

Tropical countries, which had warm temperatures, humidity, and long periods of summer and monsoons had few urban climate studies. One of the tropical regions is Southeast Asia. Southeast Asia, which consists of ten developing countries, is the geographical south-eastern region of Asia, consisting of the regions that are situated south of China, east of the Indian subcontinent, and north-west of mainland Australia which is part of Oceania (Klaus Kästle, 2013). Part of them located in mainland e.g. Thailand, Vietnam, Laos, Cambodia, while other countries are group of islands e.g. Philippines, Indonesia (Figure 1-3)

The statistics of the population of each country in 2020 show that the highest populations in five megacities: Jakarta, Manila, Ho Chi Minh, Hanoi, and Bangkok are higher than 10 million (Figure 1-3). The megacity with a high density of people and urban area is the area that is encountered with severe urban heat and climate changes. Therefore, one of these megacities was selected to be the study area. From five megacities, Bangkok was selected to be a target area in this study for two reasons. The first reason is it is one of the megacities in Southeast Asia that lacks an urban environmental climate study with the uniqueness of urban geological. The second reason is it has a highest potential for obtaining the climate data and relative spatial data.
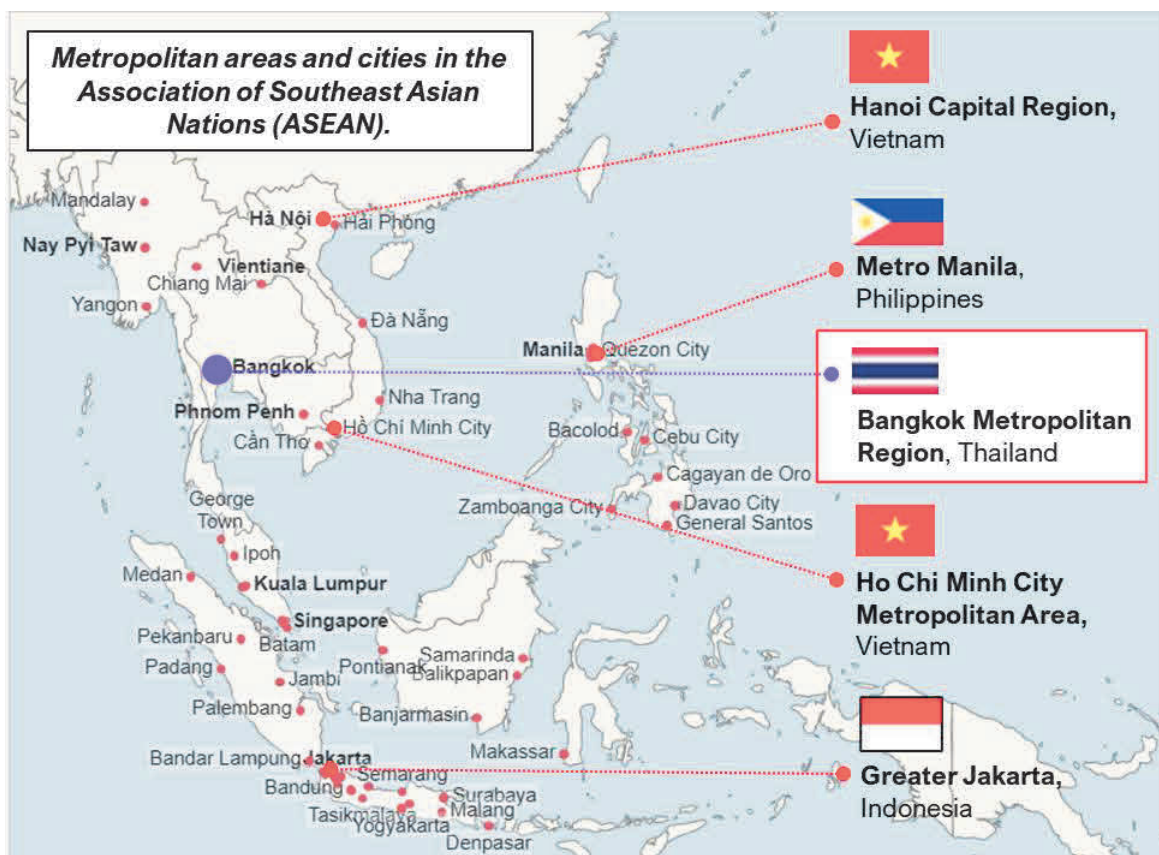
Fig. 1-3 Five megacities in Southeast Asia

Bangkok (Krung Thep Maha Nakhon) has been Thailand's capital for more than two centuries. It remains a significant economic hub and is the largest city in Thailand. Bangkok's population is continually expanding as people are drawn there by economic opportunities, largely driven by rural-to-urban migration. This rapid increase in population has caused an urban sprawl and the expansion of the cities in peripheral domains (Khamchiangta and Dhakal, 2020). A prior inquiry into BMR's urbanization (Pan et al., 2023) highlighted that over the past two decades (2000-2020), more than 70% of the developed areas have evolved from agricultural terrains with canals networks as a semi-aquatic city. Constructed in, rather than around, the Chao Phraya delta for centuries it has relied on canals for irrigation, flood mitigation and transportation.

The expansion of the Bangkok Metropolitan Area (BMA), especially in the last three decades, the canal networks have been disrupted and Bangkok has caused several environmental issues, including air and water pollution, land subsidence, and aggravated urban heat. The Thai Meteorological Department (TMD) reported an increase in maximum air temperatures across Bangkok over the last two decades. Discrepancies in temperature between the urban and rural domains, as evidenced by several studies (Pan et al., 2023; Sigit and Tanaka, 2015), indicate that Bangkok has a severe urban climate related to the UHI phenomenon. Despite several recent investigations into Bangkok's UHIs, scant attention from planners and stakeholders has been devoted to implementing urban warming mitigation strategies grounded in scientific understanding.

Although urban climate research in Thailand is increasing and mostly in Bangkok (Khamchiangta and Dhakal, 2020), it studied the UHI in terms of heat and land coverage, few studies have considered urban ventilation, actual air temperature, and regional climate of Bangkok. Most studies have used surface temperature (Khamchiangta and Dhakal, 2019, 2021; Keeratikasikorn and Bonafoni, 2018) which is calculated from remote sensing data due to resource and budget limitations (Toparlar et al., 2017). On the other hand, there are a few urban climate studies for urban land use planning. Numerical models were found at macroscale of Thailand (WRF model) or microscale (CFD simulation). In the Bangkok Metropolitan Region, the observation data was studied only on climatology, and the distribution of heat from inadequate distribution of observation data (Pakarnseree et. al, 2018) and focused only on the urban temperature on a micro-scale with its surroundings only in the center of Bangkok (Manat and Kazunori, 2011). The numerical modeling was rarely utilized; the WRF modeling— only the regional climate model that projected climate change over Southeast Asia (Chotamonsak et. al, 2011): the CFD model was used in a few studies and mostly focused on the microscale of wind distribution such as the effect of street canyon configurations and orientation (Jareemit and Srivanit, 2019).

1.2 Problem Statement and Objectives

As mentioned in the research background, the crucial limitations consist of (1) the limitation of climate data to understand the urban climate in tropical countries from the viewpoint of urban heat island mitigation: a case study of Bangkok Metropolitan Area and (2) lack of scientific evidence to clarify the situation and the severe area where urgent mitigate of urban heat island.

Based on these gaps, three research questions (RQ) were asked to shape the dissertation structure by focusing on BMA as follows:

RQ1: How to understand the urban climate in tropical countries in a data-scarce environment?

RQ2: Which spatial variables influence the Bangkok urban climate from the viewpoint of UHI mitigation?

RQ3: Where is the critical area from the urban heat island phenomenon in mesoscale and microscale of target area?

To answer the questions, the three main objectives of the dissertation are.

(1) To apply several methodologies and several scales of urban climate study to understand urban climate in tropical countries:

(2) To clarify the relationship between Bangkok's climate and the influenced spatial variables from the viewpoint of UHI mitigation from two different urban scales and:

(3) To clarify the critical area from the urban heat island phenomenon of two urban scales.

1.3   Overview of Target Areas

There are two reasons to select Bangkok as the target area from the other cities in Southeast Asia. The first reason is it is one of the megacities in Southeast Asia that lacks an urban environmental climate study and encountered with the urban heat island phenomenon from the statistics of climatology that was mentioned above. The second reason is the uniqueness of urban geological and the highest potential for obtaining the climate data and relative spatial data.

Bangkok is located in a tropical climate near the Equator with wet and dry namely Savanna. They have three seasons. One season is cool and dry—when the warm, moist inter-tropical convergence zone (ITCZ) is in the opposite hemisphere. Another season is hot and dry as the ITCZ approaches. The last season is hot and wet as the ITCZ arrives and the region experiences months of a tropical wet climate (National Geographic Society, 2020). It is a semi–aquatic city. Constructed in, rather than around, the Chao Phraya delta for centuries it has relied on canals for irrigation, flood mitigation and transportation. As the city has expanded, especially in the last three decades, the canal networks have been disrupted; filled in, paved over, and cut off from the river in favor of paved roads. Canals once connected almost every home, temple and palace in Bangkok. Canal access to the water was a central aspect of Bangkokian public life, today that access is becoming increasingly limited and privatized. Canals have a special connection to the urban design of Bangkok; besides their obvious uses for irrigation, flood control and transportation canals have another element central to their relationship to the urban life; spirit. However, Bangkok still had more than 1,000 canals from the Bangkok Administration report, but most of canals are narrow (Appendix B).

 In tropical countries, there are spatial data scarcely environment due to the limitation of budget. Similar to Bangkok before 2018, there are six national weather stations from the Thai Meteorological Department in the Bangkok Metropolitan Region (Figure 1-4). However, from late 2018 to 2019, severe environmental issues such as air quality, and urban heat, encouraged the local government to install several weather observation stations in their properties. One of the strengths inherent in selecting this study area lies in its capacity to bolster the efficacy of investigating and analyzing the pertinent features of urban climate, particularly its influence on the phenomenon of urban heat islands in tropical zones. Moreover, among the five megacities, Bangkok has a high possibility for obtaining local data from the departments of Thailand, which requires the Thai language based on the advantage of citizenship. In Southeast Asia, the main languages of each country are different with unique, related to the different cultures and distribution of geography.

Therefore, the target areas in this study consist of two scales related to the necessity and relationship between mesoscale and microscale to study urban climate, which is shown in Figure 1-2. A preliminary study on the mesoscale of Bangkok from the viewpoint of urban heat islands (UHIs) mitigation was conducted in the Bangkok Metropolitan Region (BMR), covering six provinces: Bangkok (BKK), Samut-Prakarn (SPK), Samut-Sakorn (SKN), Nakhon-Pathom (NPT), Nonthaburi (NTB), and Pathum-Thani (PTN). Encompassing an area of about 6,113.30 km² and hosting a population of nearly 10 million (as of 2019), the region is situated on the flat terrain of the Chao Phraya River basin, ranging from -1.08 to +3.12 m above sea level. Its southern boundary connects with the Gulf of Thailand. The BMR, characterized by a tropical climate, experiences three seasons: summer (March–May), monsoon (June–October), and winter (November–February). Figure 1-5 shows the target area with two different scales of study.

The secondary target areas represented the local scale and microscale urban climate of BMA. The advantage of studying mesoscale with numerical modeling is the wide range for selecting the microclimate study area. Therefore, the hypothesis of the microclimate study in Bangkok was "*Each area within a similarly critical area of the mesoscale climate zone had different local climate zones related to the urban topography and microscale spatial variables in the viewpoint of UHI mitigation*". Subsequently, two CBDs were selected as the microclimate study area for three reasons.
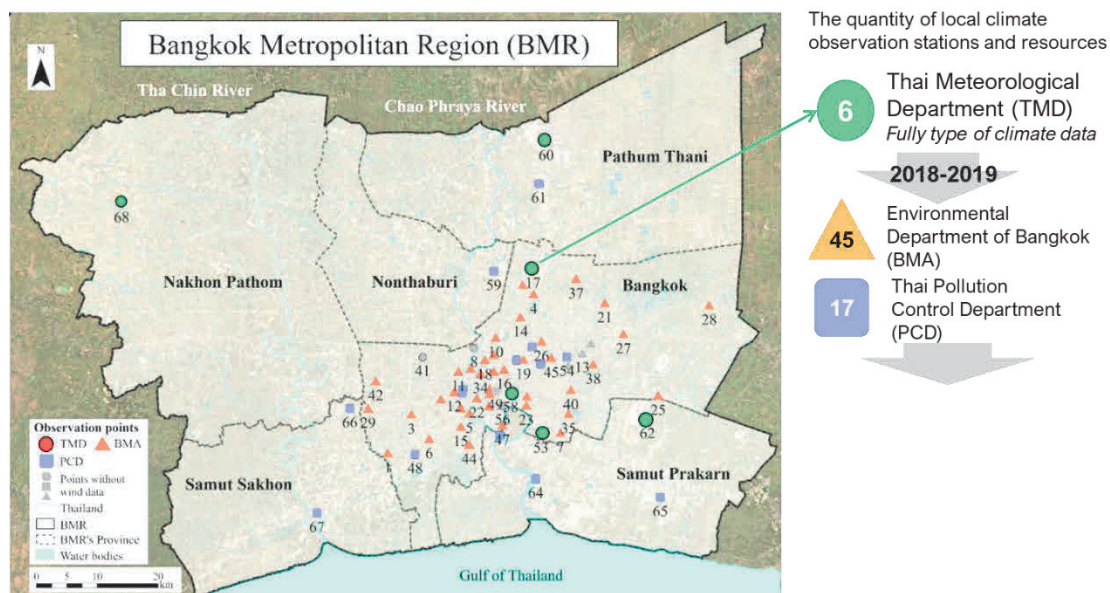
Fig. 1-4 Climate observation stations in Bangkok Metropolitan Region

The first reason is related to the findings from the mesoscale urban climate of Bangkok, the critical areas from the regional scale which had high temperatures and low wind speed (Figure 1-6) were selected. The second hierarchy is amongst the critical area from the first reason, the central business district was the main criterion because of the high density of daily life, and building the economical reason that made the CBD high daily traffic. The third reason, comparing between four CBDs of Bangkok: Yaowarat, Silom, Asoke, and Ratchadamri, which had a similar present urban planning zone (red zone: commercial), two districts were selected for comparative analysis, considered the similarity of critical type, Yaowarat and Ratchadamri which are not only had a similarity on the zone from meso-scale and BMA urban planning, they also had a similar distance from the coast which is one of the main finding variable that affected to diurnal temperature and wind speed. Moreover, both CBDs had different periods of establishment but continued to be CBDs with different urban morphology. The two CBDs of Bangkok: the Yaowarat area—the originality CBD and the Ratchdamri area—the present CBD, are selected. Both are situated in central Bangkok and share a similar latitude (13°44'26"N), The combined study area covered approximately 1.5 square kilometers.
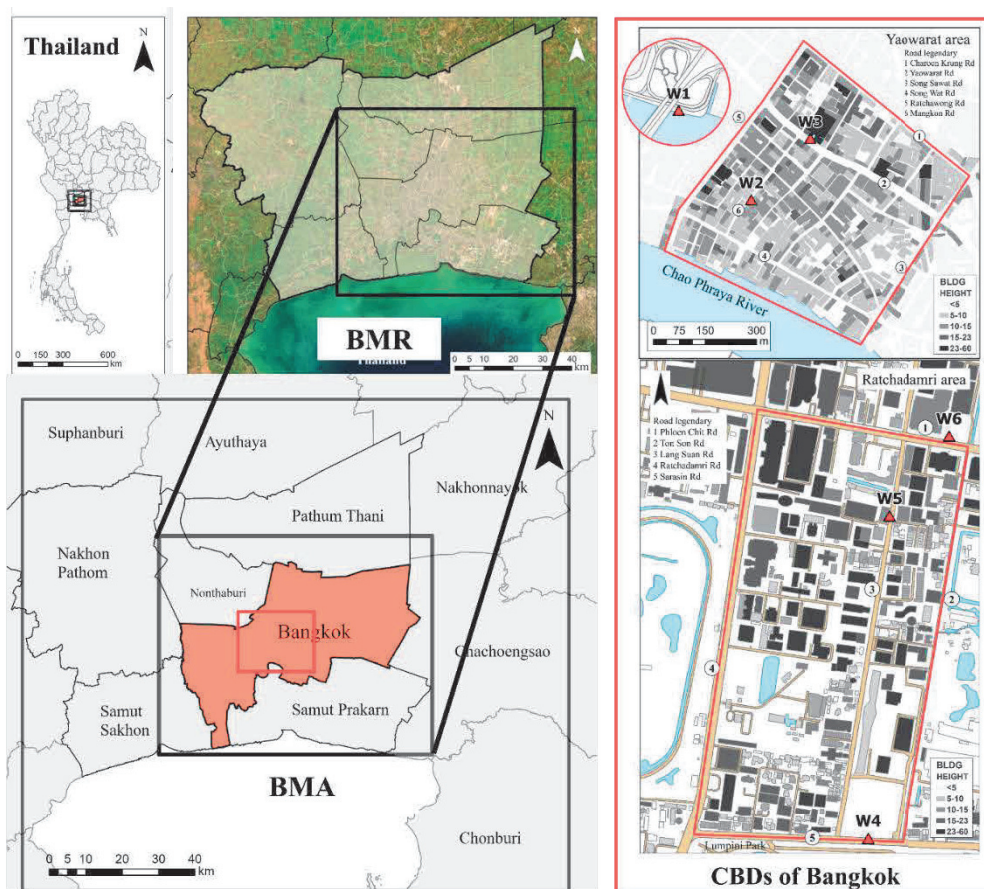
Fig. 1-5 Target area of study

1.4   Overview of Dissertation Structure and Methodologies

The dissertation is divided into seven chapters, as shown in Figure 1-6. Each chapter responds to the research questions and the main objectives with different methodologies. From Figure 1-6, this dissertation consists of four groups.

The first group is ***Chapter 1 'Introduction'***. In this chapter, the background of the study was concluded from the literature reviews, and the gap in research was reviewed to form the research questions and objectives. Subsequently, the information on the overview of the study area—from the regional scale to the district scale of the BMA was presented. The fourth part is the dissertation structure which explains the main content and the relationship between each chapter. The final part is the significance and originality of the dissertation which emphasizes and summarizes the novelty outcome from the viewpoint of tropical region's climate study.

The second and third group was divided based on the urban climate scale. The dissertation had the purpose of applying several methodologies and several scales of urban climate study to understand the urban climate in tropical countries due to the limitation of climate data to understand the urban climate in tropical countries. In this study area, the climate data from observations are distributed only on the regional and provincial scale. Therefore, the mesoscale climate was the first part of the study to clarify the critical area of Bangkok from the viewpoint of urban heat island mitigation (Chapters 2 and 3).

The second group consists of Chapters 2 and 3. This group is mainly similar to the study area scale which is the mesoscale of BMA. **Chapter 2 *'Making an Urban Environmental Climate Map of the Bangkok Metropolitan Region, Thailand'*** analyzed the relationship between air temperature, wind distributions, and spatial environmental factors based on weather data from observation stations of TMD, land use data, and remote sensing data in the BMR. The significant variables from this relationship were analyzed and used to classify the climate zone in Chapter 3.

Chapter 3 *'Urban Environmental Climate Maps of Bangkok'* scoped the study area from BMR to BMA and combined the spatial data from Chapter 2 with the numerical calculation based on WPS and WRF application with the meteorological data from NCEP. The combination of two main methods filled the gap from the adequate observed data analysis and clarified the total understanding of the urban climate in this area. However, the resource data from Chapter 2 were used to verify the accuracy of numerical calculations. The findings of both chapters are (1) the relationship between the relevant physical variables and the climate: wind speed and air temperature, in BMR and BMA, (2) the scientific evidence of regional and provincial climate zones in summer which significantly gain more understanding of the urban climate and clarified severe areas from each methodologies. Moreover, the comparison between the results of climate zones of both chapters emphasized the originality and significance of the research method.

The third group covers the information from Chapters 4–6 on the microscale of the CBD of Bangkok. The result of the combination of mesoscale climate clarified the critical area and was able to pick up the microclimate study area (Chapters 4–6). Subsequently, two CBDs in Bangkok were selected as a microscale urban area. The observation data in the mesoscale was the input data for numerical calculation in the micro-scale (Chapters 5 and 6). Each urban climate scale encompasses different factors impacting residents with different phenomena, and identifying these factors can enhance the efficacy of mitigating the urban heat island effect, as both urban climate scales positively correlate with each other.

Chapter 4 *'Field Measurements in the Two CBDs of Bangkok'* aims to collect and analyze the local weather data based on the field measurements in two CBDs of Bangkok: the Yaowarat and Ratchadamri areas which are located in the inner urban of Bangkok. Subsequently, the findings from Chapter 4 were adapted to the input data and validation of the results from the CFD simulation in Chapters 5 and 6.

Chapter 5 *'Comparative Analysis of the Urban Ventilation Characteristics between the Old and New Central Business Districts of Bangkok'* created the 3D modeling and used the numerical calculations on the CFD simulations to analyze and compare the ventilation characteristics of two CBDs. Moreover, this chapter aims to clarify the relationship between wind velocity and urban forms.

Then the findings from Chapters 4–5 were developed in ***Chapter 6 'Guidelines for Urban Land Use Planning in the Central Business District of Bangkok from the Viewpoint of Urban Heat Island Mitigation: Case Study of the Ratchadamri Area'***. This chapter created the microscale UECMs of the Ratchadamri area which analyzed and classified the local climate zones based on the wet-bulb globe temperature (WBGT) and wind speeds. Moreover, the findings of this chapter clarified the critical climate area in the microscale of Bangkok. The primary guidelines for urban land use planning in this area were presented and led to the creation of urban design in further study.

Finally, in ***Chapter 7 'Conclusion',*** the findings from Chapters 2–6 were summarized, the urban climate and the proposals design from the viewpoint of tropical regions were mentioned, and the future research direction was provided.
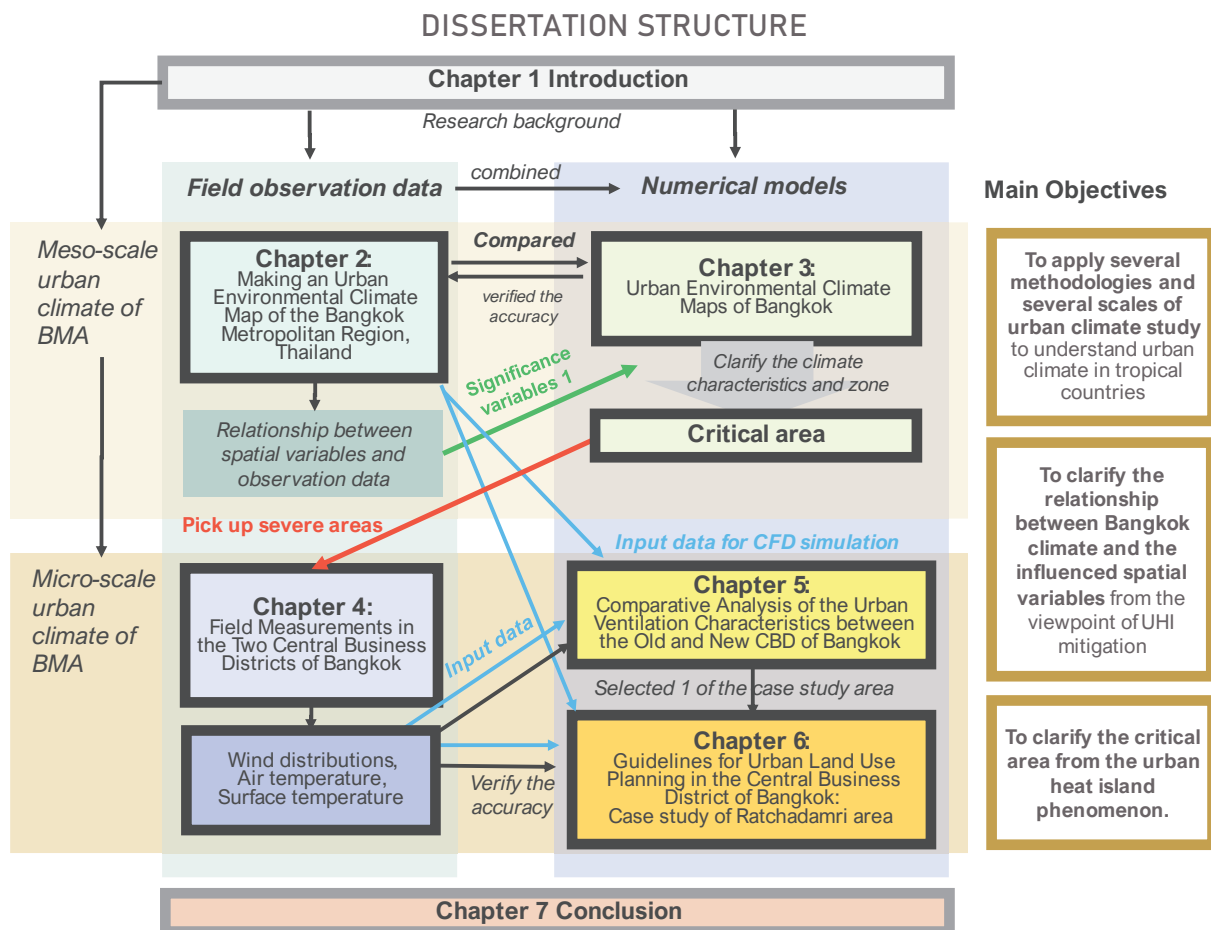
Fig. 1-6 Structure of dissertation and relationships between each chapter

1.5 The Significance and Originality of Dissertation

Although the current knowledge about the relationship between UHI and the urban climate and environmental variables was applied from worldwide cases, the understanding of urban climate under the data-scarce environment in tropical regions is still a challenge. Most tropical developing countries are typically lacking spatial environmental and climate data to support urban planning from the viewpoint of urban heat island phenomenon mitigation due to budget limitations. Similar to Bangkok, one of the megacities in Southeast Asia which is located in the tropical regions, there are only six national weather stations operated by the Thai Meteorological Department within the Bangkok Metropolitan Region. However, in response to severe environmental issues such as air quality and urban heat observed from late 2018 to 2019, the local government began installing additional weather observation stations on their properties. One of the key strengths of selecting this study area is its ability to enhance the effectiveness of investigating and analyzing crucial aspects of the urban climate, particularly its impact on the occurrence of urban heat islands in tropical zones.

Nevertheless, despite the collection of weather data at more than 60 points within the study area (Figure 2-3), it remains inadequate for achieving a comprehensive understanding of the entire region. This limitation arises from the positioning and distribution of each local station, frequently situated within the urban precincts of local government offices, thereby leading to a scarcity of diverse environmental locations that constitute a direct factor influencing the prevailing weather conditions. Therefore, two numerical applications: The Weather Research and Forecasting (WRF) model and the Computational Fluid Dynamic (CFD) simulation, were the secondary methodologies after obtaining the observation data related to the different study scales. The numerical calculation played a pivotal role in comprehending the broader context of urban climate, relying solely on weather data from observation stations proves inadequate for fulfilling this purpose. Therefore, the combination of field observation and numerical calculations on both urban scales (mesoscale and microscale) strengthens an efficient understanding of urban climate in the spatial data limitation of tropical countries from the viewpoint of urban heat island mitigation.

To summarize, in terms of practical framework, the originality of this study is the attempts to provide the developed research methodology that integrates and advances multiple urban climate methods across various urban scales to create a comprehensive understanding of the urban climate in tropical metropolises in the data-scarce environment.

To support the suitable method for the analysis in a data-scarce environment, this study attempts to decrease the limitations by creating and comparing two results from a similar urban scale (mesoscale) in cases of different methods. The strength of utilizing the actual weather data from the local government observation stations and the detailed urban spatial surrounding the stations tailored the map properly to this target area. Nevertheless, it is noteworthy that the distribution of weather stations did not adequately cover the entire region; instead, a majority of the stations were concentrated within the districts of Bangkok. On the other hand, the strength of utilizing the conventional methodology for precise calculating climate characteristics with publicly accessible data is easily applicable to other cities. However, the accessible information to everyone regardless of local characteristics or relationship to the study area.

Figures 1-7 and 1-8 show the comparison results between the field observation analysis and the numerical calculations. Figure 1-7 illustrates nocturnal and diurnal wind distribution from the field observation analysis and the numerical calculations. Related to the mentioned issues, the results from the field observation remain inadequate for achieving a comprehensive understanding of the entire region due to a scarcity of diverse environments and locations. The white circles show the different wind distributions due to the scarcity of data.

In addition, figure 1-8 illustrates the climate zone with levels of severe areas. Between these findings, the ventilation zone was more precisely based on the numerical calculation from the second map. The urban coastal zone (dark purple area) from the field observation analysis on the left side estimates a high wind speed related to the influence of the distance from the coastal line which has a high correlation with the statistical analysis. On the contrary, numerical modeling indicated that the high density of urban areas along the coastal region led to a reduction in wind speed. This finding suggests that this particular zone could be considered for implementing urban ventilation adaptation measures.

Field Observation	12 April 2019, 01:00	Numerical Modeling

Field Observation	12 April 2019, 13:00	Numerical Modeling
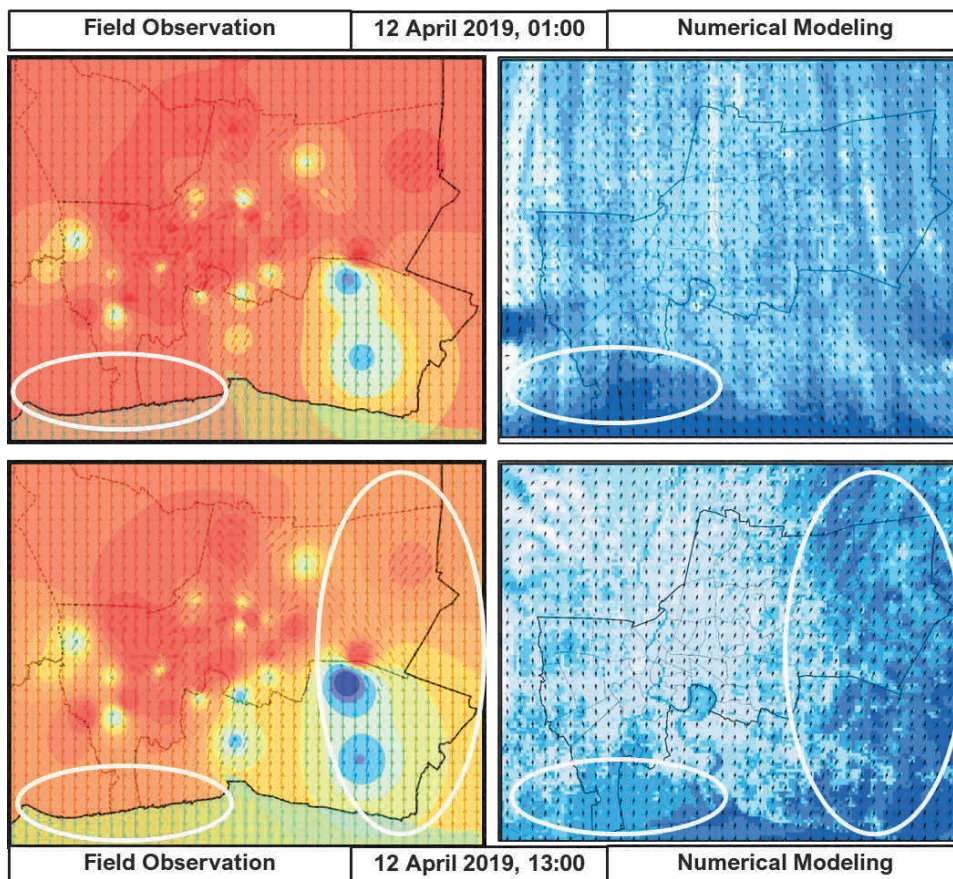
Fig. 1-7 The comparison of wind distribution from different methodologies
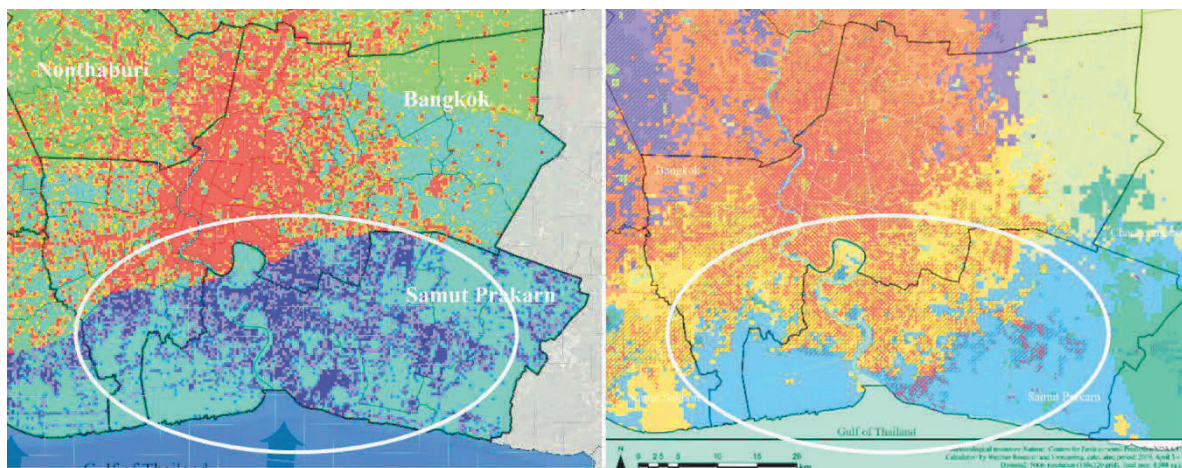
Fig. 1-8 The comparison of severe climate zones from different methodologies

References

Arnfield, A.J. (2006). Micro- and mesoclimatology. *Prog Phys Geogr, 30*, 677-689.
https://doi.org/10.1177/030913330607115.

Blocken, B. (2015). Computational Fluid Dynamics for urban physics: importance, scales, possibilities,
limitations and ten tips and tricks towards accurate and reliable simulations. *Build Environ, 91*, 219-245.
https://doi.org/10.1016/j.buildenv.2015.02.015.

Benjamin, B., Paul, J. A., Jürgen, B., Jason, C., Olaf, C., Johannes, J. F., Gerald, M., Linda, S., Iain, D., Stewart.
(2015). Mapping local climate zones for a worldwide database of the form and function of cities. ISPRS
international journal of geo-information, 4(1), 199. https://doi.org/10.3390/IJGI4010199.

Chao, R., Edward, N., Lutz, K. (2011). Urban climatic map studies: a review. International Journal of
Climatology, https://doi.org/10.1002/JOC.2237.

Fredrik, L., C. S. B. G., Andrew, G., Bei, H., Christoph, W., Kent, C., Ting, S., N.E., Theeuwes., Leena, Jrvi.,
Helen, C., Ward., I., Capel-Timms., Yuanyong, C., Per, J., Niklas, K., Dongwei, L., David, M., K., Frans,
G., Olofson., Jianguo, T., Dag, W., Lingbo, X., Zhe, Z. (2018). *Urban Multi-scale Environmental
Predictor (UMEP). Environmental Modelling and Software,*
https://doi.org/10.1016/J.ENVSOFT.2017.09.020.

Hongsuk, H. K. (1992). Urban heat island. International Journal of Remote Sensing, 13(12), 2319-2336.
https://doi.org/10.1080/01431169208904271.

Jing, Kong., Yongling, Zhao., Jan, Carmeliet., Chengwang, Lei. (2021). Urban Heat Island and Its Interaction
with Heatwaves: A Review of Studies on Mesoscale. Sustainability, doi: 10.3390/SU131910923.

Kamma, J., Manomaiphiboon, K., et al. (2020). Urban heat island analysis for Bangkok: Multi-scale temporal
variation, associated factors, directional dependence, and cool island condition. *Science Asia, 46,* 213-
223. http://dx.doi.org/10.2306/scienceasia1513-1874.2020.024.

Keeratikasikorn, C., & Bonafoni, S. (2018). Urban heat island analysis over the land use zoning plan of
Bangkok by means of Landsat 8 imagery. Remote Sensing, 10(3), 440.
https://doi.org/10.3390/rs10030440.

Khamchiangta, D., Dhakal, S. (2020). Time series analysis of land use and land cover changes related to urban
heat island intensity: Case of Bangkok Metropolitan Area in Thailand. *Journal of Urban Management,
9(4),* 1-12. https://doi.org/10.1016/j.jum.2020.09.001.

Khamchiangta, D., & S. Dhakal (2021). Future urban expansion and local climate zone changes in relation to
land surface temperature: Case of Bangkok Metropolitan Administration, Thailand. Urban Climate, 37,
100835.

Klaus Kästle (2013). "Map of Southeast Asia Region". Nations Online Project. One World – Nations Online.
Archived from the original on 20 September 2013.

Kottek, M., J., Grieser, C., Beck, B., Rudolf, & F., Rubel. (2006). World map of the Koppen-Geiger climate classification updated. *Meterologische Zeitschrift*, 15, 259-263.

Lenzholzer Sanda, Gerrit-Jan Carsjens, Robert D. Brown, Silvia Tavares, Jennifer Vanos, YouJoung Kim, Kanghyun Lee. (2020). Awareness of urban climate adaptation strategies –an international overview, *Urban Climate, 34,* 100705. https://doi.org/10.1016/j.uclim.2020.100705.

Matsuo, K., & Tanaka, T. (2019). Analysis of spatial and temporal distribution patterns of temperature in urban and rural areas: Making urban environmental climate maps for supporting urban environmental planning and management in Hiroshima. *Sustainable Cities and Society, 47*, 1-22. https://doi.org/10.1016/j.scs.2019.01.004.

Mill, G. (2014). Urban Climatology: history, status and prospects. *Urban Climate, 10,* 479-89. https://doi.org/10.1016/j.uclim.2014.06.004.

Mill, G., Iain, D., Stewart., Dev, Niyogi. (2022). The origins of modern urban climate science: reflections on 'A numerical model of the urban heat island'. Progress in Physical Geography, 46(4):649-656. doi: 10.1177/03091333221107212.

Moriyama, M., Tanaka, T. (2012). The mitigation of UHI intensity through an improved land-use plan in the urban middle area: Application to Osaka city, Japan. *Journal of Heat Island Institute International, 7*(2), 65-71. https://www.semanticscholar.org/paper/The-Mitigation-of-UHI-Intensity-through-an-Improved-Moriyama-Tanaka/8bae84702c33130925a0e096b0b406e709da609d.

National Center for Atmospheric Research (NCAR), Mesoscale and Microscale Meteorology Laboratory. (2023) Weather Research & Forecasting Model (WRF). Retrieved from https://www.mmm.ucar.edu/models/wrf.

National Oceanic and Atmospheric Administration (NOAA), U.S. Department. (2023). Trends in global average surface temperature between 1993 and 2022.

Ng, E., & Ren, C. (2015). The urban climatic map: A methodology for sustainable urban planning. Routledge.

Oke, T. R. (1982). The energetic basis of the urban heat island. *Quarterly Journal of the Royal Meteorological Society, 108(455)*, 1-24. https://doi.org/10.1002/qj.49710845502.

Oke, T.R., G. Mills, A. Christen, & J.A. Voogt. (2017). Urban Climates. 1st edition, Cambridge, United Kingdom: Cambridge University Press.

Pakarnseree, R., Chumkao, K., & Bualert, S. (2018). Physical characteristics of Bangkok and its urban heat island phenomenon. *Building and Environment, 143*, 561-569. https://doi.org/10.1016/j.buildenv.2018.07.042.

Pan, L., Lu, L., et al. (2023). Understanding spatiotemporal evolution of the surface urban heat island in the Bangkok metropolitan region from 2000 to 2020 using enhanced land surface temperature. *Geomatics, Natural Hazards and Risk, 14(1),* 2174904. http://doi.org/10.1080/19475705.2023.2174904.

Peng, T., Jialin, L., Luodan, C., Ruiliang, P., Zhongyi, W., Haitao, Z., Huilin, C., Hongbo, G. (2021). Assessing spatiotemporal characteristics of urban heat islands from the perspective of urban expansion and green infrastructure. Sustainable Cities and Society, 103208. https://doi.org/10.1016/J.SCS.2021.103208.

Ren, C., Spit, T., Lenzholzer, S., et al. (2013). Urban climate map system for Dutch spatial planning. *International Journal of Applied Earth Observation and Geoinformation, 18*, 207-221. https://doi.org/10.1016/j.jag.2012.01.026.

Rizwan, A. M., Leung, Y. C., & Liu, C. (2008). A review on the generation, determination, and mitigation of urban heat islands. *Journal of Environmental Sciences, 20,* 120-128. https://doi.org/10.1016/S1001-0742(08)60019-4.

Santamouris, M. (2007). Heat Island research in Europe: the state of the art. *Adv Build Energy Res, 1*, 123-150. https://doi.org/10.1080/17512549.2007.9687272.

Schwarz, N., Schlink, U., Franck, U., & Gromann, K. (2012). Relationship of land surface and air temperature and its implications for quantifying urban heat island indicators—An application for the city of Leipzig (Germany). *Ecological Indicators, 18*, 693-704. https://doi.org/10.1016/j.ecolind.2012.01.001.

Sigit, D. A., & Tanaka, T. (2015). The Characteristics of Urban Heat Island in Bangkok, Thailand. *Procedia Social and Behavioral Sciences, 195,* 423-428. https://doi.org/10.1016/j.sbspro.2015.06.484.

Souch, C., & S. Grimmond (2006). Applied climatology: urban climate. *Prog Phys Geogr, 30*, 270-279. https://doi.org/10.1191/0309133306pp484pr.

Stella, T., Katerina, T., Theodoros, T., Dimitrios, B. (2020). Urban Warming and Cities' Microclimates: Investigation Methods and Mitigation Strategies—A Review. Energies, 13(6), 1414. https://doi.org/10.

Tingzhen, M., Shengnan, L., Yongjia, W., Tianhao, S., Chong, P., Yueping, F., Renaud, de, R., Nyuk, H. W. (2021). Numerical Investigation on the Urban Heat Island Effect by Using a Porous Media Model. Energies, 14(15), 4681. https://doi.org/10.3390/EN14154681.

Toparlar, Y., B. Blocken, B. Maiheu, & G.J.F. van Heijst (2017). A review on the CFD analysis of urban microclimate. *Renewable and Sustainable Energy Reviews, 80*, 1613-1640. https://doi.org/10.1016/j.rser.2017.05.248.

Verein Deutscher Ingenieure. (1997). Environmental meteorology: Climate and air pollution maps for cities and regions. VDI.

Walter, L. F., Franziska, W., Ricardo, C.-D., Chunlan, L., Vincent, N. O., Nestor, G., Gustavo, J. N., Stevan, S., Claudia, E. N., Abul, Q. A., Marija, M., Juliane, B. (2021). Addressing the Urban Heat Islands Effect: A Cross-Country Assessment of the Role of Green Infrastructure. Sustainability, 13(2), 753. https://doi.org/10.3390/SU13020753.

Zhendong, Z., Chunhua, Y., Leiyu, Y., Xianchenghao, J., Jinshan, D., Longjun, Q., Bei, W., Guo, Y. Q. (2021). Impacts of land use/land cover types on interactions between urban heat island effects and heat waves. Building and Environment, 108138. https://doi.org/10.1016/J.BUILDENV.2021.108138.

Chapter 2
Making an Urban Environmental Climate Map of the Bangkok Metropolitan Region, Thailand

Analysis of Air Temperature, Wind Distributions,
and Spatial Environmental Factors

Contents

2.1   Introduction

Over the past decade, there has been a noticeable shift in both global and regional climates. This has prompted an immediate call for action by local planners and policymakers, compelling them to prioritize the safeguarding of local climates and environmental assets through climate change adaptations in urban construction. Among the pressing challenges that threaten the local climate, urban heat islands (UHIs) have emerged as a paramount concern. The term "UHI" describes the phenomenon of urban areas with altered temperatures compared to their rural surroundings (Oke, 1982). Specifically, UHIs are delineated by the temperature differential between urban and rural areas, and various metrics exist for quantifying this disparity (Schwarz et al., 2012). This phenomenon, which is ubiquitous on a global scale, manifests as a pervasive issue in densely populated metropolises with populations exceeding one million.

The causative agents of UHIs include population upsurges, urbanization dynamics, and industrial expansion (Pakarnseree et al., 2018). A comprehensive understanding of the UHI effect requires a precise elucidation of its relationship with urban spatial configurations (Li et al., 2011; Peng et al., 2016; Yao et al., 2019). As it involves both the air temperature and land surface temperature (LST) constituents, the UHI effect operates on multiple fronts (Schwarz et al., 2012; Zhou et al., 2014). Air temperature pertains to measurements captured near the urban canopy surface (Kamma et al., 2020). To quantify the UHI phenomenon, urban air temperature has been widely adopted as a reliable indicator of urban thermal characteristics in urban thermal studies (Taha, 1997; Arnfield, 2003).

Bangkok (Krung Thep Maha Nakhon) has been Thailand's capital for more than two centuries. It remains a significant economic hub and is the largest city in Thailand. The region accommodates a large population, with over 10 million individuals residing within its bounds (Khamchiangta and Dhakal, 2020; Srivanit and Kazunori, 2011). Bangkok's population is continually expanding as people are drawn there by economic opportunities, largely driven by rural-to-urban migration. This rapid increase in population, capital investment, factories, and employees has caused an urban sprawl and led to the development of transportation networks, real estate markets, escalating land valuations, and the expansion of the cities in peripheral domains (Khamchiangta and Dhakal, 2020; Srivanit and Kazunori, 2011). This rapid urbanization of Bangkok and the five surrounding provinces coalesced to form the Bangkok Metropolitan Region (BMR).

A prior inquiry into BMR's urbanization (Pan et al., 2023) highlighted that over the past two decades (2000-2020), more than 70% of the developed areas have evolved from agricultural terrains. World Bank's population data (United Nations Population Division, 2023) and the Statistical Report of Thailand (2020) (Statistical Forecasting Division, 2023) revealed a marked escalation in the nation's urban population ratio, which has surged from 22% in 1972 to 52% in 2020. The expansion of the BMR has caused several environmental issues, including air and water pollution, land subsidence, and aggravated urban heat. The Thai Meteorological Department (TMD) reported an increase in maximum air temperatures across Bangkok over the last two decades (Figure 2-1). Discrepancies in temperature between the urban and rural domains, as evidenced by several studies (Srivanit and Kazunori, 2011; Pan et al., 2023; Sigit and Tanaka, 2015), indicate that Bangkok has a severe urban climate related to the UHI phenomenon. Despite several recent investigations into Bangkok's UHIs, scant attention from planners and stakeholders has been devoted to implementing urban warming mitigation strategies grounded in scientific understanding (Srivanit and Kazunori, 2011; Matsuo and Tanaka, 2019). In Thailand, including the BMR, urban planning is based on the economic urban zoning map design, circumscribed by parameters such as building height, type, and floor area ratio (FAR). Understanding the characteristics of the urban climate is pivotal for effective urban planning; hence, policymakers must take proactive measures to mitigate the temperature, which is rising steadily year by year (Pakarnseree et al., 2018; Khamchiangta and Dhakal, 2020; Rizwan et al., 2008). The complexity of urban climatic phenomena poses significant challenges for stakeholders (Ren et al., 2013).

Therefore, urban environment climate maps (UECMs) have been devised and envisaged to augment urban planning from a climatic standpoint and inform decision-makers. In this study, we applied a map-generating methodology. Initially, UECMs drew inspiration from the Klima-Atlas, a German climate atlas, defined as "maps designed to facilitate a profound comprehension of the regional climatic conditions" (Matsuo and Tanaka, 2019). This concept spread from Germany to other European cities and the Klima-Atlas production guideline was published, standardizing Verein Deutscher Ingenieure's method (1997) (Verein Deutscher Ingenieure, 1997). Recently, these maps have been updated to incorporate urban warming measurements and air pollution distribution (Ng and Ren, 2015). These methodological frameworks can serve as guiding principles, addressing gaps in forthcoming BMR urban planning endeavors, aligning with the prevailing conditions, and fostering sustainable urban development initiatives.

To date, several studies have investigated the thermal environment changes in Bangkok and its surrounding provinces. Most of these investigations have focused on analyzing changes in LST and surfaced urban heat island (SUHI) phenomena (Thammapornpilas, 2015; Nguyen et al., 2022; Nguyen et al., 2021). Conversely, only a limited number of studies (Pakarnseree et al., 2018; Srivanit and Kazunori, 2011), have focused on near-surface temperature or air temperature owing to the inherent challenges associated with data collection. Even though near-surface temperature and LST within urban climate studies show strong correlations (Keeratikasikorn and Bonafoni, 2018; Weng, 2009), their distinct values necessitate a more targeted approach.

Therefore, this study focused on air temperature, which is a vital parameter for prospective urban climate inquiries. Nevertheless, this investigation undertook a thorough examination of each observation point using the details of land use and land cover (LULC) and built footprints to analyze the surrounding physical factors related to the air temperature and wind distribution. In particular, this study delved into distinct LULC scales, observation distances, and coastal regions, which are vulnerable to the sea breeze effect within the BMR. As a first step, this study integrated the effective variables pertaining to air temperature and wind speed into a singular regional map of the BMR, constituting a noteworthy advancement. The incorporation of geographical locations and natural water sources further enriches this study. This comprehensive analysis holds potential value for future research endeavors.

The findings derived from the correlation analysis between the air temperature distributions, wind distributions, and spatial environmental variables of the BMR could potentially be applied to urban environmental studies in other municipalities. These insights can be refined through cross-city comparisons, fostering an improved understanding of climate dynamics and urban temperature dispersion across the provincial and regional echelons at each study site. The methodologies extracted from this study can be suitably adapted to other urban centers, thereby contributing to sustainable development. Given the nexus between climate change impacts and urban landscape characteristics, it is anticipated that the research findings will serve as a valuable resource for the BMR's urban development plan and support the achievement of global objectives, namely the United Nations Sustainable Development Goals (SDGs). The SDGs encompass two relevant aspirations: sustainable cities and mitigation and adaptation to climate change. This study resonates with these overarching objectives by steering the discourse toward sustainable urbanization while advocating for effective climate-oriented planning and management mechanisms within developed countries. For reference, the abbreviations utilized throughout this study are succinctly summarized in Table 2-1.

The structure of this chapter comprises five sections. It commences with an exposition of the objectives, followed by a comprehensive overview of the materials and methods employed. The third section encapsulates the results, categorizing the findings into four distinct parts. Subsequently, the fourth section is dedicated to the discussion, wherein four specific aspects are examined. The concluding part encapsulates the overall conclusion.

2.2   Objectives

Driven by the above statements and research gaps, the authors implemented this study to bridge the knowledge of urban climate change and synthesize existing insights epitomized through the UECM. Thus, this study sought to unravel the environmental predicaments affecting the BMR and the UHI phenomenon. In this vein, this study had two key objectives: \ (1) To analyze the relationship between air temperature distribution, wind distribution, and spatial environmental factors within the BMR, and

(2) To clarify the mesoscale climate from the field observation data and relevant spatial variables, emphasize the critical area with severe climate from the viewpoint of UHI mitigation and illustrate the findings into a comprehensive UECM tailored to the BMR.

Table 2-1 Abbreviation list for this study

Abbreviation	Description	Abbreviation	Description
BKK	Bangkok	NPT	Nakhon Pathom
BMA	Bangkok Metropolitan Administration	NTB	Nonthaburi
		PTN	Pathum Thani
BMR	Bangkok Metropolitan Region	SKN	Samut Sakorn
BCR	Building Coverage Ratio	SPK	Samut Prakarn
DC	Distance from the Canals	SUHI	Surfaced Urban Heat Island
DCDS	Distance from the Coastline in the Direction of Sea breeze	TMD	Thai Meteorological
		T_{min}	Department
DR	Distance from the Rivers	T_{max}	Average Minimum
ED	Environmental Department of BMA	UCR	Temperature
FAR	Floor Area Ratio	UECM	Average Maximum
GCR	Green Coverage Ratio		Temperature
GIS	Geographic Information System	UHI	Urban Coverage Ratio
IDW	Inverse Distance Weighting	WCR	Urban Environmental Climate
LST	Land Surface Temperature	WD	Map
MLR	Multiple Linear Regression	WS	Urban Heat Island
NDVI	Normalized Difference Vegetation Index		Water Coverage Ratio
			Wind Direction
			Wind Speed
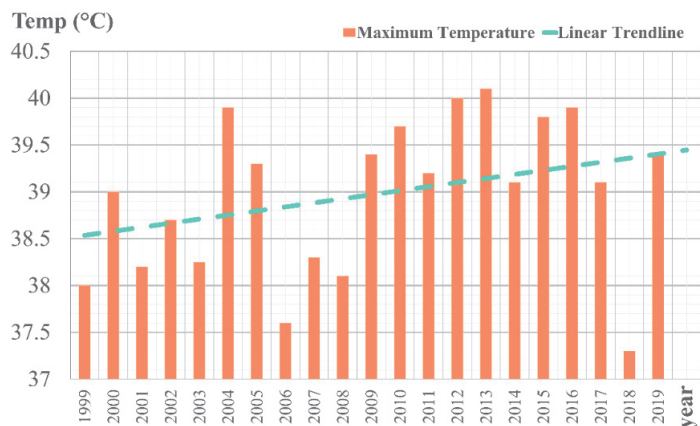
Fig. 2-1 Average maximum temperature in Bangkok (1999–2019)
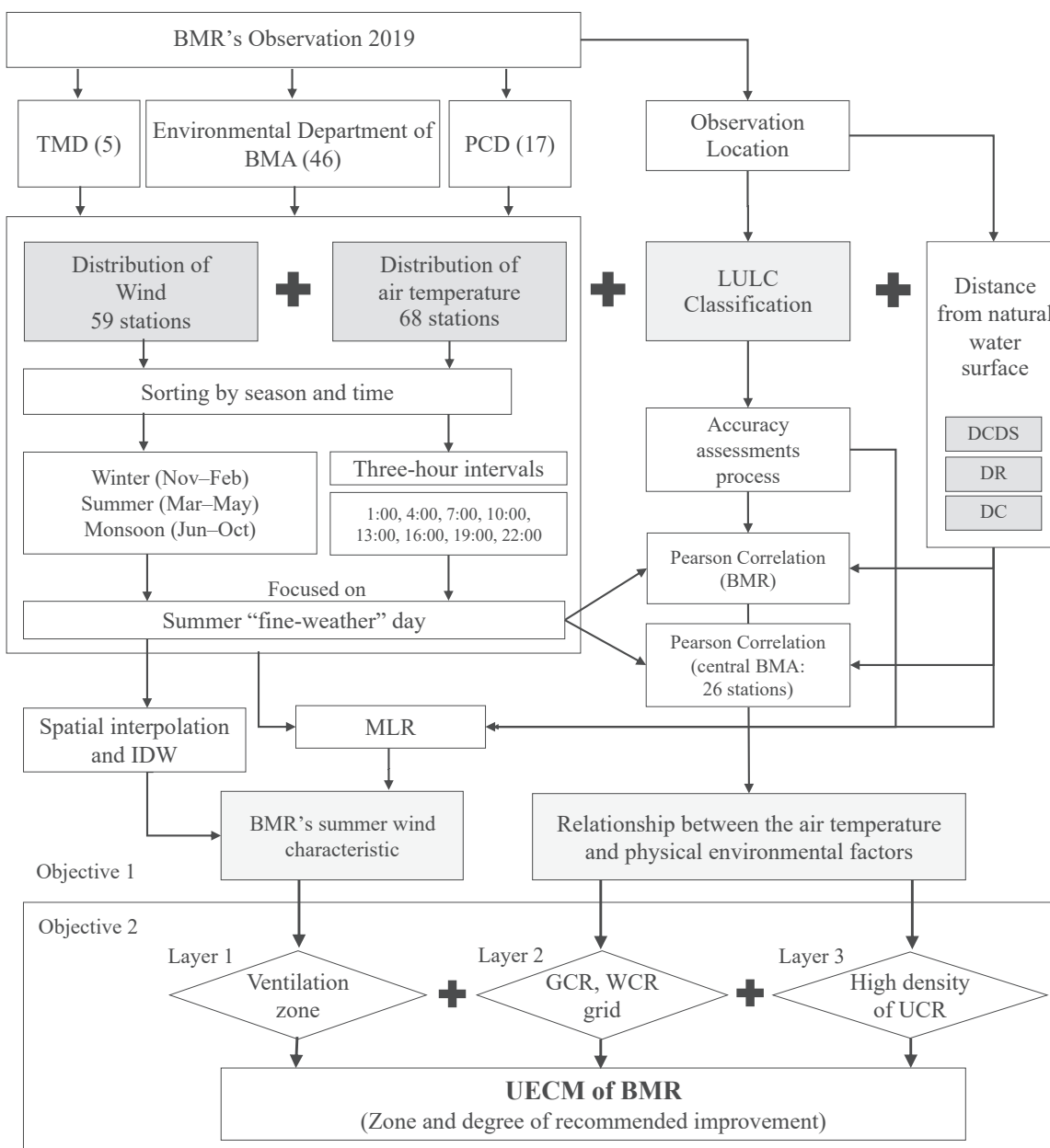
Fig. 2-2 Summary of the research framework

2.3 Materials and Methods

This section briefly discusses the methodology used in this study. The detailed process for achieving the objectives of the study is illustrated in Figure 2-2.

2.3.1 Study Area

A preliminary climate study was conducted around the BMR to examine the characteristics of Bangkok's UHIs. The BMR covers six provinces: Bangkok (BKK), Samut-Prakarn (SPK), Samut-Sakorn (SKN), Nakhon-Pathom (NPT), Nonthaburi (NTB), and Pathum-Thani (PTN). It covers an area of approximately 6,113.30 km², with a population of nearly 10 million (as of 2019) (Statistical Forecasting Division, 2023). The region is located on the Chao Phraya River basin's flat terrain, ranging from -1.08 to +3.12 m above sea level (Taichi, 2020), with the southern boundary adjoining the Gulf of Thailand. Due to its tropical climate, the BMR experiences three seasons: summer (March–May), monsoon (June–October), and winter (November–February). Figure 2-3 shows the study area and observation stations across various Thai government departments.
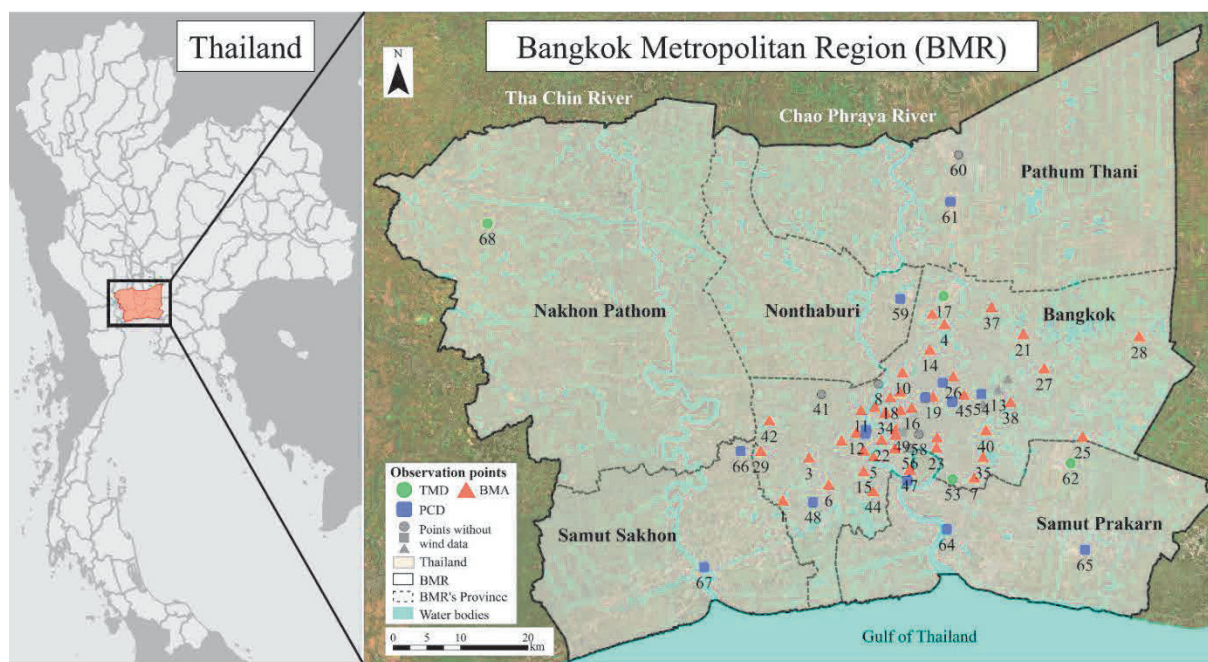
Fig. 2-3 Study areas and locations of the observed stations in the BMR

2.3.2 Climate Data Description

To understand the relationship between the local climate and spatial environmental factors, previous UECMs were organized to guide future development (Liu et al., 2017; Sasaki et al., 2018). This involved the use of secondary meteorological and geographical information sourced from Thai government agencies. The data were divided into four sections: air temperature distribution, wind distribution, LULC classifications, and the distance between each observation point and water bodies.

Meteorological data were collected from 68 stations across 3 Thai government agencies—the TMD, the Thai Pollution Control Department, and the Environmental Department of the Bangkok Metropolitan Administration (BMA)—from 2019 to 2020. Divided into three seasons—summer, monsoon, and winter—the data were collected at three-hour intervals (1:00, 4:00, 7:00, 10:00, 13:00, 16:00, 19:00, and 22:00) to capture temperature variations throughout the day. Summer data were extracted from all the data (88 days) to produce the exact summer data for the tropical country. The following criteria were used to define summer "fine weather" days (37 days)—daily precipitation of less than 1 mm, daylight hours make up at least 40% of the day, the daily maximum temperature is more than 30°C, and it is not raining (Matsuo and Tanaka, 2019; Taichi, 2020). Additionally, 159 monsoons and 118 winter days were extracted from the data based on the average daily mean temperature, average daily minimum temperature (T_{min}), and average daily maximum temperature (T_{max}). The sorted air temperature data were consistent with the limited data of the TMD stations and the methodologies of previous studies, which found that the UHI intensity varied according to season and time (Pakarnseree et al., 2018). Pearson's correlation coefficient was calculated for this analysis.

To analyze summer wind distributions, data from Station 17 on a fine-weather summer day were employed to represent the wind-blowing patterns. Station 17 is one of the main stations of the TMD, located near the Don-Mueang International Airport. A total of 59 observation stations contributed to the spatial interpolation and inverse distance weighting (IDW) analysis. In addition, multiple linear regression (MLR) was used to determine the factors affecting the wind speed.

2.3.3 LULC Classification and Coverage Ratio

Landsat 8 data, offering a medium-high spatial resolution of 30 m, were used to derive the LULC datasets. By employing a decision tree algorithm based on three indices (Fig. 2-4)—the normalized difference vegetation index (NDVI); modified normalized difference water index (MNDWI); and land use data incorporating building footprints from Geographic Information Systems (GIS) datasets of the BMA and Department of Public Works, Town, & Country Planning—LULC patterns were detected. The NDVI has been used extensively to identify vegetation based on spectral values and is one of the most popular remote-sensing vegetation indices (Yaung et al,. 2021; Patil et al., 2018). Six distinct LULC classes emerged: vegetation, water, watery vegetation, urban areas, impervious areas, and bare areas. Noticeably, the water area was overlaid with land use data from Department of Public Works, Town, & Country Planning to segregate the water surfaces of salt ponds and fisheries and to segregate watery vegetation into water forests (mangroves), and other water plant farms. Finally, the non-water areas were separated into three classes based on land use data: urban areas (buildings), impervious areas (roads and street surfaces), and bare areas (soil).

ArcGIS facilitated spatial analysis for land coverage ratio calculations, including three segments from six classifications: the urban coverage ratio (UCR), which is the percentage of a site's total ground area occupied by any human structure, including buildings, impervious areas, and roads; the green coverage ratio (GCR), which is the proportion of vegetation coverage (vegetation and watery vegetation) based on the LULC classification; and the water coverage ratio (WCR), which is, the percentage of the surface covered by water such as rivers, canals, or ponds. The coverage ratio map for each class was generated and recalibrated to a 100-m resolution (Ren et al., 2013). The coverage ratio of each station was determined within a 300-m radius, yielding insights into the physical attributes of the region based on previous studies (Rizwan et al., 2008; Shi and Zhang, 2018).

Additionally, the relationship between air temperature and environmental factors in the center of the BMR (within 26 stations) was examined, considering the average floor area ratio (FAR) and building coverage ratio (BCR) as contributing elements. The FAR, which assesses a building's floor area relative to its land size, was evaluated within a 300-m radius. The BCR was calculated using building footprints within 300 m of the vicinity. Figures 2-5 and 2-6 show LULC classification maps and the land coverage respectively, and detailed land coverage data for the 26 stations are available in Figure 2-7 and the table data of each observation point in Appendix A (Table A-1).

Landsat 8 Image
(2019)

$$NDVI = \frac{NIR - Red}{NIR + Red}$$

$NDVI \geq 0.25$ $NDVI < 0.25$

$$MNDWI = \frac{Green - SWIR1}{Green + SWIR1}$$

$MNDWI \geq -0.15$ $MNDWI < -0.15$ Land use data 2019 (DPT, BMA)

Vegetation   Watery vegetation   Water   Urban areas   Bare areas   Impervious areas

BMR LULC Classification   Accuracy assessments   1,000 random sampling points

68 Observation Locations

Calculated within surrounding 300m   Accuracy assessments report

$$GCR = 100 \times \frac{Vegetation\ area\ (sqm)}{Total\ area\ (sqm)}$$ $$WCR = 100 \times \frac{Water\ area\ (sqm)}{Total\ area\ (sqm)}$$ $$UCR = 100 \times \frac{Urban\ area\ (sqm)}{Total\ area\ (sqm)}$$ $$BCR = 100 \times \frac{Building\ Footprint\ (sqm)}{Total\ area\ (sqm)}$$

$$FAR = \frac{Total\ Floor\ area\ (sqm)}{Building\ Footprint\ (sqm)}$$

LULC Classification (coverage ratio)

Note: Red: visible red wavelength, Green: visible green wavelength, NIR: near infrared, and SWIR: shortwave infrared.

Fig. 2-4 The designed framework of the LULC classification
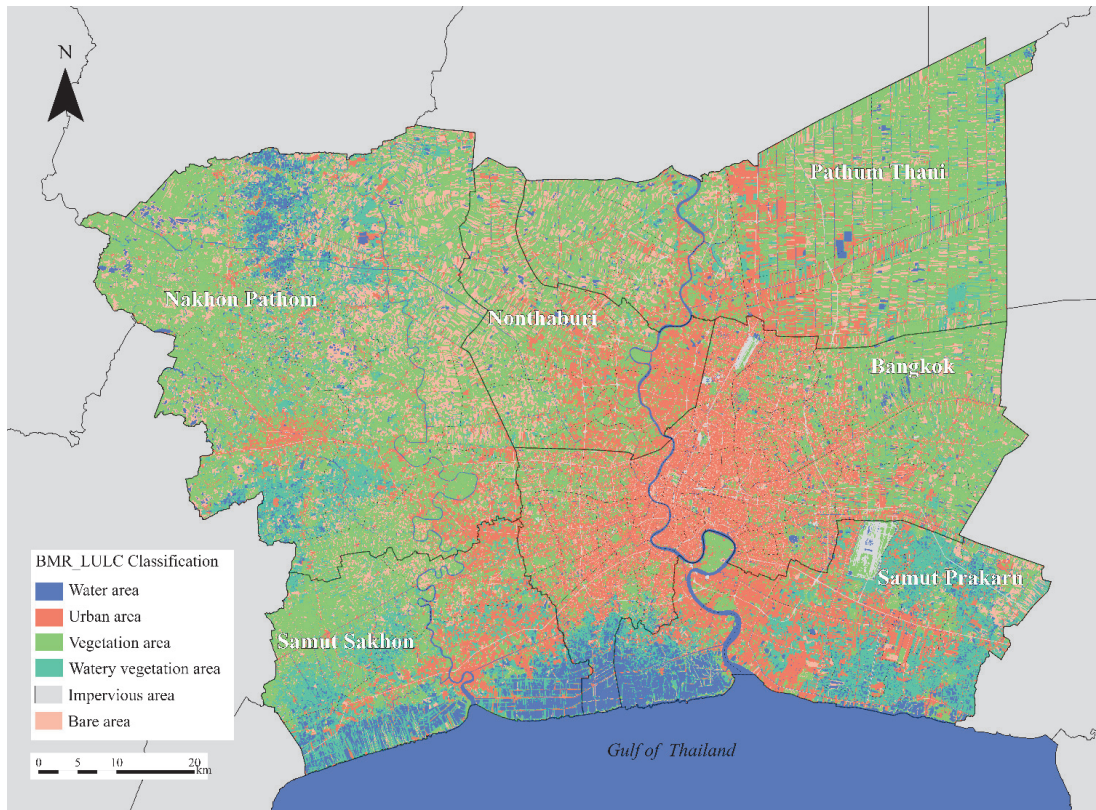
Fig. 2-5 LULC classification map of the BMR
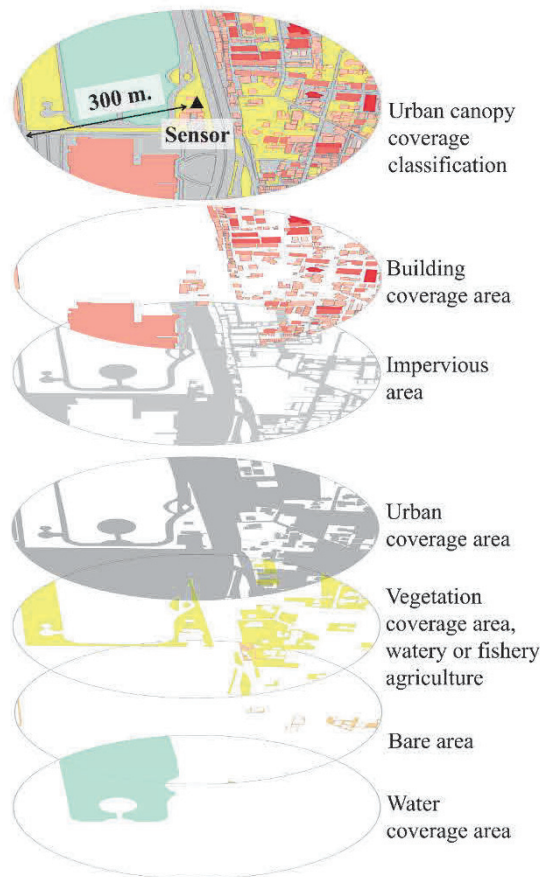
Fig. 2-6 Classification of surrounding land coverage of the observed station
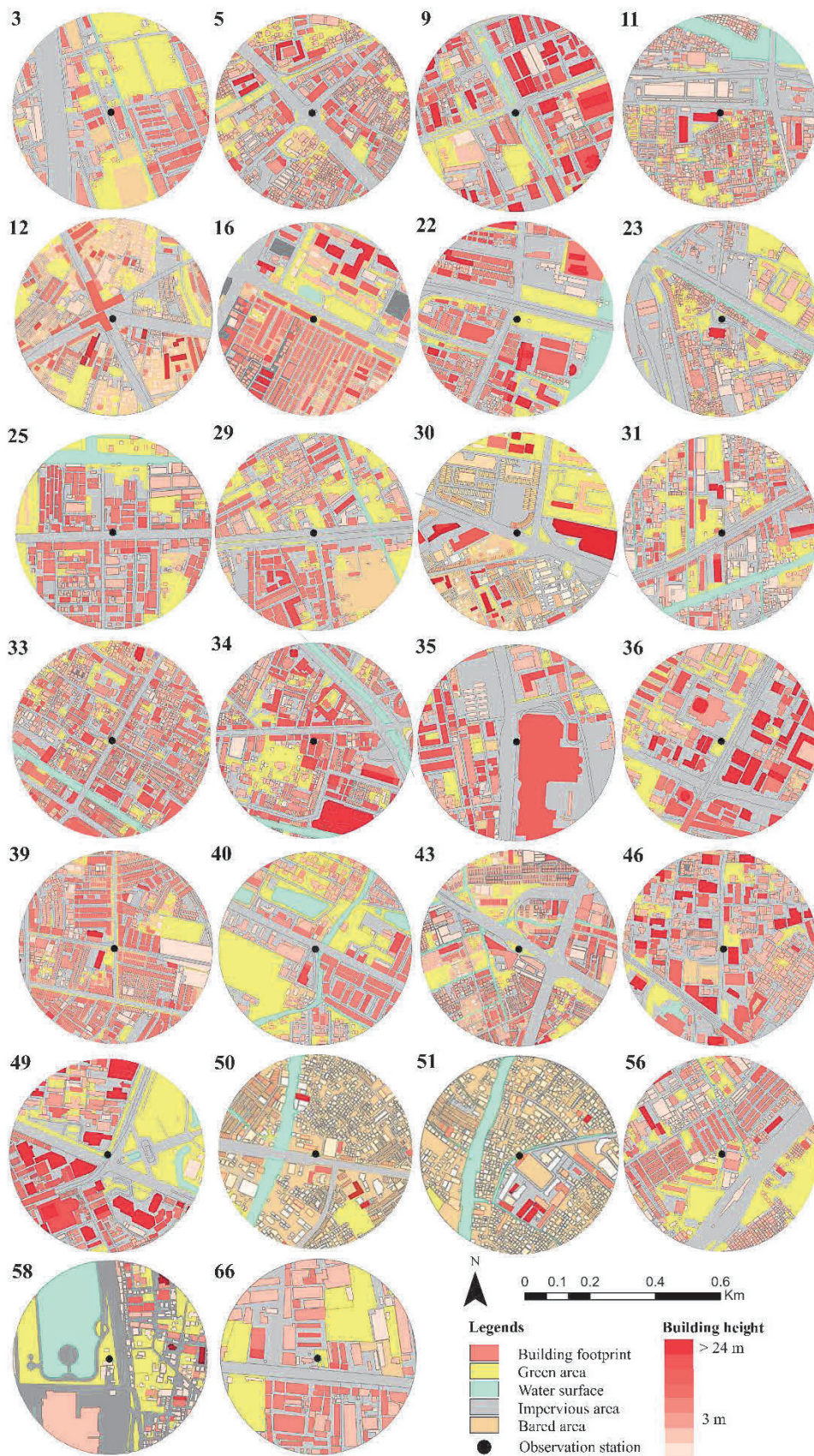
Fig. 2-8 Land coverage of 26 stations in the inner area of BMR

2.3.4 Accuracy Assessment of the LULC Classification

The accuracy of the LULC classification was verified using high-resolution Google Earth images from 2019. A representative sample of approximately 1,000 reference points distributed proportionately across different classes (approximately 1.2% of the total dataset) was established for validation (Alawamy et al., 2020; Stehman, 2009). A confusion matrix analysis encompassing the user's accuracy, producer's accuracy, overall accuracy, and kappa coefficient was employed to assess the classification accuracy (Diek et al., 2017; Sarkar, 2018).

2.3.5 Other Physical Factors

Using Euclidean distance tools within the GIS, the distance in meters between each observation point and the water surface was categorized into three indices. First, the distance from the coastline in the direction of the sea breeze (DCDS) was determined by calculating the gap between the Gulf coastline and each observation point. T h i s methodology was adopted from previous studies (Matsuo and Tanaka, 2019; Sasaki et al., 2018). Second, the distance from the river (DR) was computed by calculating the distance between the Chao Phraya and Tha-Chin Rivers and each observation point. The third index was distance from the canal (DC). The list of canals was obtained from the BMA and other provincial governors' databases. The BMA's canal data consisted of 1,161 canals, which were primarily documented in the Thai language. As a result, 33 canals characterized by an average width exceeding 15 m were selected to determine the distance between their borderline and 26 stations located in the central area of the BMR. Figure 2-8 shows map of rivers and canals for calculating the DC. Additional details regarding the list of canals is presented in Appendix A (Table A-2).

2.3.6 Making the Primary UECM of the BMR

The creation of the primary UECM of the BMR involved a systematic process based on the relationships established in the preceding section. The influence of each factor was divided into three main layers on the map (Figure 2-2). The initial layer was developed using spatial interpolation and IDW techniques, combined with the range of DCDS, and overlaid onto an average summer temperature distribution map. This combination delineated an effective sea breeze zone.

The subsequent layer focused on the influence of the vegetation areas on urban temperature. This layer was visualized on a square grid map of the BMR, with each grid covering an area of 90,000 m² within a 300×300 m resolution. The BMR, encompassing 86,208 grids, was extensively analyzed in this manner. The first step involved calculating the GCR for each grid, which was derived from the sum of the vegetation and watery vegetation areas on the LULC map (Figure 2-5).

Subsequently, a spatial analysis tool was employed to aggregate the GCR, leading to the classification of the raster into four groups based on the GCR threshold: less than 10%, 10–30%, 30–50%, and > 50%. These groups were visually represented by color-coded pixels, namely, red, orange, yellow, and green. Additionally, the WCR was determined, to reflect the predominant value for each grid. Instances, where the WCR exceeded 50%, were depicted in blue. The third layer, corresponding to the UCR influence, was subsequently generated. It depicted grids with UCR values exceeding 90%. This layer was generated using a methodology similar to that used for the GCR map. UCR-influenced grids were visually represented using hatching patterns. Finally, the three layers were superimposed to create an integrated UECM for the BMR. This synthesis was achieved through focal statistical analysis, operating at a resolution of 300 m.
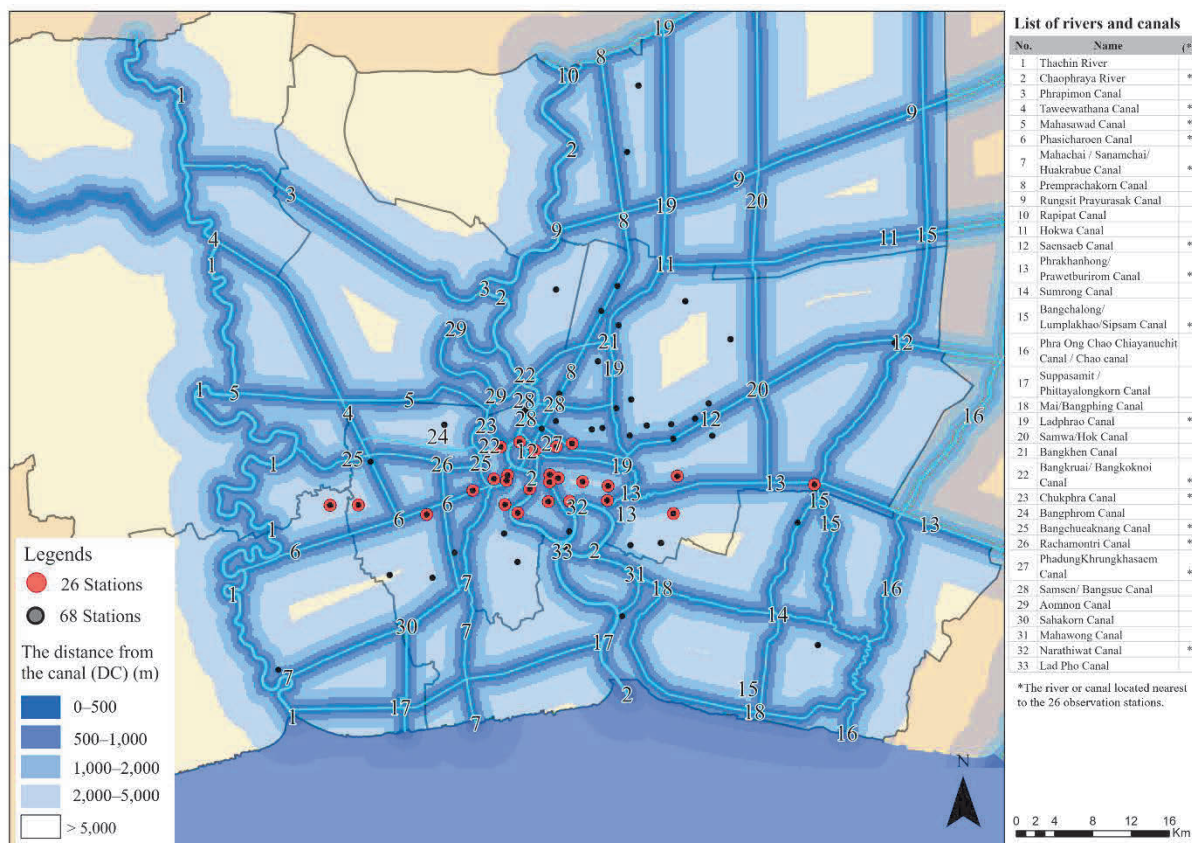
Fig. 2-8 Map of rivers and canals for calculating the DC

2.4   Result

2.4.1   Relationship between Air Temperature Distribution and Spatial Environmental Factors in the BMR

At the regional scale, an investigation of the average daily minimum temperature (T_{min}) and average daily maximum temperature (T_{max}) for each season in 2019 was conducted about spatial environmental factors across the observation points within the BMR. Table 2 presents the correlation coefficients between the five spatial environmental factors and the air temperature in the BMR. This study produced the following three findings:

1) DCDS Relationships: The DCDS exhibited various relationships across seasons and times. It displayed a negative correlation with T_{min} in all seasons (-0.349, -0.252, and -0.463, respectively) and a positive correlation with T_{max} during summer (0.650) and the monsoon (0.332). Consequently, areas farther from the coast experienced higher diurnal air temperatures during summer but lower nocturnal temperatures, which were attributed to greater diurnal-nocturnal temperature variations.

2) DR and WCR Relationships: The DR exhibited a negative correlation with minimum temperature during summer and winter (-0.490 and -0.537, respectively). The WCR displayed a negative correlation with T_{max} in summer, with the highest correlation observed during winter.

3) UCR and GCR Effects: The UCR showed a positive correlation with T_{min} in all seasons, resulting in increased nocturnal temperatures in urban areas. Conversely, the GCR demonstrated a strong negative correlation with T_{min} in all seasons, suggesting that rural areas with higher green coverage experienced lower nocturnal temperatures. Increasing green areas within urban regions has emerged as a viable solution for mitigating nocturnal urban heat.

The analysis of stations with high and low DCDS ratios indicated a significant impact on air temperature, particularly in areas distant from the coastline. However, observation stations located 24–40 km from the coastline in central Bangkok remained unaffected by the DCDS (Figures 2-8 and 2-11). Hence, to discern the factors influencing the urban temperature within this range, a comprehensive analysis was conducted on 26 central urban stations in Bangkok. Pearson's correlation coefficients were recalculated for the DR, BCR, FAR, and DC (Table 3). The results demonstrated the following:

1) **UCR Dominance:** The UCR exhibited the most significant positive correlation with T_{min} during the monsoon and winter seasons at both the regional and provincial scales, surpassing the effects of the BCR and FAR.

2) **DC and DR Influence:** Both the DC and DR exhibited negative correlations with T_{min} across all seasons, with the DC displaying a stronger negative correlation in the summer and monsoon seasons.

3) **Relevance of the GCR and WCR:** The GCR maintained a robust negative correlation with T_{min}, whereas the WCR displayed a weaker correlation with temperature.

In essence, land coverage (GCR and BCR) and proximity to water resources (DCDS, DR, and DC) were the key determinants of temperature distribution. Notably, the DCDS predominantly influenced daytime conditions, whereas the other factors primarily affected nocturnal conditions.

Table 2-2 Correlation coefficient between the physical factors and the air temperature every season in the BMR

Physical Factors	Summer		Monsoon		Winter	
	T_{max}	T_{min}	T_{max}	T_{min}	T_{max}	T_{min}
DCDS	0.650**	-0.349*	0.332*	-0.252*	0.111	-0.463**
DR	0.268	-0.490**	0.185	-0.243	-0.107	-0.537**
UCR	0.001	0.543**	0.092	0.543**	0.155	0.681**
GCR	0.095	-0.591**	-0.02	-0.592**	-0.148	-0.737**
WCR	-0.247*	-0.09	-0.219	-0.088	-0.077	-0.124

Notes: ** The correlation coefficient is significant (on both sides) at the 0.01 level,
   * The correlation coefficient is significant (on both sides) at the 0.05 level
   Level of correlation: (-)0.3 < r < (-)0.45 = weak, (-)0.45 < r < (-)0.6 = medium strong
   correlation, r > (-)0.6 = strong correlation

Table 2-3 Correlation coefficient between the physical factors and the air temperature every season in the central urban area of the BMR

Physical Factors	Summer		Monsoon		Winter	
	T_{max}	T_{min}	T_{max}	T_{min}	T_{max}	T_{min}
DC	-0.122	-0.519**	-0.193	-0.473*	-0.122	-0.499**
DR	0.236	-0.456*	0.077	-0.331	-0.065	-0.547**
UCR	-0.021	0.322	0.096	0.563**	-0.002	0.519**
BCR	0.001	0.255	0.207	0.397*	0.249	0.474*
FAR	-0.131	0.384*	-0.079	0.460*	0.02	0.477*
GCR	0.095	-0.489**	-0.02	-0.569**	-0.148	-0.557**
WCR	0.066	-0.049	0.1	0.056	-0.111	-0.068

Notes: ** The correlation coefficient is significant (on both sides) at the 0.01 level,
   * The correlation coefficient is significant (on both sides) at the 0.05 level
   Level of correlation: (-)0.3 < r < (-)0.45 = weak, (-)0.45 < r < (-)0.6 = medium strong
   correlation, r > (-)0.6 = strong correlation

Table 2-4 Results of a stepwise MLR analysis for the indicators that influence the summer diurnal wind speed by different models

Model	Variable Entered	R	R^2	Adj R^2	Std Error of the estimate
1	BCR	0.592	0.350	0.339	0.63419
2	BCR, DCDS	0.692	0.479	0.460	0.57283

Note: Dependent indicator is the average maximum wind speed in summer (13:00 hours)

Table 2-5 Summary of results for MLR coefficients of the best prediction model for investigating the influence on the summer diurnal wind speed (13:00 hours)

Model 2	Un Std. Coeff.		Std. Coeff.	F.	Sig.
	B	Std. error	Beta		
(Constant)	3.612	0.356		10.1548	<0.001
BCR	-0.029	0.005	-0.6111	-6.3255	<0.001
DCDS	-3.13E-05	0.000	-0.3597	-3.7237	<0.001

2.4.2   Summer Wind Characteristics in the BMR and Influential Factors

An analysis of 37 days characterized by fine-weather patterns was undertaken to elucidate the summer wind behavior in the BMR (Yokoyama et al., 2017). Figure 2-8 illustrates the wind blowing pattern at Station 17, revealing two predominant patterns: patterns A and B. Pattern A featured a consistent southward wind flow with higher diurnal wind speeds. Pattern B, however, exhibited variability in wind direction throughout the day. The data from Pattern A were used for further analysis. Using IDW interpolation, the wind distribution contours were analyzed for April 12 using wind data from 59 observation points. Figure 8 shows the simulated wind distribution at 1:00 and 13:00 on April 12 at a height of 10 m. Urban and core urban areas exhibited lower ventilation efficiencies, with average nocturnal wind speeds below 1 m/s, in contrast to rural regions with speeds of 7–8 m/s. Sea breezes emerged as a significant influencer of afternoon wind speed, and MLR analysis was applied to ascertain the factors impacting wind speed. Table 4 shows the stepwise MLR results, highlighting the BCR and DCDS as key contributors to summer diurnal wind speed variation (1 p.m.), jointly explaining approximately 47.9% of the variation (R^2 = 0.479). The model proposed in Equation 1 predicts the summer diurnal wind speed based on urban morphological features, offering insights into enhancing wind speed through urban planning considerations.

$$WS = 3.612 - 0.029 \times BCR - (3.13 \times 10^{-5}) \times DCDS \quad \textbf{[Eq. 1]}$$
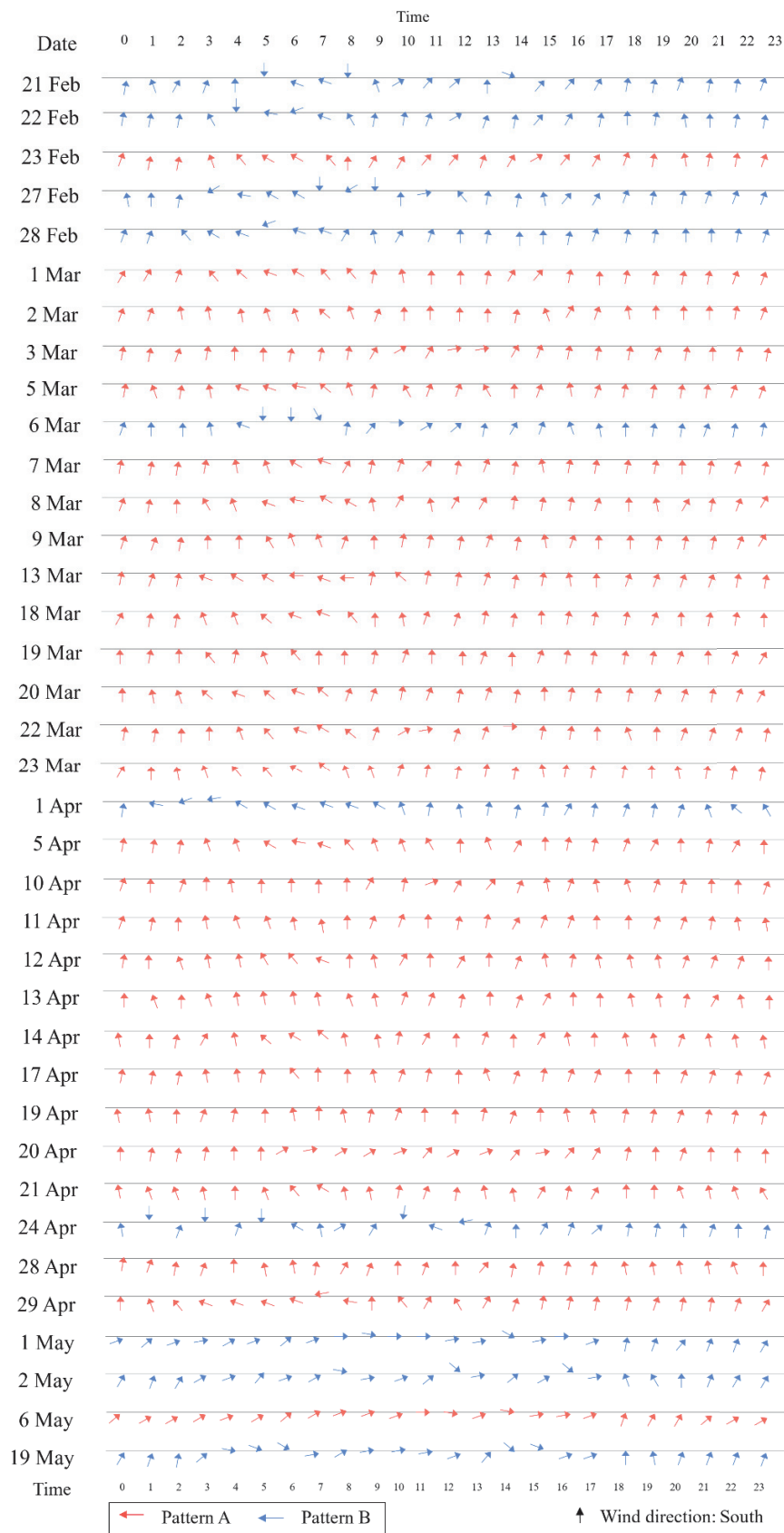
Fig. 2-9 The wind-blowing patterns of each summer fine-weather day at Station 17
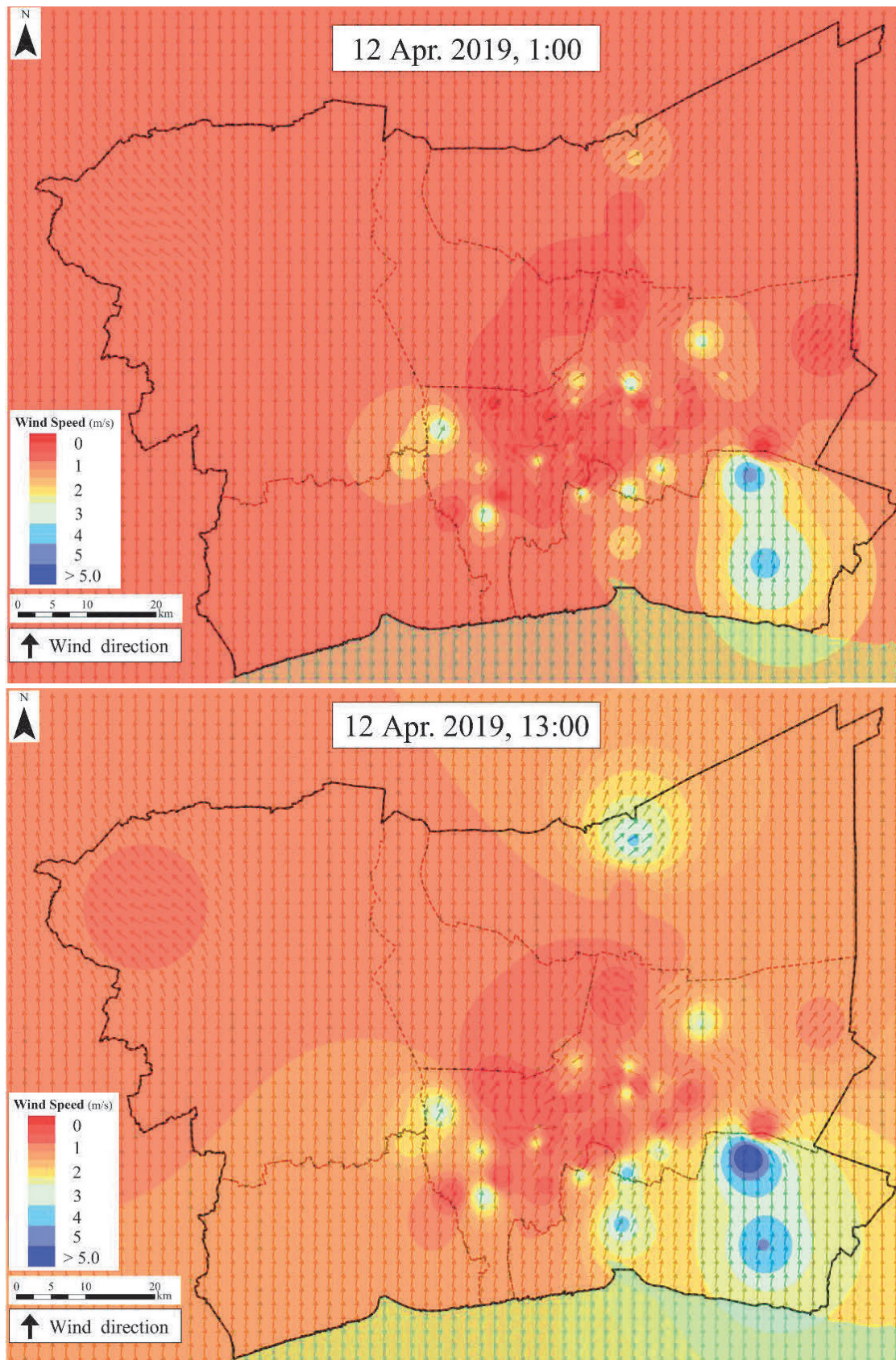
Fig. 2-10 The wind distribution with the IDW interpolation analysis into the winding contour at 1:00 hours and 13:00 hours on April 12, 2019

2.4.3   Correlation between Urban Climate Distribution and Spatial Environmental Factors in the BMR

The primary factors exhibited a correlation with summer T_{max}, including the DCDS and WCR. Conversely, summer T_{min} was correlated with the GCR, DR, and UCR. Wind speed exhibited no discernible correlation with temperature. It is important to note that each season and timeframe exhibited distinct relationships with spatial environmental factors, as depicted in Figures 2-11 and 2-12. Figure 2-11 shows the scope of the influence of the DCDS on the diurnal distribution of T_{max} in summer. The dark red points signify regions characterized by elevated T_{max} values, situated in the central Bangkok area, and locations where the DCDS value exceeded 40 km. In contrast, the white points denote regions of lower T_{max}, that are primarily positioned near the coastline. Figure 2-12 shows the influence of the GCR on the nocturnal distribution of T_{min} during summer. Remarkably, urban areas showed higher T_{min} values than rural areas. Moreover, the extent of the various water resources had a discernible impact on the scope of the study area. Therefore, although the DR could be a potent determinant of regional and provincial temperature patterns, the DC was more influential at the provincial level. Additionally, the DCDS and BCR exhibited a notable effect on wind speed. A comprehensive overview of the relationship between spatial environmental factors and urban climate distribution is presented in Figure 2-13.
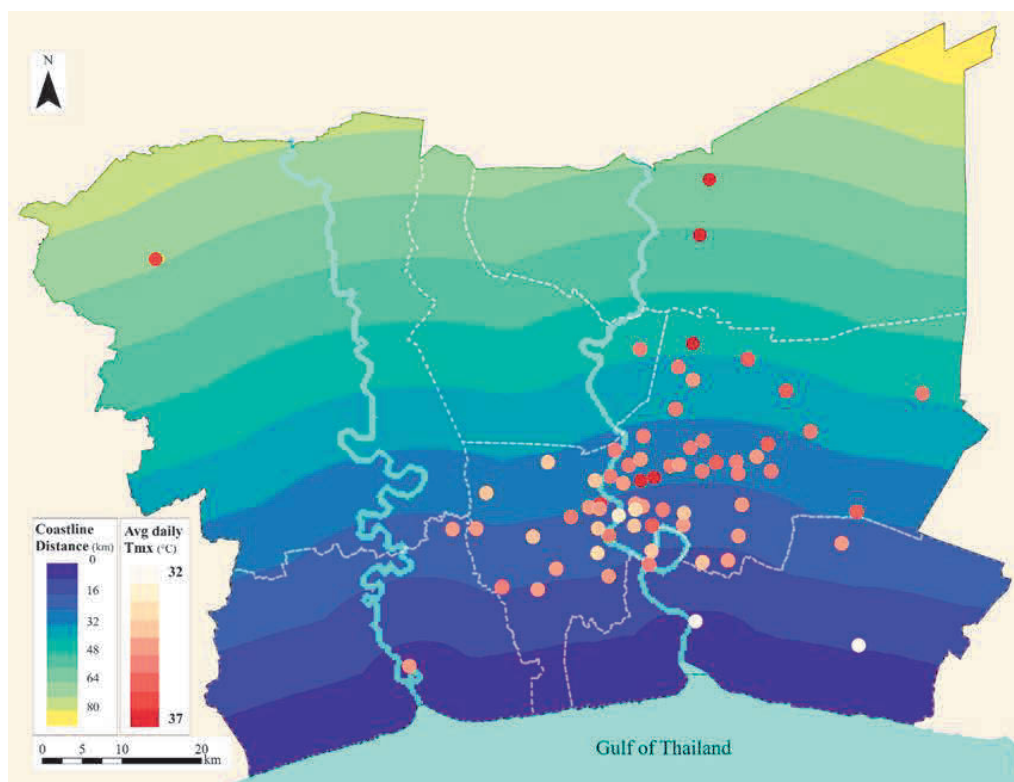
Fig. 2-11 The coastline distance range with the average maximum temperatures in summer
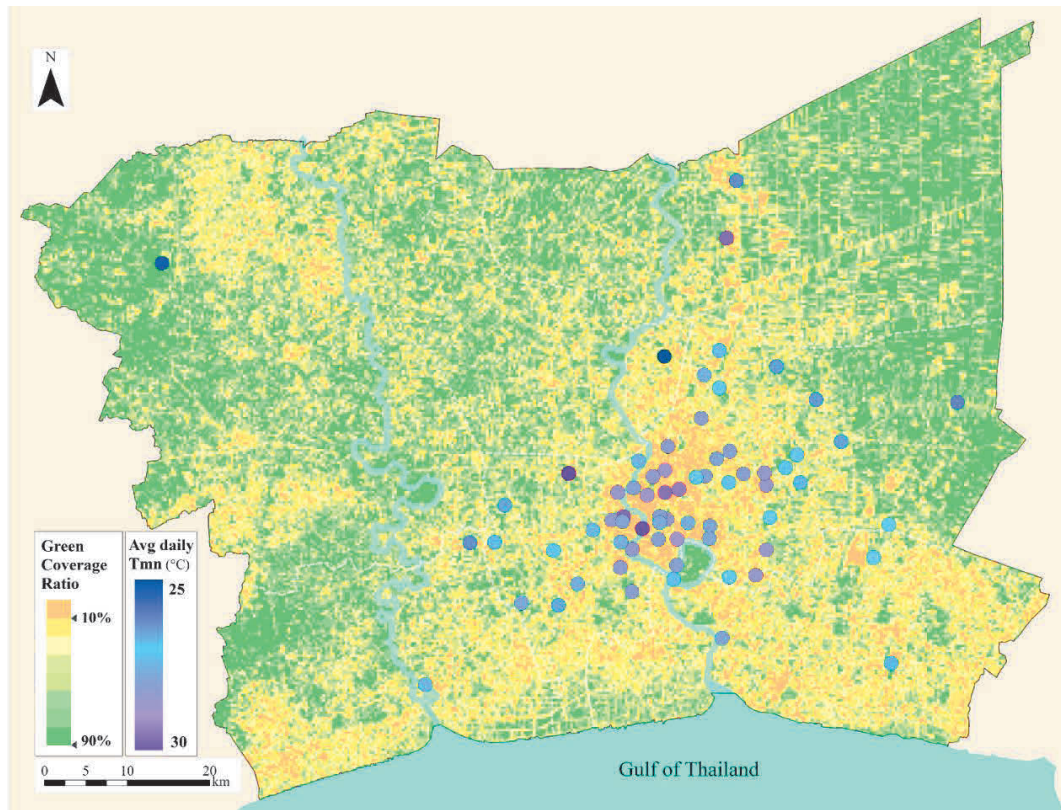
Fig. 2-12 The green coverage ratio with the average minimum temperatures in summer

Note: Blue arrow is positive correlation, Red arrow is negative correlation,
Black arrow is both positive and negative correlation
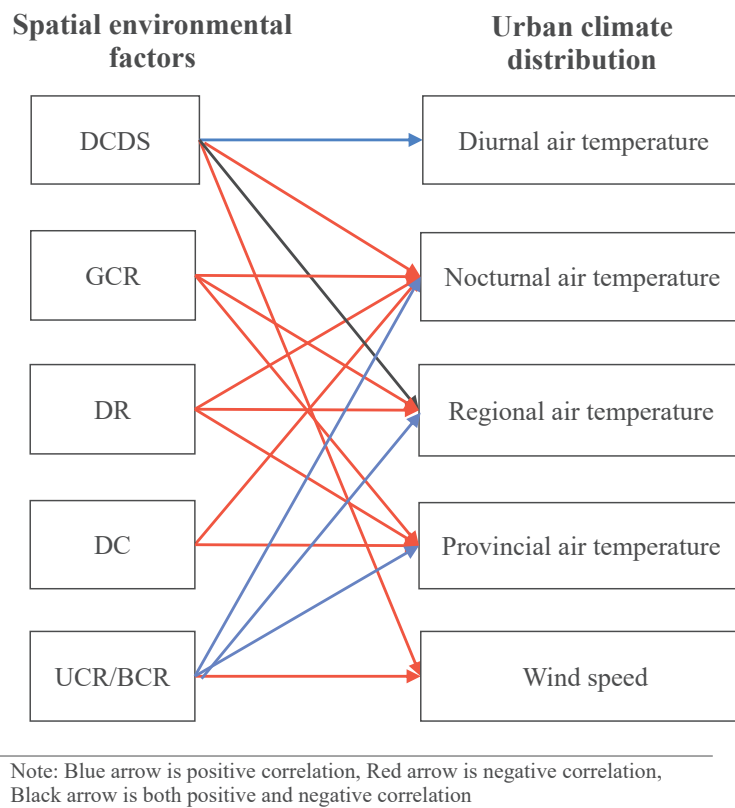
Fig. 2-13 Relation diagram between spatial environmental factors and urban climate distribution

2.4.4   The UECM of the BMR

The UECM was developed based on the aforementioned outcomes. The GCR, DR, and DC exerted considerable influences on the nocturnal summer air temperature. Conversely, the DCDS and WCR played significant roles during the daytime summer conditions. In addition, the DCDS and UCR had a noteworthy impact on the ventilation patterns. Consequently, the author stratified the impact of each factor into three primary layers within the UECM (Figure 2-14). Subsequently, these three overlaid layers were amalgamated into a single map, culminating in a comprehensive UECM for the BMR (Figure 2-16).

2.4.4.1 Territorial Zoning of the BMR Based on Sea Breeze Influence on Ventilation

The initial layer, the territorial zone, offers insights into the potential of sea breezes in terms of wind speed and air temperature. This layer was categorized into three distinct zones, delineated by a black dashed line, reflecting the scope of the DCDS and sea breeze effects during summer. The territorial zone included the following delineations:

1) Zone 1 spans the first 0–24 km of the coastline in the Gulf of Thailand. It encompasses regions characterized by consistently robust sea breeze ventilation throughout the day. This area includes a significant portion of SPK, one district of SKN, and two districts in the southern part of BKK. Encompassing approximately 1,512 km^2, this zone displays heightened sea breeze efficiency.

2) Zone 2 extends up to 40 km from the coastline of the Gulf of Thailand. This area demonstrates moderate sea breeze ventilation during the day (10:00–19:00), with its characteristics influenced by the IDW of wind distribution (as depicted in Figure 8). However, during the night, ventilation in this zone is related to the LULC patterns. Encompassing approximately 1,870 km^2, Zone 2 covered extensive areas of BKK, SKN, and the southern part of the NPT. Enhancing ventilation in this zone will require comprehensive consideration of both factors.

3) Zone 3 exhibits a minimal sea breeze influence and is situated more than 40 km from the coastline. The wind speeds in this zone are predominantly governed by other factors, particularly the LULC classifications. Encompassing substantial regions of NPT, PTN and NTB, and the northern segment of BKK, Zone 3 underscores the interplay between wind patterns and LULC characteristics.

2.4.4.2 Mapping Green Coverage Ratio in the BMR

The subsequent layer was classified into four groups based on the GCR thresholds and color-coded to represent varying ranges of the GCR (at a mesh resolution of 300 m × 300 m):

1) Green area (GCR 50%)
2) Yellow area (GCR of 30–50%)
3) Orange area (GCR of 10–30%)
4) Red area (GCR below 10%)

Given the strong correlation between the GCR and temperature, the GCR emerged as the main factor encapsulated within the UECM. Figures 2-14 and 2-15 show a substantial portion of the BMR featuring a GCR exceeding 50%, primarily concentrated along the periphery (NPT, PTN, NTB, and SKN). Figure 2-15 shows the proportional distribution of each grid type across the provinces and the entire BMR, with SPK exhibiting the lowest GCR area and the highest WCR.

2.4.4.3 High Density of the Urban Area in the BMR

The third layer was constructed to correspond to the influence of the UCR. The UCR exhibited correlations with both ventilation and temperature at regional and local scales. Notably, the data coverage was inversely proportional to the GCR. As such, the authors exclusively presented areas of risk characterized by a UCR surpassing 90%, without factoring in the GCR (illustrated by the black-hatched grid overlay over a red-shaded region). These high-risk areas were predominantly concentrated in BK K and the central regions of each province. Within the BMR, these areas accounted for 6% of the total area, whereas in the BKK, they encompassed nearly 18% (Figure 2-15). SPK and NTB constituted 8.15% and 6.84% of the respective areas. The N T B exhibited extensive vegetation cover and a heightened concentration of urban development owing to its proximity to the BKK, extending outward from the city center. Furthermore, the urban landscapes of NTB are closely linked to Bangkok's territory, which is driven by escalating land prices. Notably, SPK hosts Thailand's largest airport, S uvarnabhumi International Airport, along with a significant industrial zone, rendering it a densely urbanized area.

2.4.4.4 Degrees of Recommendations for Nine Zones within the UECM of the BMR

The BMR was subdivided into nine distinct zones, each associated with varying degrees of recommendations for LULC and ventilation enhancement. Zones 1, 2, and 3 exhibited a high degree of recommendation for LULC improvement, characterized by a GCR of less than 30% and a substantial UCR exceeding 70%. Conversely, Zones 1, 2, and 5 had a pressing need for sea breeze ventilation improvements, featuring elevated UCR values and inadequate diurnal ventilation. Urgent intervention was warranted in Zones 1 and 2, which needed both LULC and ventilation improvements. Moderately recommended improvements spanned Zones 3–6, whereas Zones 7–9 had relatively fewer recommendations for both aspects. Within the BMR, Zone 7 was the most extensive area, whereas Zones 3, 4, 6, and 8 collectively accounted for less than 4%. The distribution of the area of each zone within each province is shown in Figure 2-17. The pressing zone within the BMR comprised approximately 14% of the total area, with the majority situated in BKK and NTB at 25% and 27%, respectively. In the case of NTB, NPT, and PTN, positioned to the west and north of BKK, Zone 7 was predominated. In the coastal provinces of SPK and SKN, the primary focus was on improving green areas within Zone 3.
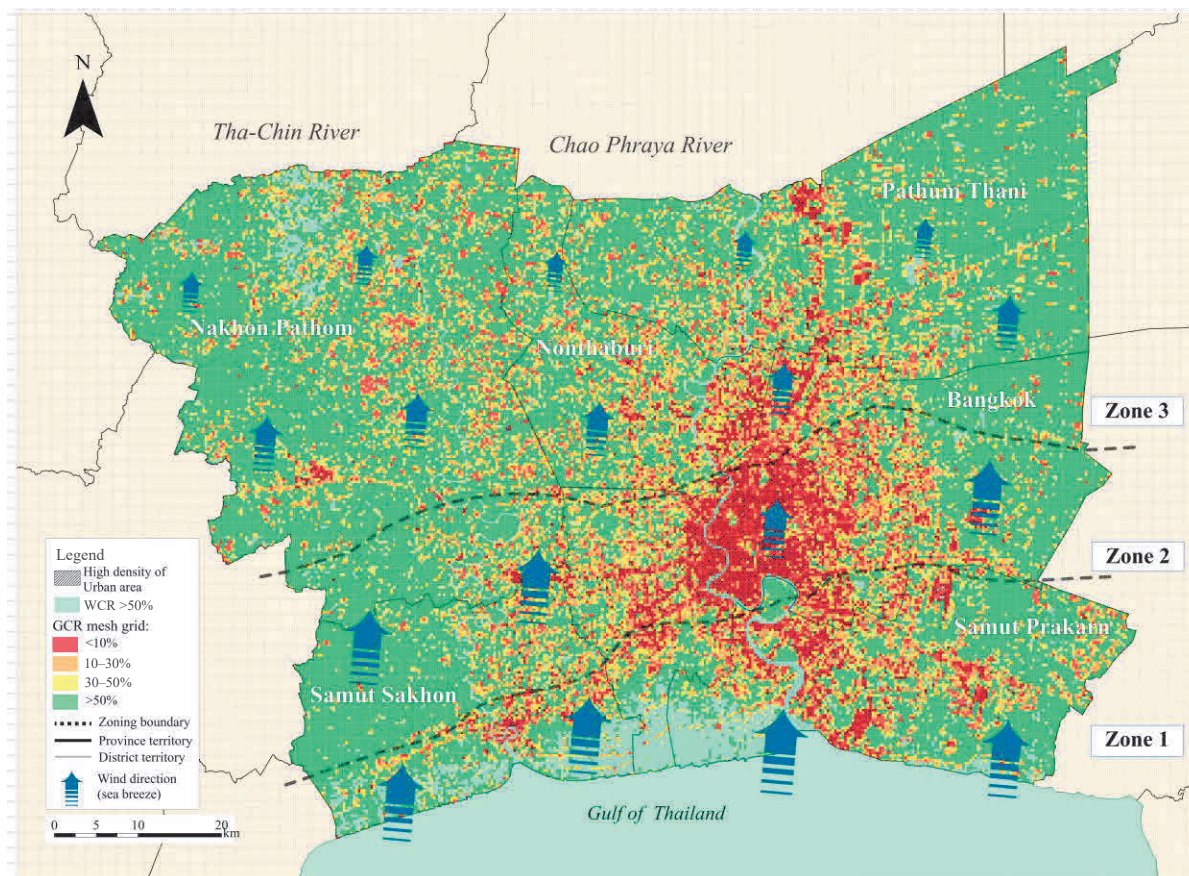
Fig. 2-14 Three overlayed layers from the environmental factors of the BMR
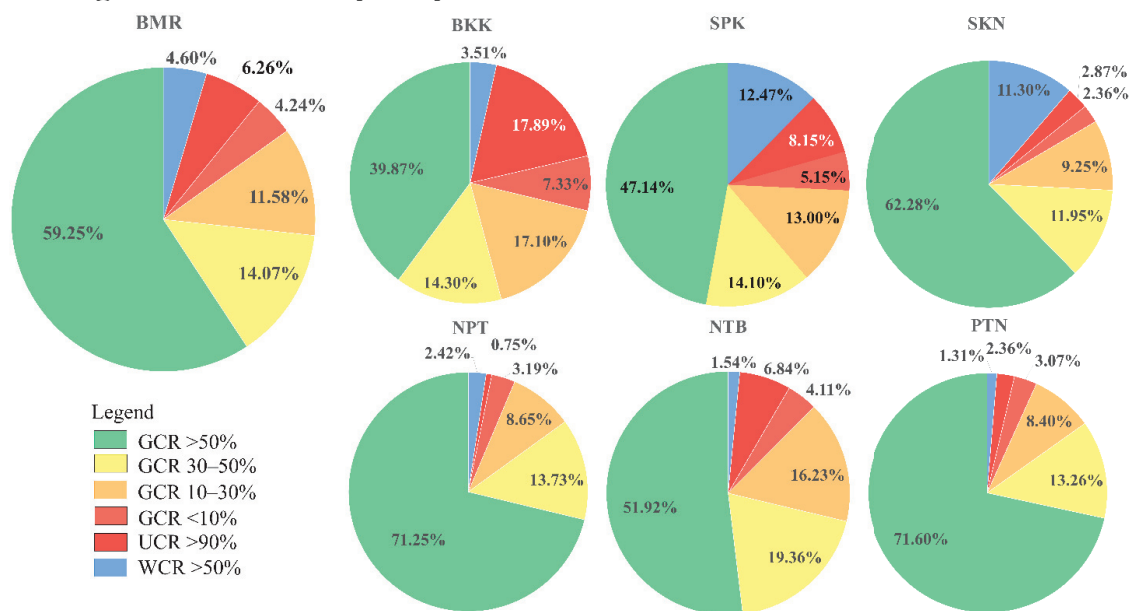
Fig. 2-15 The percentage of each coverage area in each province of the BMR
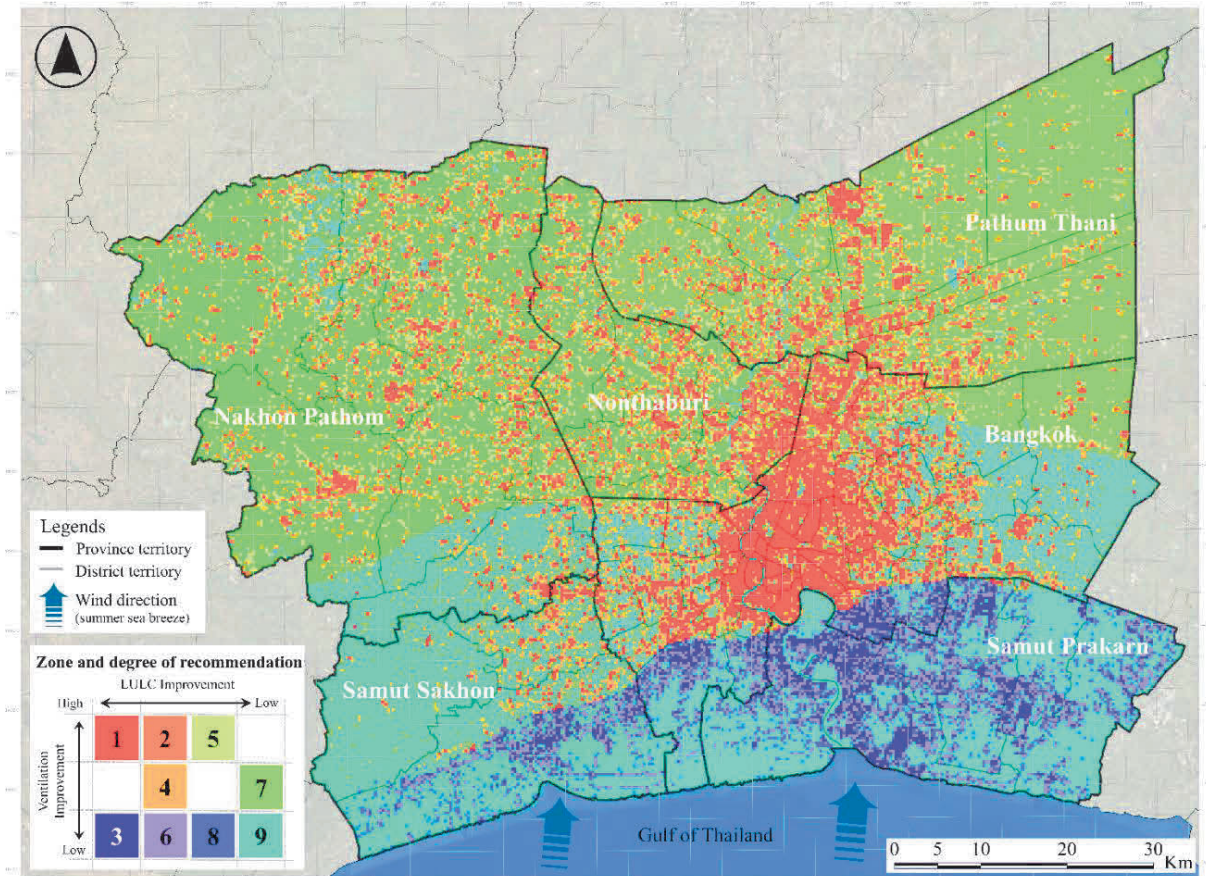
Fig. 2-16 A UECM of the BMR, Thailand
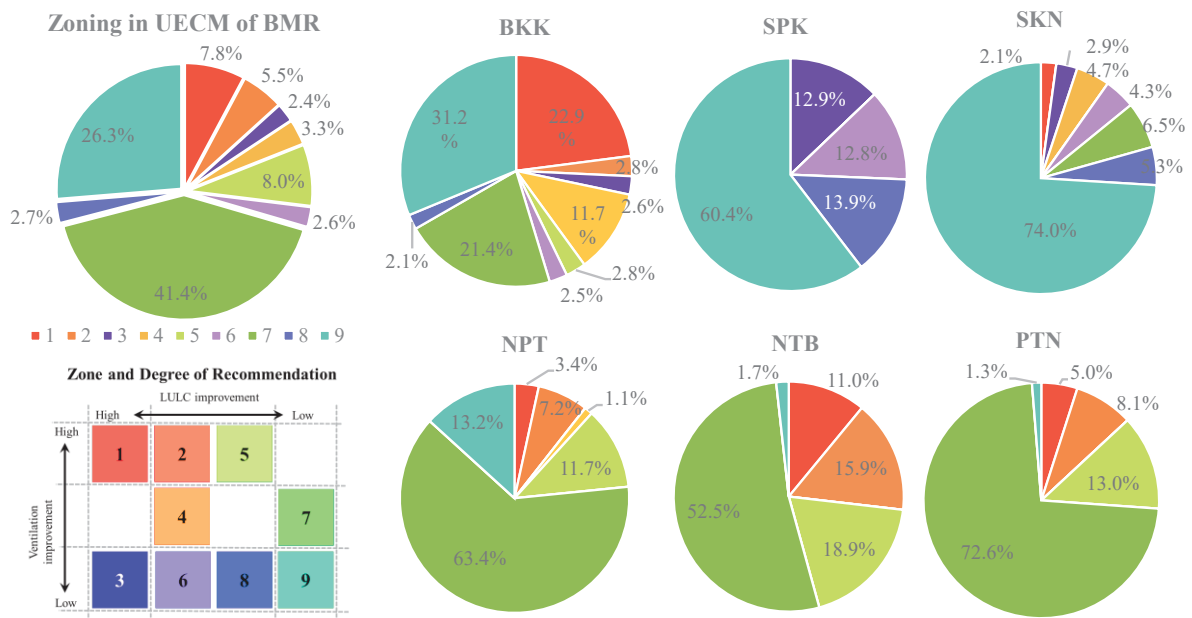
Fig. 2-17 Summary of the percentage of each zone in the BMR from the UECM

2.5   Discussion

2.5.1   Data Usage and Analysis

In this study, climate observation data and satellite imagery were integrated to create a unified map. The methodology of this study was employed in previous studies (Matsuo and Tanaka, 2019); however, this research took a unique approach by independently scrutinizing each observation point through a detailed analysis of LULC information and building footprints. This allowed for a comprehensive examination of the physical factors affecting air temperature and the incorporation of additional data from other observation stations. The inclusion of the DCDS and DR in this study drew on prior research conducted in Japan (Matsuo and Tanaka, 2019; Sasaki et al., 2018; Yokoyama et al., 2017), while adapting and introducing a novel factor, DC, specific to the study area. Remarkably, this research is the first to combine wind and temperature distribution data to construct a UECM for the BMR. Unlike many previous climate studies in Bangkok or the BMR that focused solely on distribution data, this study adopted a more comprehensive approach. In addition, this research underscores the practical utility of UECM for stakeholders, positioning it as a pivotal tool for shaping sustainable development plans at both the provincial and regional levels.

Additionally, Table 2-6 provides an assessment of the accuracy of the classified LULC classes by evaluating the user accuracy, producer accuracy, kappa coefficient, and total accuracy using kappa statistics (Fleiss et al., 2004). The results exhibited a high level of precision, demonstrated by an overall kappa coefficient of nearly 80%, confirming the reliability of the LULC map.

2.5.2   Bangkok Topography and Its Physical Relationships

This study investigated the correlation between sensors and water resource distance variables DR, DC, and DCDS. The statistical analysis revealed a robust association between the DC, DR, and DCDS, and air temperature, especially within a 300-m radius (Srivanit and Kazunori, 2011; Matsuo and Tanaka, 2019; Sasaki et al., 2018). Although proximity to water bodies can ameliorate temperature, limitations arise when obstructive buildings hinder these benefits. Building orientation within urban areas significantly influence the wind speed, surface temperature, and air temperature at the district level. This issue pertains to central Bangkok, which is characterized by numerous canals yet experiences high temperatures (Figures 2-8). Enhancing these areas will involve district-scale simulations to craft development plans that strategically optimize obstacle placement in accordance with the analytical findings.

While the results in Table 2-2 illustrate a strong correlation between environmental factors and T_{min} during summer, T_{max} exhibited rare correlations. However, mitigating nocturnal temperatures in urban areas can help narrow the gap between urban and rural temperatures, which is a hallmark of the UHI-related efforts. Therefore, the GCR, DR, and DC have emerged as the primary factors for tempering nocturnal urban temperatures. As the BMR predominantly comprises of a flat terrain, geographical characteristics play a secondary role in determining the temperature distribution patterns. Nonetheless, the correlation coefficients in Table 2 indicate DCDS's consistent relationship with temperature on a regional scale. Elevated diurnal air temperatures may result from a reduced sea breeze influence (Matsuo and Tanaka, 2019; Sasaki et al., 2018), while lower nocturnal temperatures could be linked to a higher GCR. Although the BCR correlated with both ventilation and temperature, the availability of building coverage data was limited to Bangkok. To develop the regional UECM for the BMR, the UCR was utilized instead of the BCR, considering the urban and impervious areas from the LULC map. Notably, the UCR exhibited a negative correlation with the GCR owing to the characteristics of these data resources.

Table 2-6 Accuracy assessment of the LULC classification map of the BMR

Class Value	C_1	C_2	C_3	C_4	C_5	C_6	Total	User Accuracy (%)	Kappa Coefficients
C_1	64	1	0	5	0	4	74	86.50	0
C_2	0	193	12	3	0	1	209	92.30	0
C_3	2	25	376	5	2	17	427	88.10	0
C_4	3	5	26	101	0	8	143	70.60	0
C_5	0	1	1	0	23	0	25	92.00	0
C_6	1	5	28	2	1	85	122	69.70	0
Total	70	230	443	116	26	115	**1000**	0	0
Producer Accuracy (%)	91.40	83.90	84.90	87.10	88.50	73.90	0	**84.20**	0
Kappa	0	0	0	0	0	0	0	0	**78.20**

Note: C_1: water area; C_2: urban area; C_3: vegetation area; C_4: watery vegetation; C_5: impervious area; C_6: bare area.

2.5.3   Urban Climate Characterization and Development Strategies for the BMR

The BMR was separated into nine zones to facilitate a comprehensive investigation of urban climate characteristics. Each zone had distinct geographical attributes and exhibited varying ratios of vegetation to urban areas, which directly influenced air temperature and ventilation patterns. While a substantial portion of the BMR falls within low-risk zones (Zones 7–9) that do not require immediate intervention and display moderate daytime air ventilation, approximately 15% of the BMR (Zones 1 and 2) remains at risk and requires increased attention. Notably, these risk-prone zones are concentrated in the central urban regions of each province, particularly in Bangkok. These zones encompass over a quarter of both BKK and NTB, and experience elevated day and nighttime temperatures coupled with inadequate ventilation. Only the areas near the Chao Phraya River may experience higher wind speeds, while others may encounter obstructions from urban structures.

If urban planning in these areas is aligned with the insights from this study, it could enhance airflow dynamics in Bangkok. Consequently, both provinces should conduct comprehensive analyses of climatic conditions and environmental factors to produce maps based on the local climate zone typology classification. These maps would serve as valuable tools for analysis and inform future developmental strategies. The remaining four provinces can be categorized based on their proximity to the coastline.

In the case of the coastal provinces SPK and SKN, a significant portion of their areas maintain existing land-use patterns due to effective wind circulation from the coastline. Mangrove areas function as green spaces and conservation zones for marine life. In contrast, NPT and PTN primarily allocate land for agricultural purposes, enabling the preservation of conventional land-use practices. While both provinces are situated considerably far from the coastline, the nocturnal wind speeds in open spaces tend to be elevated, which is attributed to the terrestrial air movement.

Despite the overall resilience of these four provinces to environmental crises within their urban precincts, in-depth scrutiny of the central urban zones revealed potential issues. Substantial urban development in these localities has resulted in compromised daytime wind circulation and elevated temperatures, similar to those experienced in the central areas of Bangkok, which are prone to environmental challenges. Thus, future urban development strategies in the suburban periphery of the BKK should be carefully studied. For future urban planning, the authors recommend that the BMR and each local government should have a UECM and usable climatic resources for mitigation, which are provided in each zone.

This result correlates with those of previous studies (Pakarnseree et al., 2018; Pan et al., 2023) on the LST and SUHI within BKK from 2000 to 2015 and 2020, respectively. Temperature-related risk areas in Bangkok were primarily concentrated in Zones 1 and 2. However, the expansion of these risk-prone areas is attributed to urbanization without comprehensive environmental planning. Moreover, compared with previous studies, this UECM study introduced a distinct scale encompassing the entire BMR and classified sea-breeze-influenced ventilation zones. Interventions aimed at reducing heat and enhancing ventilation have focused on high-density urban areas in central Bangkok, where green spaces are relatively scarce. Previous studies (Pakarnseree et al., 2018; Moriyama and Tanaka, 2012); Rajagopalan et al., 2014) underscored the positive impacts of high-rise buildings and unobstructed spaces in urban landscapes, which facilitates improved air circulation through thoroughfares.

Furthermore, scholarly discourse has highlighted the importance of effective building layouts and the incorporation of green spaces (Thammapornpilas, 2015; Moriyama and Tanaka, 2012). Consequently, in the analysis of urban districts or localized contexts, other factors that influence environmental challenges must be considered. These variables encompass the ratio of building height to road width, along with the configuration of elevated edifices. Moreover, the incorporation of green areas manifests as a diversity of attributes and styles tailored to each area, contingent upon contextual factors, budgetary constraints, and envisioned utility, as appraised by urban planners and landscape architects (Chang and Li, 2014; Aleksandrowicz et al., 2017).

Earlier studies in the BMR hinged on LST data to elucidate this phenomenon; however, this study bridged the methodological gap in urban climatology by grounding its analysis in air temperature data. This underlines the potential of near-surface temperature analysis for creating an urban climate map conducive to UHI amelioration. In addition, it revealed a more pronounced spatiotemporal variance than LST data (Chen et al., 2016; Rahaman et al., 2022). Significant efforts must be made to improve BMR thermal data and refine urban thermal investigations by harnessing an assortment of climate data (Yao et al., 2019).

2.5.4   Limitations

This study has several limitations. The utilization of air temperature measurements within the UHI framework was aimed at encapsulating the thermal heterogeneity of the study area. However, limitations arising from the constrained quantity and distribution of climatic monitoring stations in the BMR could play a role in establishing variability when examining the correlation between air temperature and urban spatial characteristics (Yao et al., 2019; Arnfield, 2003). Variations in station distribution across the study region were evident, with a notable concentration within Bangkok, the capital city. Therefore, the authors advocate an increase in the number of meteorological stations within the BMR. This expansion is imperative for cultivating an expansive database that caters to the scrutiny of sustainable urban planning and administration. Such an initiative would underpin future enhancements in urban heat mitigation, which is distinct from each province's environmental context.

Another constraint pertains to the utilization of the 2019 LULC datasets, potentially necessitating a reconsideration of the application of the UECM. This adjustment is relevant to the findings of several previous studies (Rahaman et al., 2022; Zhang et al., 2022) and indicates that alterations in land coverage can influence temperature. Consequently, a comprehensive study involving the creation of maps and prediction of future urban expansion should be conducted. This would facilitate the development of city plans that align with the environmental and urban contexts. Moreover, in relation to the factors presented in Tables 2-3 and 2-4, it is apparent that both the DR and DC exhibited a substantial correlation with urban thermal profiles. However, their intricate relationships were precluded from detailed depictions within the BMR's UECMs owing to cartographic limitations imposed by the regional map proportions.

Furthermore, advancing this study would entail the creation of UECMs across various scales, from the mesoscale to the district level. This extension would involve incorporating additional variables, such as the sky view factor, canyon street ratio, and building surface materials. In addition, it is essential to explore alternative methodologies, such as computational fluid dynamics simulations, weather research and forecasting models, multi-scale simulators for the geo-environment, and machine learning algorithms, as indicated in previous research (Palusci and Cecere, 2022; Buddee and Hengrasmee, 2019).

2.6   Conclusion

In this study, a UECM of the BMR was constructed based on a correlation analysis between air temperature distribution, wind distribution, and spatial environmental factors. This construction relied on extensive long-term data collected from 68 temperature sensors and 59 wind velocity sensors distributed across multiple field observation points. Subsequent climate zoning and clarified the area with different recommendations for urban planning. The main conclusions of this chapter are as follows:

1) The results of the correlation analysis between the physical factors and air temperature reaffirmed the pivotal role of physical attributes in shaping urban temperature patterns and ventilation distribution within the BMR.

2) The key factors exhibiting a correlation with air temperature distribution included land coverage (GCR, UCR, and BCR) and proximity to water bodies (DCDS, DR, and DC). Notably, the DCDS had a significant influence on diurnal temperature, whereas other factors predominantly influenced nocturnal conditions.

3) By employing MLR analysis, a comprehensive assessment of the wind distribution in flat terrains was undertaken. The investigation revealed that both the DCDS and BCR had substantial impacts on diurnal wind speeds in summer.

4) The BMR was categorized into nine distinct zones, based on three ventilation zones linked to summer sea breezes from the Gulf of Thailand and five temperature mitigation area classes. **Notably, Zones 1 and 2, mostly located in central BKK, emerged as priority zones for UHI mitigation efforts**. Recommendations for these zones include enhancing the LULC with increased green areas and open spaces to enhance ventilation.

5) The key findings could be transposed onto a simplified map illustrating current areas and projected environmental impacts. This underscores the role of the U E C M as a potent t o o l for fostering understanding and awareness among local urban planners, stakeholders, and governors regarding their respective regions. Furthermore, it established a risk ratio for UHI within each BMR province.

6) These findings have the potential to guide enhancements of urban environments and offer insights into urban heat mitigation and adaptation. They emphasized the significance of precise climate data collection as a foundation for future urban environmental inquiries, contributing to more accurate city planning and sustainable development. Moreover, the methodologies employed in this study could be adapted to other cities or refined to achieve higher resolutions, potentially operating at a district scale.

Nevertheless, despite the collection of weather data at more than 60 points within the study area, it remains inadequate for achieving a comprehensive understanding of the entire region. This limitation arises from the positioning and distribution of each local station, frequently situated within the urban precincts of local government offices, thereby leading to a scarcity of diverse environmental locations that constitute a direct factor influencing the prevailing weather conditions. Therefore, the next chapter aims to analyze mesoclimate of BMA by using numerical modeling and combined with the observation data.

References

Aleksandrowicz, O., Vuckovic, M., Kiesal, K., Mahdavi, A. (2017). Current trends in urban heat island mitigation research: Observations based on a comprehensive research repository. *Urban Climate, 21*, 1-26. https://doi.org/10.1016/j.uclim.2017.04.002.

Alawamy, J. S., Balasundram, S. K., et al. (2020). Detecting and analyzing land use and land cover changes in the region of Ai-Jabal Al-Akhdar, Libya using time-series Landsat data from 1985 to 2017. *Sustainability, 12*, 4490. https://doi.org/10.3390/su12114490.

Arnfield, J. (2003). Two decades of urban climate research: A review of turbulence, exchanges of energy and water, and the urban heat island. *International Journal of Climatology, 23*, 1-26. https://doi.org/10.1002/joc.859.

Buddee, P., Hengrasmee, S. (2019). The Prospect of Urban Geometry Impact on Urban Heat Island: A Case Study of Bangkok. *JARS, 16*(1), 167533. https://doi.org/10.56261/jars.v16i1.167533.

Chang, C., Li, M. (2014). Effects of urban parks on the local urban thermal environment. *Urban Forestry & Urban Greening, 13*(4), 672-681. https://doi.org/10.1016/j.ufug.2014.08.001.

Chen, A., Yao, L., Sun, R., Chen, L. (2014). How many metrics are required to identify the effects of the landscape patterns on land surface temperature. *Ecological Indicators, 45*, 424-433. https://doi.org/10.1016/j.ecolind.2014.05.002.

Chen, A., Zhao, X., Yao, L., Chen, L. (2016). Application of a new integrated landscape index to predict potential urban heat island. *Ecological Indicators, 69*, 828-835. https://doi.org/10.1016/j.ecolind.2016.05.045.

Diek, S., Fornallaz, F., et al. (2017). Barest pixel composite for agricultural areas using Landsat time series. *Remote Sensing, 9,* 1245. https://doi.org/10.3390/rs9121245.

Fleiss, J. L., Levin, B., Paik, M. C. (2004). *The Measurement of Interrater Agreement*. In *Statistical Methods for Rates and Proportions* (3rd ed.). John Wiley & Sons: Hoboken, NJ, USA. ISBN 0471526290.

Kamma, J., Manomaiphiboon, K., et al. (2020). Urban heat island analysis for Bangkok: Multi-scale temporal variation, associated factors, directional dependence, and cool island condition. *Science Asia, 46,* 213-223. http://dx.doi.org/10.2306/scienceasia1513-1874.2020.024.

Keeratikasikorn, C., & Bonafoni, S. (2018). Urban heat island analysis over the land use zoning plan of Bangkok by means of Landsat 8 imagery. *Remote Sensing, 10(3),* 440. https://doi.org/10.3390/rs10030440.

Khamchiangta, D., Dhakal, S. (2020). Time series analysis of land use and land cover changes related to urban heat island intensity: Case of Bangkok Metropolitan Area in Thailand. *Journal of Urban Management, 9(4),* 1-12. https://doi.org/10.1016/j.jum.2020.09.001.

Li, J., Song, C., Cao, L., Zhu, F., Meng, X., & Wu, J. (2011). Impacts of landscape structure on surface urban heat islands: a case study of Shanghai, China. *Remote Sensing of Environment, 115*, 3249-3263. https://doi.org/10.1016/j.rse.2011.07.008.

Liu, S., Song, D., & Yu, B. (2017). The objective and methodology of urban climate map for the city of Xiamen. *Procedia Engineering, 180,* 462-470. https://doi.org/10.1016/j.proeng.2017.04.205.

Matsuo, K., & Tanaka, T. (2019). Analysis of spatial and temporal distribution patterns of temperature in urban and rural areas: Making urban environmental climate maps for supporting urban environmental planning and management in Hiroshima. *Sustainable Cities and Society, 47*, 1-22. https://doi.org/10.1016/j.scs.2019.01.004.

Moriyama, M., Tanaka, T. (2012). The mitigation of UHI intensity through an improved land-use plan in the urban middle area: Application to Osaka city, Japan. *Journal of Heat Island Institute International, 7*(2), 65-71. https://www.semanticscholar.org/paper/The-Mitigation-of-UHI-Intensity-through-an-Improved-Moriyama-Tanaka/8bae84702c33130925a0e096b0b406e709da609d.

Ng, E., & Ren, C. (2015). The urban climatic map: A methodology for sustainable urban planning. Routledge.

Nguyen, C. T., & Chidthaisong, A., et al. (2022). How do disparate urbanization and climate change imprint on urban thermal variation? A comparison between two dynamic cities in Southeast Asia. *Sustainable Cities and Society, 82*, 103882. https://doi.org/10.1016/j.scs.2022.103882.

Nguyen, C. T., Diep, N. T. H., Iabchoon, S. (2021). Direction of urban expansion in the Bangkok metropolitan area, Thailand under the impact of a national strategy. *Vietnam Journal of Earth Sciences, 43,* 380-398. http://doi.org/10.15625/2615-9783/16313.

Oke, T. R. (1982). The energetic basis of the urban heat island. *Quarterly Journal of the Royal Meteorological Society, 108(455)*, 1-24. https://doi.org/10.1002/qj.49710845502.

Pakarnseree, R., Chumkao, K., & Bualert, S. (2018). Physical characteristics of Bangkok and its urban heat island phenomenon. *Building and Environment, 143*, 561-569. https://doi.org/10.1016/j.buildenv.2018.07.042.

Palusci, O., Cecere, C. (2022). Urban Ventilation in the Compact City: A Critical Review and a Multidisciplinary Methodology for Improving Sustainability and Resilience in Urban Areas. *Sustainability, 14*, 3948. http://doi.org/10.3390/su14073948.

Pan, L., Lu, L., et al. (2023). Understanding spatiotemporal evolution of the surface urban heat island in the Bangkok metropolitan region from 2000 to 2020 using enhanced land surface temperature. *Geomatics, Natural Hazards and Risk, 14(1),* 2174904. http://doi.org/10.1080/19475705.2023.2174904.

Patil, A. S., Panhalkar, S. S., et al. (2018). Impact of land use land cover change on land surface temperature using geoinformatics techniques. *International Journal of Research Analysis and Reviews, 5,* 550-559. Retrieved from https://www.researchgate.net/publication/331588813_IMPACT_OF_LAND_USE_LAND_D_COVER_CHANGE_ON_LAND_SURFACE_TEMPERATURE_USING_GEOINFORMATICS_TECHNIQUES.

Peng, J., Xie, P., & Liu, Y. (2016). Urban thermal environment dynamics and associated landscape pattern factors: A case study in the Beijing metropolitan region. *Remote Sensing of Environment, 173,* 145-155. https://doi.org/10.1016/j.rse.2015.11.027.

Rahaman, Z. A., Al Kafy, A., et al. (2022). Assessing the impacts of vegetation cover loss on surface temperature, urban heat island and carbon emission in Penang City, Malaysia. *Building and Environment, 222*, 109335. https://doi.org/10.1016/j.buildenv.2022.109335.

Rajagopalan, P., Lim, K.C., Jamei, E. (2014). Urban heat island and wind flow characteristics of the tropical city. *Solar Energy, 107*, 159-170. https://doi.org/10.1016/j.solener.2014.05.042.

Ren, C., Spit, T., Lenzholzer, S., et al. (2013). Urban climate map system for Dutch spatial planning. *International Journal of Applied Earth Observation and Geoinformation, 18*, 207-221. https://doi.org/10.1016/j.jag.2012.01.026.

Rizwan, A. M., Leung, Y. C., & Liu, C. (2008). A review on the generation, determination, and mitigation of urban heat islands. *Journal of Environmental Sciences, 20,* 120-128. https://doi.org/10.1016/S1001-0742(08)60019-4.

Sarkar, A. (2018). Accuracy assessment and analysis of land use land cover change using geoinformatics technique in Ranigani Coalfield Area, India. *International Journal of Environmental Science and Natural Resources, 11,* 25-34. https://doi.org/10.19080/IJESNR.2018.11.555805.

Sasaki, Y., Matsuo, K., Yokoyama, M., Sasaki, M., & Tanaka, T., et al. (2018). Sea breeze effect mapping for mitigating summer urban warming: For making urban environmental climate map of Yokohama and its surrounding area. *Urban Climate, 24,* 529-550. https://doi.org/10.1016/j.uclim.2017.07.003.

Schwarz, N., Schlink, U., Franck, U., & Gromann, K. (2012). Relationship of land surface and air temperature and its implications for quantifying urban heat island indicators— An application for the city of Leipzig (Germany). *Ecological Indicators, 18*, 693-704. https://doi.org/10.1016/j.ecolind.2012.01.001.

Shi, Y., & Zhang, Y. (2018). Remote sensing retrieval of urban land surface temperature in hot-humid region. *Urban Climate, 24*, 299-310. https://doi.org/10.1016/j.uclim.2017.01.001.

Sigit, D. A., & Tanaka, T. (2015). The Characteristics of Urban Heat Island in Bangkok, Thailand. *Procedia Social and Behavioral Sciences, 195,* 423-428. https://doi.org/10.1016/j.sbspro.2015.06.484.

Srivanit, M., & Kazunori, H. (2011). The influence of urban morphology indicators on summer diurnal range of urban climate in Bangkok metropolitan area, Thailand. *International Journal of Civil & Engineering, 11(05),* 34-46. Retrieved from https://www.researchgate.net/publication/286451137_The_Influence_of_Urban_Morphology_Indicators_on_Summer_Diurnal_Range_of_Urban_Climate_in_Bangkok_Metropolitan_Area_Thailand.

Statistical Forecasting Division, Bangkok: National Statistical Office, Thailand. Statistical Yearbook Thailand 2020. http://service.nso.go.th/nso/nsopublish/pubs/e-book/SYB-2020/18/index.html. (Accessed 18 April 2023).

Stehman, S. V. (2009). Sampling designs for accuracy assessment and analysis of land use land cover. *International Journal of Remote Sensing, 30,* 5243-5272. https://doi.org/10.1080/01431160903131000.

Sun, R., Lu, Y., Chen, L., & Yang, L. (2013). Assessing the stability of annual temperature for different urban functional zones. *Building and Environment, 65,* 90-98. https://doi.org/10.1016/j.buildenv.2013.04.001.

Taha, H. (1997). Urban climates and heat islands: albedo, evapotranspiration, and anthropogenic heat. *Energy and Buildings, 25,* 99-103. https://doi.org/10.1016/S0378-7788(96)00999-1.

Taichi, T. (2020). Use of high-resolution elevation data to access the vulnerability of the Bangkok metropolitan area to sea level rise. *Hydrological Research Letters, 14(4),* 136-142. https://doi.org/10.3178/hrl.14.136.

Thammapornpilas, J. (2015). Urban spatial development to mitigate urban heat island effect in the inner area of Bangkok. *Journal of Environmental Design and Planning: Nakhara, 11,* 29-40. Retrieved from https://ph01.tci-thaijo.org/index.php/nakhara/article/view/104849.

United Nations Population Division. (2023). World Urbanization Prospects. Urban population (% of total population) 1960-2021. https://data.worldbank.org/indicator/SP.URB.TOTL.IN.ZS?locations=TH. (Accessed 18 April 2023).

Verein Deutscher Ingenieure. (1997). Environmental meteorology: Climate and air pollution maps for cities and regions. VDI.

Weng, Q. (2009). Thermal infrared remote sensing for urban climate and environmental studies: Methods, applications, and trends. ISPRS *Journal of Photogrammetry and Remote Sensing, 64*, 335-344. https://doi.org/10.1016/j.isprsjprs.2009.03.007.

Yao, L., Xu, Y., & Zhang, B. (2019). Effects of urban function and landscape structure on the urban heat island phenomenon in Beijing, China. *Landscape Ecology and Engineering, 15,* 379-390. https://doi.org/10.1007/s11355-019-00388-5.

Yaung, K. L., & Chidthaisong, A., et al. (2021). Land Use Land Cover Changes and Their Effects on Surface Air Temperature in Myanmar and Thailand. *Sustainability, 13,* 10942. http://doi.org/10.3390/su131910942.

Yokoyama, M., Tanaka, T., Sugiyama, T., Sadohara, S. (2017). Making climate zoning maps in Yokohama-comparison among different resolution calculation. *Journal of Heat Island Institute International, 12*(2), 107-114. http://www.heat-island.jp/web_journal/JGM8SpecialIssue/P-33_yokoyama.pdf.

Zhang, M., Zhang, C., Al Kafy, A., Tan, S. (2022). Simulating the Relationship between Land Use/Cover Change and Urban Thermal Environment Using Machine Learning Algorithms in Wuhan City, China. *Land, 11*(1), 14. https://doi.org/10.3390/land11010014.

Zhou, W., Qian, Y., Li, W., & Han, L. (2014). Relationships between land cover and the surface urban heat island seasonal variability and effects of spatial and thematic resolution of land cover data on predicting land surface temperature. *Landscape Ecology, 29*, 153-167. https://doi.org/10.1007/s10980-013-9950-5

Chapter 3
Urban Environmental Climate Maps of Bangkok

Based on the spatiotemporal temperature and ventilation zones from the numerical calculation of the WRF model

Contents

3.1   Introduction

From a preliminary study using temperature from observation data conducted in 2019 in Chapter 2, it became clear that the Bangkok Metropolitan Region (BMR) had a variation pattern of temperature and wind distribution related to the spatial and temporal analysis. The influencing factors were not only different between the two scales of the study area but also the periods. The findings of the relationship led to clarification of the severe climate on the mesoscale of BMR and were illustrated by the Urban Environment Climate Maps (UECMs) of BMR. However, to classify the climate zoning by the temperature and wind distribution in the study area, only the weather data from 68 observation points is insufficient to understand the precise climate characteristics in the condition of the data-scarce environment. Therefore, this chapter aims to fill the gap of the limitations of Chapter 2 by using a numerical calculation to clarify the climate characteristics of Bangkok and the critical climate area.

This chapter asserts the critical importance of comprehending the temperature and wind distribution at the regional and provincial scale, specifically within the Bangkok Metropolitan Area (BMA). It elaborates on the process of generating Urban Environmental Climate Maps (UECMs) for Bangkok, building upon the groundwork laid in the preceding chapter. The intricate details of this methodology involve numerical calculations conducted within the Weather Research and Forecasting (WRF) application. These calculations utilize mesoscale weather data and geographic information system (GIS) land use classification data obtained from the Thai Government.

The Weather Research and Forecasting (WRF) model stands out as a highly adaptable and extensively utilized Numerical Weather Prediction (NWP) system, serving both atmospheric research and operational forecasting purposes. This collaborative development involved institutions such as the National Center for Atmospheric Research (NCAR), the National Oceanic and Atmospheric Administration (NOAA), and the European Centre for Medium-Range Weather Forecasts (ECMWF). Conceived in the late 1990s, WRF's development engaged a collaborative partnership including the U.S. Air Force, the Naval Research Laboratory, the University of Oklahoma, and the Federal Aviation Administration (FAA) (NCAR, 2023).

For researchers, WRF can produce simulations based on actual atmospheric conditions or idealized conditions. WRF offers operational forecasting as a flexible and computationally efficient platform while reflecting recent advances in physics, numerics, and data assimilation contributed by developers from the expansive research community. WRF is currently in operational use at the National Centers for Environmental Prediction (NCEP) and other national meteorological centers—including the Thai Meteorological Department (TMD) —as well as in real-time forecasting configurations at laboratories, universities, and companies. WRF has a large worldwide community of registered users (a cumulative total of over 57,800 in over 160 countries as of 2021), and NCAR provides regular workshops and tutorials on it (NCAR, 2023). An active and engaged user community, comprised of researchers, meteorologists, and climatologists globally, contributes to the ongoing development and improvement of WRF. The model's open-source nature fosters collaboration, transparency, and innovation within the atmospheric science community.

WRF's versatility enables the simulation of complex atmospheric conditions, making it an indispensable tool for scientists and meteorologists. Researchers leverage the model for numerical experiments, enhancing their understanding of meteorological phenomena and contributing to advancements in atmospheric science. This dynamic and collaborative resource continues to play a pivotal role in advancing our knowledge of the Earth's atmosphere. Notably, urban climate scientists, including Matsuo and Tanaka (2019), Giorgos et al. (2010), and Fei et al. (2011), have utilized WRF, analyzing its results to develop climate maps at different scales.

Thailand has implemented specific policies concerning environmental impact studies, notably the Environmental Impact Assessment (EIA). This assessment is mandated for large architectural projects exceeding a total area of 10,000 sq m. or a height surpassing 23 m. The EIA serves as a procedural framework for studying and evaluating potential impacts resulting from the implementation of any project, undertaking, or state-sanctioned operation. These impacts may directly or indirectly affect natural resources, environmental quality, health, sanitation, life quality, or other interests of individuals and communities. The EIA process involves public participation, aiming to determine measures that can prevent and rectify identified impacts.

The EIA is recognized as a crucial tool in fostering sustainable development, aiming to strike a balance between economic growth, environmental protection, and social considerations. However, it is noteworthy that the current environmental assessment approach primarily focuses on a case-by-case study of individual projects and may not comprehensively cover all environmental impacts at the district scale. There is a recognized need for an urban environmental assessment that encompasses a group of buildings, providing a more holistic understanding of the overall existing situation. Such an approach would contribute to a more comprehensive evaluation of the environmental impact within urban areas, ensuring a more effective and integrated approach to sustainable development and environmental management.

The fourth revision of the Bangkok land use planning is currently undergoing a review process, and public input is being solicited for its finalization in 2024. This represents an advancement from the third revision, published and used since 2013 to the present, which primarily focused on land use classification and associated restrictions, including floor area ratio (FAR), open area ratio (OSR), and building construction criteria (Bangkok Metropolitan Administration (BMA), 2023). This research aims to contribute by integrating local climate science with the analysis of land use data, presenting the findings in an accessible format for both experts and non-experts. The objective is to facilitate a clear understanding of the significance of studying environmental impacts at the city level, particularly in the context of policy design and planning with local governments.

In addressing the research questions, this chapter elucidates the climate distribution data derived from the numerical calculations performed using the WRF model. The integration of findings from Chapter 2 and this chapter highlights distinctions in climate characteristics resulting from varied resources and methodologies. Subsequently, UECMs of Bangkok are formulated.

The chapter is organized into five main sections. It commences with an outline of the objectives, followed by a detailed exploration of the methodology and data usage. This section is further divided into three parts; the study area and period of calculations; the classification of WRF input data; the analysis of WRF output data and the accuracy assessment of the WRF output. The third section delves into the results and discussions, encompassing four key points; spatiotemporal temperature and temperature zones; spatiotemporal ventilation and ventilation zones; the UECMs of the BMA, and the accuracy assessment of the WRF output. The fourth and fifth sections encapsulate the conclusions drawn from the study and outline its limitations, concluding with suggestions for further research.

3.2   Objectives

1. To analyze the spatial and temporal temperatures and wind distribution based on the combination of the observation data and numerical calculations: the WRF model in the mesoscale of Bangkok.

2. To clarify the severe climate area of Bangkok from the viewpoint of UHI mitigation and illustrate in the Urban Environmental Climate Maps of the Bangkok Metropolitan Area

3.3   Methodology and Data Usage

In this chapter, the utilization of data is bifurcated into two primary components: input data for calculations and output data for analysis. Both datasets undergo computation in the WRF Preprocessing System (WPS) and the WRF application. Consequently, this section is structured into three subparts: elucidation of the study area and the period of calculations, delineation of the classification of input data for calculations in WRF, and the exploration of the analysis of WRF output data and cluster analysis.

3.3.1 Study Area and The Period of Calculations

In this chapter, the focus shifts from the Bangkok Metropolitan Region (BMR) discussed in the previous chapter to the Bangkok Metropolitan Area (BMA). However, the calculation of weather data in the WRF model necessitates the use of two domains: the parent domain and the nested domain. Figure 3-1 provides details on both domains, with Domain 2 covering the entire BMA, and Domain 1 encompassing Bangkok along with parts of 14 surrounding provinces. To facilitate the WRF application calculations, both domains have a resolution of 1,500 m for Domain 1 and 500 m for Domain 2.

Concerning the period under study, Chapter 2 elucidated the Fine-Weather Day (FWD) during the summer of 2019 using data from the Thai Meteorological Department (TMD). The wind patterns for each FWD, specifically wind pattern A, were depicted in Figures 2-9 and 3-2. Consequently, this chapter has chosen the continuous period of those days characterized by the prevailing wind direction in summer, specifically wind pattern A. The calculation periods in WRF span from 3rd to 13th April 2019, with additional details about the calculation conditions presented in Table 3-1.

Table 3-1 Calculation conditions

Calculation period	2019/04/03 00:00:00 – 2019/4/13 18:00:00
Horizontal grid	Domain1: 1,500 m resolution 100x90 grid
	Domain2: 500 m resolution 150x120 grid
Vertical grid	32 layers (Surface – 20 km, unequal interval)
Meteorological data	NCEP FNL Operational Model Global Tropospheric Analyses, continuing from July 1999 (6 hours intervals)
Land use data	Domain1: USGS land use data Domain2: USGS land use index based on land use data from the Department of Public Works and Town & Country Planning and Department of City Planning and Urban Development, BMA
Elevation data	Domain1&2: Digital elevation model (30m resolution)
Microphysics	Reisner2 scheme
Radiation	Mstrnx scheme
PBL scheme	Mellor-Yamada Level2.5 scheme
Urban canopy	Single-layer urban canopy model
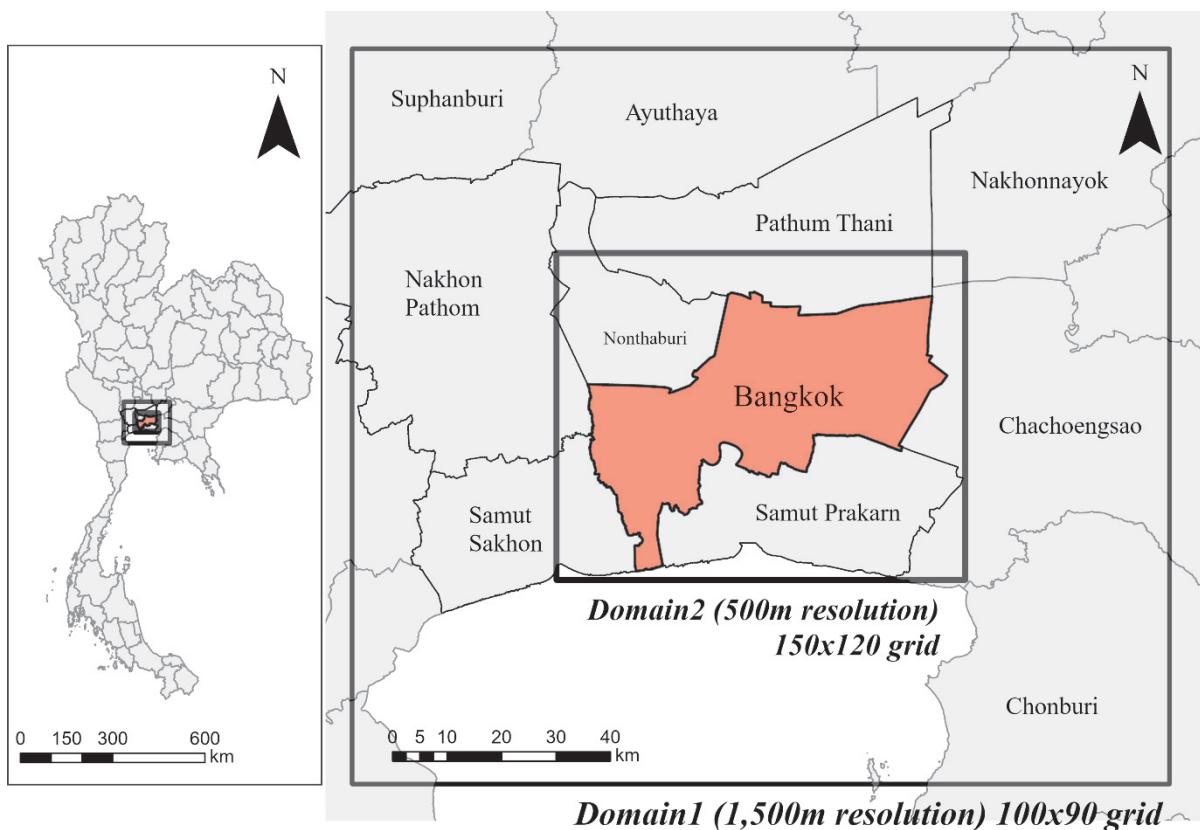
Figure 3-1 Calculation area
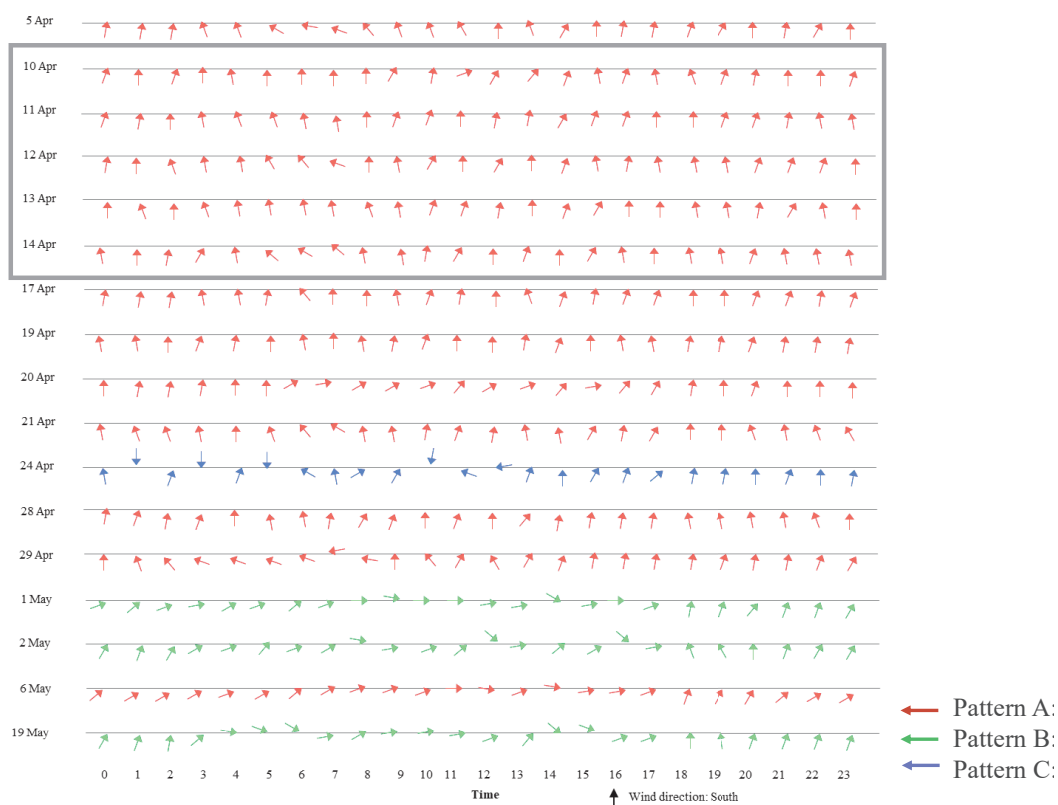
Fig. 3-2 (Part of) Wind pattern of each FWD in summer and the selected period of calculation

3.3.2 Classification of Input Data for Calculation in WRF

In the realm of input data for calculation in the Weather Research and Forecasting (WRF) model, this chapter amalgamates information from three distinct classifications (Table 3-1): meteorological data, land use data, and elevation data. Meteorological data, sourced from the NCEP FNL Operational Model Global Tropospheric Analyses, spans from July 1999 with 6-hour intervals, aligning with the period of calculation. The second dataset encompasses land use data procured from multiple sources, including the Department of Public Works and Town & Country Planning, the Department of City Planning and Urban Development (BMA), and the classification of the normalized difference vegetation index (NDVI) value.

Thailand's land use data was subsequently converted to the United States Geological Survey (USGS) index, with specifics outlined in Table 3-2. The third dataset encompasses elevation data derived from the Digital Elevation Model (DEM) with a 30 m resolution. Furthermore, the classification of land use data (LU_INDEX) for WRF in Domain 2 was elucidated, particularly in categorizing urban areas (LU_INDEX is 1) into three distinct values (31–33) via the urban canopy model. Each urban type was classified based on the NDVI range, as depicted in Figure 3-3, with the calculation of six urban parameters for each type. The conditions for these urban parameters are detailed in Table 3-3 and constitute input data for the calculation.

Figures 3-4 and 3-5 illustrate the land use data for both domains. Subsequently, all input data transformed the Geographic Information System (GIS) base into an NC (Numerical Control) file. The NC format, a text-based file, contains instructions for CNC (Computer Numerical Control) machines. Finally, the 'Namelist.WPS' in the WPS combined all three input data, followed by calculations on the WRF model.

3.3.3 Analysis of WRF Output Data and the Accuracy Assessment

In the evaluation of the WRF output data and subsequent cluster analysis, the outcomes of WRF calculations were retrieved from the application, focusing on selected variables—the temperature at a 2 m height and vectors of wind data at a 10 m height—during specific periods, specifically from 3–13 April 2019 with analysis periods spanning 10–13 April 2019 (Fig.3-2). Initially, the output data takes the form of an NC file. To facilitate analysis, this data was transformed into CDL files, designed to encapsulate information crucial for the exchange of basic primary color grading information between different software systems. Subsequently, both sets of climate data were subjected to K-mean cluster analysis. This analysis technique was employed to craft spatiotemporal temperature and ventilation maps. Moreover, the validation of WRF output data was calculated from two periods on 12 April 2019: 1 A.M. and 1 P.M. from the temperature and wind distribution data.

Table 3-2 The classification of land use data

USGS		Thailand		
LU Code	Classification	LUID	LU Code	Classification
1	Urban and built-up area	U1	11	City, Town, Commercial
		U2	12	Village
		U3	13	Institutional land
		U4	14	Communication and utility
		U5	15	Industrial land
		U6	16	Other built-up land
2	Dryland Cropland and pasture	A2	22	Field crop
		A3	23	Perennial crop
		A4	24	Orchard
		A5	25	Horticulture
		A6	26	Shifting cultivation
		A7	27	Pasture and farm-house
3	Irrigated Cropland and pasture	A1	21	Paddy field
		M5	55	Salt flat
4	Mixed 2-3	A0	20	Integrated farm/Diversified farm
5	Cropland/Grassland mosaic			
6	Cropland/Woodland mosaic			
7	Grassland	U7	17	Golf course
8	Shrubland			
9	Mixed 7-8	M1	51	Rangeland
		M2	52	Marsh and Swamp
10	Savanna			
11	Deciduous Broasleaf Forest			
12	Deciduous Needleleaf Forest			
13	Evergreen Broasleaf			
14	Evergreen Needleleaf			
15	Mixed forest	F1	31	Evergreen forest
		F2	32	Deciduous forest
		F5	35	Forest plantation
		F6	36	Agro-forestry
		F7	37	Beach forest
16	Water Bodies	A9	29	Aquacultural land
		W1	41	Natural water body
		W2	42	Artificial water body
17	Herbaceous Wetland	A8	28	Aquatic plant
18	Wooden Wetland	F3	33	Mangrove forest
		F4	34	Swamp forest
19	Barren or sparsely vegetland	M3	53	Mine, Pit
		M4	54	Other miscellaneous land
		M7	57	Garbage dump
20	Herbaceous Tundra			
21	Wooded Tundra			
22	Mixed Tundra			
23	Bare Ground Tundra			
24	Snow			
31	UCM1			
32	UCM 2			
33	UCM 3			
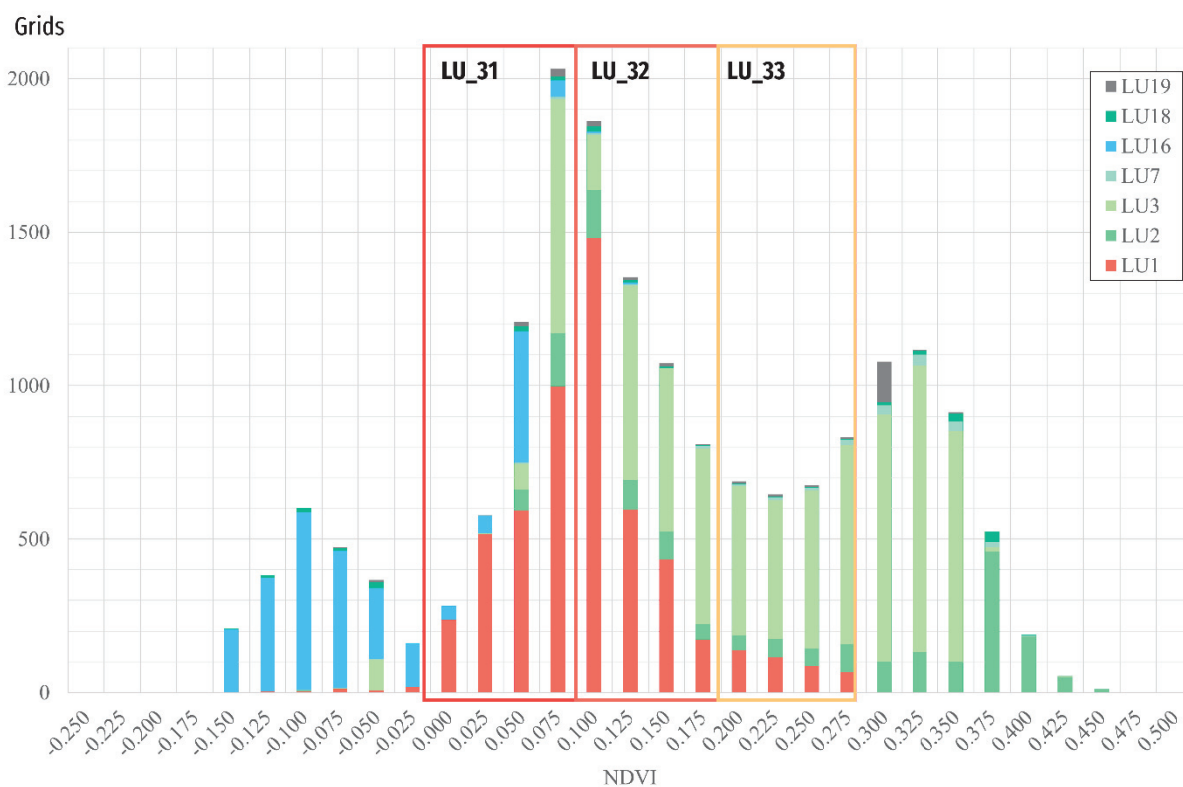
Fig. 3-3 Range of NDVI value and land use classification of Domain2

Table 3-3 The urban parameters

LU_INDEX (urban type)	NDVI	Urban Parameters					
		UCR	BH (m)	Std. of RH (m)	BL (m)	Road Width (m)	Avg AHF (W/m2)
31 Commercial and Industry	<0.075	0.9	23.1	4.0	6	16	80.27
32 High-dense-residence	0.075< X <0.175	0.75	10.6	3.0	6.39	14.8	70
33 Low-dense-residence	>0.175	0.65	5.6	1.0	5.9	6	25

Notes: UCR = Urban Coverage Ratio (%), BH = Building Height, Std. = standard deviation,
RH = Roof Height, BL = the Building Length of one side of the building,
AHF = Anthropogenic Heat Flux (W/m2),
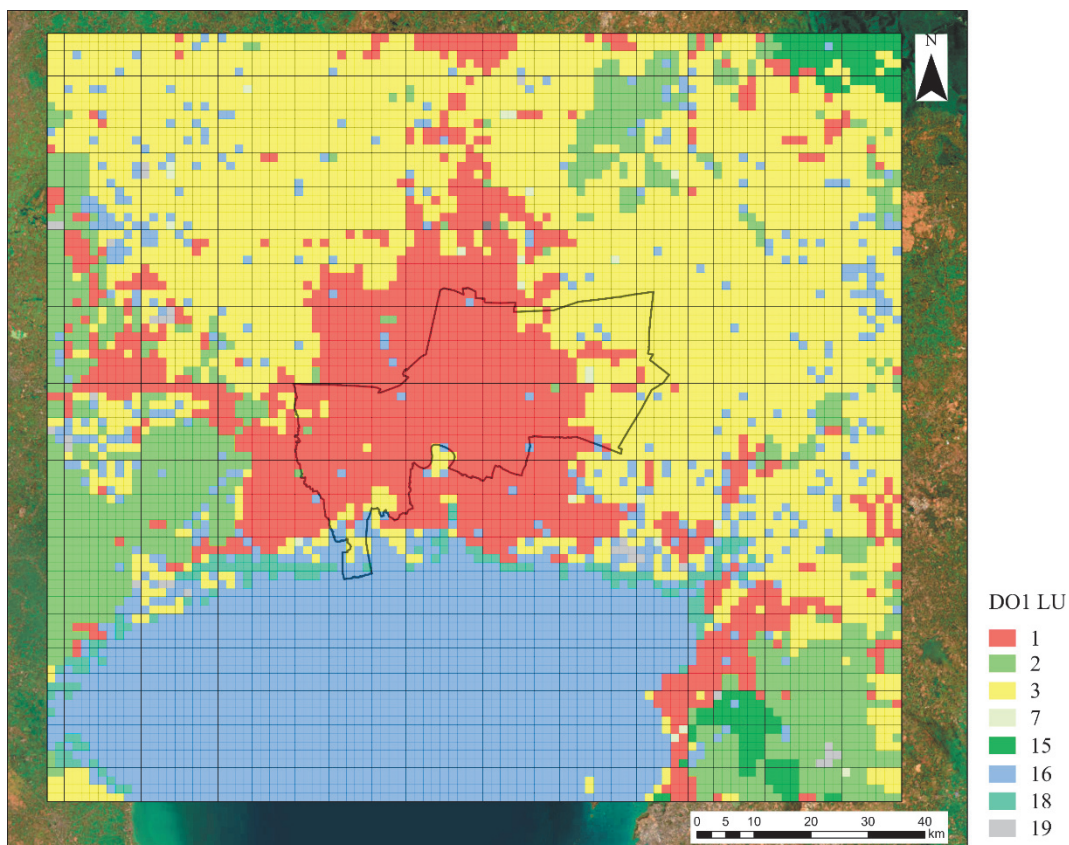
Fig. 3-4 Classification of land use index of Domain1
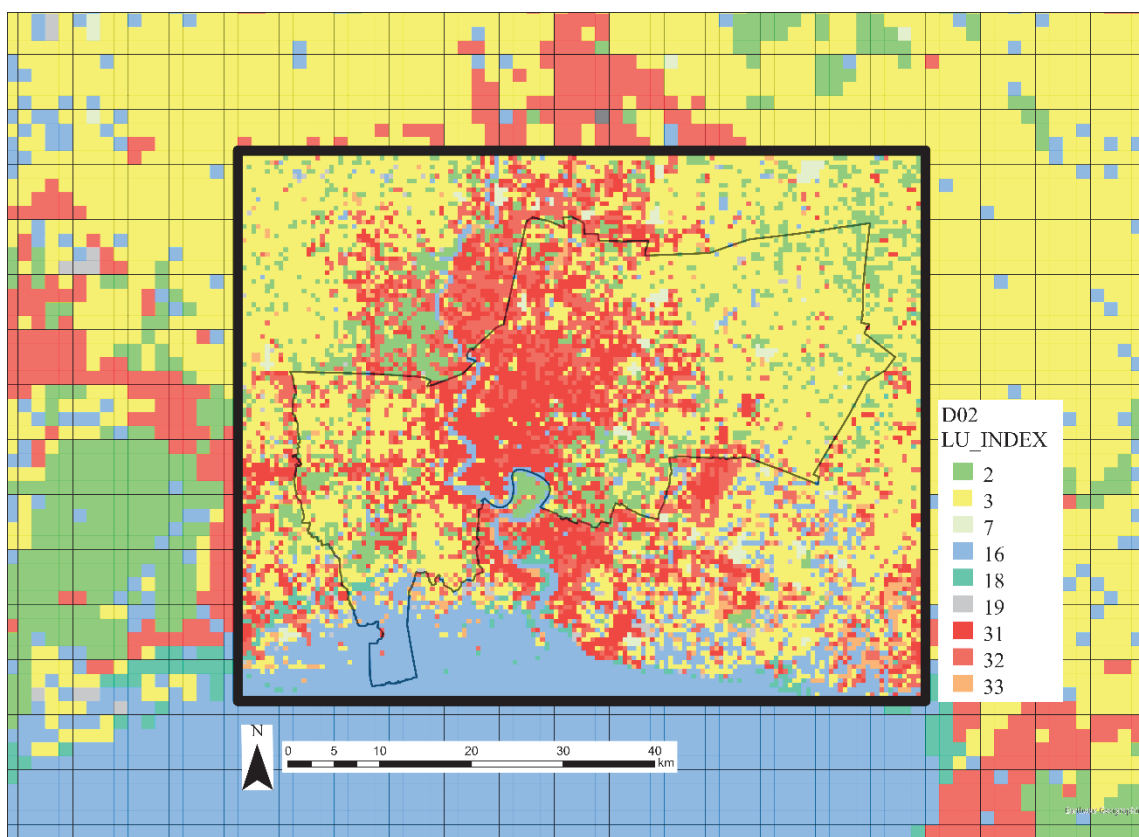
Fig. 3-5 Classification of land use index of Domain2

3.4   Results and Discussions

The analysis of WRF outputs yielded temperature data at the 2-meter level (T2) and wind vector data at the 10-meter level (U10 and V10) for each grid within both domains. The climate analysis focused on data from Domain 2, characterized by a high resolution of 500 meters. The selected period for analysis spans from April 10, 2019, 00:00:00 to April 13, 2019, 23:00:00, based on the Thailand time zone (GMT+7). The temperature and wind speed data were then averaged on an hourly basis over the four days. These aggregated data were subsequently categorized into distinct zones, forming the basis for discussion in this section. The results are presented in three parts, with the initial two sections highlighting different climate data, followed by the third section addressing the UECMs of BMA.

3.4.1   Spatiotemporal Temperature and Temperature Zone of BMA

The analysis of temperature at the 2-meter level (T2) in Domain 2 focused on studying the temporal temperature patterns, as presented in Table 3-4 and Figure 3-6. The temperature data for the BMA reveals a discernible daily cycle, marked by fluctuating mean temperatures across the 24-hour period. Notably, the mean temperature peaks around 15:00 and gradually decreases from the evening onwards. The temperature range, representing the difference between maximum and minimum temperatures, varies between approximately 3.51°C and 5.06°C. The most significant temperature variations are observed during the evening and early morning, indicating cooler nights, with the lowest temperatures typically recorded around 6:00. The daily temperature trends follow a consistent pattern despite minor hourly fluctuations within a few degrees Celsius. Additionally, Figures 3-7 and 3-8 illustrate the distinct temperature distributions during different periods—at 1:00 and 13:00.

When examining the temporal temperature across three types of urban areas—Commercial and Industry (LU31), High-dense-residence (LU32), and Low-dense-residence (LU33)—significant patterns emerge. Figure 3-9 illustrates the average temperatures (Avg) and temperature differences (Max-Min) across these distinct urban zones. High-density residence areas consistently record the highest average temperatures throughout the day, indicating a propensity for elevated temperatures compared to commercial and industrial areas (LU31) and low-dense residence areas (LU33). The temperature differences (Max-Min) exhibit variability among zones, with LU32 displaying the most substantial fluctuations, signifying significant variations between daily maximum and minimum temperatures.

Conversely, LU33 demonstrates the smallest differences, suggesting a more stable and predictable temperature pattern. The hourly temperature trends across all zones adhere to a typical diurnal variation, with LU32 consistently experiencing the highest temperatures during peak hours. In summary, this analysis provides valuable insights into the unique temperature dynamics of different urban areas, emphasizing variations in average temperatures and temperature fluctuations throughout the day.

Temperature Zone of BMA

The classification of temperature through K-mean cluster analysis has delineated the BMA into six distinct zones, each exhibiting unique temperature patterns. Table 3-5 and Figure 3-10 provide detailed insights into the characteristics of each zone.

Spatial and temporal temperature data across the six zones (Zone 1 to Zone 6) offer a comprehensive depiction of temperature variations over a 24-hour period. At 1:00, Zone 1 registers the highest temperature at 31.36°C, while Zone 4 records the lowest at 29.11°C. Consistent temperature trends persist through subsequent hours, with variations discernible among zones. Notably, temperatures peak around 15:00 (3 PM) across all zones, with Zone 3 recording the highest temperature at 38.06°C. The hourly temperature patterns exhibit synchronicity, gradually declining during the night.

Zone 1 encompasses the largest area, spanning 4,789 grids (1,197.25 sq km), while Zone 4 is the smallest, covering 993 grids (248.25 sq km). Generally, Zones 3 and 1 experience higher temperatures both day and night, Zones 2 and 6 maintain moderate temperatures, and Zones 4 and 5 exhibit slightly lower temperatures, indicating warmer conditions during the day and cooler conditions at night. During nighttime, the order of temperature for each pair of zones changes to 1, 3, 6, 2, 5, and 4, respectively.

This detailed dataset allows for an in-depth analysis of both spatial and temporal temperature variations. It provides valuable insights into the unique characteristics of each zone and temperature fluctuations over time. This contributes to a better understanding of local climate change.
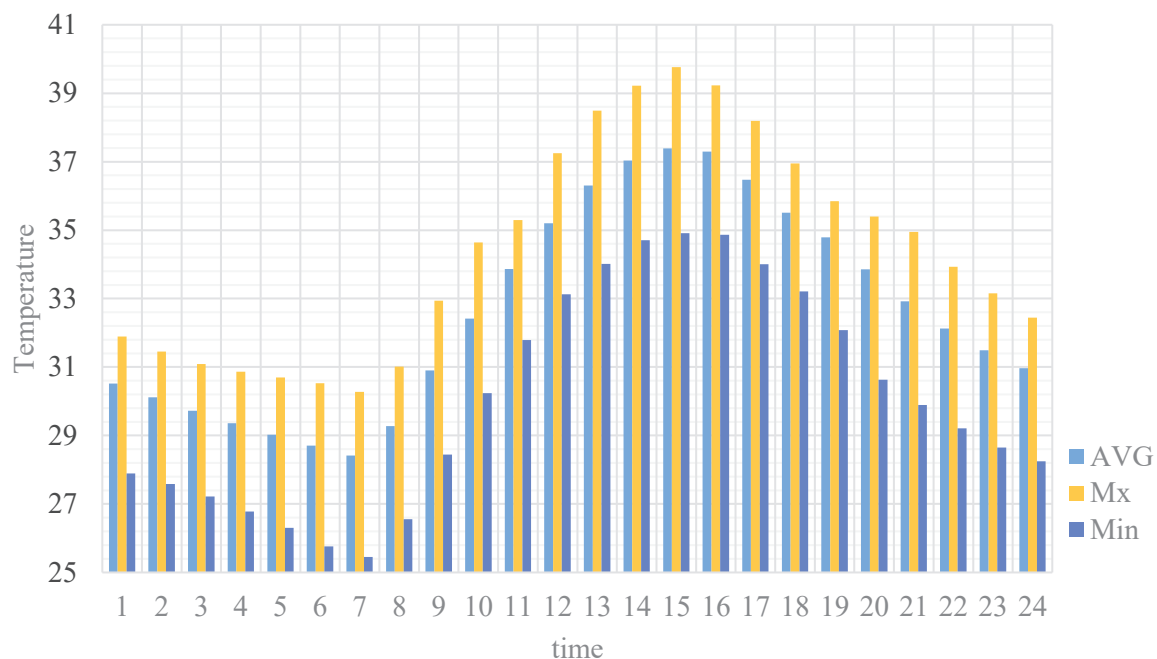
Fig. 3-6 Temporal temperature of BMA

Table 3-4 Temporal temperature data in the summer of BMA

Time	Temperature (°C)			
	Mean	Max	Min	Max-Min
1:00	30.52	31.89	27.90	4.00
2:00	30.11	31.45	27.58	3.86
3:00	29.72	31.09	27.22	3.86
4:00	29.36	30.87	26.77	4.09
5:00	29.02	30.69	26.30	4.40
6:00	28.71	30.52	25.76	4.76
7:00	28.42	30.27	25.45	4.82
8:00	29.27	31.01	26.55	4.46
9:00	30.90	32.94	28.44	4.50
10:00	32.42	34.64	30.24	4.40
11:00	33.87	35.29	31.79	3.51
12:00	35.21	37.24	33.13	4.11
13:00	36.30	38.50	34.02	4.48
14:00	37.03	39.22	34.71	4.51
15:00	37.39	39.76	34.91	4.85
16:00	37.30	39.23	34.87	4.36
17:00	36.47	38.19	34.00	4.19
18:00	35.50	36.95	33.21	3.75
19:00	34.79	35.85	32.08	3.77
20:00	33.86	35.40	30.63	4.76
21:00	32.92	34.95	29.89	5.06
22:00	32.13	33.93	29.21	4.72
23:00	31.49	33.16	28.65	4.51
0:00	30.97	32.45	28.25	4.20
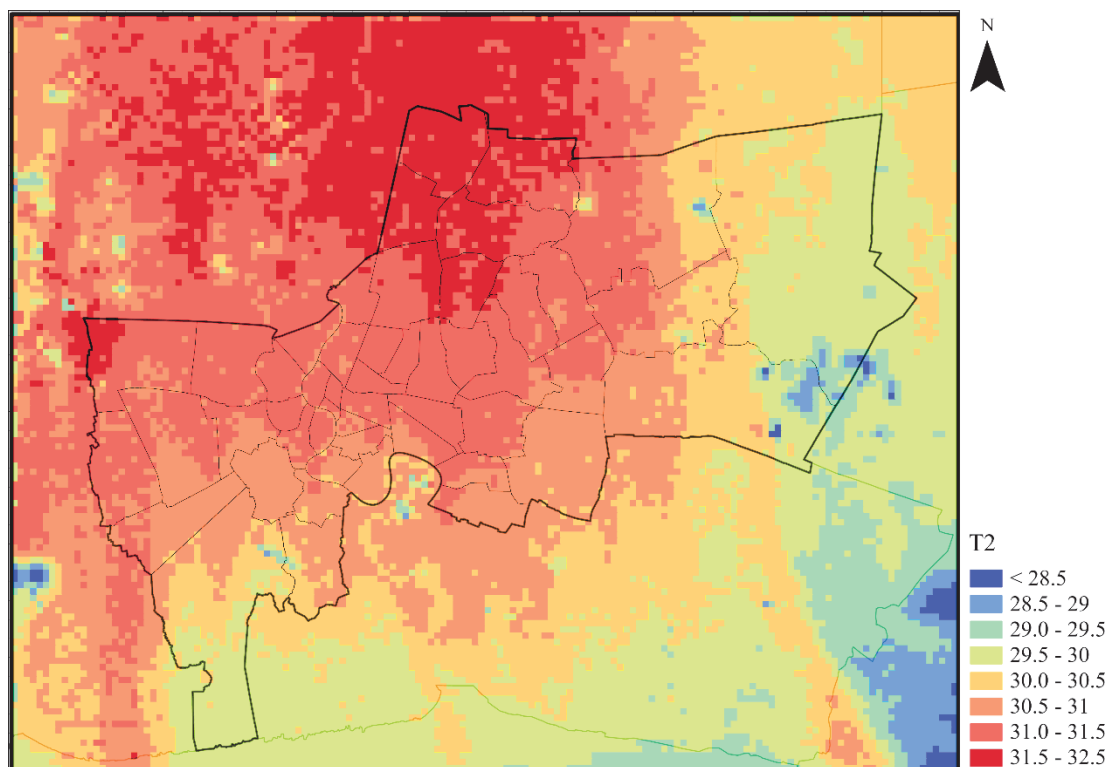
Fig. 3-7 Temperature distribution at 1:00 on 12 April 2019
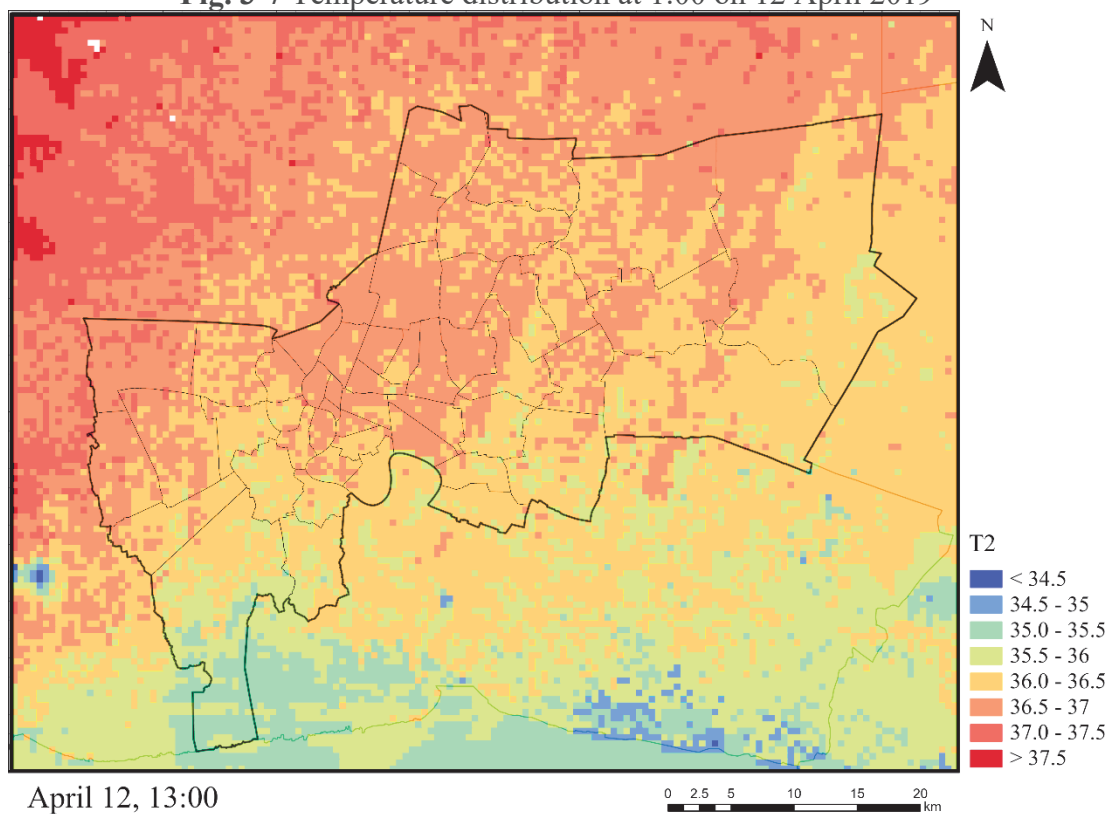
April 12, 13:00

Fig. 3-8 Temperature distribution at 13:00 on 12 April 2019
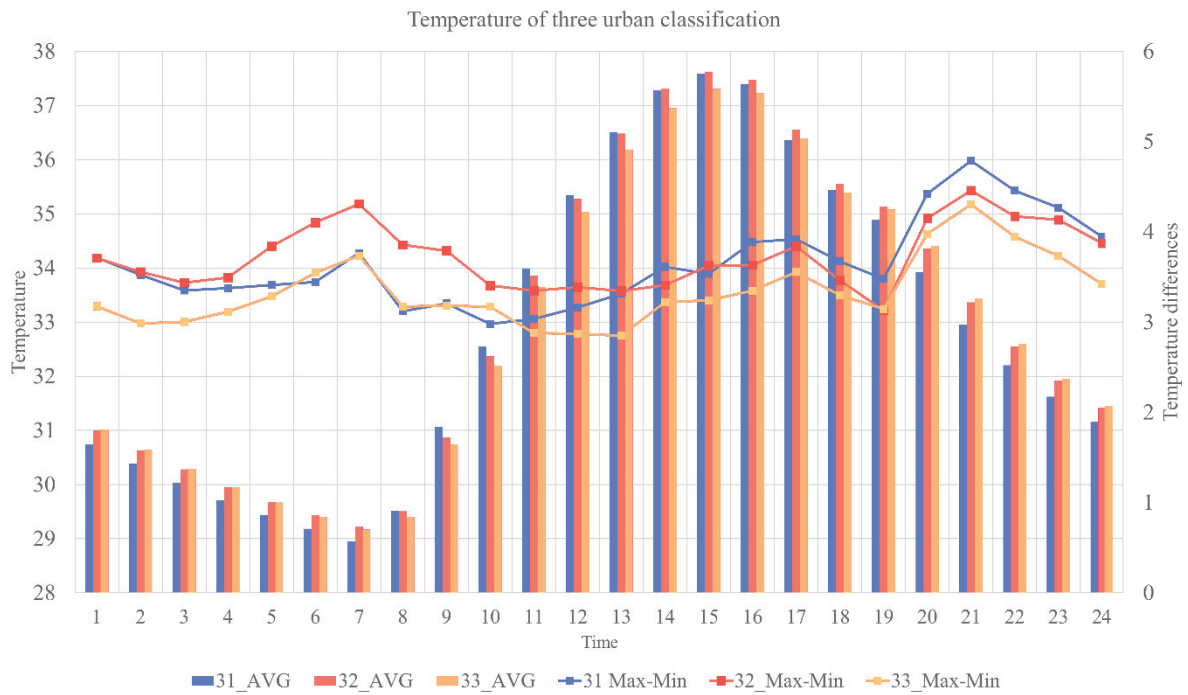
Fig. 3-9 Spatio temporal temperature of three types of urban area
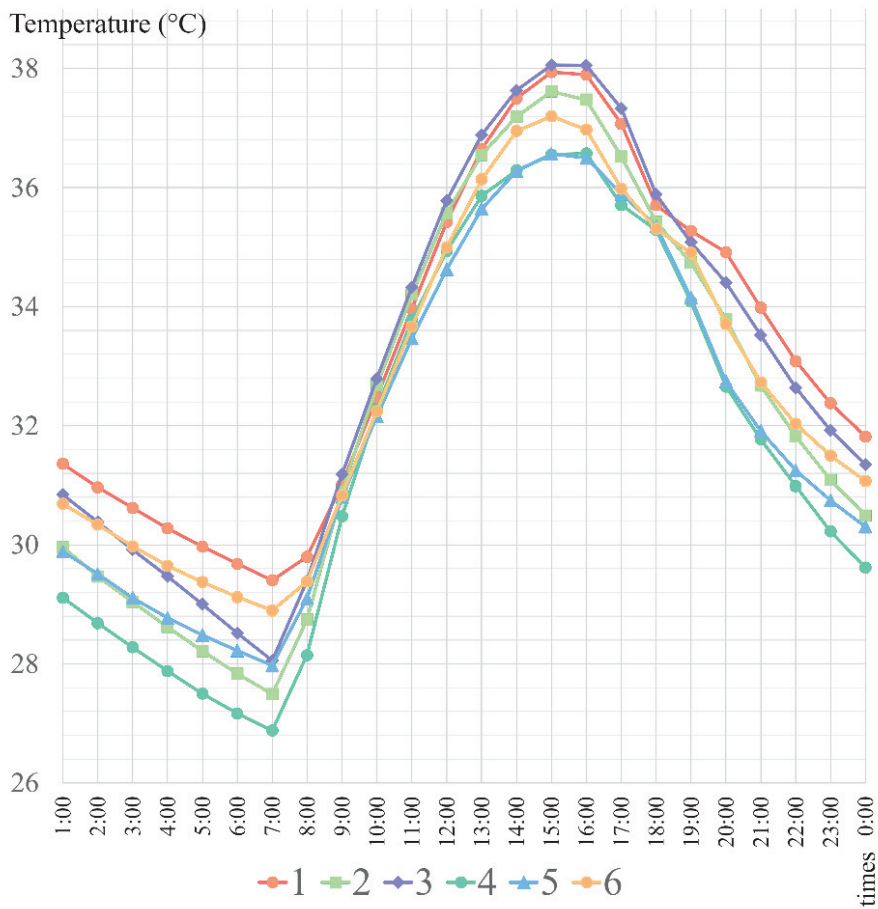
Fig. 3-10 Spatio temporal temperature of six zones

Table 3-5 Spatio-temporal temperature zone of BMA

Times	Spatial and temporal temperature (°C)					
	Zone 1	Zone 2	Zone 3	Zone 4	Zone 5	Zone 6
1:00	31.36	29.96	30.84	29.11	29.89	30.69
2:00	30.96	29.47	30.38	28.68	29.51	30.34
3:00	30.62	29.04	29.92	28.28	29.11	29.97
4:00	30.28	28.62	29.47	27.88	28.77	29.65
5:00	29.97	28.21	29.00	27.50	28.48	29.37
6:00	29.68	27.84	28.51	27.17	28.22	29.12
7:00	29.40	27.49	28.05	26.88	27.97	28.90
8:00	29.80	28.74	29.40	28.15	29.10	29.38
9:00	31.02	30.89	31.18	30.48	30.80	30.83
10:00	32.48	32.68	32.79	32.28	32.16	32.25
11:00	33.96	34.20	34.33	33.77	33.47	33.67
12:00	35.42	35.57	35.78	34.93	34.63	35.00
13:00	36.65	36.55	36.89	35.86	35.64	36.14
14:00	37.50	37.19	37.63	36.29	36.28	36.95
15:00	37.94	37.61	38.06	36.55	36.57	37.20
16:00	37.90	37.48	38.05	36.58	36.50	36.97
17:00	37.07	36.52	37.33	35.71	35.89	35.98
18:00	35.71	35.42	35.89	35.29	35.35	35.31
19:00	35.27	34.74	35.08	34.08	34.15	34.90
20:00	34.91	33.79	34.40	32.66	32.74	33.71
21:00	33.98	32.68	33.52	31.77	31.91	32.73
22:00	33.09	31.82	32.64	30.99	31.25	32.03
23:00	32.38	31.09	31.92	30.22	30.74	31.50
0:00	31.82	30.49	31.35	29.62	30.30	31.07
Cases	4,789	2,763	2,019	993	3,771	3,665

3.4.2   Spatiotemporal Wind Velocity and Ventilation Zone of BMA

The wind data at the 10 m height of Domain 2 was primarily analyzed to study the temporal ventilation which is shown in Table 3-6 and Figure 3-11.

The wind data for BMA in 2019 reveals distinctive patterns in hourly wind speed variations. Generally, wind speed (WS_Avg) experiences a decline during the early morning hours until around 6:00, followed by a gradual increase. Notably, the highest average wind speed occurs in the evening, peaking at 21:00. Throughout the day, there is substantial variability in wind speed values, highlighting the dynamic nature of atmospheric conditions. The range between minimum and maximum wind speeds (WS_min and WS_max) is considerable, emphasizing the fluctuating wind patterns. Daily wind speed patterns indicate lower speeds during the early morning hours, a steady increase from 8:00 onwards, reaching a peak in the evening, and a subsequent gradual decline after 18:00. Extreme wind speed values, both minimum and maximum, are observed during the night and early morning, suggesting potential variations in atmospheric stability. The median wind speed (WS_Median) follows a similar pattern to the average, providing insight into the central tendency of the wind speed distribution.

Additionally, Figures 3-12 and 3-13 provide visual representations of the distinct wind velocity distributions during different periods—specifically, at 1:00 and 13:00 for both BMA and Bangkok, respectively. In both figures, the prevailing wind direction is from the south, exerting a notable influence on ventilation, particularly during diurnal periods. Notably, the inner areas of BMA exhibit the lowest wind speeds during the day. This information holds significance for comprehending the diurnal variability in the local wind climate of Bangkok and carries implications for urban planning and environmental assessments. The identified wind patterns can contribute valuable insights for designing structures, optimizing urban layouts, and assessing environmental conditions, especially in the context of ventilation and air quality management.

Ventilation Zone of BMA

The wind speed data was classified by K-mean analysis and divided BMA into six distinct zones with different ventilation patterns. Table 3-7 and Figure 3-14 show the details of each zone.

The spatio-temporal wind speed data across six different zones (Zone 1 to Zone 6) reveals interesting patterns in wind dynamics over a 24-hour period. At 1:00, Zone 5 exhibits the highest wind speed at 6.40 m/s, while Zone 1 has the lowest at 3.39 m/s. Throughout the day, wind speeds vary among zones, with Zone 5 consistently having the highest values and Zone 1 having the lowest values at 2.32 m/s. Notably, the wind speeds are generally lower during the early morning hours and gradually increase during the day. At 15:00, all zones experience an uptick in wind speed, with Zone 5 recording the highest at 4.92 m/s. The hourly wind speed patterns suggest a synchronization among zones, with fluctuations and peaks observed at different times. The cases column indicates the number of instances recorded, with Zone 1 having the highest count at 7,274 grids which means most of BMA has the lowest wind speed.

Compared to the previous study about the ventilation zone of BMA, Manat's study (Manat et al., 2022) presented the ventilation zones based on the spatial form and all indicators were calculated with standard GIS-based. The similarity critical area is the similar area which is the inner urban of Bangkok. However, this detailed dataset provides valuable insights into the spatiotemporal variations in wind speed across different zones, offering a comprehensive understanding of the wind dynamics in the studied region based on the wind simulation by WRF.
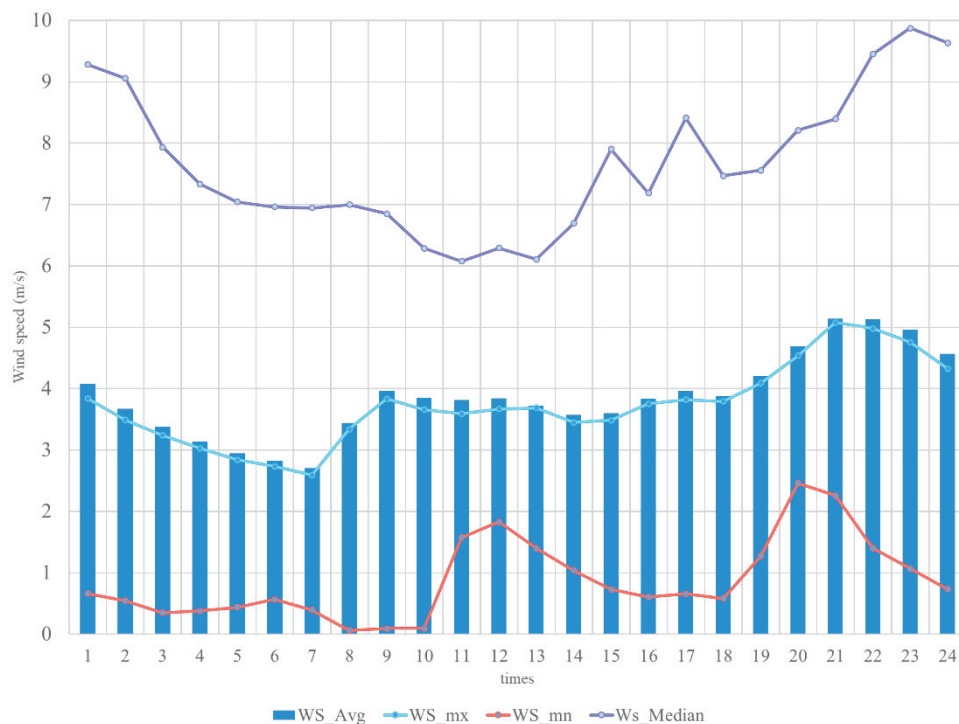
Fig. 3-11 Wind speed data of Domain 2

Table 3-6 Wind speed data in s the summer of BMA

Times	WS_Avg	WS_Median	WS_min	WS_max
1:00	4.08	3.84	0.66	9.28
2:00	3.67	3.49	0.55	9.06
3:00	3.37	3.24	0.35	7.93
4:00	3.14	3.03	0.38	7.33
5:00	2.94	2.84	0.44	7.04
6:00	2.82	2.74	0.57	6.96
7:00	2.70	2.59	0.40	6.94
8:00	3.44	3.34	0.06	7.00
9:00	3.96	3.84	0.10	6.85
10:00	3.85	3.66	0.09	6.29
11:00	3.82	3.59	1.58	6.08
12:00	3.84	3.67	1.83	6.29
13:00	3.73	3.69	1.40	6.11
14:00	3.57	3.45	1.04	6.69
15:00	3.60	3.49	0.73	7.90
16:00	3.84	3.76	0.61	7.19
17:00	3.97	3.82	0.66	8.41
18:00	3.88	3.80	0.58	7.47
19:00	4.21	4.09	1.27	7.56
20:00	4.69	4.54	2.46	8.21
21:00	5.14	5.08	2.26	8.39
22:00	5.13	4.98	1.40	9.45
23:00	4.96	4.76	1.07	9.88
0:00	4.56	4.33	0.73	9.64

April 12, 13:00
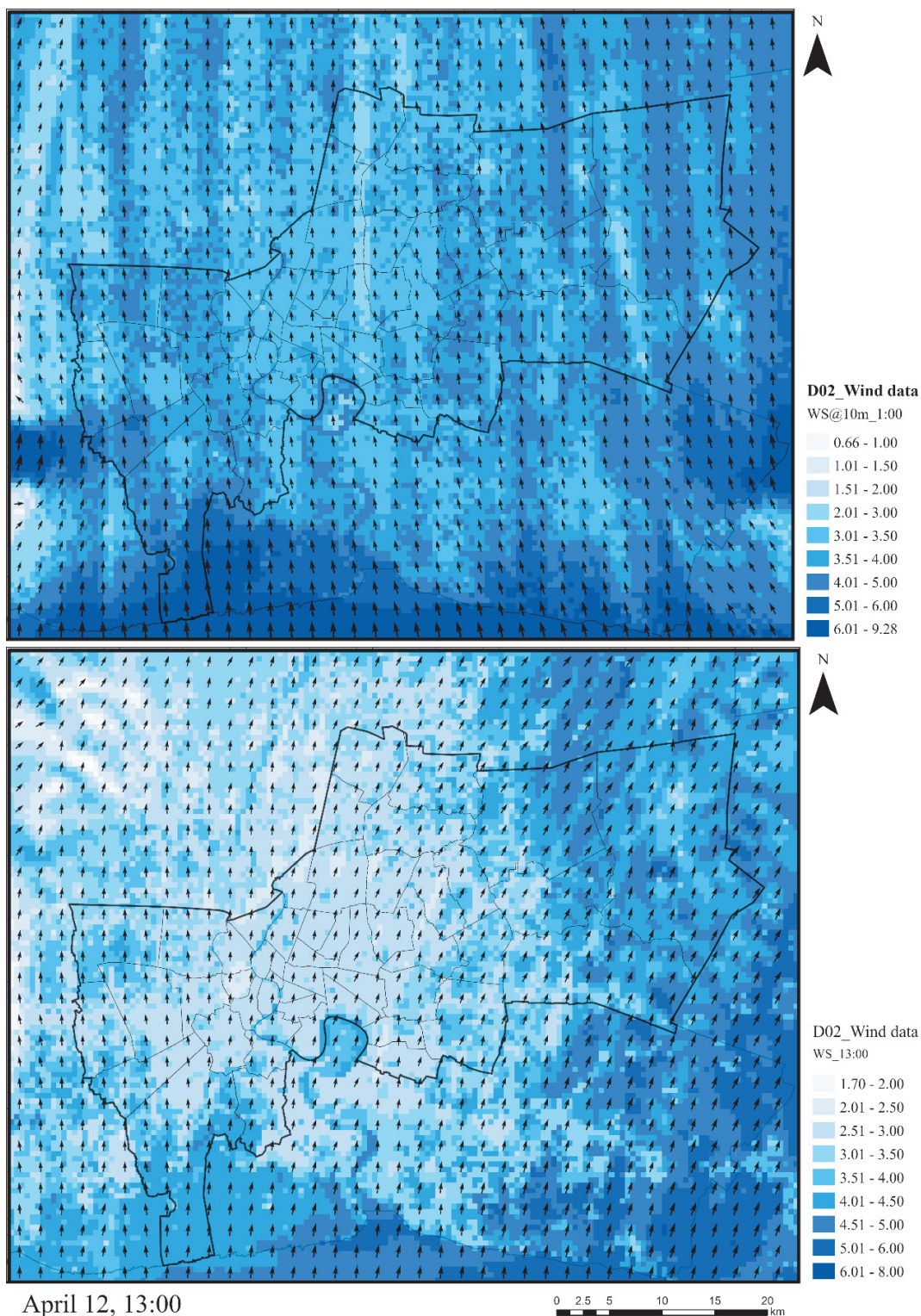
Fig. 3-12 Wind distribution at 1:00 and 13:00 on 12 April 2019 of Domain 2
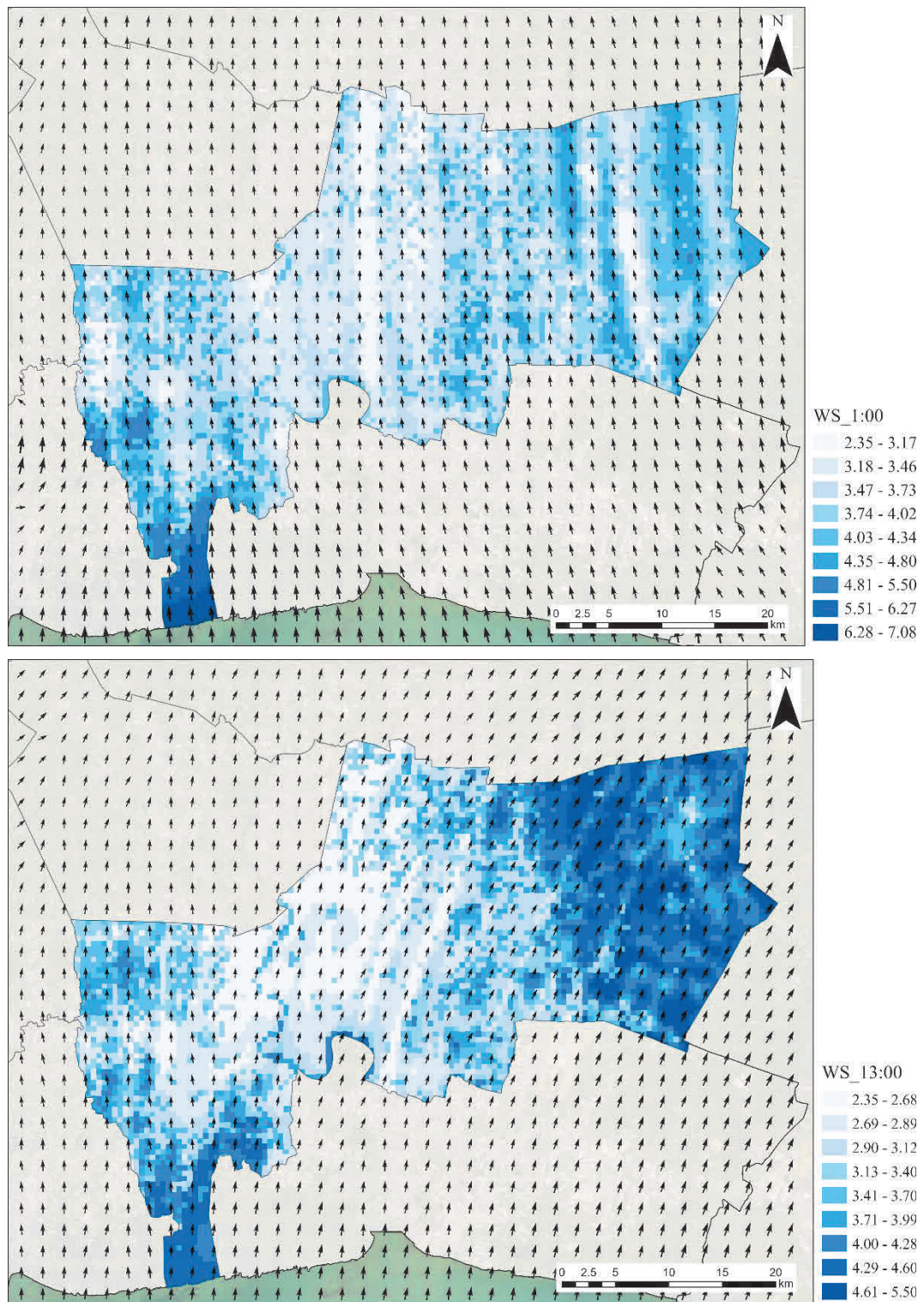
Fig. 3-13 Wind distribution at 1:00 and 13:00 on 12 April 2019 in Bangkok

Table 3-7 Spatio-temporal ventilation zone of BMA

Times	Spatio-temporal wind speed (m/s)					
	Zone 1	Zone 2	Zone 3	Zone 4	Zone 5	Zone 6
1:00	3.39	3.86	4.19	4.39	6.40	6.27
2:00	3.08	3.42	3.73	4.00	5.50	5.78
3:00	2.85	3.11	3.42	3.77	4.70	5.30
4:00	2.68	2.85	3.26	3.53	4.22	4.76
5:00	2.55	2.62	3.11	3.24	4.03	4.37
6:00	2.45	2.47	2.97	3.13	3.98	4.10
7:00	2.32	2.32	2.77	3.07	3.81	4.07
8:00	2.65	3.54	3.03	4.36	4.13	5.00
9:00	2.97	4.21	3.38	5.19	4.32	5.65
10:00	2.87	4.16	3.27	5.16	3.74	5.33
11:00	2.88	4.11	3.27	5.08	3.63	5.32
12:00	2.97	4.10	3.39	4.94	3.80	5.44
13:00	2.95	3.97	3.36	4.56	4.26	5.09
14:00	2.84	3.69	3.55	4.03	4.60	5.22
15:00	2.91	3.78	3.47	4.20	4.40	4.92
16:00	3.14	4.13	3.49	4.41	4.46	5.29
17:00	3.18	4.20	3.52	4.54	5.20	5.20
18:00	3.17	3.82	4.09	4.20	5.29	5.07
19:00	3.41	3.82	5.33	4.40	6.46	5.98
20:00	4.08	4.55	5.37	4.75	6.99	5.98
21:00	4.40	4.98	5.79	5.42	7.27	6.12
22:00	4.33	4.92	5.62	5.44	7.83	6.66
23:00	4.14	4.79	5.18	5.29	7.77	6.82
0:00	3.77	4.37	4.64	4.95	7.26	6.69
Grids	7,274	3,222	1,342	3,910	1,251	1,001
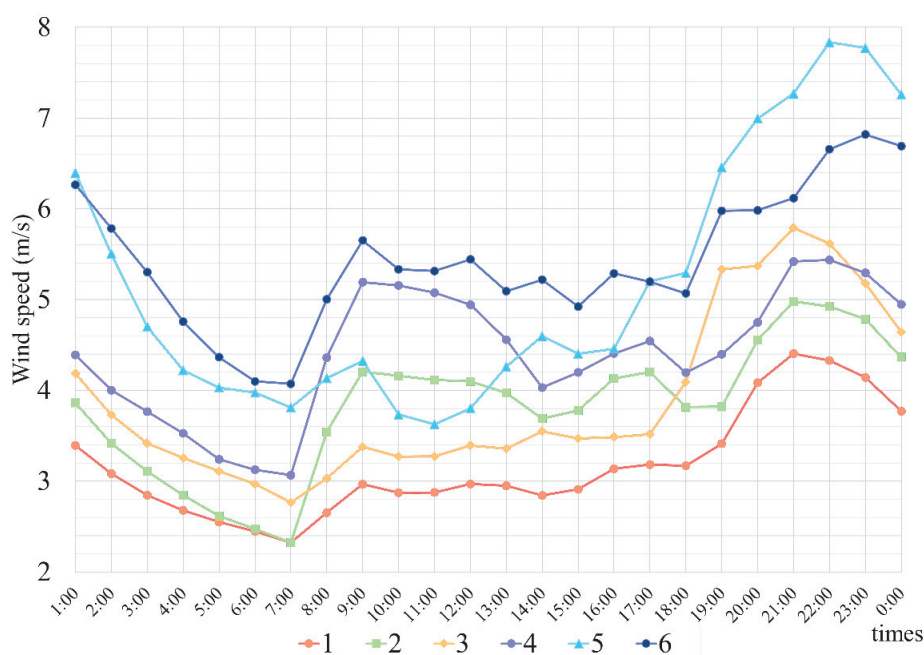
Fig. 3-14 Spatiotemporal ventilation zone of BMA

3.4.3   UECMs of BMA

UECMs of BMA are made based on three combinations from the spatial analysis maps which are a temperature zoning map of BMA, a ventilation zoning map of BMA, and the high density of urban area map.

Temperature Zoning Map of BMA

First, regarding the temperature zone, the spatiotemporal temperature zoning map was created. Each zone was represented in a different color by the following:

Zone 1—Orange Zone: The highest temperature zone throughout the day with the largest area, This zone covers the central and northern parts of Bangkok. Most of the area is the urban area in commercial zone and low to high-density residential zone of the BMA urban land use planning third edition (2013)—the latest published (Figure 3-15).

Zone 2—Green Zone: The moderate to high diurnal temperature and low nocturnal temperature zone. This zone covers the eastern part of Bangkok which is the rural and agricultural zone and the conservation zone.

Zone 3—Purple Zone: The highest diurnal temperature zone and moderate nocturnal temperature zone. This zone covers both rim sides of Bangkok which is the connected area between Zones 1, 2, and 6 and mixed between the low-density residential area and the rural and agricultural area.

Zone 4—Dark Green Zone: The lowest temperatures zone throughout the day. It covers a small area of the eastern part of BMA which is the rural and agricultural zone.

Zone 5—Blue Zone: The low-temperature zone and most of the coastal areas. This zone covers the southern part of Bangkok which is the coastal district and water area.

Zone 6—Yellow Zone: The moderate diurnal temperature and high nocturnal temperature zone. This zone covers a large area from the western to the central area of Bangkok. Most of the area is a similar zone to Zone 1.

Figure 3-16 shows the details related to each zone location and also ranks up their temperature characteristics by the average diurnal temperature (10:00–18:00) and average nocturnal temperature (18:00–10:00).
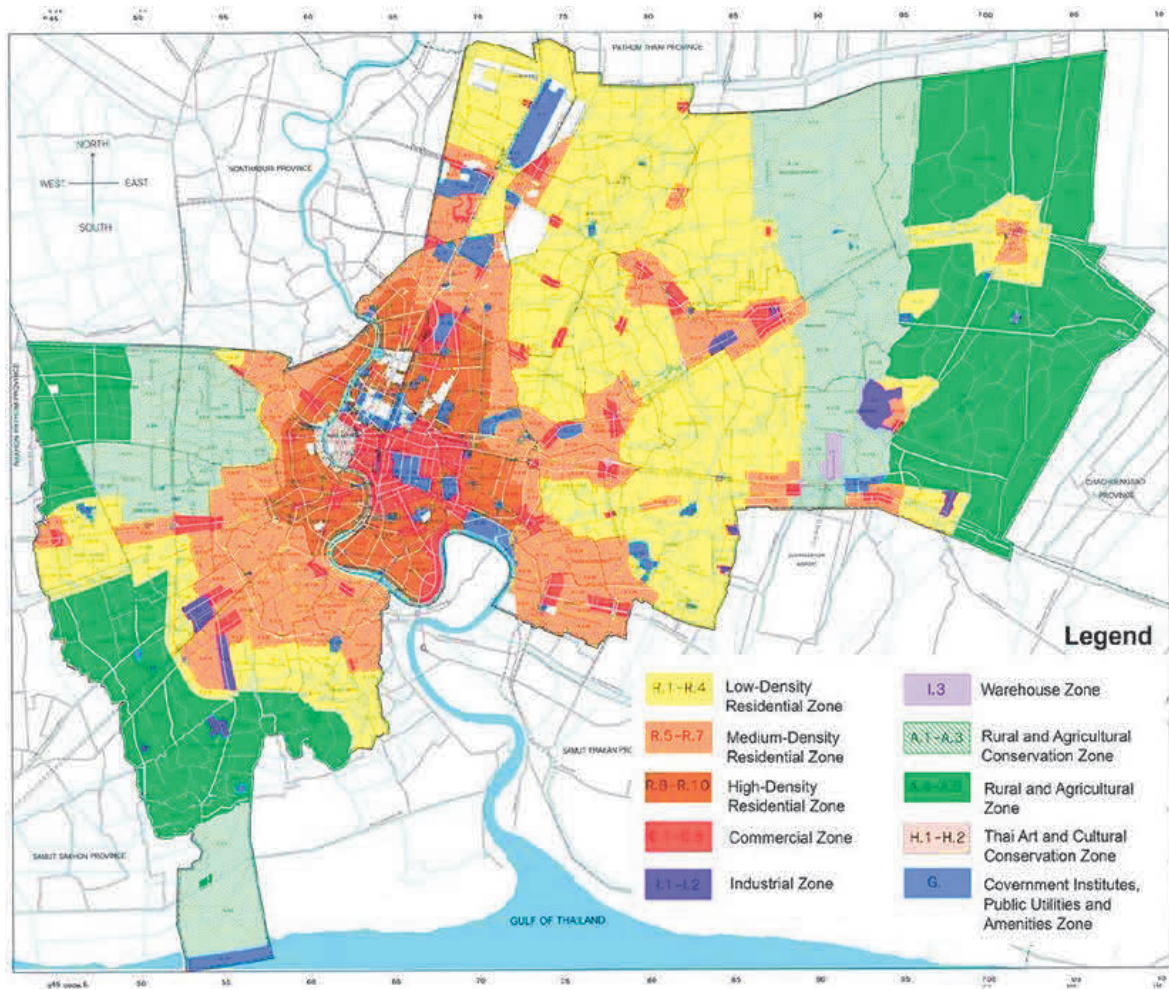
Fig. 3-15 The urban land use planning map of BMA (2013)

Bangkok Temperature Zoning Map
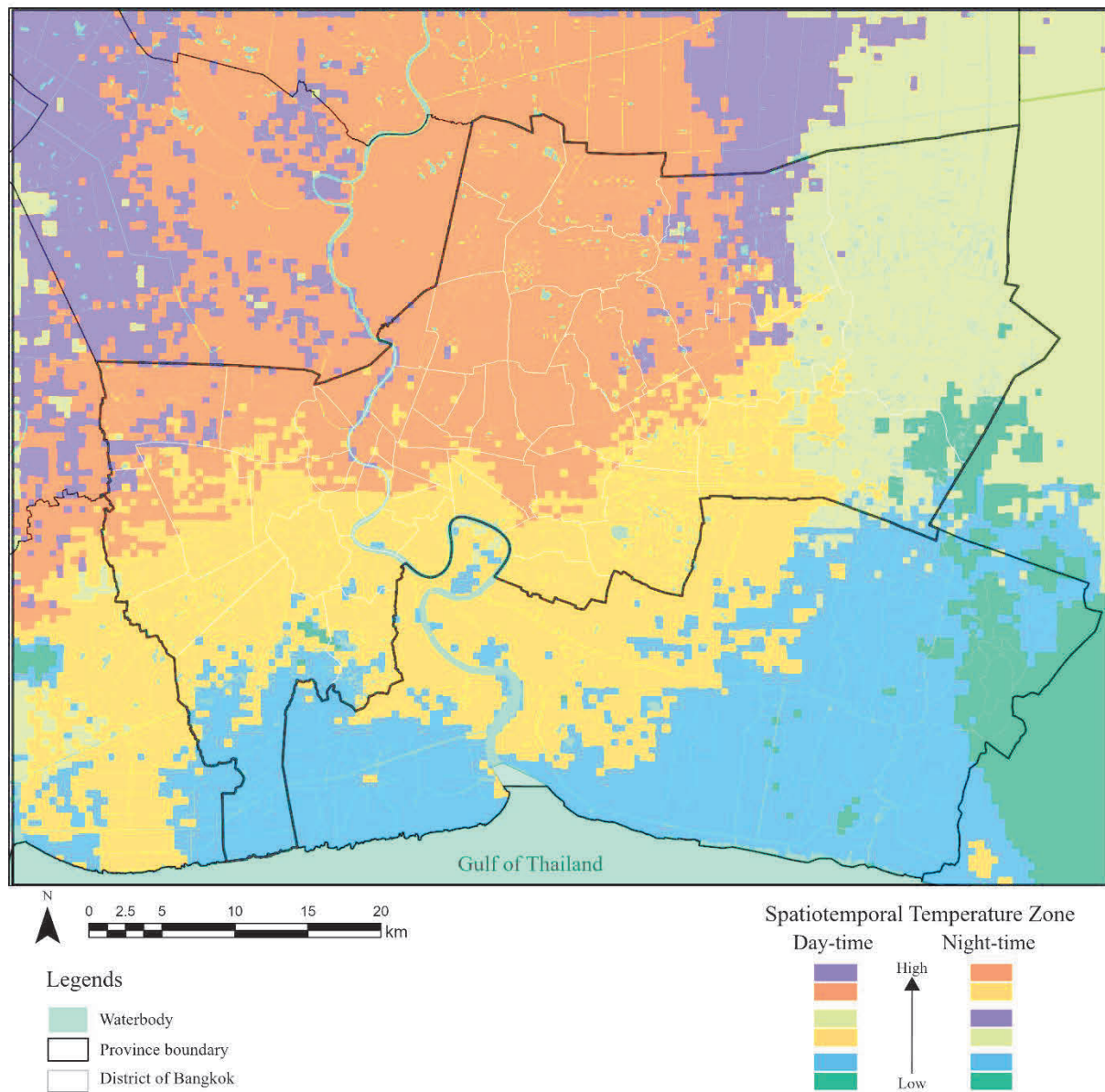
Fig. 3-16 Bangkok Temperature Zoning Map

Ventilation Zoning Map of BMA

In the second part, the spatio-temporal ventilation zoning map was created. Each zone was represented in a different color by the following:

Zone 1—Red Zone: The lowest wind speed zone throughout the day with the largest area of Bangkok. Most of the area is similar to Zone 1 of the temperature zone. The wind can not pass through the central BMA urban area. Therefore the wind speed is the lowest.

Zone 2—Green Zone: The moderate diurnal wind speed and low nocturnal wind speed zone. This zone covers part of eastern and western BMA which is the rural and agricultural zone and the low residential zone. It seems like the wind from the coast—prevailing wind—passes the same direction through BMA and connects to Nonthaburi and Pathum Thani which are located in a similar longitude.

Zone 3—Yellow Zone: The moderate wind speed zone. This zone covers both rim sides of Bangkok which is the connected area between Zones 1, 2, and 6 and mixed between the low-density residential area and the rural and agricultural area.

Zone 4—Purple Zone: The high diurnal wind speed and moderate nocturnal wind speed zone. It covers the east part of BMA which is the rural and agricultural zone. This zone has a high wind speed related to the rural and agricultural space of Samut-Prakarn allowing the seasonal wind from the coast to pass through the area but on night, the wind speed was dropped related to the distance from the coast.

Zone 5—Light Blue Zone: The high wind speed zone. This zone covers the southern part of BMA which is the coastal district, mangrove forest, and water area.

Zone 6—Blue Zone: The high wind speed zone. This zone covers the south and west sides of Samut Prakarn and does not cover BMA. Most of the area also had low temperatures throughout the day.

BMA consists of five ventilation zones and most of the area is the low wind speed zone. This issue is related to the urban land use planning of BMA. The rural and agricultural zone on the east side of the BMA has better ventilation. The future land use planning of BMA is supposed to consider this issue and plan to develop new environmental policies. Figure 3-17 shows the details related to each zone location and also ranks up their wind speed characteristics by the average diurnal wind speed (10:00–18:00) and average nocturnal wind speed (18:00–10:00).

Bangkok Ventilation Zoning Map
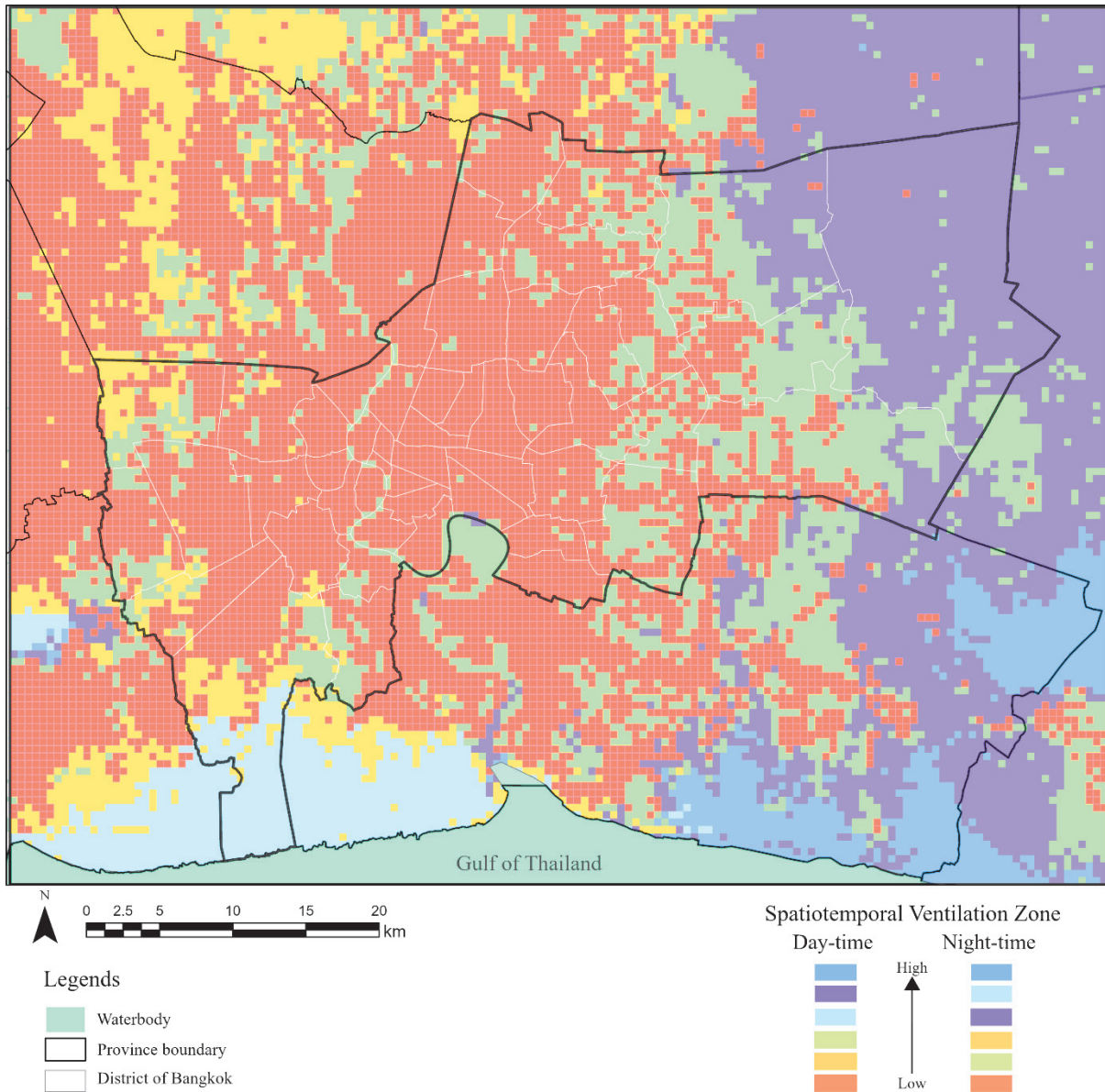
Fig. 3-17 Bangkok Ventilation Zoning Map

Integration with High-Density Urban Area Map

The third part of the UECM of BMA was overlayed by the high density of the urban area map which is the result from Chapter 2 and is shown in Figures 2-14 and 3-18. The layer represents the focus area to mitigate the UHI and is related to the microclimate study for further study.

UECM of BMA

Finally, the UECM of BMA is shown in Figure 3-19, the lowest wind speed zone (Zone 1) was overlayed with the black hatch areas, and the high-density urban area is shown in the red hatch area. These findings confirm the importance of the weather simulation data which is distributed and covers all the study areas and is the scientific evidence to support urban planning from the viewpoint of environmental impact and urban planning. Compared with a previous study, most of the local climate zone (LCZ) was analyzed and classified based on the land use and land coverage (LULC) classification following Oke's theory (Oke et al, 2018) which is spreading internationally, including in Thai climate study (Khamchiangta and Dhakal, 2020 & 2021; Kamma, 2020; Srivanit, 2011).

The temperature and ventilation zonation maps emerge as significant findings, underscoring that temperature distribution is shaped not only by Local Climate Zones (LCZ) and Land Use and Land Cover (LULC) but also by geographic factors, environmental conditions, and prevailing wind directions. The weather in a given area is intricately linked to the interplay of these diverse influences on the landscape.

This comprehensive understanding of temperature zonation contributes valuable insights into the complex dynamics of urban climates, providing a nuanced perspective beyond the singular impact of LCZ and LULC. By considering the broader environmental context and geographic features, the temperature zonation map enriches our comprehension of how local climate influences manifest in the temperature patterns across different zones within the BMA.
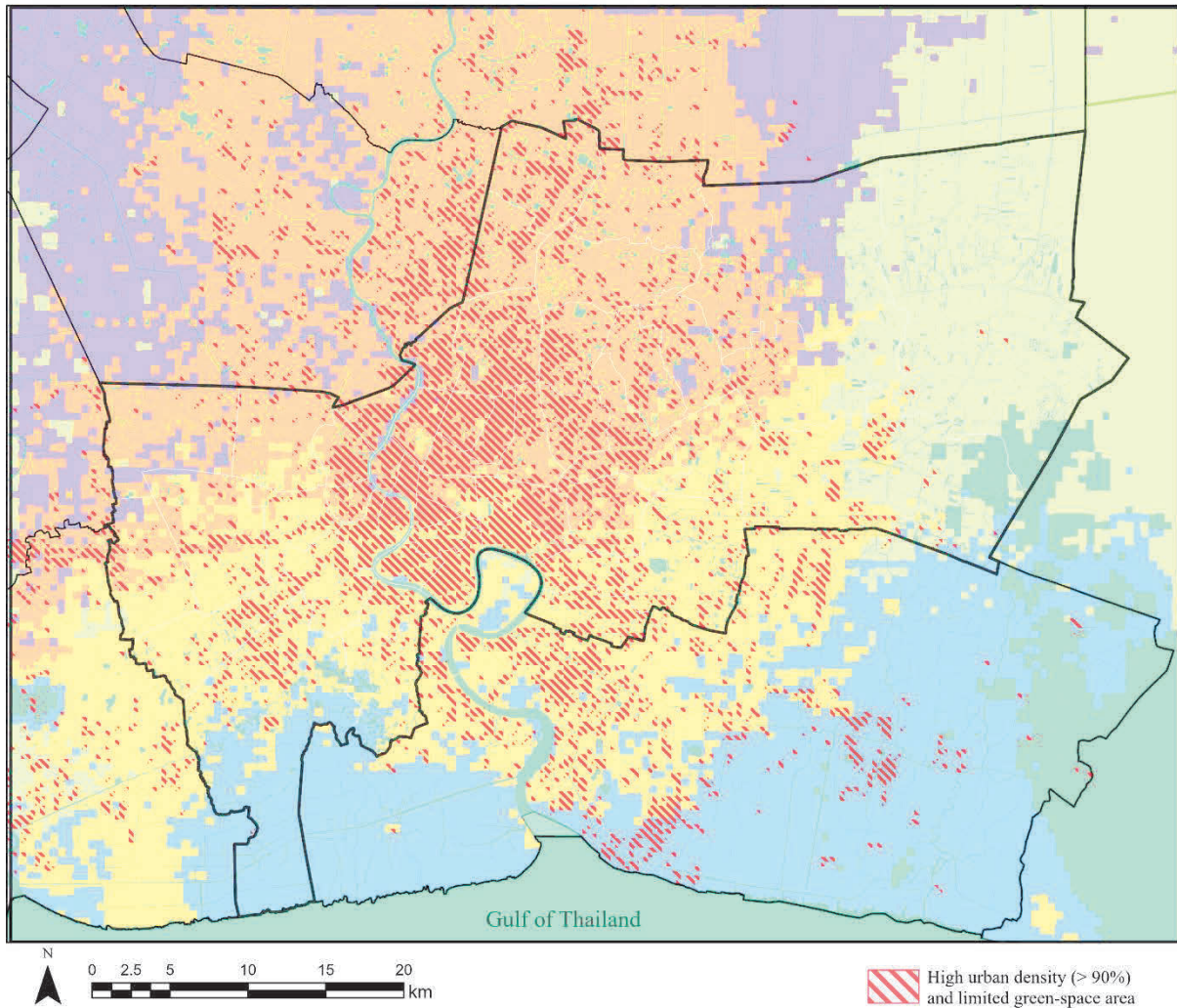
Fig. 3-18 Overlaying the high-density area of UCR to the Bangkok temperature zoning map

Urban Environmental Climate Map of Bangkok
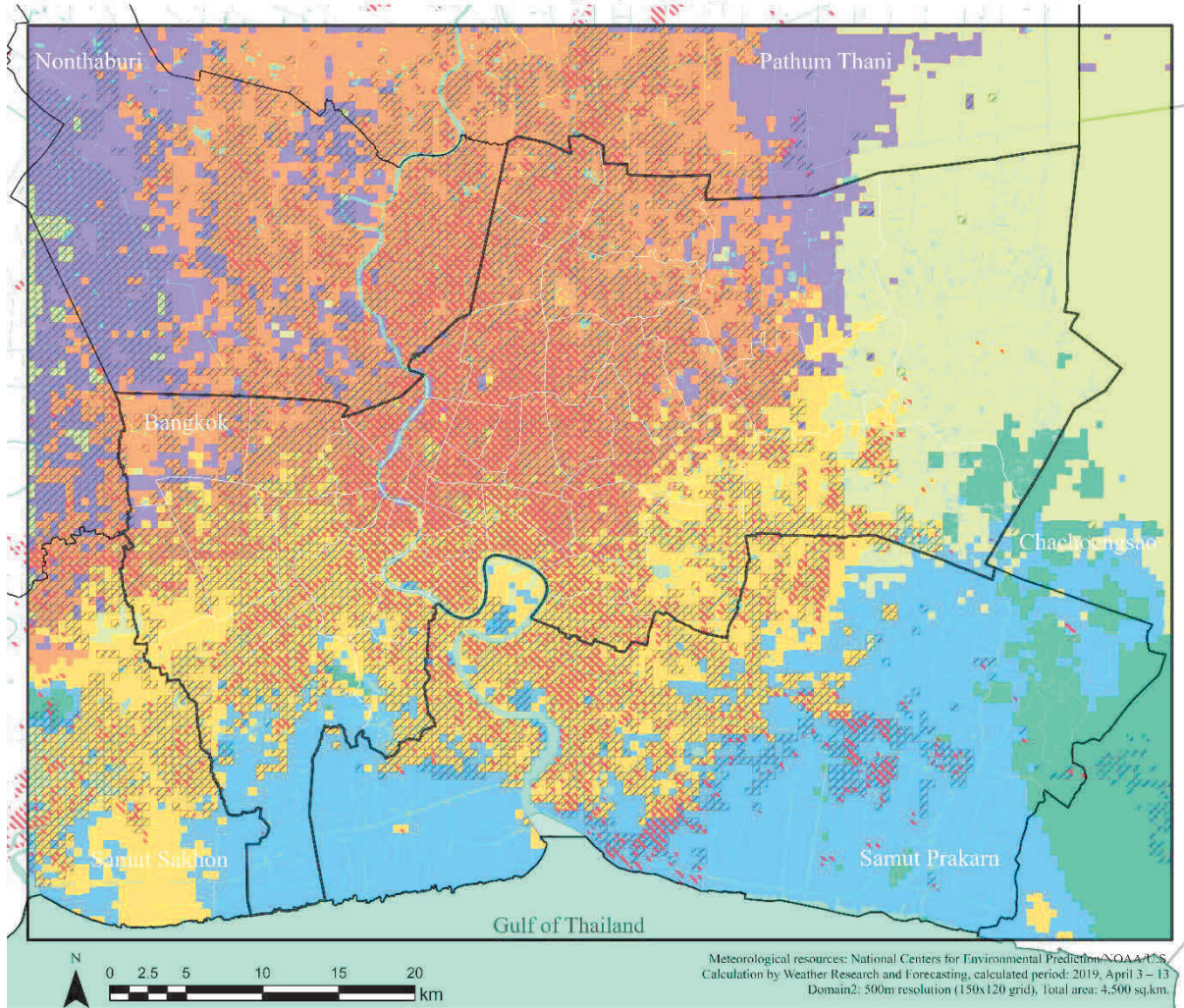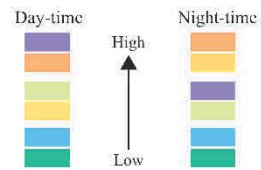
Fig. 3-19 Urban Environmental Climate Map of Bangkok

3.4.4 The Accuracy Assessment of WRF Output

The accuracy assessment of WRF output was verified. The result from Figure 3-20 shows a high correlation between the results from WRF calculation and observation data in the temperature distribution data. Related to 40 samples of the observation station per period, the correlation coefficient was 0.68 and 0.77 with the R-square values 0.46 and 0.59 respectively. The output from the WRF model had a higher value than the observation data in both periods, especially in the afternoon. The assumption is the difference of scale and relevant variables between the point stations and the 500 m resolution area from the WRF output. Conversely, related to the wind speed data (4 samples from the national weather stations), the correlation coefficient at 1 P.M. was high (0.61) with the R-square value 0.37, but low at 1 A.M. Wind direction of both periods was from the southwest to southeast. The assumption is both stations are influenced by microscale variables. At Station 58, the observation data was low because the wind was blocked from a huge building (the National Convention Hall). At Station 7, it had an opposite correlation between the two periods. The open space in the direction of diurnal wind allowed higher wind speed than the nocturnal wind speed that was blocked by the surrounding buildings. The correlation between wind speed data is shown in Figure 3-21 and Figure 3-22 illustrates the wind direction of Stations 7 and 58.

In addition, the comparison of two outputs from two methodologies in the meso scale of Bangkok climate analysis (Figures 1-6 and 1-7) revealed the different climate conditions, especially in the value of wind speed, in some areas. The density of urban areas and building coverage influence the decreasing wind speed even though the area is along the coastline. Therefore, this complex area could be considered for improving ventilation.

Moreover, this comparison emphasized and supported the dissertation methodologies, which aim to apply several urban climate methodologies for understanding the urban climate in the climate data-scarce environment in tropical regions. However, each methodology had strengths and weaknesses. The strength of utilizing the actual observation data from the local government and stations and the clarification of the spatial surrounding environment of the stations tailored the map properly to this target area. Nevertheless, it is noteworthy that the distribution of weather stations is inadequate for understanding the entire region; instead, a majority of the stations were concentrated within the districts of Bangkok.

On the other hand, the strength of utilizing the conventional methodology for precise calculating climate characteristics with publicly accessible data is easily applicable to other cities. However, the accessible information to everyone regardless of local characteristics or relationship to the study area. In summary, the combination of both methodologies filled the limitations of each other and was the suitable developed research methodology.
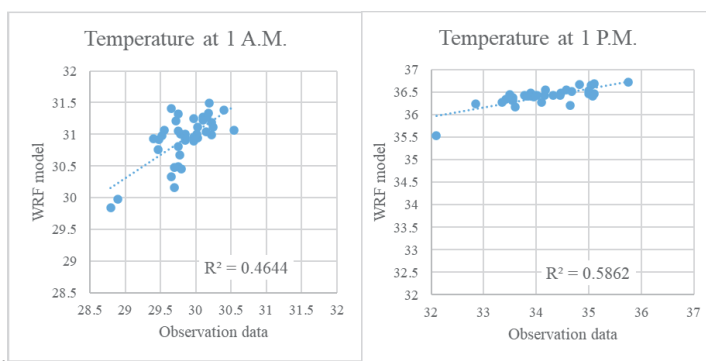
Figure 3-20 Correlation between the results from WRF output and observation data (temperature)
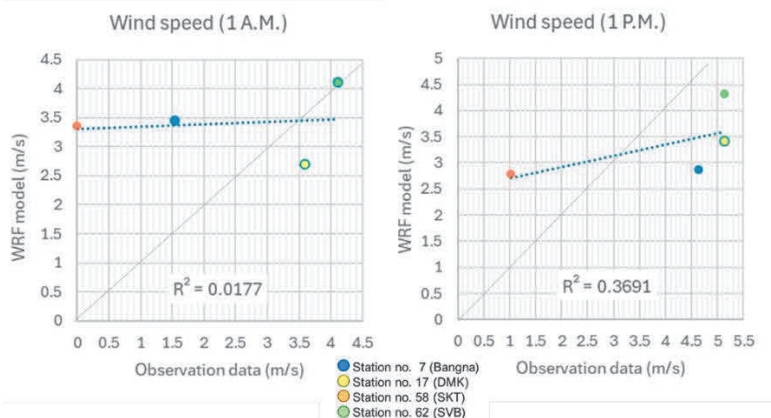
Figure 3-21 Correlation between the results from WRF output and observation data (wind speed)
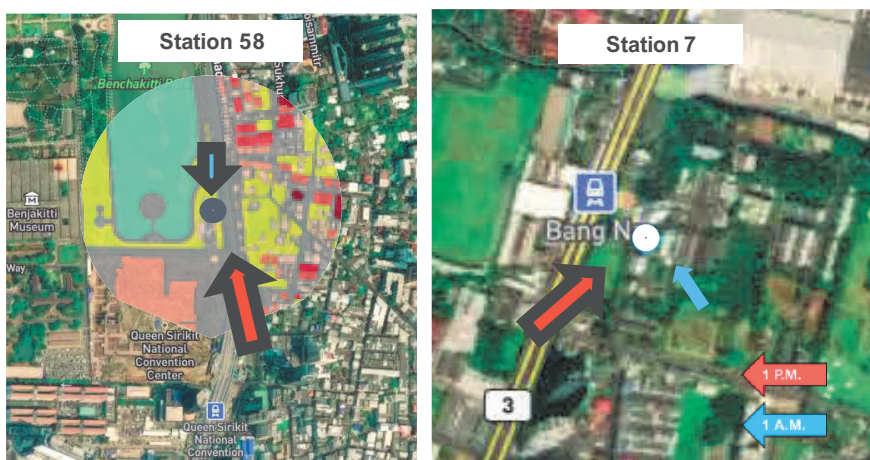
Figure 3-22 Wind direction in two low wind speed stations.

3.5   Conclusion

This chapter advances the understanding of Bangkok Metropolitan Area's (BMA) meso-urban climate characteristics during the summer, focusing on temperature and wind distribution. Utilizing numerical calculations with the WRF model and cluster analysis, this study synthesizes scientific data and statistics to create temperature and ventilation zoning maps. The integration of these maps, along with insights from the preceding chapter, culminates in the creation of the Urban Environmental Climate Maps (UECM) for BMA.

The primary findings include:

1. The UECM provides a comprehensive overview of BMA's spatial and temporal temperature zoning, ventilation characteristics, and high-density urban areas. The six temperature zones, ranging from central Bangkok (Zone 1) to the rural east (Zone 4), reveal the diversity of Meso-climate phenomena.

2. Implications extend to future urban planning endeavors, emphasizing the need for targeted strategies in areas with poor ventilation and high-density urban development. This scientific evidence underscores the role of weather simulation data in informed urban planning decisions, considering environmental impact and local climate conditions.

3. The key findings can be simplified in the form of maps depicting current conditions and projected environmental impacts, fostering understanding and awareness of critical climate areas on the actual provincial scale with specific critical areas.

4. These insights have the potential to guide urban environment enhancements, offering valuable perspectives on urban heat mitigation and adaptation. The precise climate data collected in this study serves as a foundation for future urban climate inquiries, contributing to accurate city planning and sustainable development. The study lays the groundwork for informed decision-making in creating sustainable and climate-resilient urban environments in Bangkok. Furthermore, the methodologies employed can be adapted to other cities or refined for higher resolutions, potentially operating at a district scale.

In summary, this chapter clarified the precise microclimate of BMA and highlighted the severe area with a high temperature and low wind speed along the day. In terms of practical framework, these combined methodologies provide a nuanced understanding of temperature and wind distribution in the climate data-scarce environment of Thailand and other developing countries in tropical regions.

3.6   Limitations and Further Study

The study found obstacles and weaknesses that could provide improvements for future studies. The limitations of this study and topics for further study are as follows:

1. **Data Resolution:** The precision of UECMs hinges on the resolution of input data, such as weather simulations and land-use maps. Utilizing higher-resolution data sources holds the potential to significantly improve the accuracy of temperature and wind speed predictions.

2. **Temporal Dynamics:** This study predominantly addresses diurnal variations, providing a snapshot of daily urban climate patterns in summer. Future research should expand its scope to explore seasonal changes and long-term trends, offering a more comprehensive understanding of urban climate dynamics.

3. **Future Study Area**: Moreover, in response to the main objective of this research, this chapter's findings lead to the focused areas which are the critical areas of Bangkok microclimate which is located in the center.

In summary, addressing these limitations and pursuing suggested avenues for future research will contribute to the refinement and applicability of UECMs, ensuring their utility in guiding sustainable urban development in Bangkok and beyond.

References

Department of Public Works and Town & Country Planning. (2020). GIS data of land use of the Bangkok Metropolitan Region and surrounding.

Department of City Planning and Urban Development, BMA. (2020). GIS data of land use in Bangkok.

Fei, Chen., Hiroyuki, Kusaka., Robert, Bornstein., Jason, Ching., C., S., B., Grimmond., Susanne, Grossman-Clarke., Thomas, Loridan., Kevin, W., Manning., Alberto, Martilli., Shiguang, Miao., David, J., Sailor., Francisco, Salamanca., Haider, Taha., Mukul, Tewari., Xuemei, Wang., Andrzej, A., Wyszogrodzki., Chaolin, Zhang., Chaolin, Zhang. (2011). The integrated WRF/urban modelling system: development, evaluation, and applications to urban environmental problems. International Journal of Climatology, doi: 10.1002/JOC.2158.

Giorgos, Papangelis., Maria, Tombrou., A., Dandou., Themis, Kontos. (2012). An urban "green planning" approach utilizing the Weather Research and Forecasting (WRF) modeling system. A case study of Athens, Greece. Landscape and Urban Planning, doi: 10.1016/J.LANDURBPLAN.2011.12.014

Kamma, J., K. Manomaiphiboon, N. Aman, T. Thongkamdee, S. Chuangchote, & S. Bonnet (2020). Urban heat island analysis for Bangkok: multi-scale temporal variation, associated factors, directional dependence, and cool island condition. *Science Asia, 46*, 213-223. http://dx.doi.org/10.2306/scienceasia1513-1874.2020.024.

Khamchiangta, D., & S. Dhakal (2020). Time series analysis of land use and land cover changes related to urban heat island intensity: Case of Bangkok Metropolitan Area in Thailand. *Journal of Urban Management, 9(4)*, 1-12. https://doi.org/10.1016/j.jum.2020.09.001.

Khamchiangta, D., & S. Dhakal (2021). Future urban expansion and local climate zone changes in relation to land surface temperature: Case of Bangkok Metropolitan Administration, Thailand. Urban Climate, 37, 100835.

Matsuo K., & T. Tanaka (2019). Analysis of spatial and temporal distribution patterns of temperature in urban and rural areas: Making urban environmental climate maps for supporting urban environmental planning and management in Hiroshima. *Sustainable Cities and Society, 47*, 1-22. https://doi.org/10.1016/j.scs.2019.01.004.

National Center for Atmospheric Research (NCAR), Mesoscale and Microscale Meteorology Division & UCAR/NCAR/CISL/TDD. (2023). WRF Model Software (3.9.0) [Computer software]. Retrieved from http://www.wrf-model.org

National Center for Atmospheric Research (NCAR), Mesoscale and Microscale Meteorology Laboratory. (2023) Weather Research & Forecasting Model (WRF). Retrieved from https://www.mmm.ucar.edu/models/wrf.

National Centers for Environmental Prediction (NCEP), National Weather Service/NOAA/U.S. Department of Commerce. 2000, updated daily. *NCEP FNL Operational Model Global Tropospheric Analyses, continuing from July 1999*. Research Data Archive at the National Center for Atmospheric Research, Computational and Information Systems Laboratory. https://doi.org/10.5065/D6M043C6. Accessed 10 November 2022.

Oke, T.R., G. Mills, A. Christen, & J.A. Voogt (2017). Urban Climates. 1st edition, Cambridge, United Kingdom: Cambridge University Press.

Srivanit, M., & H. Kazunori (2011). The influence of urban morphology indicators on summer diurnal range of urban climate in Bangkok metropolitan area, Thailand. *International Journal of Civil & Engineering, 11(05),* 34-46.

Srivanit, M., Jareemit, D., Liu, J. (2022). A Classification Urban Precinct Ventilation Zones Using Key Indicators of Spatial Form: Case Study in Bangkok. In: Kang, T., Lee, Y. (eds) Proceedings of 2021 4th International Conference on Civil Engineering and Architecture. Lecture Notes in Civil Engineering, vol 201. Springer, Singapore. https://doi.org/10.1007/978-981-16-6932-3_39.

Chapter 4
Field measurements in
Two Central Business Districts of Bangkok

Contents

4.1   Introductions

4.2   Objectives

4.3   Methodologies and Materials

    4.3.1 Study Area

    4.3.2 Bangkok Climate Conditions

    4.3.3 Detail of the Field Measurement

4.4   Results and Discussions

    4.4.1 Wind data

    4.4.2 Air temperature and black globe temperature data

    4.4.3 Surface temperature data

    4.4.4 Field measurement design planning

4.5   Conclusion

4.6   Limitation and Direction of Future Study

    References

4.1   Introductions

Decades of empirical investigations have unequivocally established the dynamic nature of climatic fluctuations, manifested both at the global and regional scales. Urban Heat Islands represent a pervasive and pressing global challenge (Schwarz et al., 2012; Oke et al., 2017). As mentioned in the research background in Chapters 1 and 2, this phenomenon disproportionately affects metropolises with populations exceeding one million inhabitants, including Bangkok, Thailand. Understanding and addressing the intricacies of UHIs becomes an imperative task for urban planners, policymakers, and researchers alike, given the pronounced ramifications these thermal anomalies exert on local climates and environmental stability.

Field measurements employ a traditional approach to analyzing urban microclimates using conventional meteorological measurement devices (Rizwan et al., 2008; Santamouris, 2007; Mill et al., 2014). Field observations began in the early nineteenth century with Luke Howard's work (Oke, 2018). Data was collected daily over 25 years, providing a significant knowledge base for the study of urban climates. This methodology is still popular and is a fundamental step in understanding the present climate situation in each area. Since the early 2000s, the development of realistic urban microclimate models, advanced computational resources, and numerical simulation approaches has become increasingly popular (Souch and Grimmond, 2006; Arnfield, 2006; Blocken, 2015). However, observations continue to play a central role in evaluating urban climate effects and developing an understanding of the responsible processes. Given the growth in the number and size of cities, the relative paucity of urban meteorological stations, and the need for regular atmospheric observations in cities, it is more crucial than ever.

Previous research on the climate of the Bangkok Metropolitan Region, which includes Bangkok, has demonstrated that urban characteristics vary with location and spatial environments. Various outcomes and relationships exist between the climate and the surrounding urban environment (Matsuo and Tanaka, 2019; Srivanit and Kazunori, 2011). Although recent research data (Srivanit and Kazunori, 2011; Khamchiangta and Dhakal, 2020) have been gathered from studying the UHI of Bangkok, Thailand, to date, few studies have considered urban ventilation and actual air temperature. Most studies have used surface temperature due to resource and budget limitations (Toparlar et al., 2017).

In addition, the lack of climate data in inner-urban areas necessitates further research into the urban climate analysis of the central business districts (CBDs) of Bangkok to comprehend and guide its application in urban planning. A dearth of climate data within inner urban areas necessitates a more comprehensive exploration into the analysis of urban climate within the CBDs of Bangkok. Such an endeavor is essential for a deeper understanding and the informed application of findings in the realm of urban planning. Bangkok's expansion has caused environmental issues such as air pollution, excessive urban heat, and weak ventilation, especially in the inner urban area of Bangkok or central district business (CBD).

Related to the previous chapter, which studied and created the Bangkok Environmental Climate Zoning Map and specified the critical area from the urban heat island phenomenon (Figures 3-19 and 3-20), this chapter continued the study in the Bangkok Metropolitan Area on other scales and methodologies. Therefore, to study the microclimate of Bangkok from Chapters 4 to 6, the hypothesis is "Each area within a similarly critical area of the mesoscale climate zone had different local climate zones related to the urban topography and microscale spatial variables in the viewpoint of UHI mitigation".

Therefore, there are three conditions for selecting the target areas; (1) located in a similar critical zone (had high temperatures and low wind speed) from the finding of mesoscale BMA climate: (2) the central business district or downtown which has a high daily traffic populations, high density of urban area, and had a typical urban topography of Bangkok and: (3) for comparison the microclimate characteristics, two different urban topography areas will be selected. Bangkok had four main CBDs at different periods and unique characteristics. However, only two CBDs are located in a similar critical zone (Orange area, Figure 4-1). Subsequently, the Bangkok microclimate was studied in two CBDs, namely the Yaowarat area and the Ratchadamri area. Moreover, Yaowarat and Ratchadamri not only had a similarity in the zone from mesoscale and BMA urban planning, but they also had a similar distance from the coast which is one of the main finding variables that affected diurnal temperature and wind speed.

Within this context, this chapter aims to collect weather data from two CBDs of Bangkok by field measurement. Moreover, it seeks to understand the urban climate of both areas by comparatively analyzing both areas and identifying the unique situation related to the spatial characteristic component of each area. The findings of this study will be one of the important case studies providing insight into the climate field measurement in Thailand and making stakeholders aware of the importance of city weather data collection and data analysis.

Moreover, it could be adapted to other cities or countries and be used to verify the accuracy of numerical calculation in Chapters 5 and 6.

Hence, this chapter is structured into five sections as follows. The first section outlines the objectives. Following that, the material and methodology are introduced, providing information about the study areas, supplementary data, and the detailed field measurements performed to collect weather data in both areas. The subsequent section presents the results and discussions, divided into four parts related to different measurements, along with a discussion of the field measurement design planning in Bangkok. Moving forward, the conclusion is summarized, and, finally, the limitations and directions for future study are outlined.
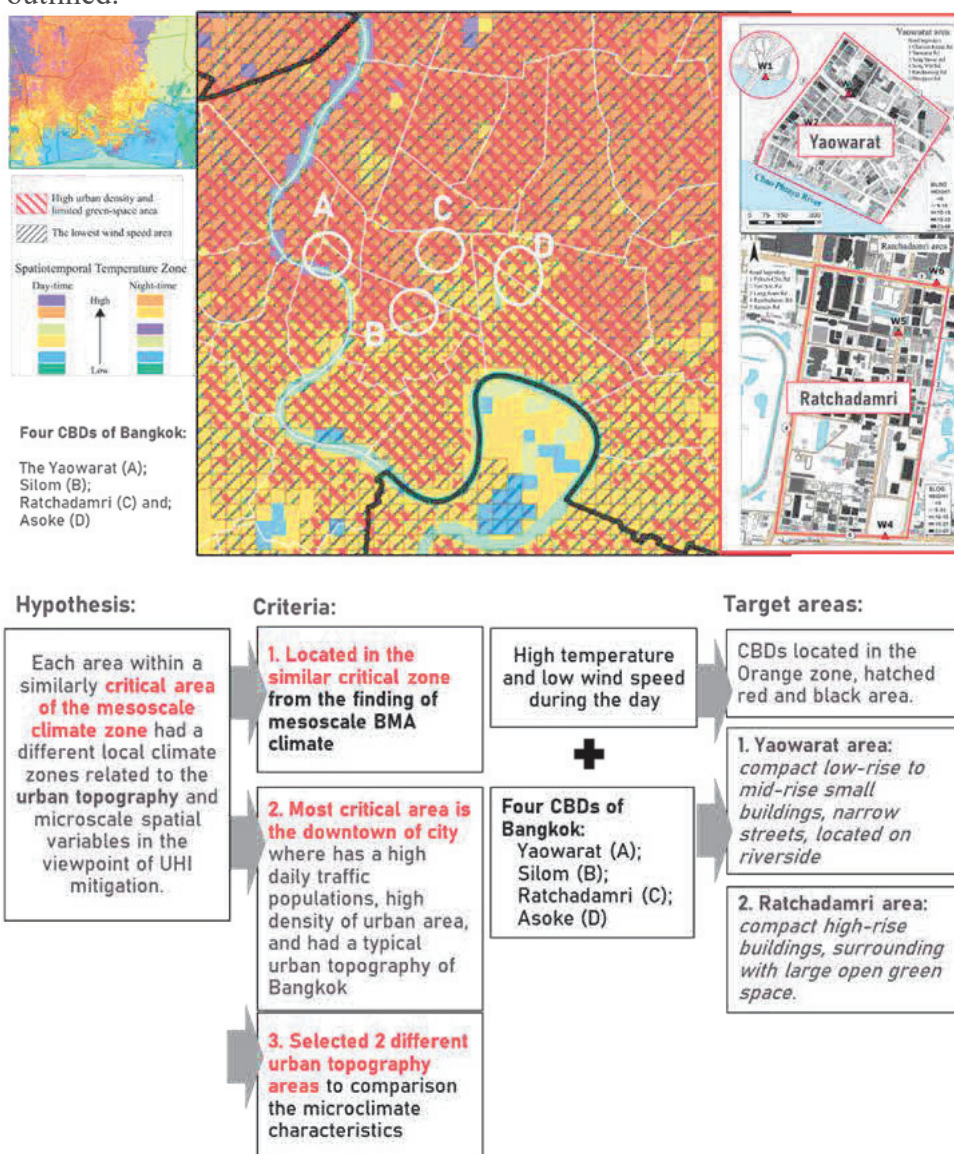
Fig. 4-1 Hypothesis of microclimate study in Bangkok and the criteria to select the study area

4.2 Objectives

1) To collect the field observation data focused on air temperature, surface temperature, and wind distribution data from the two CBDs of Bangkok.

2) To verify the accuracy of the microclimate numerical modeling of Bangkok in Chapters 5 and 6 by using the field observation data.

4.3 Methodology and Materials

To serve the objective, this section is divided into three parts: the study area, Bangkok climate conditions and the field measurement period, and details of the field measurement.

4.3.1 Study area

Bangkok, featuring several CBDs with diverse characteristics, provided the backdrop for this study. To investigate urban climate, two CBDs, Yaowarat and Ratchadamri, both situated in central Bangkok and sharing a similar latitude (13°44'26"N), were selected.

Yaowarat, located in Chakkrawat, Samphanthawong district, is historically significant as Bangkok's original and oldest CBD. Its establishment is closely linked to the creation of two key roads, Charoen Krung Road in 1861, and Yaowarat Road in 1891, solidifying its status as Bangkok's inaugural CBD. Known for its association with the Thai Chinese community, Yaowarat stands as one of the world's largest Chinatowns. Characterized by a dense urban area, featuring 2- to 5-story commercial buildings, small streets, and alleys bustling with shops and vendors, Yaowarat provides a vibrant urban landscape. Bounded by Charoen Krung Road to the north, Song Sawat Road to the east, Song Wat Road to the south along the Chao Phraya River, Ratchawong Road to the west, and Yaowarat Road at its center, this district has maintained its significance over the years. The introduction of a metro line in 2019, particularly the Wat Mangkorn station, has further enhanced accessibility. Presently, Yaowarat remains a bustling commercial hub with high land prices, offering valuable insights into urban ventilation dynamics.

Ratchadamri, located in the Pathumwan district, holds the distinction of having the highest land prices in Thailand in 2022. Emerging as a new economic hub with large real estate projects and high-rise buildings, this area is defined by five main roads: Phloen Chit Road to the north, Ton Son Road to the east, Lang Suan Road in the central, Ratchadamri Road to the west, and Sarasin Road to the south. South of Ratchadamri lies Lumpini Park, one of the largest green spaces in central Bangkok. Established in the 1920s, this inner-city park covers an expansive area and adds a significant green element to the urban landscape.

To investigate urban microclimates in Bangkok, these two areas were chosen for their distinct urban characteristics and high population density. This selection aimed to provide insights into ventilation dynamics and temperature distribution, laying the groundwork for mitigating the UHI effect. The combined study area covered approximately 1.5 square kilometers. Refer to Figure 4-1 for an overview of the location and area of three CBDs in Bangkok—Yaowarat, Silom, and Ratchadamri. Detailed information about the study area and the specific locations of field measurement points can be found in Figures 4-2 and 4-3, respectively.

Fig. 4-2 Study area and fixed station's location in Yaowarat district
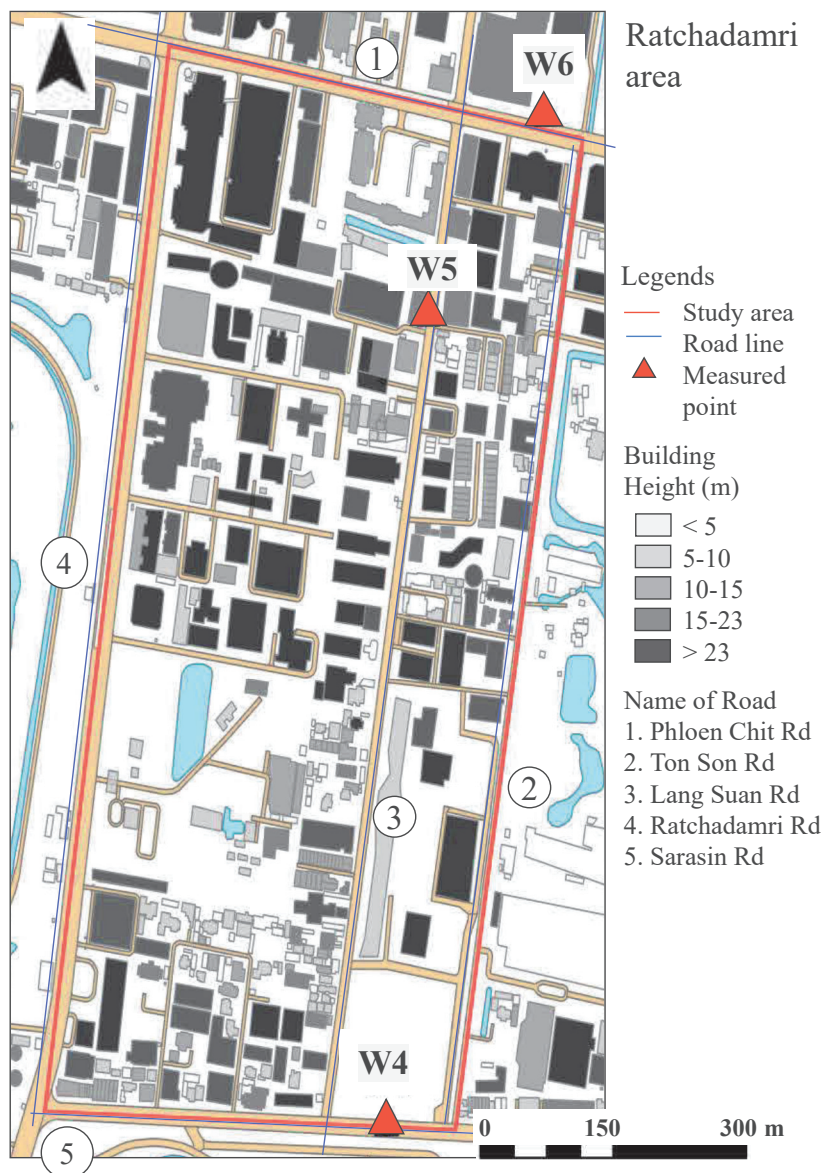
Fig. 4-3 Study area and fixed station's location in Ratchadamri district

4.3.2 Bangkok climate conditions and the period of the field measurement

The timing and season were crucial considerations for the field survey. The optimal conditions for studying the thermal environment, particularly to understand thermal distribution, occur during the summer period in Thailand, spanning from March to May. However, due to the constraints imposed by the COVID-19 pandemic from 2020 to 2021, the field measurement was rescheduled for October 2022. While this period does not represent the peak temperature observed during the hot and humid season (May to October), it still experiences elevated temperatures and is the longest season in Thailand.

To determine the field survey period, weather data for Thailand in 2019 from two stations, Don Muang Airport Station (DMK) and Suvarnabhumi Airport Station (SVB), provided by the Thai Meteorological Department (TMD, 2019), were analyzed. The weather conditions were categorized into three parts:

Temperature Conditions: The highest air temperature (31.9 °C) occurred in April, gradually decreasing until September, with a subsequent rise in October (29.4 °C), marking the period of seasonal transition (see Figure 4-4). Additionally, the average temperature on rainless days showed a peak in May (32.1°C), with a slight increase in October (30.1°C). SVB consistently recorded lower temperatures than DMK due to differences in their surroundings, with SVB situated amidst agriculture and farming industries, while DMK, the original international airport, is surrounded by urban areas.

Comparing average air temperatures and temperatures only during rainless days (FWD) at both stations revealed a similar pattern. During the monsoon season (May to October), temperatures increased by 1–2 degrees, closely resembling the summer season. This comparison underscored the relationship between temperature patterns in the monsoon season and summer.

Rainfall Volumes: SVB experienced the highest rainfall volumes in May, June, and September, while DMK recorded peak volumes in June and October (refer to Figure 4-6). The monsoon season in Bangkok typically brings rainfall volumes ranging from 100 to 200 ml, originating from the southwest direction, directly impacting the Bangkok Metropolitan Region coast. Conversely, the dry season featured rainfall volumes of less than 70 ml, with moisture carried by the cold wind from the northeast.

Wind Speed and Wind Direction: Wind rose diagrams for each month in 2019 (Figure 4-8) illustrated that wind direction shifted from south-southwest (SSW) in summer to south-southeast (SSE) in September and east-southeast (ESE) in October, preceding the onset of winter in November. Wind speeds were higher in summer, averaging around 5 m/s, compared to the winter average of approximately 3 m/s.

In summary, while October shares similarities with summer in terms of high temperatures and fewer rainy days, there are slight differences in wind direction. October was deemed the optimal time for the field survey in Bangkok, considering these conditions. Consequently, the field survey was conducted on October 19, 20, 23, and 24, 2022, aligning with the criteria for "fine weather day" conditions outlined in Chapter 2, which include daily precipitation of less than 1 mm, daylight hours constituting at least 40% of the day, a daily maximum temperature exceeding 30°C, and no rainfall (Oke, 1982; Matsuo and Tanaka, 2019). Weather data were exclusively collected during daylight hours from 8:30 to 17:30.

Average Temperature (2019)

	Jan	Feb	Mar	Apr	May	Jun	Jul	Aug	Sep	Oct	Nov	Dec
SVB	27.5	28.9	29.7	31.5	30.9	29.8	29.1	28.7	28.3	29.4	28.5	27
DMK	27.7	29.7	30.5	31.9	31	29.9	29.7	29.1	28.6	29.4	28.5	27

Average temperature without rainy day (2019)

	Jan	Feb	Mar	Apr	May	Jun	Jul	Aug	Sep	Oct	Nov	Dec
SVB	27.7	28.9	29.7	31.7	32.1	30.4	29.6	29.6	29.7	30.1	28.8	27
DMK	28.8	29.7	30.5	32.1	32.1	30.6	30.6	30	29.7	30.1	28.6	27
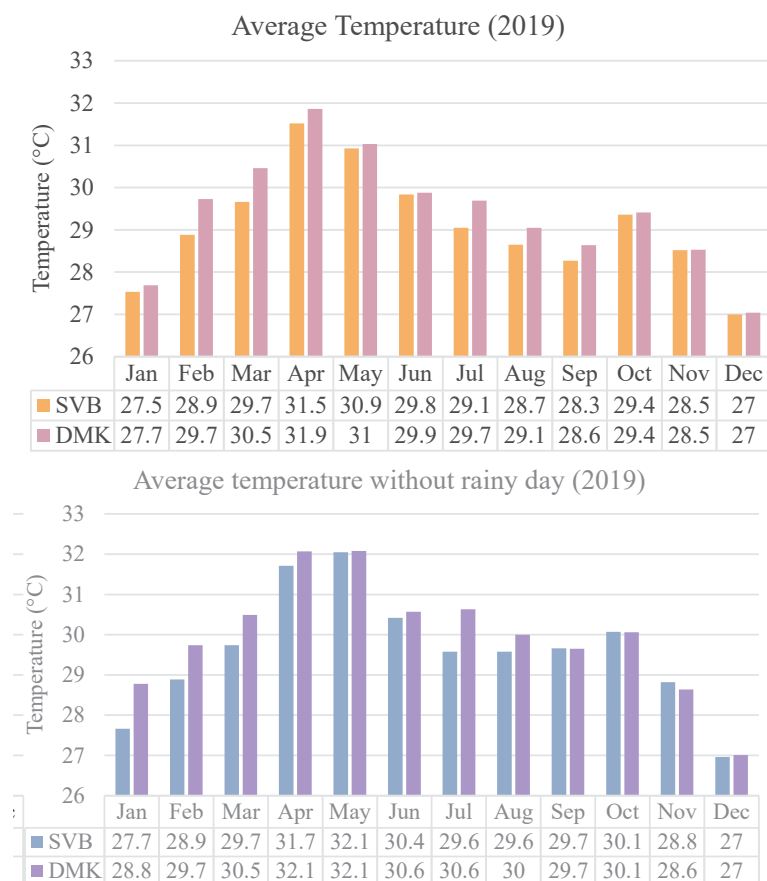
Fig. 4-4 Comparing the average temperature between SVB and DMK

Suvarnabhumi Airport Station (2019)

Don Muang Airport Station (2019)
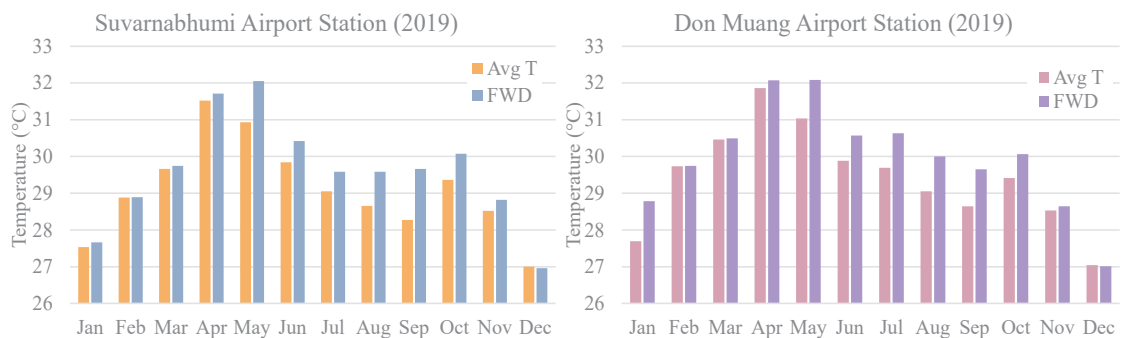
Fig. 4-5 Comparing two conditions of the average temperature,
(left) SVB and (right) DMK

Rainfall volume (2019)

	Jan	Feb	Mar	Apr	May	Jun	Jul	Aug	Sep	Oct	Nov	Dec
SVB	0.6	65.3	10.2	0.2	195.7	55.2	183.8	69.2	173.7	67.1	36.2	0
DMK	0.8	0	0	95.8	119.4	238.5	100.1	98.6	156.7	175.5	10.8	0
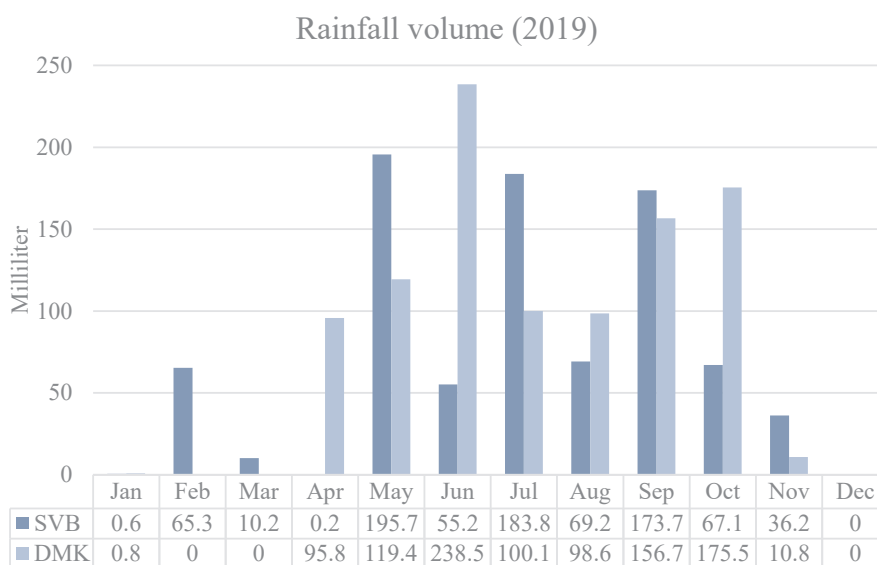
Fig.4-6 Rainfall volumes in 2019
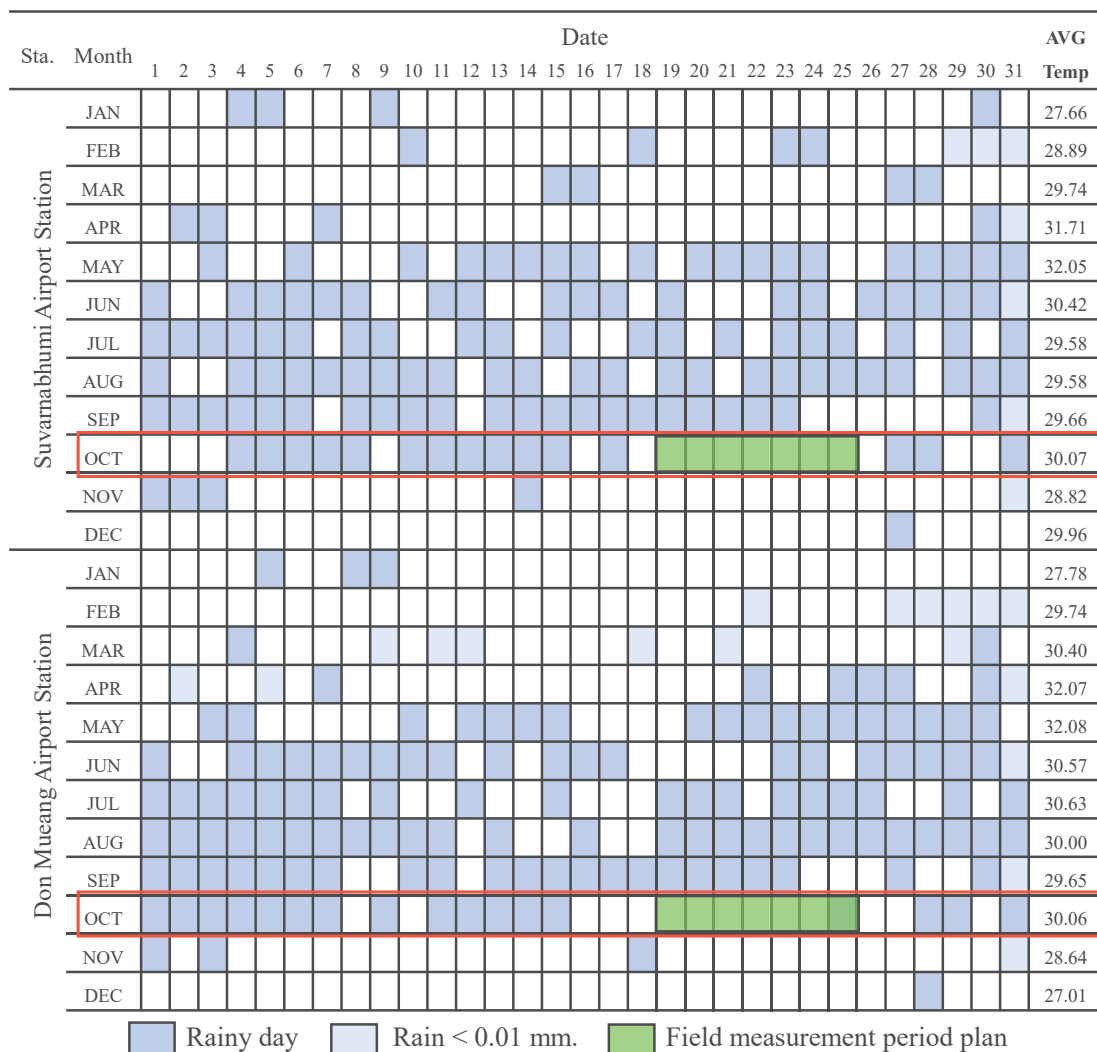
Fig.4-7 The summary of rainy days from two stations in 2019 and the field measurement periods

Fig. 4-8 Windroses of Bangkok in 2019

4.3.3 Detail of the Field Measurements

During the measurement period, four types of weather data were collected, encompassing wind distribution (wind direction and wind speed), air temperature, black globe temperature, and surface temperature. These climate data types were consistent with those used in prior urban climate studies (Matsuo et al., 2019; Oke et al., 2017). Notably, these weather data were acquired through two distinct field measurement methods: fixed observation stations and mobile surveys, each utilizing different tools and equipment illustrated in Figure 4-9.

Fixed Stations:

The fixed-point survey aimed to measure wind data, air temperature, and black globe temperature. Wind speed was assessed using a three-cup anemometer, and wind direction was determined using an arrow-feather wind vane. Measurements were taken at a height of approximately 2 meters from the ground, with a one-second measurement interval. Air temperature was measured with a temperature sensor, shielded against radiation, set at the same level as the wind data collector, also at a one-second interval. The measurement period extended from 8:30 a.m. to 5:30 p.m. Black globe temperature was measured using a temperature sensor with a 75 mm diameter black globe ball.

For the Yaowarat area (W1-W3), three stations were designated: W1, the riverside station with open space and a large garden; W2, an area featuring mid-rise buildings with high density, compact buildings, and narrow roads; W3, a location with high-rise buildings and a wide road. The Ratchadamri area (W4-W6) included three stations as well: W4, an open-space area opposite Lumpini Park; W5, situated on a wide road and surrounded by medium to high buildings; W6, located on a wide road with obstacles and concrete parking lots. Figures 4-10 and 4-11 depict the characteristics of W1-W3 and W4-W6, respectively, while Figure 4-12 illustrates the six fixed stations and their surroundings.

The surface temperature was measured by an infrared thermometer on different materials surrounding the fixed stations (W1–W6). Measurements were taken 10 times per point every hour from 8:30-17:30, using the average temperature during shaded and non-shaded periods. The distance between the equipment and surface material ranged from 2-5 meters, with a 90° angle to the target. Surface materials were categorized into four types: concrete buildings, pavements, asphalt roads, and greenery (tree leaves or grass). W1, located next to the river, also measured the surface temperature of the waterbody. Figure 4-13 provides a conceptual illustration of surface temperature measurements.

Mobile Survey:

A mobile survey was conducted to measure air temperature and black globe temperature. Air temperature was measured using a thermocouple sensor inserted into a naturally ventilated tube covered with aluminum foil on the outer surface tube, with a measurement height of approximately 1 meter. The measurement interval was 1 second, and all equipment was attached to an electric scooter (see Figure 4-14). Additionally, GPS recording was installed on the electric scooter at 1-second intervals. The equipment was driven along six routes (45 spots) in the Yaowarat area and five routes (37 spots) in the Ratchadamri area, as shown in Figures 4-15 and 4-16. Each target spot was measured for 5 minutes at five intervals throughout the day (8:30, 10:30, 12:30, 14:00, and 17:30), resulting in five rounds of mobile surveys per day for each CBD.

Equipment figure	Name	Measurement
	Temperature sensor Tr52-i: Thermal record TR-5106 Fluoropolymer coated sensor	Air temperature (Fixed-point survey) Black globe temperature (Fixed-point and mobile survey)
	Thermocouple Tr55-i: Data recorder AD-1214 K type thermocouple sensor	Air temperature (Mobile survey)
	Black globe 75 mm.	Black globe temperature (Fixed-point and mobile survey)
	Solar radiation cover	Air temperature (Fixed-point and mobile survey)
	Three cup type wind speed Wind vane direction	Wind speed and wind direction (Fixed-point)
	Hobo recording set	Recording the wind data (Fixed-point)
	Infrared Thermometer: HORIBA IT-550	Surface temperature (Fixed-point)
	GPS: Garmin: etrex 10J	Confirm the measurement spot (Mobile survey)

Fig. 4-9 Field measurement tools and type of equipment
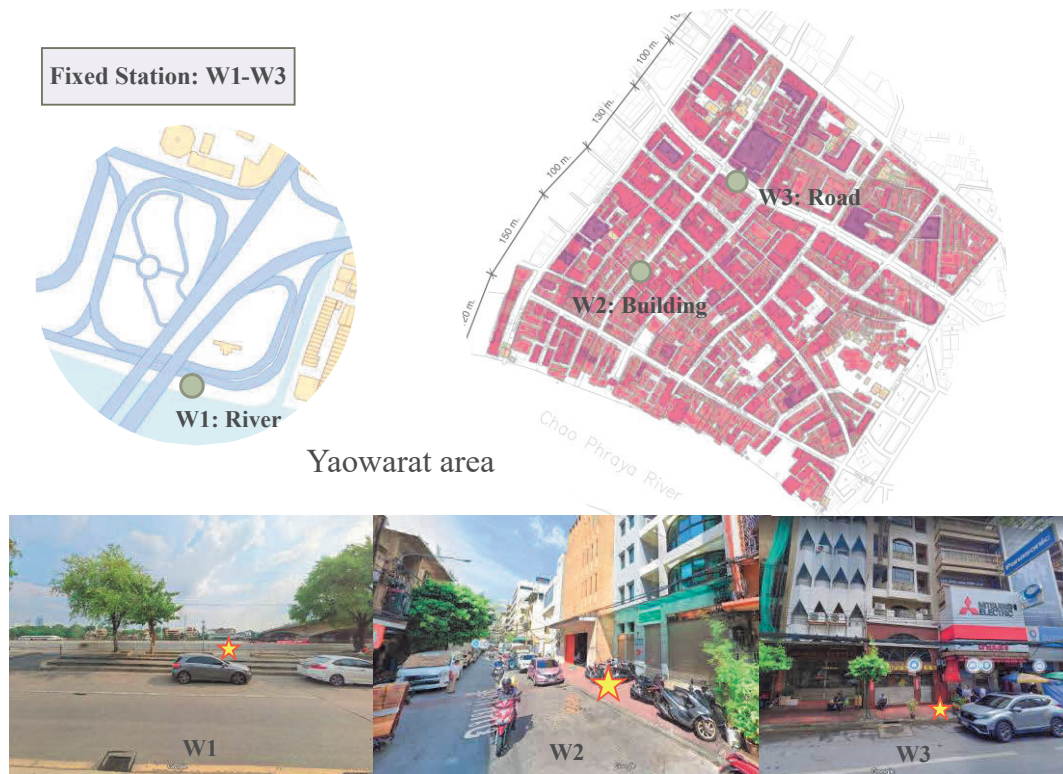
Fig. 4-10 Three fixed stations in the Yaowarat area
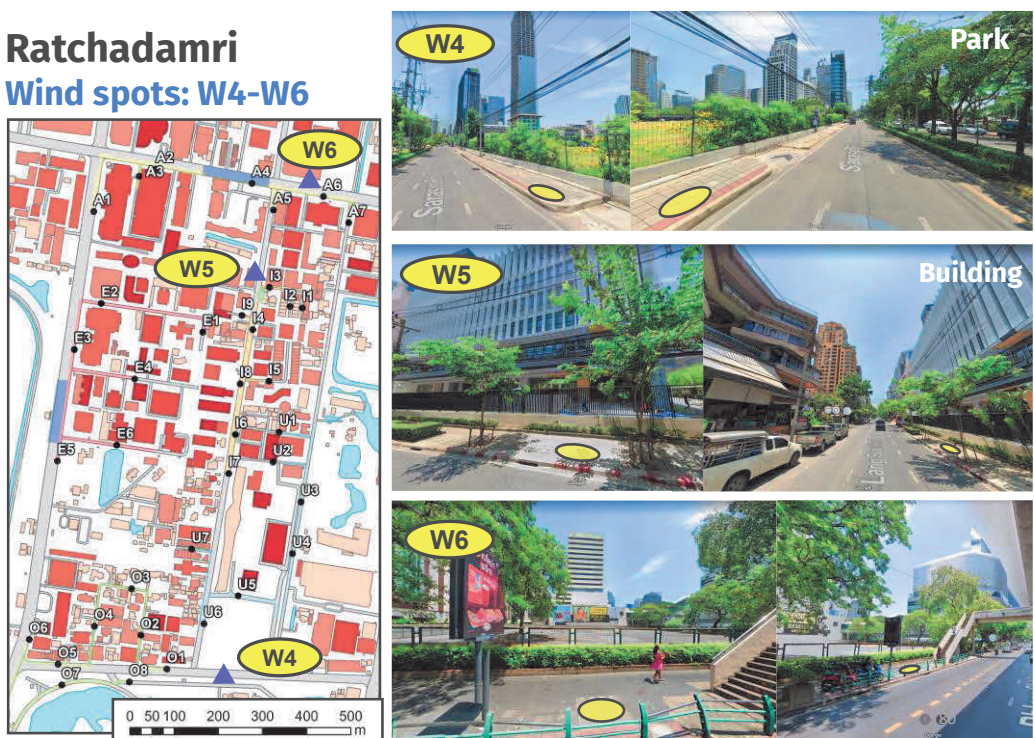
Fig. 4-11 Three fixed stations in the Ratchadamri area (W4-W6)

W1　　　　　　　　**W2**　　　　　　　　**W3**

W4　　　　　　　　**W5**　　　　　　　　**W6**

W1　　　　　　　　**W2**　　　　　　　　**W3**

W4　　　　　　　　**W5**　　　　　　　　**W6**

Building Height (m)

□ < 5　　□ 5-10　　□ 10-15　　□ 15-23　　■ > 23
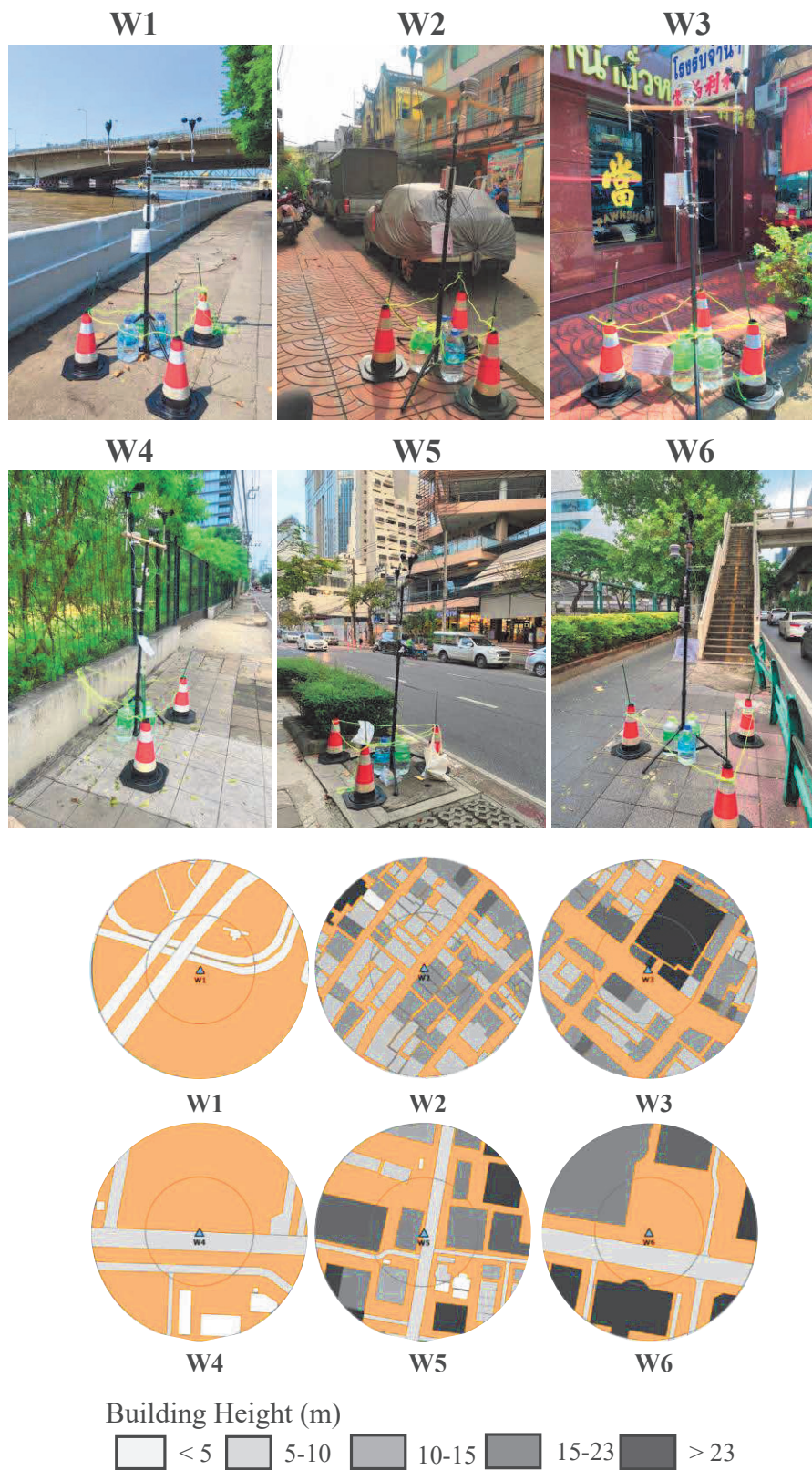
Fig. 4-12 Six fixed-point stations and their surroundings
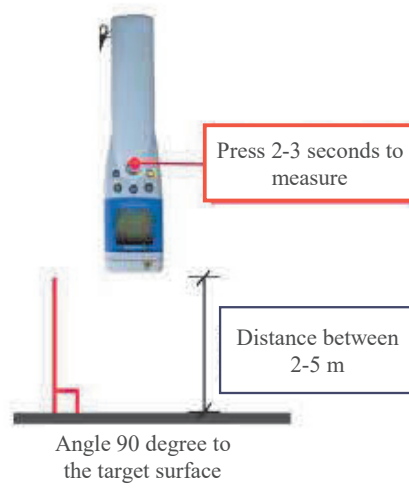
Fig. 4-13 The surface temperature measurement at the fixed point
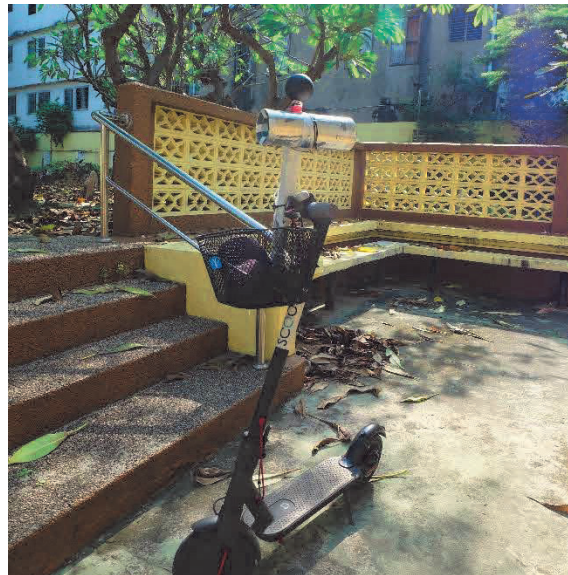
Fig. 4-14 Mobile survey by the electrical scooters in Bangkok
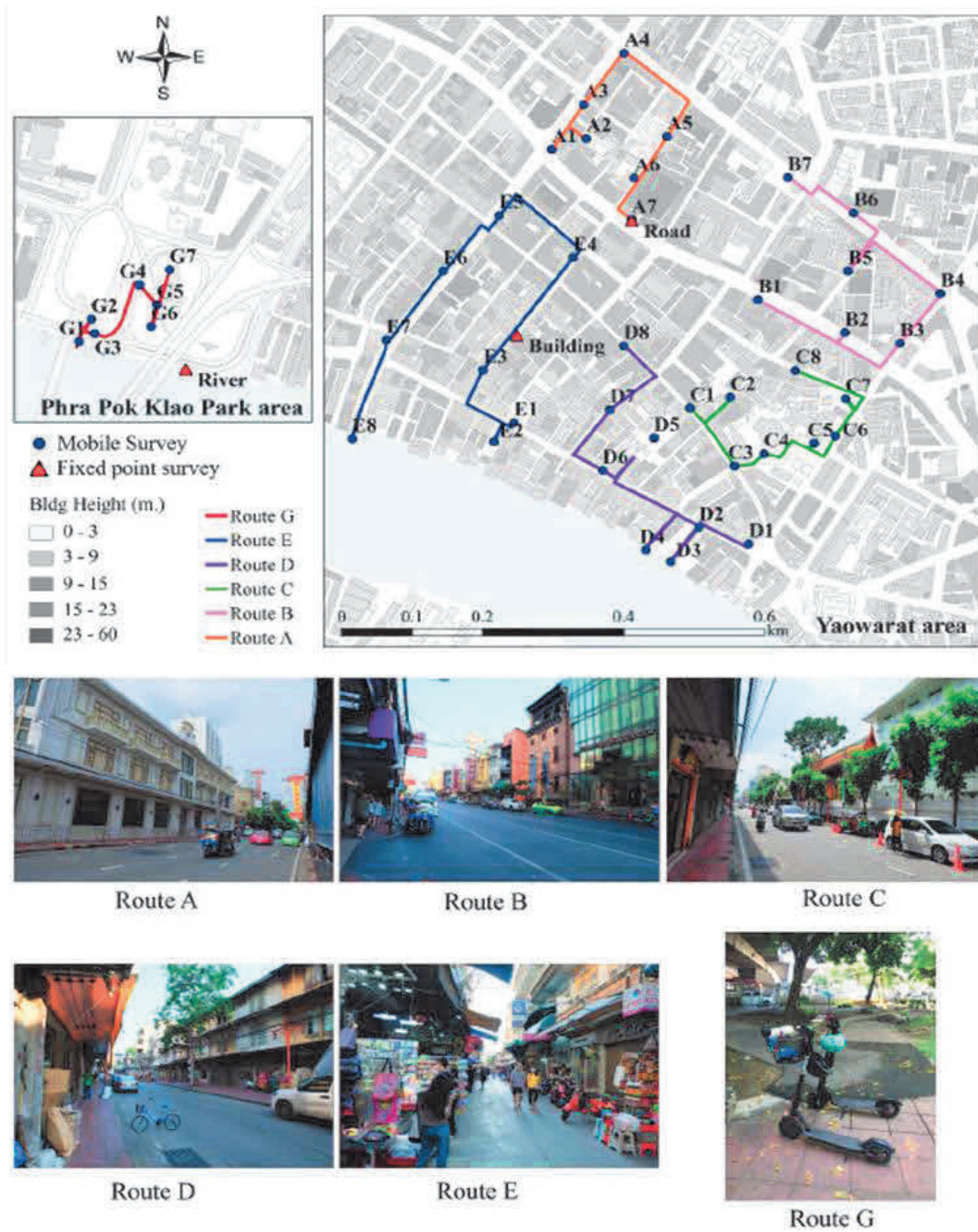
Fig. 4-15 Spots and routes for the mobile survey in the Yaowarat area
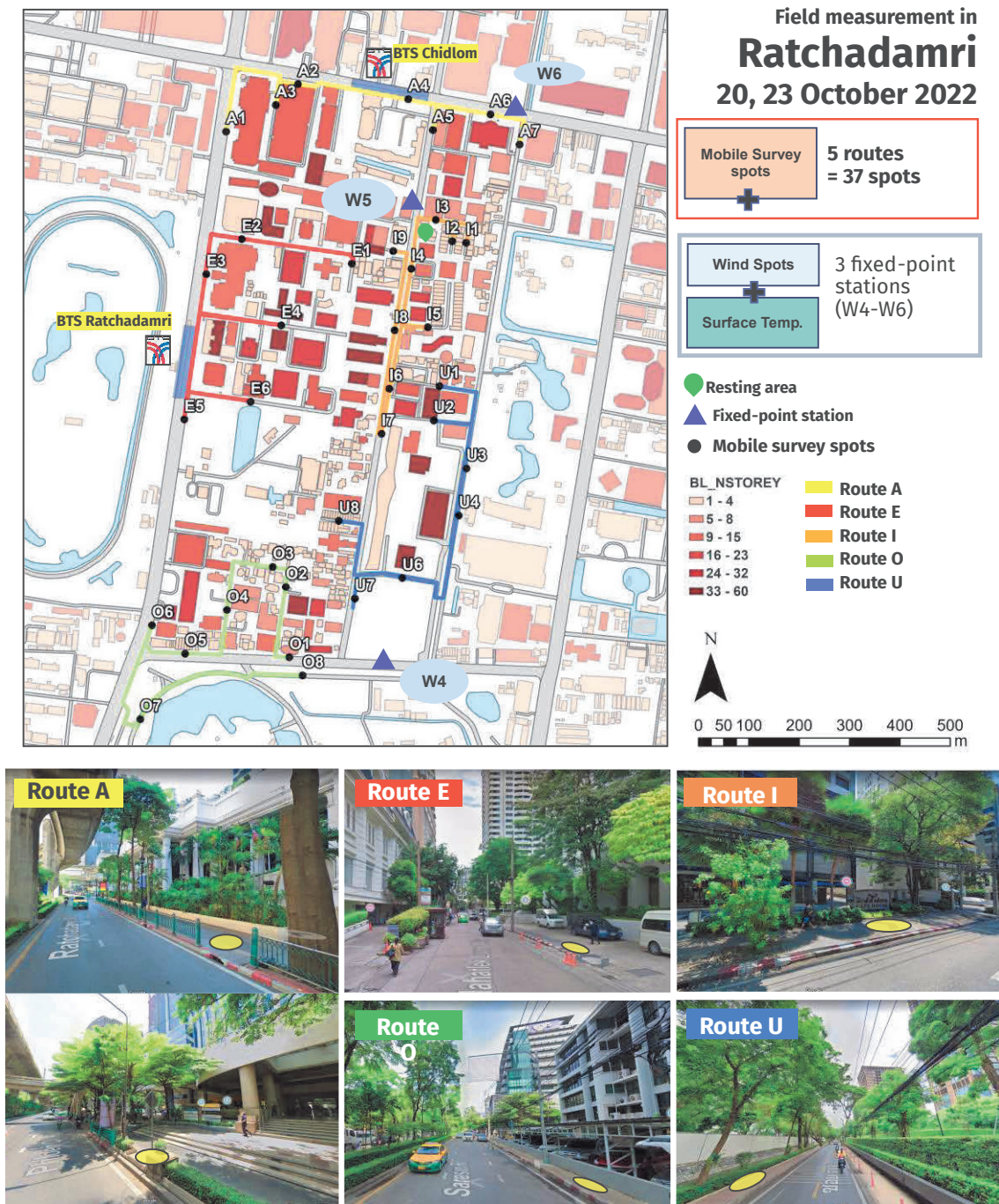
Fig. 4-16 Spots and routes for the mobile survey in the Ratchadamri area

4.4 Results and Discussions

This chapter presents its findings in four distinct sections. The first three parts detail the results of each climate data classification in each CBD, while the fourth part discusses the field measurement design planning and criteria.

4.4.1 Wind data

Examining the field measurement results from the six fixed stations, illustrated in Figure 4-17, surface areas represent wind velocity (WV) with continuous variables indicated on the left vertical axis, and dots represent wind direction (WD) shown with discrete variables on the right. Both CBDs exhibited poor WV, resembling prevailing wind patterns. WD from the six stations showed two distinct patterns: consistent wind direction throughout the day and a shift in wind direction around 14:00. Some stations exhibited different directions, such as South and West (e.g., W3), influenced by specific characteristics of each measurement point's surroundings, particularly road orientation.

Yaowarat featured a mix of compact low-rise to mid-rise structures. The prevailing WD in Yaowarat was from the North and East, as evidenced by the results of W1, located without surrounding obstacles and parallel to the Chao Phraya River. However, it is crucial to acknowledge that the inner urban area can exhibit varying WD, influenced by factors like urban layout, road orientation, and specific measurement locations, as indicated in prior research (Oke et al., 2017). The approach flow around urban buildings is disrupted by upwind structures, resulting in a complex wind pattern, manifested in distinctive flow patterns within urban canyons. For instance, W3 exhibited mostly the South wind direction, situated behind the building line perpendicular to the approach flow (ENE–E), creating a recirculation vortex that reversed the WD.

Ratchadamri showcased a mix of compact mid to high-rise and open high-rise buildings. In the Ratchadamri area, W5 recorded the highest WV on both days, while W4 had the lowest. Despite WV patterns between W4, W5, and W6 in Ratchadamri, the WD from three points did not align with Bangkok's prevailing wind, mostly originating from the North and West.

The highest WV among the six stations was observed around the riverside. W1, representing an open area, exhibited the highest average WV at 1.08 m/s, with the maximum WV occurring in the afternoon at 2.74 m/s. In contrast, both W2 and W3, situated amidst shophouses and buildings characterizing the Yaowarat urban topography, had significantly lower WV values, almost reaching 0 m/s (0.06 and 0.23, respectively). Despite the road being parallel to the wind's direction (W2), wind penetration through the urban area was hindered by compact low-rise buildings. The advantage of the riverside area, characterized by its high WV, could be enhanced if more open spaces were created adjacent to the riverside areas, enabling the river's winds to flow through the inner urban region via wider roads, thereby significantly benefiting Yaowarat.

Considering the results of field measurements and urban topography, W1 and W4 both represent open space areas. However, a curious question arises regarding why W4 exhibits a high OSR but a lower WV compared to W1, despite having a similar environmental context. Regarding W4, despite its lack of immediate building surroundings, its proximity to a 4-meter-high linear stretch of bushes (Fig. 4-12) is a notable micro-level factor impacting its WV. Verification of these issues should be pursued through other methodologies such as numerical calculations via computer fluid dynamic simulation.
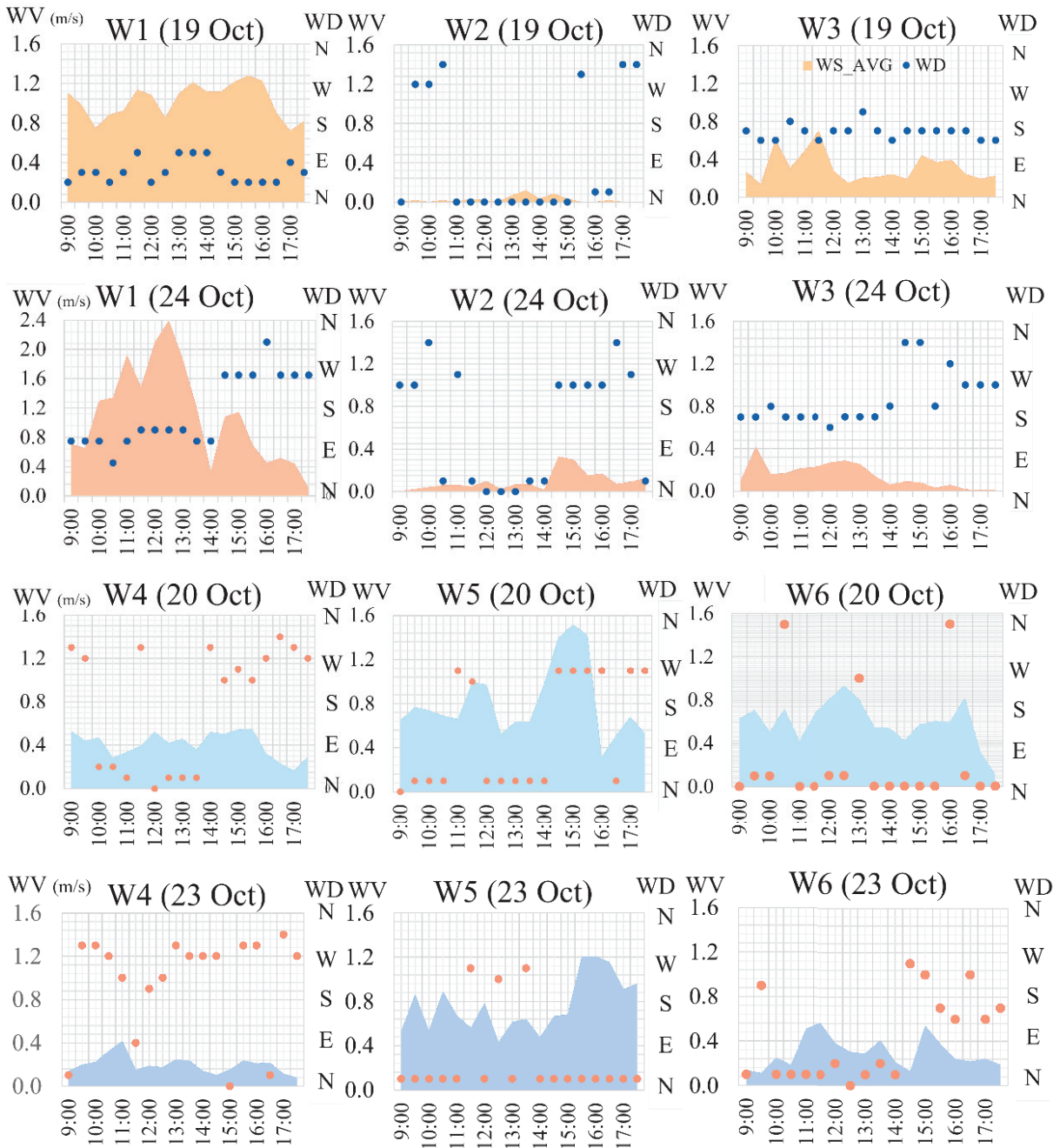
Fig. 4-17 Wind data from six fixed stations in four days of actual measurement

4.4.2 Air Temperature and Black Globe Temperature Data

        This section focuses on the collection and presentation of air temperature and black globe temperature data, utilizing two distinct measurement methods—the mobile survey for temperature distribution across various areas and data from fixed stations to elucidate the interplay between temperature, time, and the surrounding environment. The tables and figures (Tables 4-1 to 4-4, Figures 4-18 to 4-23) offer a comprehensive overview of the collected data.

        Temperature in the Yaowarat Area:

        In Yaowarat, air temperature from fixed stations displayed a consistent pattern over two days. W1 recorded the lowest temperature throughout the day, while W3 experienced some of the highest temperatures (Figure 4-18). The peak temperature occurred around, ranging from approximately 29–33°C, reaching almost 36°C at W3.

        Results from the mobile survey, presented as average values per survey time and location, indicated lower morning temperatures in the northwest area compared to the southeast area. The latter maintained relatively high temperatures throughout the day. Figure 4-19 highlights hot spots in Yaowarat, particularly at 11 a.m., where A7 and B1-B4 recorded the highest temperatures (33.5–35.3°C). Notably, spots A1, A7, and B2, receiving direct sunlight, exhibited higher temperatures than B1, shaded by a nearby building. By 1 p.m., the highest temperatures expanded to surrounding spots, predominantly in routes A and B. This thermal expansion continued at 3 p.m., with spots in routes A and B maintaining high temperatures, and spots in route D experiencing increased air temperatures.

        Adjacent to the riverside area, spots G1 and E8, lacking parking facilities, maintained stable temperatures between 30–32°C throughout the day. However, parking areas like D3 and D4 exhibited higher temperatures in the afternoon, decreasing in the evening. Notably, impervious open spaces differed in temperature, with spot B7 near the metro station recording lower air temperature due to its greenery pocket. Even spots D3 and D4, adjacent to the river, exhibited high air and solar radiation temperatures, with D4's small parking lot recording higher temperatures than D3, the larger parking lot.

Comparisons among green areas (G4, G5, G7, and D5) revealed varying temperatures, with spot G5, blending brick pavement with natural soil, mitigating temperatures the most. Meanwhile, spot D5, with a few trees, natural soil, and brick pavement, recorded high solar radiation temperatures. In the mid-rise building area with narrow roads, characterized by high building density and low wind speed, air temperature remained relatively constant throughout the day. However, around high buildings on wide roads, air temperature varied due to building shade and sun direction. The cooling airflow from air conditioning units in front of shophouses, notably in spot E4, resulted in abnormally low air temperatures.

Figure 4-18 illustrates the significant deviation of black globe temperature from air temperature, with W1 exhibiting stable temperatures— with a low gap between the highest and lowest temperatures (6°C)—and W2 recording lower temperatures in the morning, increasing in the afternoon. W3 displayed instability, experiencing a significant temperature increase by 14°C from 9 a.m. to 11 a.m. In the afternoon, it had some abnormal cases, notably at 3 p.m. on the first day, with a significant temperature decrease due to building awning shading. Figure 4-20 further illustrates the spatiotemporal distribution of black globe temperatures, emphasizing high temperatures in the southern part of the Yaowarat area.

Temperature in the Ratchadamri Area:

Figure 4-23 shows that the average temperature in Ratchadamri begins at 27.57°C and gradually increases to 32.24°C with the maximum average temperature between both days of measurement being 35.65°C at 5 p.m. The distribution temperature from the mobile survey in Ratchadamri is shown in Figures 4-21 and 4-22. The air temperature was lower in the northern area in the morning compared to that in the southeast area. Consequently, the air temperature distribution showed the south area maintained a relatively high temperature throughout the day.

On the other hand, the north and east areas—most of the spots on Route A and U— which are surrounded by high-rise buildings and greenery, maintained a relatively low temperature throughout the day. In the afternoon, the spots at Langsuan Road, which is a wide road, had increasing temperatures. The black globe temperatures in Figure 4-22 showed a similar direction to the air temperature. The south area and spot E6 had the highest temperature while the east area had the coolest. Notably, the second day had more clouds, and the temperature was higher than the first day, reflecting the typical weather conditions in Thailand during the summer and monsoon season with high temperature, poor ventilation, higher humidity, and more cloudiness in the afternoon.

The temperature in the Ratchadamri area

Figure 4-23 shows that the average temperature in Ratchadamri begins at 27.57°C and gradually increases to 32.24°C with the maximum average temperature between both days of measurement being 35.65°C at 5 p.m. When exclusively examining the data from the fixed stations, the air temperature was consistently lowest at W6 throughout the entire day, whereas the highest temperatures were recorded at W4 (Figure 4-18). The peak temperatures were typically observed around 1 p.m., with the temperature rising from approximately 29°C to 31–33°C, and gradually decreasing to 31°C in the afternoon.

The distribution temperature from the mobile survey in Ratchadamri is shown in Figures 4-21 and 4-22. The air temperature was lower in the northern area in the morning compared to that in the southeast area. Consequently, the air temperature distribution showed the south area maintained a relatively high temperature throughout the day. On the other hand, the north and east areas—most of the spots on Route A and U—which are surrounded by high-rise buildings and greenery, maintained a relatively low temperature throughout the day. In the afternoon, the spots at Langsuan Road, which is a wide road, had increasing temperatures.

Moreover, the black globe temperatures depicted in Figure 4-22 exhibited a similar trend to the air temperature. The southern area and spot E6 recorded the highest temperatures, while the eastern area had the coolest temperatures. Two notable divergences between the two temperature readings were observed: at 1 p.m., most spots along Langsuan Road and the inner area displayed elevated temperatures, and at 5 p.m., spots A1, A2, A5, E3, and I4 registered higher temperatures compared to other locations. Notably, the second day had more clouds, and the temperature was higher than the first day, reflecting the typical weather conditions in Thailand during the summer and monsoon seasons with high temperatures, poor ventilation, higher humidity, and more cloudiness in the afternoon.

Comparing Temperature Between Both Areas

Upon comparing air temperature between the two CBDs (Figure 4-23), the difference between the average maximum and minimum temperatures in Yaowarat and Ratchadamri was similar at 9.24°C and 9.36°C, respectively. However, at 9 a.m., the Ratchadamri area had a lower temperature (27.57°C) than the Yaowarat area (29.32°C). The temperature difference between the two CBDs from morning to 1 p.m. was 2°C, gradually closing to 1°C at 5 p.m.

Focusing only on fixed station data, W3 and W6, representing high urban density located next to a wide road in each CBD, exhibited different temperature patterns. Figure 4-18 shows that W6 had higher temperatures on both days, with a significant difference of 3.5–5°C. Additionally, W2 and W5 showed slightly different temperatures (1.5–2°C) due to their spatial characteristics. W2, surrounded by low and mid-rise buildings, is located on a narrow road (6-8 m), while W5, surrounded by mid-rise and high-rise buildings, is situated on a wide road (15 m). In contrast, W1 and W4, representing open spaces, exhibited a similar temperature pattern.

Therefore, this field measurement provides an overview of temperature distributions in the two CBDs of Bangkok, marking the initial step toward understanding local microclimates. This study holds originality in the preliminary Bangkok microclimate investigation. Moreover, the methodology, adapted from previous research, has been revised and tailored to be more relevant to the study area and tropical climate zone.
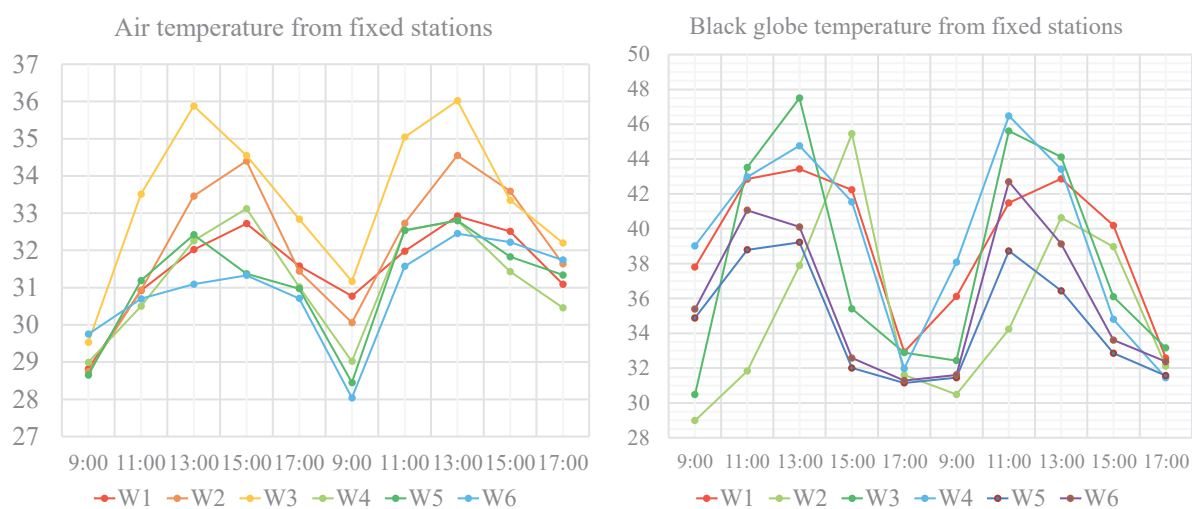
Fig. 4-18 Air temperature and black globe temperature from six fixed stations
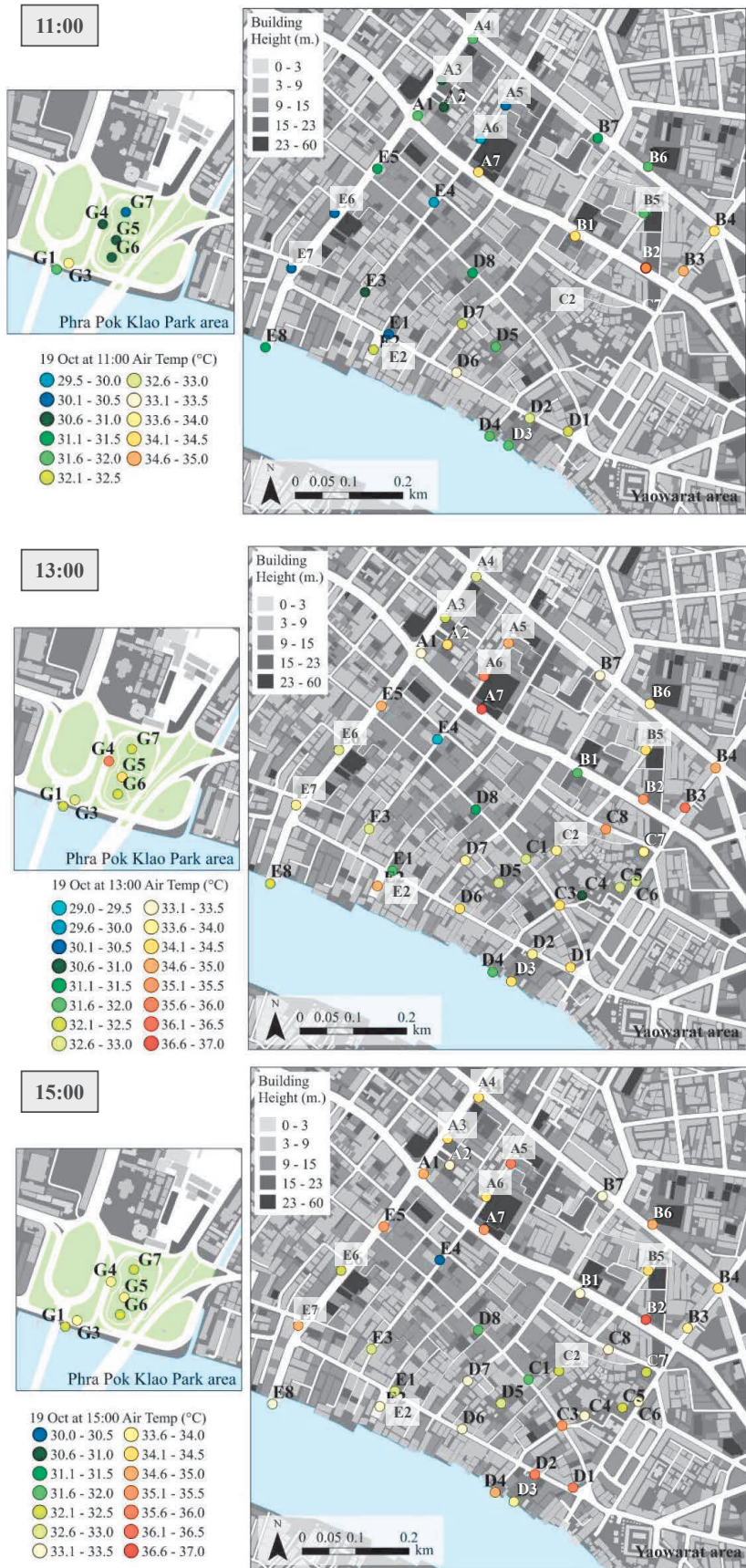
Fig. 4-19 Air temperature distribution on 11:00, 13:00, and 15:00, 19th October 2022
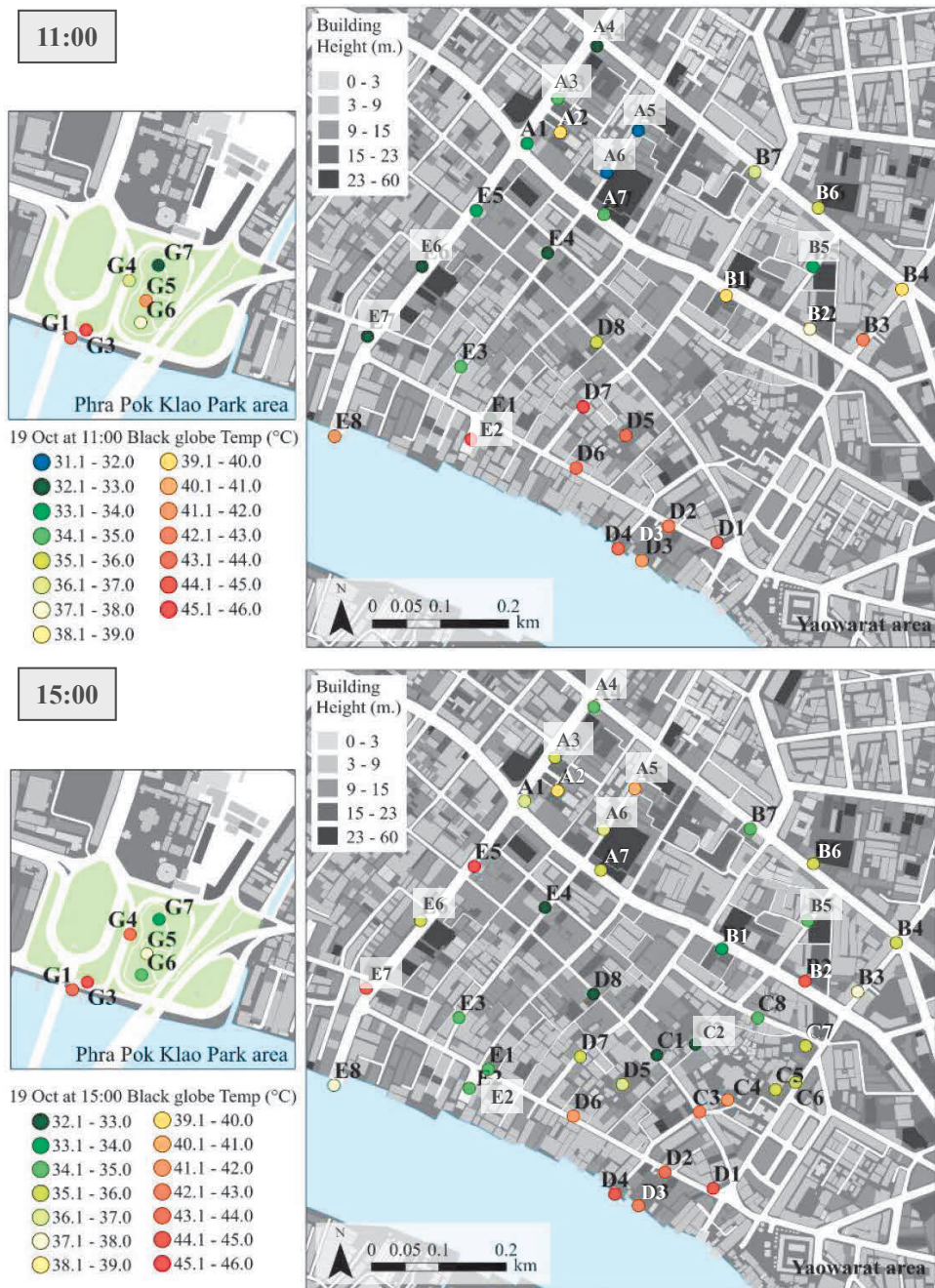
Fig. 4-20 Black globe temperature distribution on 11:00 and 15:00, 19th October 2022
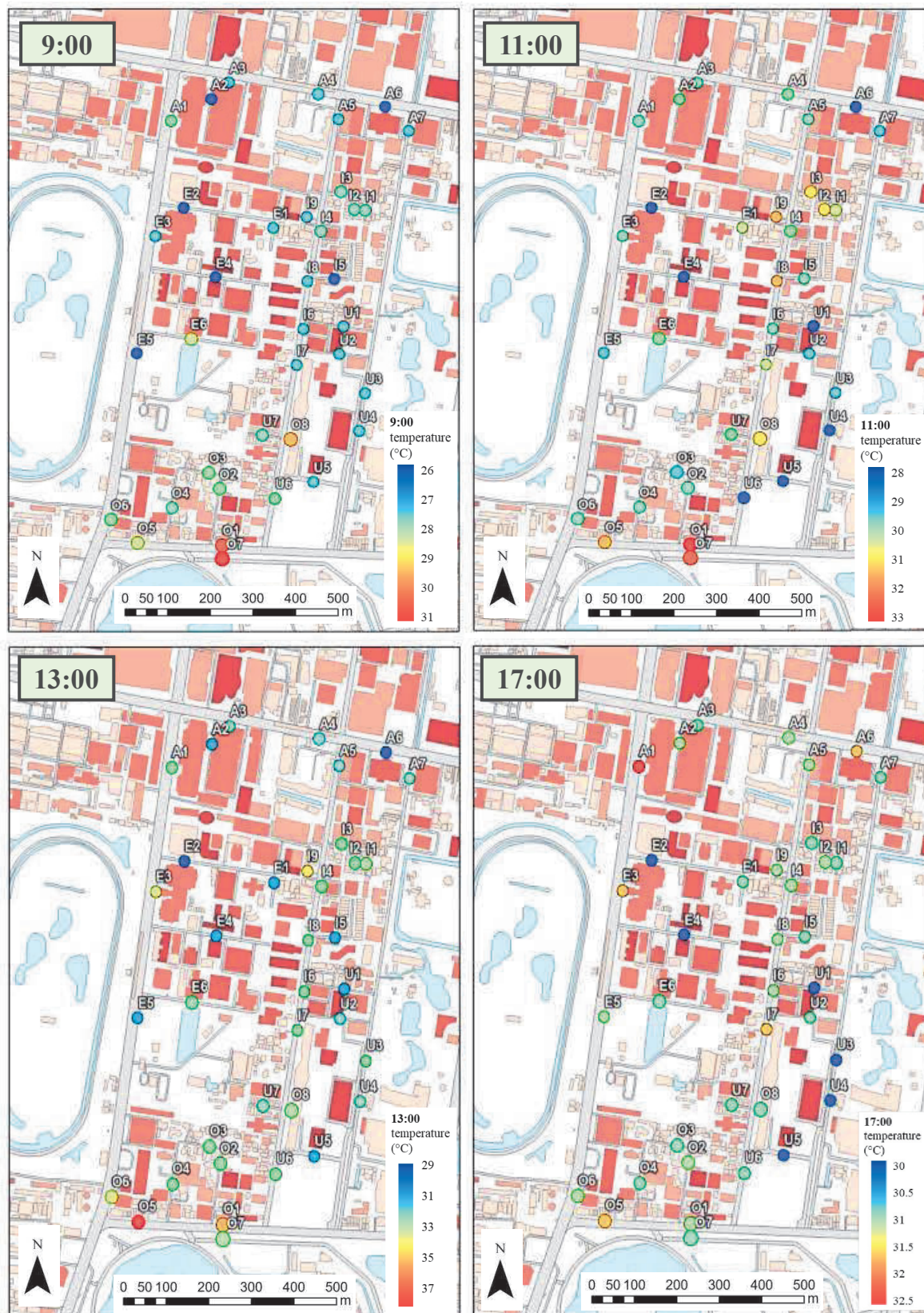
Fig. 4-21 Air temperature distribution at 9:00, 11:00, 13:00, and 17:00,
20th October 2022 in the Ratchadamri area
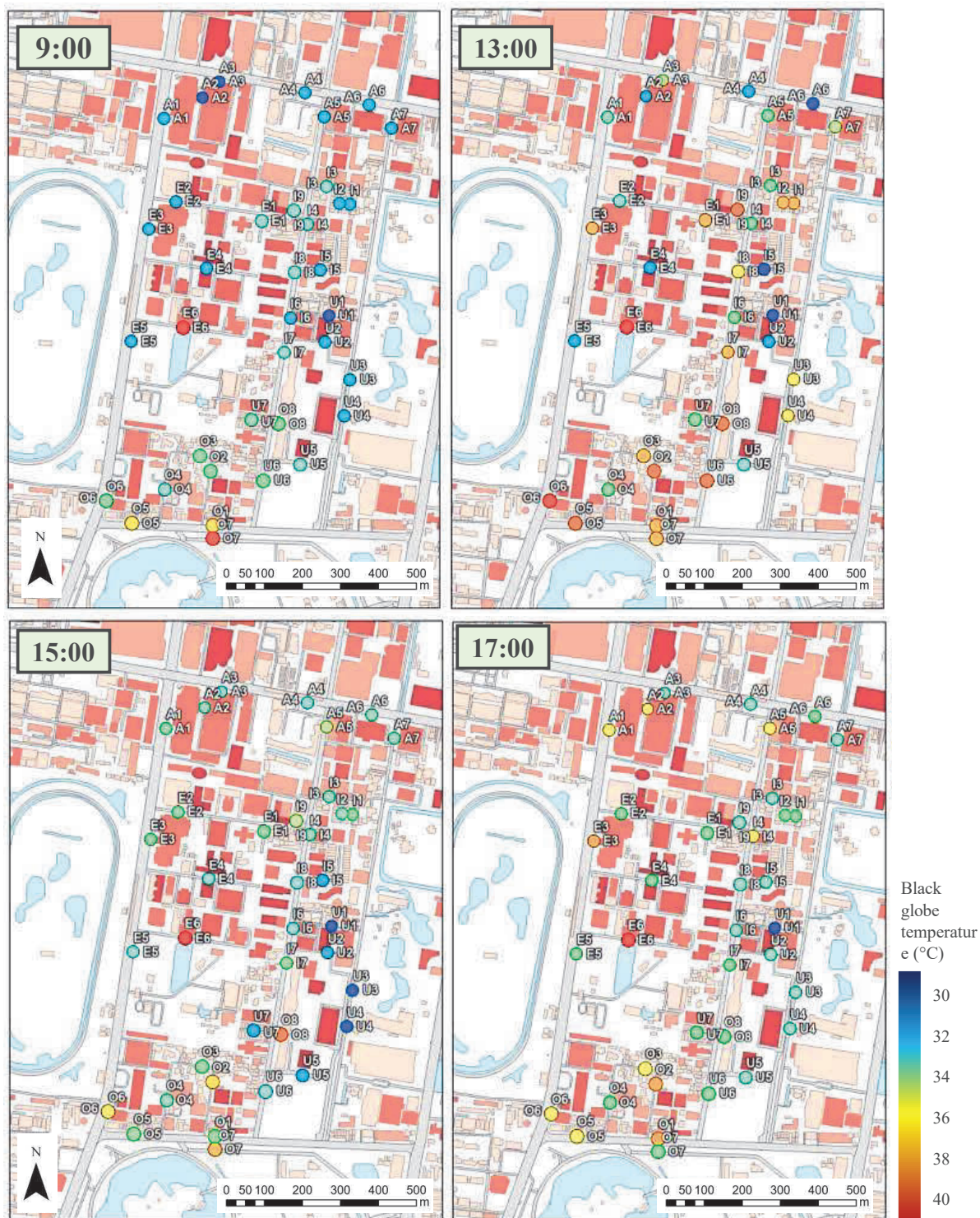
Fig. 4-22 Black globe temperature distribution at 9:00, 13:00, 15:00, and 17:00, 20th October 2022 in the Ratchadamri area

Table 4-1 The air temperature data of the Yaowarat area

| Spot	19 October 2022					24 October 2022				
	9:00	11:00	13:00	15:00	17:00	9:00	11:00	13:00	15:00	17:00
A1	28.80	31.99	33.11	34.80	33.12	29.51	32.71	35.25	34.14	31.83
A2	28.79	30.92	34.02	33.39	32.58	30.07	32.67	34.62	33.32	31.92
A3	27.85	30.57	32.25	34.28	32.52	29.48	32.49	34.09	33.87	31.50
A4	28.21	31.64	32.81	34.16	32.70	29.33	31.97	35.14	33.16	31.59
A5	27.74	30.01	34.81	35.60	32.72	29.19	31.36	34.06	34.94	31.56
A6	27.81	29.70	35.73	34.11	32.64	28.06	31.23	34.38	32.73	31.73
A7	28.32	34.42	36.85	35.09	33.04	29.19	33.67	35.86	33.48	32.56
B1	28.11	34.48	31.80	33.01	31.72	30.72	31.40	33.08	33.59	31.22
B2	28.31	35.33	35.16	36.87	32.46	30.27	33.56	36.04	33.68	31.96
B3	29.35	34.69	36.04	33.89	32.38	30.46	33.15	35.85	34.36	32.43
B4	29.91	34.19	34.80	34.33	32.72	32.02	32.95	34.65	33.91	32.09
B5	28.25	31.91	34.17	34.08	32.35	29.58	31.63	35.69	33.40	32.29
B6	28.54	31.57	33.83	34.91	32.75	30.79	32.65	34.78	32.42	31.47
B7	28.03	31.18	33.42	33.40	32.62	29.64	32.67	34.41	32.69	31.95
C1	28.20	-	32.83	31.97	30.54	29.88	32.55	36.61	32.16	31.25
C2	28.04	-	33.59	32.12	31.15	29.65	32.24	36.06	31.11	30.90
C3	28.12	-	34.07	35.35	31.91	29.76	32.93	36.25	33.30	31.73
C4	29.73	-	30.95	33.12	31.63	30.62	33.43	36.92	33.32	31.76
C5	27.75	-	32.70	32.46	31.18	29.75	34.11	36.96	33.61	31.81
C6	28.44	-	32.99	33.43	32.71	29.65	36.39	35.40	32.70	31.34
C7	28.72	-	33.73	32.02	32.01	31.11	32.33	36.59	32.38	31.32
C8	29.54	-	35.34	33.11	32.55	31.76	34.78	36.58	33.08	31.90
D1	29.03	32.33	34.29	35.68	32.28	30.49	33.68	36.61	33.66	31.97
D2	29.11	32.53	33.56	35.84	32.29	30.69	34.02	36.34	34.06	32.23
D3	27.88	31.82	34.25	33.77	32.07	30.23	32.97	35.29	31.91	30.81
D4	29.38	31.58	31.91	34.96	32.76	30.79	32.84	36.80	33.84	30.71
D5	28.97	31.78	32.55	32.55	32.06	30.05	33.53	33.64	33.25	31.37
D6	29.79	33.04	34.18	33.25	32.14	30.58	33.84	34.86	33.44	31.97
D7	28.54	32.16	33.97	33.42	32.20	30.15	32.27	34.53	33.21	31.81
D8	29.50	31.05	31.19	31.96	31.55	30.65	31.35	32.61	32.24	31.21
E1	27.86	30.22	31.67	32.73	31.87	30.09	32.50	35.04	33.54	31.58
E2	30.02	32.44	34.72	33.00	31.83	31.01	33.81	35.21	33.05	32.03
E3	28.05	30.96	32.82	32.66	32.01	29.73	32.12	35.11	32.93	31.92
E4	27.94	29.51	29.45	30.42	31.31	29.06	30.55	33.86	32.33	31.31
E5	28.36	31.01	34.92	35.16	32.36	29.98	32.60	34.23	33.35	31.87
E6	28.30	30.15	32.55	32.38	31.98	29.62	32.13	35.15	32.32	31.73
E7	28.27	30.34	33.50	34.61	32.19	29.91	31.80	34.89	34.19	31.91
E8	29.57	31.37	32.25	33.43	32.36	30.65	31.41	34.05	31.31	31.34
G1	27.96	31.73	32.20	32.33	32.47	29.90	33.10	33.87	33.53	31.80
G2	-	-	-	-	-	-	-	-	-	-
G3	29.02	33.76	32.57	33.51	33.51	30.51	34.30	36.30	34.44	31.95
G4	27.89	30.71	35.64	33.63	32.58	29.04	32.31	34.09	33.48	31.78
G5	29.04	30.75	34.26	33.51	31.82	29.59	33.41	33.49	34.41	31.54
G6	27.95	30.51	32.05	32.12	31.71	28.82	33.90	33.52	32.62	31.08
G7	28.10	30.38	32.08	32.03	31.51	27.60	32.89	32.17	32.59	31.14
W1	28.82	30.92	32.02	32.72	31.58	30.77	31.98	32.92	32.51	31.09
W2	28.74	30.93	33.46	34.40	31.44	30.06	32.73	34.55	33.59	31.64
W3	29.53	33.51	35.88	34.55	32.84	31.17	35.04	36.02	33.35	32.20

Note: The black area is the lack of data, the gray area is the shade spot while collecting the data, and the blue area is the cloudy period.

Table 4-2 The black globe temperature data of the Yaowarat area

Spot	19 October 2022					24 October 2022				
	9:00	11:00	13:00	15:00	17:00	9:00	11:00	13:00	15:00	17:00
A1	30.21	33.62	34.79	36.28	33.50	30.66	34.55	37.10	35.11	32.10
A2	34.26	39.16	40.26	39.49	32.60	38.35	42.53	40.77	35.30	32.30
A3	30.70	34.00	35.19	35.63	32.50	32.78	35.70	36.26	34.70	31.80
A4	30.14	32.91	34.10	34.04	32.30	31.88	34.41	36.30	34.20	31.85
A5	29.10	31.70	38.82	40.67	32.40	31.00	33.60	36.40	40.59	31.70
A6	29.00	31.20	42.80	36.06	31.90	30.54	33.50	35.89	35.01	31.90
A7	30.04	34.64	40.80	35.10	32.20	31.97	37.75	37.99	34.55	32.42
B1	32.50	39.62	33.34	34.00	31.70	37.02	33.89	34.96	35.00	32.00
B2	30.45	37.59	42.99	44.08	33.10	33.16	40.84	45.61	39.50	32.60
B3	36.93	42.81	44.39	37.54	32.50	39.93	44.46	45.95	36.72	32.98
B4	34.50	39.06	37.86	35.71	32.70	43.02	37.13	39.25	36.10	33.04
B5	30.87	33.74	36.11	34.40	31.85	33.56	34.97	37.55	35.83	32.50
B6	34.74	35.06	40.48	35.75	32.30	38.13	39.10	37.83	35.22	31.90
B7	33.08	36.61	36.52	34.36	31.90	35.30	39.17	42.42	35.87	32.60
C1	29.90	-	40.78	33.00	31.37	31.50	34.76	37.95	33.50	31.70
C2	29.00	-	41.36	32.60	31.20	30.40	32.98	39.00	32.60	31.20
C3	30.50	-	43.22	42.96	32.10	31.30	35.10	44.95	35.17	32.30
C4	40.35	-	44.49	41.53	31.80	39.51	39.44	46.15	37.46	32.60
C5	33.35	-	45.95	35.78	31.26	33.85	44.69	47.69	37.36	32.30
C6	32.00	-	47.81	35.81	31.90	32.39	44.63	40.29	35.86	32.60
C7	40.17	-	45.71	35.70	31.60	40.57	42.95	44.37	39.30	32.63
C8	41.04	-	48.09	34.60	32.00	42.16	44.03	45.29	36.40	32.59
D1	38.65	44.11	44.19	44.16	32.60	38.71	41.09	44.09	37.69	32.83
D2	38.50	42.73	43.68	43.48	32.30	38.53	40.39	44.82	37.46	32.70
D3	37.62	42.00	44.48	42.85	35.40	38.74	40.22	47.00	36.25	32.28
D4	40.01	43.66	44.93	44.41	34.88	39.91	41.33	48.10	40.30	31.73
D5	40.04	43.71	36.31	36.10	31.90	38.58	41.80	40.24	37.13	31.87
D6	40.43	43.76	46.37	41.84	31.90	34.38	44.00	39.56	37.20	32.54
D7	32.36	45.00	45.54	35.98	31.70	33.00	43.86	42.70	35.66	32.30
D8	40.32	35.48	33.93	32.63	30.46	37.87	37.57	35.82	33.50	31.36
E1	29.80	32.64	41.85	34.11	32.26	32.30	34.00	43.45	34.82	32.03
E2	37.74	45.82	44.54	34.73	31.90	38.89	39.53	44.39	35.84	32.24
E3	30.16	34.43	42.46	34.30	32.10	33.60	35.69	44.55	34.50	32.10
E4	29.45	32.20	35.76	32.18	30.80	30.90	37.95	40.53	34.03	31.30
E5	30.10	33.52	43.95	45.49	32.10	32.10	36.42	38.49	36.26	32.28
E6	30.50	32.60	43.82	35.33	31.26	32.01	36.30	41.74	36.21	32.00
E7	30.20	32.50	45.99	44.37	31.40	31.90	35.60	43.05	38.34	32.20
E8	39.69	41.20	44.69	37.37	31.50	38.36	42.65	44.00	34.85	31.60
G1	35.56	43.60	34.20	43.38	34.81	35.29	44.59	43.32	40.64	32.90
G2	-	-	-	-	-	-	-	-	-	-
G3	34.04	45.57	42.25	45.31	35.14	38.31	42.19	46.80	44.05	33.02
G4	29.85	36.88	46.95	43.94	32.75	32.01	35.89	39.72	38.26	32.25
G5	38.34	41.77	39.44	37.44	31.70	39.60	40.80	38.30	37.21	31.81
G6	30.93	37.37	35.86	34.31	31.14	33.07	42.19	36.05	34.56	31.20
G7	30.34	32.60	34.01	33.60	30.92	32.77	35.15	35.10	33.20	31.10
W1	37.80	42.85	43.43	42.23	32.93	36.11	41.49	42.87	40.19	32.58
W2	28.99	31.83	37.88	45.46	31.61	30.49	34.23	40.64	38.97	32.12
W3	30.48	43.52	47.50	35.41	32.89	32.43	45.61	44.12	36.10	33.16

Note: The black area is the lack of data, the gray area is the shade spot while collecting the data, and the blue area is the cloudy period.

Table 4-3 The air temperature data of the Ratchadamri area

Spot	20 October 2022					23 October 2022				
	9:00	11:00	13:00	15:00	17:00	9:00	11:00	13:00	15:00	17:00
A1	27.61	29.29	32.68	32.98	32.21	28.21	30.50	31.35	32.38	30.81
A2	26.45	29.60	30.36	31.46	31.07	27.71	30.15	30.44	31.82	30.88
A3	26.57	29.05	31.37	31.37	30.69	27.37	29.46	30.63	30.76	31.35
A4	26.91	29.69	30.69	32.69	31.01	27.20	30.48	31.73	31.00	31.05
A5	26.82	29.13	30.53	33.04	31.34	27.31	29.95	33.12	31.62	30.68
A6	26.11	28.33	29.54	30.58	31.53	26.93	29.24	30.77	31.25	30.78
A7	26.54	28.85	31.09	31.93	31.00	26.93	30.87	32.67	31.07	30.66
E1	26.51	30.85	30.29	32.11	30.88	28.09	30.30	32.59	31.90	30.66
E2	26.23	28.14	29.69	30.53	30.27	27.72	29.42	32.95	31.62	30.45
E3	26.77	29.17	33.88	33.04	31.74	27.91	30.94	33.11	31.74	30.85
E4	26.43	28.42	30.22	31.13	30.40	27.37	29.88	31.78	30.73	30.54
E5	26.31	28.89	30.46	31.73	31.16	27.45	30.12	31.57	31.06	30.84
E6	28.67	30.19	31.95	33.43	30.98	28.78	32.44	33.62	31.54	31.17
I1	27.25	30.78	33.41	32.54	30.76	28.25	30.91	32.71	32.35	31.22
I2	27.02	31.16	32.37	31.29	31.06	28.01	30.70	34.01	31.98	31.22
I3	27.02	31.00	32.10	31.85	30.68	27.67	30.68	32.36	31.50	30.70
I4	27.33	30.16	32.80	32.12	31.39	27.97	30.55	32.04	31.88	31.11
I5	26.40	29.09	30.35	31.32	30.95	27.39	29.26	30.96	30.98	30.38
I6	26.83	29.47	32.47	31.24	31.41	27.61	30.21	32.84	32.09	30.90
I7	26.70	30.91	32.84	33.47	31.71	27.98	29.70	32.59	31.91	30.94
I8	26.68	31.58	32.28	31.73	31.25	27.95	30.71	32.12	32.30	30.95
I9	26.62	31.61	34.11	32.47	31.42	27.97	28.83	34.50	32.44	30.93
O1	30.08	32.70	35.48	32.98	31.42	28.64	30.86	34.34	32.62	31.39
O2	28.29	29.16	32.68	32.56	31.01	27.41	29.91	32.60	31.79	30.90
O3	28.15	28.78	32.59	32.66	30.87	27.84	30.30	32.78	31.07	30.49
O4	27.49	29.15	32.02	32.38	30.63	27.21	30.23	31.87	30.79	30.48
O5	28.76	31.67	36.81	33.34	31.58	27.15	32.44	34.21	31.13	31.21
O6	28.17	29.15	33.66	33.31	31.47	27.03	30.51	33.80	30.79	30.43
O7	30.59	32.08	33.38	33.80	30.60	29.80	31.69	31.23	32.60	30.82
O8	29.66	31.02	33.25	34.17	30.78	26.91	30.60	33.70	31.68	30.71
U1	26.64	28.34	30.04	30.96	30.34	27.41	29.63	31.67	31.11	30.11
U2	26.76	28.55	30.53	31.73	30.74	27.72	29.73	32.08	31.43	30.73
U3	26.85	28.73	32.11	31.40	30.15	27.72	30.49	33.16	30.77	29.72
U4	26.69	28.38	31.08	31.54	30.24	27.06	29.36	31.66	31.02	30.02
U5	26.81	28.44	30.41	31.78	30.40	26.46	30.17	31.96	31.33	31.22
U6	27.90	28.43	32.55	32.96	30.51	27.84	31.14	33.31	31.96	30.86
U7	27.04	29.51	31.47	33.05	30.51	27.26	31.26	33.38	32.09	31.06
W4	28.99	30.50	32.26	33.12	31.02	29.02	32.53	32.80	31.43	30.46
W5	28.65	31.19	32.42	31.37	30.97	28.45	32.54	32.80	31.83	31.34
W6	29.75	30.70	31.09	31.33	30.71	28.04	31.57	32.45	32.22	31.74

Note: The black area is the lack of data, the gray area is the shade spot while collecting the data, and the blue area is the cloudy period.

Table 4-4 The black globe temperature data of the Ratchadamri area

Spot	20 October 2022					23 October 2022				
	9:00	11:00	13:00	15:00	17:00	9:00	11:00	13:00	15:00	17:00
A1	28.20	30.90	35.83	34.60	32.00	28.90	32.91	36.17	33.20	31.20
A2	27.89	36.84	33.64	33.70	31.80	29.10	33.57	34.43	32.80	31.50
A3	27.90	33.68	39.34	32.40	31.00	29.23	32.17	33.60	31.90	31.07
A4	28.29	31.67	33.64	32.33	31.00	28.41	31.60	32.66	31.53	31.20
A5	28.20	31.80	36.80	37.50	31.60	29.30	33.03	38.96	36.71	30.80
A6	28.30	31.00	32.33	33.11	31.30	28.70	31.79	33.83	33.44	30.80
A7	28.70	36.03	39.67	33.10	30.90	29.88	41.32	41.46	33.10	30.60
E1	29.31	40.37	42.22	35.56	31.50	30.20	32.89	38.92	33.10	31.20
E2	28.23	32.43	34.37	34.38	31.50	29.40	31.90	35.50	32.90	31.20
E3	28.30	41.00	42.41	35.90	32.30	29.66	33.70	35.47	32.90	31.36
E4	28.23	31.93	33.94	32.71	31.20	28.80	32.50	33.49	31.62	30.70
E5	28.80	31.50	33.23	32.78	31.40	28.70	31.81	32.62	31.51	30.80
E6	39.70	43.92	45.89	43.87	32.73	33.41	42.27	44.16	34.27	31.50
I1	28.67	41.16	42.90	35.16	31.10	31.08	38.42	36.83	33.40	32.08
I2	29.00	41.87	42.31	33.25	31.30	29.97	44.48	42.12	33.20	32.30
I3	29.10	35.50	36.72	33.50	31.00	29.50	36.26	35.33	32.20	31.40
I4	29.06	32.14	36.76	33.49	31.70	29.30	34.60	35.20	32.70	31.66
I5	28.20	29.96	32.56	31.78	30.70	28.90	31.88	32.30	31.30	30.60
I6	28.53	31.10	37.01	32.12	30.90	29.60	34.10	43.03	33.41	31.20
I7	29.10	36.44	42.99	36.70	31.20	31.98	42.59	41.10	36.41	31.40
I8	29.25	40.50	40.47	33.00	30.80	30.30	42.78	40.82	33.50	31.10
I9	29.90	40.93	43.03	37.53	30.71	30.60	41.10	44.28	33.33	31.10
O1	35.44	40.67	42.33	36.30	32.30	38.19	38.15	46.72	35.60	33.88
O2	31.28	33.94	43.60	39.04	32.29	31.30	34.70	39.33	33.76	32.07
O3	31.17	32.10	42.44	35.76	32.00	32.50	35.63	40.19	33.20	32.10
O4	29.26	31.50	37.56	33.24	31.20	29.56	33.60	35.91	32.00	31.40
O5	35.47	39.17	43.07	36.20	31.80	29.80	43.52	45.93	32.40	31.61
O6	31.47	33.91	44.78	38.70	31.80	29.80	37.40	46.06	33.10	31.10
O7	38.41	40.50	42.16	40.74	31.21	42.82	44.61	38.27	39.98	31.50
O8	32.30	35.14	43.38	41.31	31.10	32.18	39.30	43.19	39.56	31.10
U1	27.60	29.30	32.73	30.85	30.40	29.20	30.70	34.81	32.16	30.40
U2	28.30	31.50	33.11	31.43	31.00	29.72	33.10	34.30	32.20	31.20
U3	28.63	37.18	40.50	30.95	31.00	29.42	33.80	39.94	31.50	30.70
U4	28.30	31.56	40.34	30.93	30.77	28.54	32.16	36.30	31.20	30.40
U5	29.40	31.96	34.35	31.02	31.00	29.72	34.12	35.05	31.57	30.90
U6	32.10	33.74	43.15	32.05	31.20	32.60	37.24	40.23	34.68	31.28
U7	30.20	34.24	37.93	31.93	31.20	30.79	35.13	36.27	33.50	31.10
W4	39.02	42.97	44.76	41.54	31.98	38.08	46.48	43.42	34.80	31.44
W5	34.88	38.79	39.22	32.01	31.15	31.45	38.73	36.44	32.86	31.57
W6	35.39	41.06	40.11	32.58	31.29	31.61	42.70	39.13	33.61	32.37

Note: The black area is the lack of data, the gray area is the shade spot while collecting the data, and the blue area is the cloudy period.

Table 4-5 Summary of temperature data from two CBDs The black globe temperature data of the Ratchadamri area

Type of measurement/ Time-series	The air temperature data					The black globe temperature data				
	9:00	11:00	13:00	15:00	17:00	9:00	11:00	13:00	15:00	17:00
YWR_Tavg	29.32	32.30	34.23	33.41	31.92	34.40	38.49	41.27	37.23	32.21
YWR_Tmax	31.02	35.86	36.91	35.91	33.04	42.03	45.72	48.10	44.77	34.28
YWR_Tmin	27.67	30.03	30.81	30.77	30.62	29.70	32.09	34.15	32.39	30.78
RDR_Tavg	27.57	30.15	32.24	31.90	30.90	30.65	36.01	38.72	34.01	31.34
RDR_Tmax	30.20	32.62	35.65	33.40	31.98	41.26	45.20	46.31	41.92	33.31
RDR_Tmin	26.29	28.49	29.99	30.63	29.93	28.01	30.00	32.31	31.03	30.40
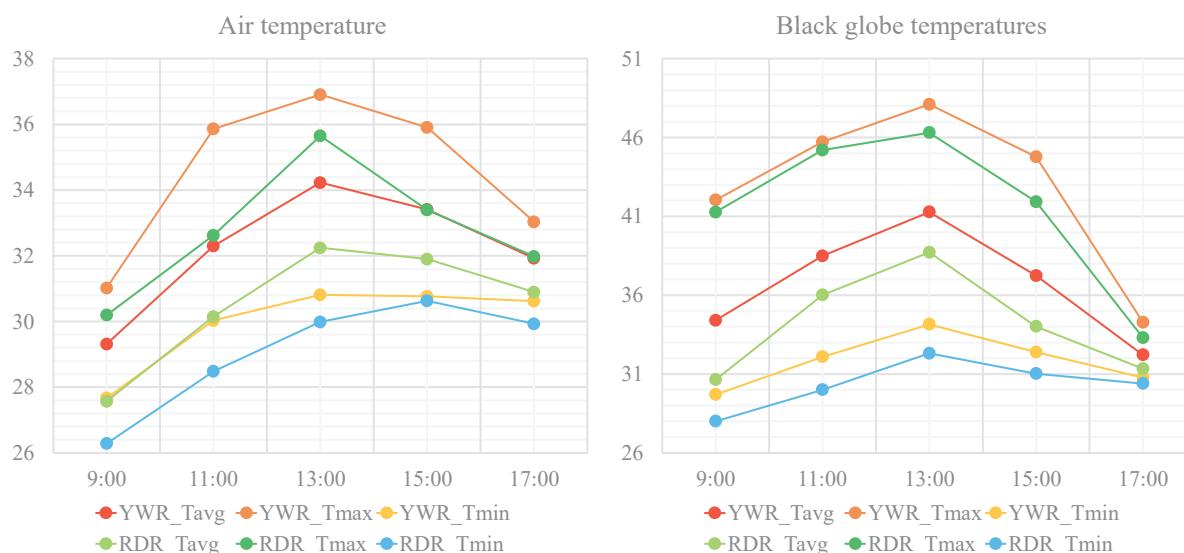
Fig. 4-23 Overview of air temperature and black globe temperature in both CBDs

4.4.3 The Surface Temperature Data

Surface temperature data from both areas are presented in Figures 4-24 to 4-25, and Tables 4-6 and 4-7, highlighting the impact of shade on decreasing surface temperature. Tables 4-6 and 4-7 specifically demonstrate the effect of shade on various surface materials. A summary of surface temperature by material and a comparison between both areas is provided in Figure 4-26 and Table 4-8. Notably, four materials—concrete pavement, asphalt road, tree, and concrete buildings—exhibited similar patterns. In the morning, surface materials in the Ratchadamri area were higher than those in Yaowarat. However, in the afternoon, temperature characteristics were inversely aligned, with surface temperature in the Ratchadamri area decreasing at a faster rate. As a result, Yaowarat had higher surface temperatures than Ratchadamri in the afternoon.

The highest surface temperature was recorded on the asphalt road, reaching 46.45°C and 46.91°C at 11:30–12:30. Concrete pavement, nearly equivalent to the road, exhibited temperatures of 46.16°C in Ratchadamri and 44.04°C in Yaowarat. Both materials showed a gradual convergence at 17:30. Regarding tree surfaces, the difference between Ratchadamri and Yaowarat was most pronounced in the morning, with gaps of almost 5°C from 8:30–11:30. However, by 17:30, the trend reversed, and Yaowarat had higher temperatures. In terms of building temperatures, Ratchadamri consistently showed higher temperatures by around 3–4°C, except for a slight inversion of 1–2°C in the afternoon. Waterbody surface temperature data were collected only from the Yaowarat area, revealing a gradual increase from the morning (27.5°C) to noon. In the afternoon, the temperature stabilized, maintaining approximately 30°C.

Therefore, the surface temperature in each study area offers individual measures, allowing for the analysis of spatial relationships. These results, illustrating surface temperature variations across different materials, serve as valuable input for future studies.

Table 4-6 Surface temperature of W1-W3

Point	Material	8:30	9:30	10:30	11:30	12:30	13:30	14:30	15:30	16:30	17:30
W1: 19 Oct	Pavement	30.38	37.16	37.3	42.48	48.41	47.89	47.78	45.25	41.32	37.84
	Road	32.14	36.99	42.32	47.11	51.52	51.42	49.59	44.69	40.48	36.58
	Tree	26.06	28.8	29.66	32.44	35.74	40.02	42.15	43.04	39.76	35.41
	Water	27.33	26.59	27.9	28.32	29.9	28.05	28.23	28.87	29.39	29.19
W1: 24 Oct	Pavement	33.83	40	43.25	45.4	47.56	48.83	44.13	44.57	41.11	38.3
	Road	30.66	34.65	36.08	36.1	43.04	43.56	41.82	39.83	38.78	36.15
	Tree	29.14	30.37	32.69	33.47	35.44	38.27	39.11	37.31	35.74	34.01
	Water	27.73	28.42	29.7	29.03	30.07	29.95	30.97	30.07	30.44	29.92
W2: 19 Oct	Pavement	27.96	28.51	29.35	29.87	30.47	38.64	41.69	44.02	36.1	34.66
	Road	27.8	28.31	29.26	29.24	39.49	46.96	47.45	36.39	30.253	32.91
	Tree	27.47	28.74	30.29	31.86	32.04	31.5	31.86	32.16	31.3	31.15
	Bldg	27.89	28.36	29.46	30.04	31.04	32.47	34.35	35.82	33.4	32.58
W2: 24 Oct	Pavement	28.3	29.4	29.92	31.32	32.29	33.33	33.04	35.72	33.35	32.95
	Road	27.94	28.58	29.93	31.23	38.06	31.69	31.81	37.1	31.09	32.07
	Tree	28.19	29.78	31.23	32.53	33.31	35.61	34.36	32.62	31.15	30.92
	Bldg	28.33	29.35	30.05	31.39	32.11	37.17	36.41	33.97	32.64	32.05
W3: 19 Oct	Pavement	27.04	29.5	35.42	39.71	53.76	51.15	43.51	38.36	37.09	35.22
	Road	28.73	32.29	45.12	42.15	55.11	55.22	44.28	41.43	39.26	35.43
	Bldg	27.67	29.94	32.63	34.06	40.53	36.59	34.79	34.21	33.62	32.4
	Tree	28.61	29.3	31.87	33.32	39.98	35.79	35.01	34.46	31.48	34.02
W3: 24 Oct	Pavement	29.89	31.96	34.2	43.92	47.75	44.38	40.48	39.56	37.65	34.25
	Road	30.55	37.56	38.43	48.53	51.46	49.39	41.57	39.83	38.39	33.02
	Bldg	29.88	32.52	33.38	35.09	37.47	35.91	33.85	33.93	32.89	34.66
	Tree	29.48	31.64	32.33	34.14	36.88	38.2	36.42	34.93	33.67	36.69

Notes: Bldg. = concrete building and gray color represents shade.

Table 4-7 Surface temperature of W4-W6

Point	Material	8:30	9:30	10:30	11:30	12:30	13:30	14:30	15:30	16:30	17:30
W4: 20 Oct	Pavement	30.66	35.77	41.05	47.43	46.71	44.22	44.62	41.61	38.21	36.94
	Road	31.06	37.1	40.93	46.03	46.08	44.72	43	41.75	38.34	36.03
	Tree	27.25	31.79	31.5	31.47	30.1	34.41	32.48	32.26	31.54	30.24
	Grass	29.89	34.82	36.74	38.37	37.59	38.12	34.51	33.52	31.58	29.83
W4: 23 Oct	Pavement	31.77	37.96	42.18	46.48	49.24	50.96	49.63	47.22	41.3	38.27
	Road	31.5	36.66	41.4	45.45	47.18	46.86	46.67	43.37	41.59	37.3
	Tree	16.78	9.66	30.57	32.17	32.44	33.84	33.67	33.3	31.52	29.86
	Grass	29.32	34.89	32.4	36.73	37.75	38.65	36.9	36.03	32.53	30.07
W5: 20 Oct	Pavement	29.86	31.34	35.62	45.6	38.69	37.46	33.65	33.38	32.84	32.13
	Road	31.38	33.67	36.72	43.05	37.91	32.77	33.26	34.11	33.16	32.36
	Tree	24.84	27.71	29.07	32.29	33.115	33.94	32.71	32.27	32.13	31.58
	Bldg	35.18	34.79	35.84	43.47	39.82	36.17	34.33	33.39	32.57	31.9
W5: 23 Oct	Pavement	27.71	35.57	40.27	36.99	40.6	38.66	36.27	34.3	33.15	31.9
	Road	32.27	39.11	45.17	49.28	39.7	39.86	36.19	34.69	33.43	32.56
	Tree	23.57	26.55	30.35	30.2	30.94	31.5	32.31	32.17	31.8	31.23
	Bldg	39.62	39.69	40.44	37.57	38.14	34.3	33.22	31.62	30.87	31.41
W6: 20 Oct	Pavement	32.93	32.75	40.2	46.78	50.95	43.05	38.96	36.01	35.72	35.54
	Road	33.75	32.61	38.17	48.98	52.58	39.76	35.94	35.27	34.45	34.11
	Bldg	28.14	27.81	30.08	31.32	34.39	33.36	31.77	32.06	32.2	31.6
	Tree	28.8	27.41	28.39	29.11	28.06	29.99	30.79	30.27	30.74	30.42
W6: 23 Oct	Pavement	32.65	37.98	44.03	47.76	50.76	52.63	41.04	38.05	38.82	37.14
	Road	34.27	37.05	42.44	48.68	51.39	42.81	37.84	35.31	34.75	34.01
	Bldg	26.93	28.19	29.88	30.67	32.46	33.25	32.44	32	31.52	31.56
	Tree	25.2	27.08	29.7	30.14	31.56	30.82	30.52	30.75	30.61	30.61

Notes: Bldg. = concrete building and gray color represents shade.
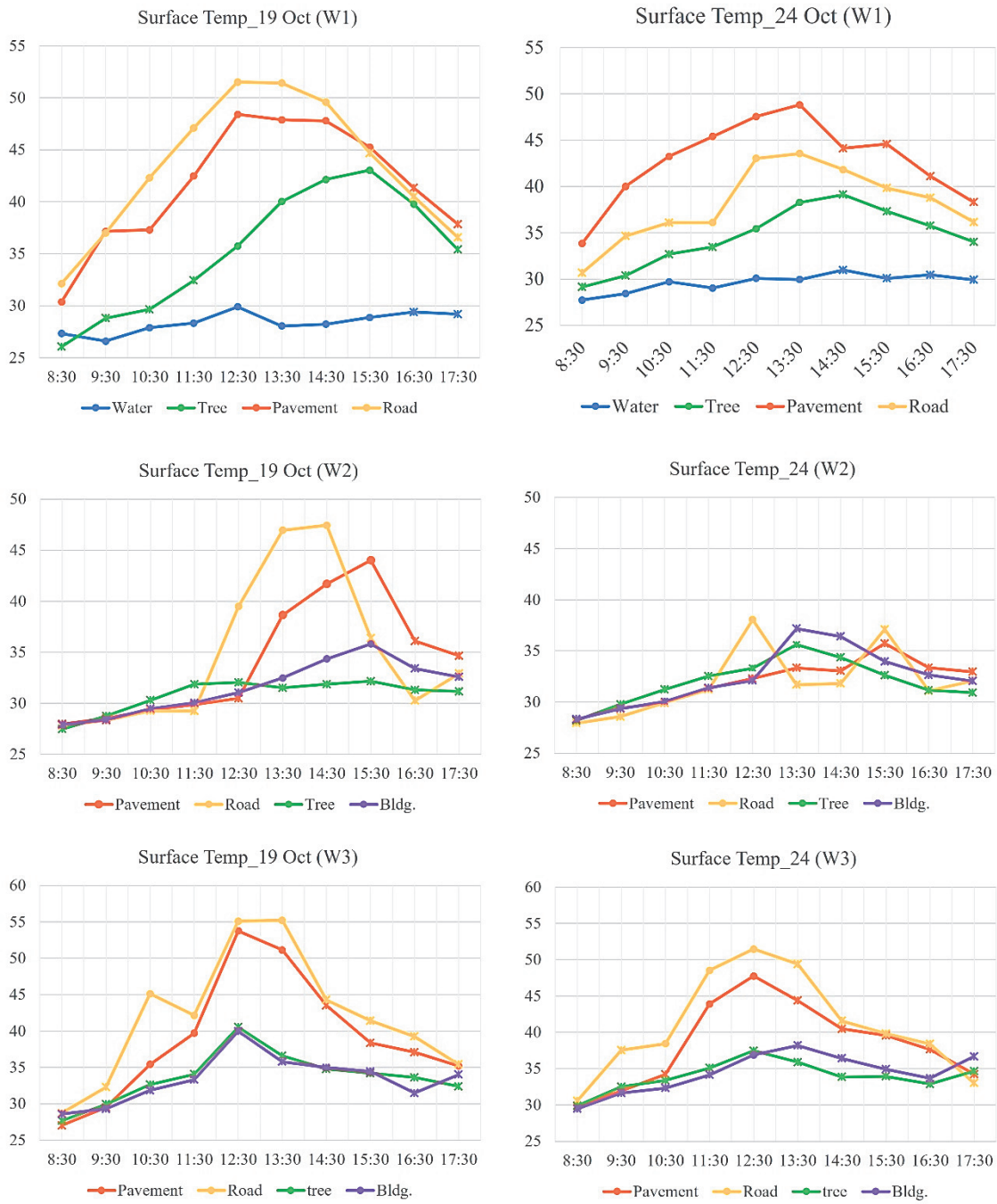
Fig. 4-24 Surface temperature of W1-W3

Fig. 4-25 Surface temperature of W4-W6

Table 4-8 The average surface temperature by materials

Area	Material	8:30	9:30	10:30	11:30	12:30	13:30	14:30	15:30	16:30	17:30
Y	Pavement	29.57	32.76	34.91	38.78	43.37	44.04	41.77	41.25	37.77	35.54
R		30.93	35.23	40.56	45.17	46.16	44.50	40.70	38.43	36.67	35.32
Y	Road	29.64	33.06	36.86	39.06	46.45	46.37	42.75	39.88	36.38	34.36
R		32.37	36.03	40.81	46.91	45.81	41.13	38.82	37.42	35.95	34.40
Y	Tree	28.16	29.77	31.35	32.96	35.57	36.57	36.49	35.75	33.85	33.70
R		29.89	34.82	36.74	38.37	37.59	38.12	34.51	33.52	31.58	29.83
Y	Building	28.44	30.04	31.38	32.65	35.29	35.54	34.85	34.48	33.14	32.92
R		32.47	32.62	34.06	35.76	36.20	34.27	32.94	32.27	31.79	31.62
Y	Water	27.53	27.51	28.80	28.68	29.99	29.00	29.60	29.47	29.92	29.56

Note: Area Y = Yaowarat area, Area R = Ratchadamri area
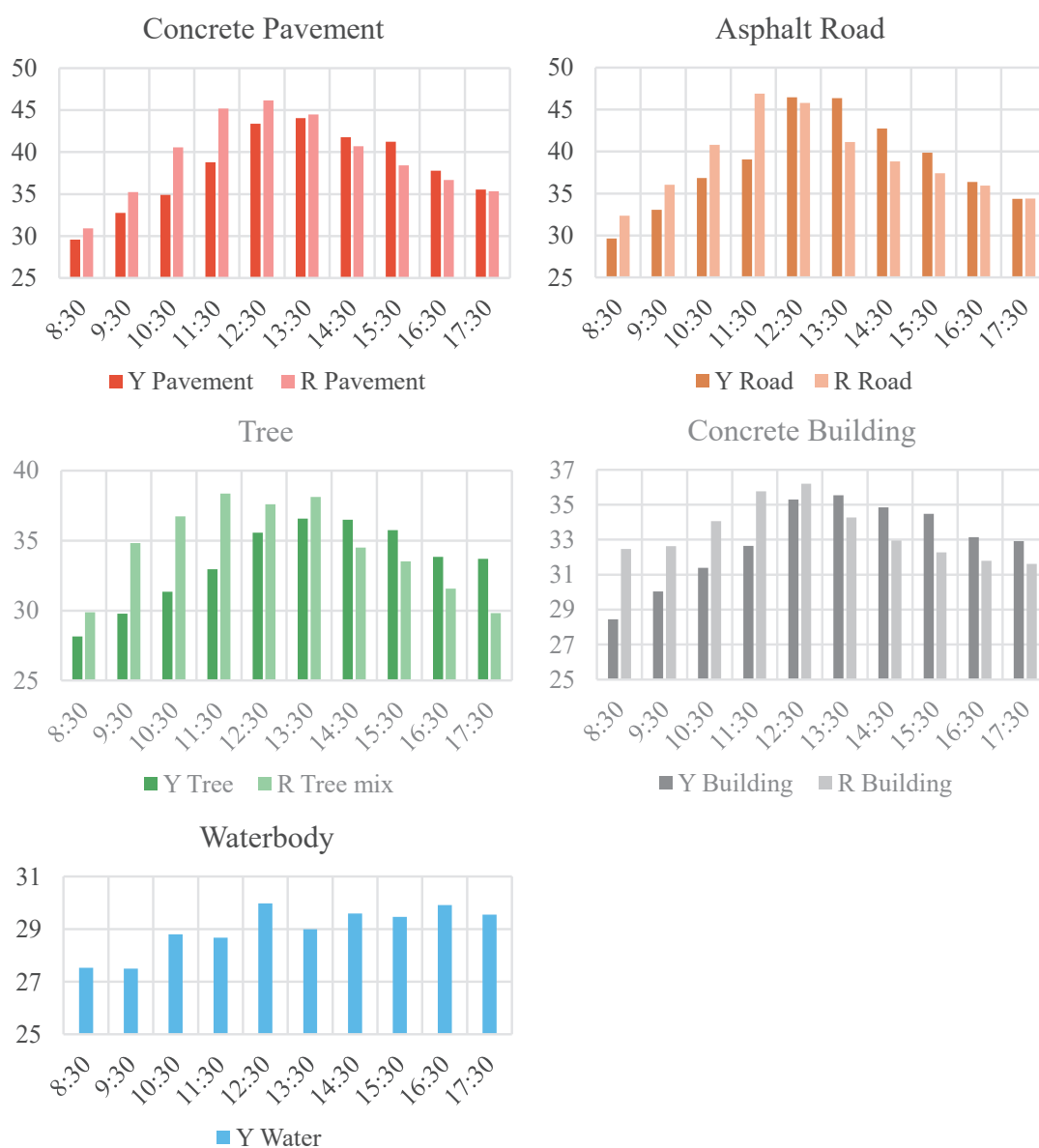
Fig. 4-26 The average surface temperature by materials in both areas

4.4.4 Field Measurement Design Planning

The detailed design planning of the field measurement played a crucial role in directly influencing the collected climate data. The scope of the measurement area for the two CBDs was carefully planned with specific criteria:

1. The total area for each CBD was approximately 0.5–1 square kilometers.

2. Both areas had a high urban density, with a building coverage ratio exceeding 50%.

3. The total area could effectively collect weather data in public spaces.

Following these criteria, the routes for the mobile survey and the locations for fixed stations were designed. Each CBD had 5–6 routes for mobile surveys, considering limitations such as human resources, the distance between observation spots, the period for each round of the survey, and the urban characteristics. Each route included 6–10 observation spots, with distances between spots and rest areas of less than 1 km. The time required to collect weather data was kept under an hour for each route. Electronic scooters were used for all mobile surveys due to narrow pathways, the lack of bicycle lanes in Bangkok, and the efficiency of scooters in terms of time and energy compared to walking. The criteria for selecting observation spots in the mobile survey were based on their surroundings, road width and direction, land coverage classification, and the designation of all points as public spaces.

For fixed stations, each area had three stations, determined by equipment limitations and set-up time. Various urban topographies were considered as criteria for measuring urban ventilation in areas with different urban characteristics. The first station was in a vacant area without obstacles, serving as a standard for unobstructed wind data. The second and third stations were located in urban areas with medium to high building density, focusing on different road orientations. Each CBD had three fixed stations: W1 and W4 were in vacant areas with wide open spaces, while W2, W3, W5, and W6 were in the inner-urban area, representing different footpaths in Mangkon Road, Yaowarat Road, Lang Suan Road, and Sarasin Road, respectively.

The efficiency of spot and location design planning was evident in the collected weather data. Some mobile survey spots had to be relocated onsite due to unpredictable situations, such as prohibitions, property owner objections, changes in land coverage due to construction, and the opening of air-conditioned buildings for commercial purposes in the Yaowarat area, leading to abnormal temperature readings. Similar challenges were encountered at the fixed station W4, where the presence of 4-meter-high bushes affected wind speed data. The open space intended to represent the Ratchadamri area had to be relocated, given that most open spaces were private and impractical for equipment setup.

4.5 Conclusion

The chapter effectively accomplished its objectives, which aimed to gather temperature and wind data from Bangkok's two CBDs and characterize their climate features. The focus on the distinctive urban qualities and high population density of Yaowarat and Ratchadamri justified their selection. The data collection in October 2022 considered optimal conditions for studying the urban microclimate in Bangkok. The results, categorized into wind data, air temperature, black globe temperature, and surface temperature, yielded the following findings:

1. **Wind Data Analysis:** Complex wind patterns were identified, influenced by urban layouts, road orientation, and specific measurement locations.

2. **Air Temperature Distribution:** Peak temperatures around 13:00 and variations influenced by urban characteristics were observed in both Yaowarat and Ratchadamri. Black globe temperatures showed significant deviations, emphasizing the impact of shading and building orientation.

3. **Surface Temperature Surveys:** Shade demonstrated a clear effect on decreasing temperatures, with variations observed among different materials.

4. **Comparison of Temperature Patterns:** Variations in morning and afternoon temperatures between Yaowarat and Ratchadamri were highlighted.

The planning of field measurements, including mobile survey routes and fixed station locations, played a crucial role in data collection efficiency. Selection criteria for observation spots considered surroundings, road characteristics, land coverage, and public spaces. Challenges, such as spot relocations due to unforeseen circumstances and the influence of environmental factors on data collection, were encountered.

In summary, this study offers valuable insights into the local microclimates of Yaowarat and Ratchadamri, laying a foundational step for future research. The methodology, adapted and refined from prior studies, demonstrates originality and relevance to the tropical climate zone. This chapter successfully presents and discusses the results of field measurements, underscoring the importance of meticulous design planning in obtaining meaningful climate data from the chosen CBDs in Bangkok.

4.6 Limitation and Direction of Future Study

The study found obstacles and weaknesses that could provide improvements for future studies. The limitations of this study and topics for further study are as follows:

- Unforeseen situations, such as prohibitions, changes in land coverage due to construction, and property owner restrictions, led to the relocation of some mobile survey spots, affecting data consistency.

- Certain fixed stations, like W4, experienced lower wind speed due to the presence of 4-meter-high bushes, showcasing the impact of immediate surroundings on data accuracy.

- The study focused on a specific period in October, and the findings may not fully represent seasonal variations, particularly in comparison to the hot and humid season.

- Further microclimatic analysis: conduct a more extensive and detailed analysis of microclimatic conditions, considering additional parameters and variations over multiple seasons to enhance the comprehensiveness of the study.

- Utilize numerical simulations, such as computer fluid dynamics, to validate and complement field measurement results, providing a more in-depth understanding of airflow and thermal patterns.

- Long-Term Monitoring: implement long-term weather data monitoring to capture the dynamics and changes in urban microclimates over an extended period, enabling the observation of trends and patterns.

By addressing these limitations and incorporating these future study plans, researchers can enhance the robustness and applicability of insights gained from the field measurements in this chapter.

Acknowledgment

Architectural and Urban Planning Laboratory

Professor Tanaka Takahiro	Assistant Professor Shota Tamura
Ms. Umpika Mettatam	Mr. Tomoya Migitera
Mr. Riki Yamaga	Mr. Taku Goto
Mr. Nishimura Jumpei	Mr. Matsuura Michihiro
Mr. Yuki Yamamoto	Mr. Daiki Shiromoto
Mr. Ryota Araki	Mr. Naoya Kutsuna
Mr. Taisei Moriyama	Mr. Daiki Shigematsu

References

Arnfield, A.J. (2006). Micro- and mesoclimatology. *Prog Phys Geogr, 30*, 677-689. https://doi.org/10.1177/030913330607115.

Blocken, B. (2015). Computational Fluid Dynamics for urban physics: importance, scales, possibilities, limitations and ten tips and tricks towards accurate and reliable simulations. *Build Environ, 91*, 219-245. https://doi.org/10.1016/j.buildenv.2015.02.015.

Khamchiangta, D., & S. Dhakal (2020). Time series analysis of land use and land cover changes related to urban heat island intensity: Case of Bangkok Metropolitan Area in Thailand. *Journal of Urban Management, 9(4)*, 1-12. https://doi.org/10.1016/j.jum.2020.09.001.

Matsuo K., & T. Tanaka (2019). Analysis of spatial and temporal distribution patterns of temperature in urban and rural areas: Making urban environmental climate maps for supporting urban environmental planning and management in Hiroshima. *Sustainable Cities and Society, 47*, 1-22. https://doi.org/10.1016/j.scs.2019.01.004.

Mill, G. (2014). Urban Climatology: history, status and prospects. *Urban Climate, 10,* 479-89. https://doi.org/10.1016/j.uclim.2014.06.004.

Oke, T.R. (1982). The energetic basis of the urban heat island. *Quarterly Journal of the Royal Meteorological Society, 108(455)*, 1-24. https://doi.org/10.1002/qj.49710845502.

Oke, T.R., G. Mills, A. Christen, & J.A. Voogt (2017). Urban Climates. 1st edition, Cambridge, United Kingdom: Cambridge University Press.

Rizwan, A.M., Y.C. L. Dennis, & C. Liu (2008). A review on the generation, determination, and mitigation of urban heat island. *Environ Sci, 20*, 120-128. https://doi.org/10.1016/S1001-0742(08)60019-4.

Santamouris, M. (2007). Heat Island research in Europe: the state of the art. *Adv Build Energy Res, 1*, 123-150. https://doi.org/10.1080/17512549.2007.9687272.

Schwarz, N., U. Schlink, U. Franck, & K. Gromann (2012). Relationship of land surface and air temperature and its implications for quantifying urban heat island indicators-An application for the city of Leipzig. *Ecological Indicators, 18*, 693-704. (in German)

Souch, C., & S. Grimmond (2006). Applied climatology: urban climate. *Prog Phys Geogr, 30*, 270-279. https://doi.org/10.1191/0309133306pp484pr.

Srivanit, M., & H. Kazunori (2011). The influence of urban morphology indicators on summer diurnal range of urban climate in Bangkok metropolitan area, Thailand. *International Journal of Civil & Engineering, 11(05),* 34-46.

Thai Meteorological Department (TMD) (2023). Average Wind Rose of Bangkok. http://www.aws-observation.tmd.go.th/aws/awsWindRose., last accessed 2023/10/10.

Toparlar, Y., B. Blocken, P. Vos, G.J.F. van Heist, W.D. Janssen, T. Hooff, H. Montazeri, & H.J.P. Timmermans (2015). CFD simulation and validation of urban microclimate: A case study for Bergpolder Zuid, Rotterdam. *Building and Environment, 83,* 79-90. https://doi.org/10.1016/j.buildenv.2014.08.004.

Chapter 5
Comparative Analysis of the Urban Ventilation Characteristics between the Old and New
Central Business Districts of Bangkok

Relationships between Wind Velocity and Urban Forms

Contents

5.1 Introduction

Building upon insights gained from comprehensive field measurements in Bangkok's central business districts (CBDs) detailed in the previous chapter, this section delves into a critical aspect of urban climatology—urban ventilation. The prior chapter elucidated temperature patterns, wind data, and microclimatic nuances in Yaowarat and Ratchadamri. Now, our focus shifts to a deeper exploration of urban ventilation, pivotal in understanding and mitigating the urban heat island (UHI) phenomenon.

The intricate relationship between urban ventilation and the broader urban climate becomes evident when considering the complexity of factors influencing the urban environment (Sundborg, 1950; Oke et al., 2017). As rapid urbanization transforms cityscapes, the need to decipher the impact of wind flow, especially its speed and direction, on local climates becomes increasingly pressing. This chapter strategically bridges insights from field measurements with the broader context of urban climatology, emphasizing the role of urban ventilation in the tropical setting of Bangkok.

Urban ventilation, characterized by wind patterns, holds the key to unlocking a deeper understanding of the local microclimates observed in Yaowarat and Ratchadamri. Limited attention has been given to urban ventilation in Bangkok compared to studies on the UHI effect (Unsakul et al., 2017; Takkanon, 2017; Heshani and Winijkul, 2022). The previous chapter highlighted the influence of factors such as building density, road orientation, and open spaces on temperature distributions related to the previous study (Pakarnseree et al., 2018; Kamma et al., 2020; Khamchiangta and Dhakal, 2020). Then, this chapter focuses on how these factors interact with wind flow, impacting ventilation within the urban structure.

To comprehensively address the challenges posed by the urban environment in Bangkok, a dual approach is undertaken. First, traditional field measurements provide a tangible and real-time understanding of existing conditions. Second, advanced computational simulations, specifically computational fluid dynamics (CFD), offer advantages in studying urban microclimates at various scales.

Recently, CFD has been frequently used as a predictive methodology, and it plays an important role in transferring urban microclimate knowledge into engineering and design practices for urban planning (Toparlar et al., 2017). CFD simulations can be employed to study urban microclimates at different scales, ranging from the meteorological mesoscale over the meteorological microscale to the building scale and the indoor environment (Moonen et al., 2012; Blocken, 2014; Blocken, 2015).

The main advantage of CFD is the opportunity to perform comparative analyses based on different scenarios (Blocken, 2014; Blocken, 2015). However, there is a lack of studies validating CFD analysis with field measurement data in tropical climates, especially in Bangkok, Thailand (Toparlar et al., 2017).

In this chapter, the integration of these methodologies becomes paramount for a holistic assessment of urban ventilation in the studied CBDs. The significance of this chapter lies in its capacity to provide practical insights and strategies to enhance urban ventilation. Through a synthesis of field measurements and the predictive capabilities of CFD simulations, our objective is not only to enrich academic discourse but also to guide urban planning practices toward the creation of sustainable and climate-resilient urban environments.

Moreover, this study aligns seamlessly with global objectives, particularly the United Nations Sustainable Development Goals (SDGs). Two specific SDGs relate to our work: those focusing on the development of sustainable cities and efforts towards climate change mitigation and adaptation. This research contributes to the global agenda by shedding light on the concept of sustainable cities and advocating for effective climate change-related planning and management in developed nations.

Hence, this chapter is structured into five sections as follows. The first section outlines the objectives. Following that, the methodology is introduced, providing information about the study area, a brief of field measurement data, spatial analysis, and the CFD simulations supplementary data. The subsequent section presents the results and discussions, divided into four parts—the ventilation characteristics of both CBDs, the relationship between wind speed and urban physical variables, data usage and methodology, and the CFD simulation validation. Moving forward, the conclusion is summarized, and, finally, the limitations and directions for future study are outlined. The study framework is shown in Figure 5-1.

5.2 Objectives

Hence, driven by the statements and research gaps mentioned above, this research objective aims to analyze and compare the urban ventilation characteristics between the two CBDs of Bangkok based on the combined results from field measurement and CFD simulations.

Objectives

To analyze and compare urban ventilation characteristics between two CBDs of Bangkok based on the combination from field measurement and CFD simulations to understand the overall urban ventilation in both areas

Research Outline

Study areas ✚ Methodology and data usage

Yaowarat area

Ratchadamri area

Field measurement

Spatial analysis

CFD simulations

Classification of physical variables

Correlation analysis between WV and physical variables

Results and Discussions

Urban Ventilation Characteristics and comparison between both CBDs ✚ Relationship between wind velocity and urban physical variables ✚ Data usage and methodologies ✚ Limitations and further study

Conclusion

Fig. 5-1 Research framework of Chapter 5

5.3 Methodology and Data Usage

In this chapter, the data usage was combined from two data resources, which are the field measurement data from Chapter 4 and the results from the CFD simulation. The methodology of this chapter was divided into four parts: the primary part was the study area, The second part was the detail of field measurement. Then, the third part comprised a spatial analysis with geographic information system (GIS) and statistics analysis. Finally, the fourth part was the detail of the CFD simulation and modeling.

5.3.1 Study Area

Bangkok hosts several Central Business Districts (CBDs), each with unique historical and urban characteristics. For this study, the focus narrowed to two key CBDs— Yaowarat and Ratchadamri—both centrally located and sharing a similar latitude (13°44'26"N).

Yaowarat, positioned in Chakkrawat, Samphanthawong district, stands as Bangkok's original and oldest CBD, steeped in historical significance. Renowned as one of the world's largest Chinatowns, Yaowarat features a vibrant urban fabric with 2- to 5-story commercial buildings, small streets, and alleys bustling with activity. With its unique mix of low to medium-height structures, Yaowarat offers valuable insights into urban ventilation dynamics, attracting commerce and boasting some of the city's highest land prices. Ratchadamri, located in the Pathumwan district, emerged as a new economic hub with the highest land prices in Thailand in 2022. Dominated by high-rise buildings and significant real estate projects, the area encompasses major roads like Phloen Chit, Ton Son, Lang Suan, Ratchadamri, and Sarasin. South of this district lies Lumpini Park. With its modern economic prominence and a juxtaposition of high-rise structures and greenery, Ratchadamri presents a distinct urban landscape.

Selected for their diverse urban characteristics and high population density, Yaowarat and Ratchadamri collectively form a study area of approximately 1 square kilometer. This deliberate selection facilitates a nuanced exploration of ventilation dynamics, laying the foundation for addressing the UHI effect. Further details about the study area, including specific field measurement locations, can be referenced in Figure 5-2.
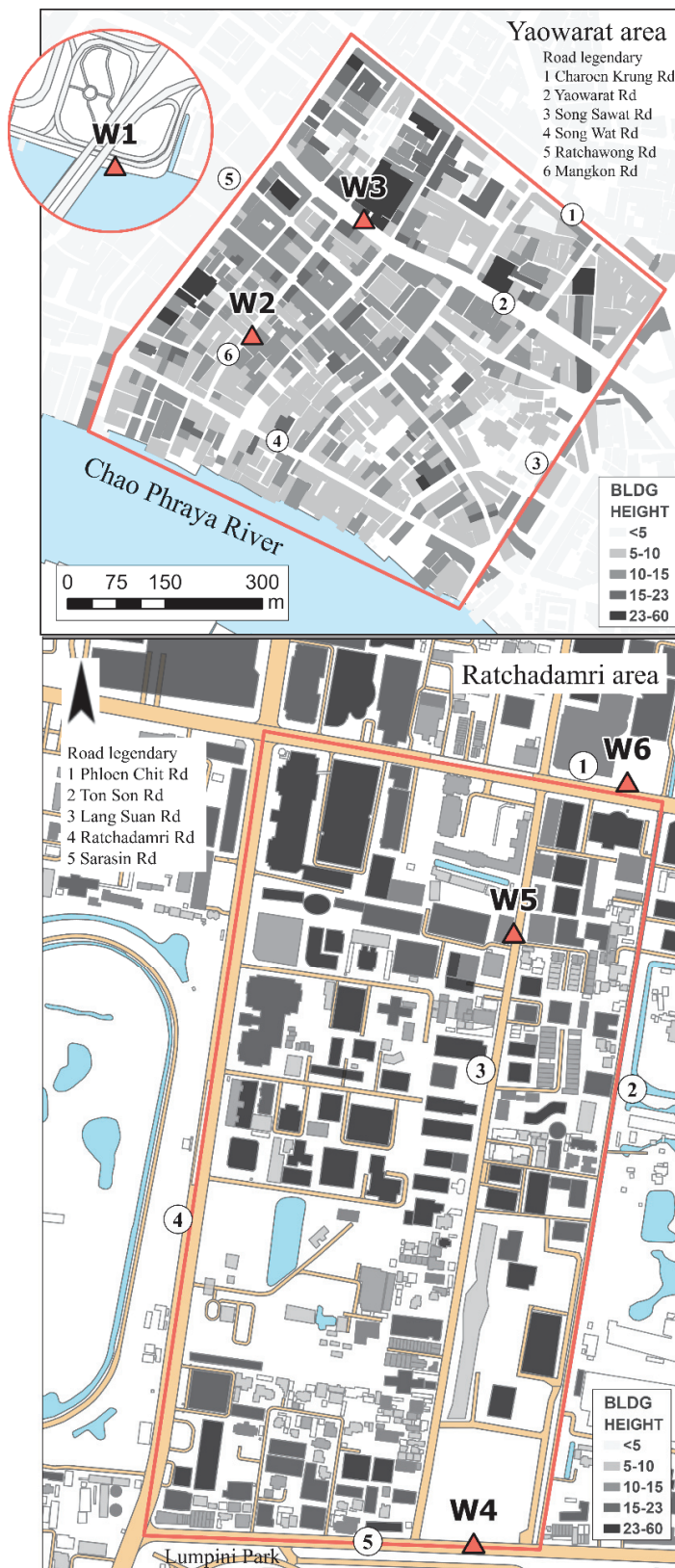
Fig. 5-2 The two study areas

5.3.2 The Field Measurement Data

In this chapter, the data usage was combined from two data resources, which are the field measurement data from Chapter 4 and the results from the CFD simulation. The field measurement surveys were conducted on October 19, 20, 23, and 24, 2022. Each study area measured the wind distributions in two days with three fixed stations (W1–W6). To measure the wind velocity (WV) and wind direction (WD), this study used a three-cup anemometer and an arrow-feather wind vane, respectively. The equipment for measuring was set up approximately two meters above ground level and had a 1-second interval from 8:30 to 17:30 each day. In addition, the various urban topographies were used as criteria for measuring urban ventilation. The detail is shown in Chapter 4. Figure 5-3 shows the photo from each field measurement station and the topography surrounding it within 100 m.
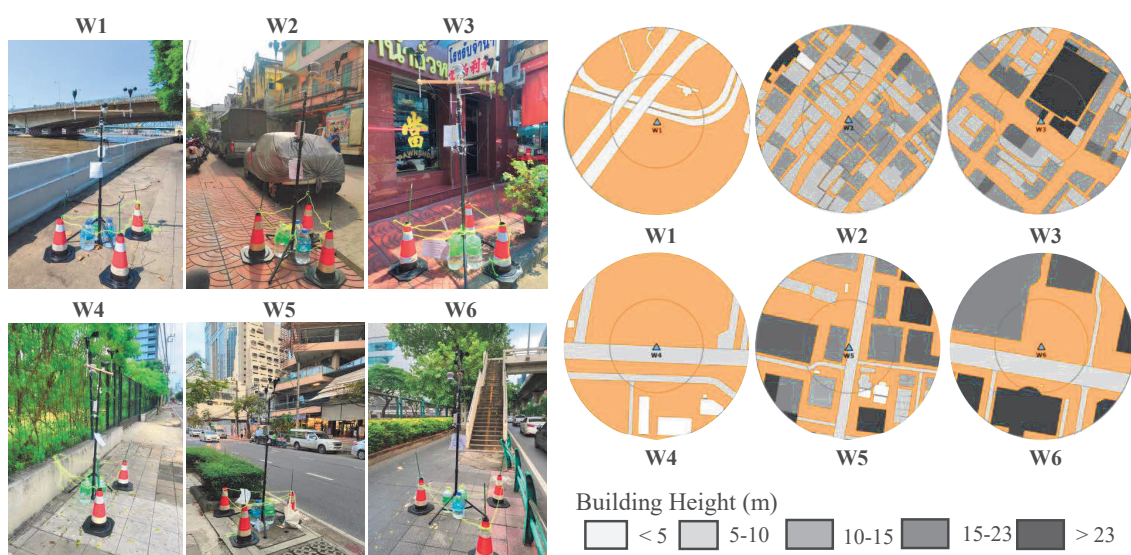
Fig. 5-3 Field measurement stations (W1–W6)

5.3.3 Spatial Analysis

The spatial analysis consists of two phases. The first phase was a classification of urban physical variables and the second phase was the correlation analysis between the wind velocity from the result of CFD simulation and urban physical variables.

Classification of Urban Physical Variables

According to the previous research data (Matsuo and Tanaka, 2019; Pakarnseree et.al, 2018; Srivanit and Kazunori, 2018; Kamma et al., 2020) and findings from Chapters 2–4, several variables affected the urban climate. The type of land coverage and its coverage ratio, comprising the measurement points, are two major considerations. Moreover, the urban microclimate — studied within 2 km^2 — was related to its context, such as the width of the road, the height-to-width (H/W) ratio, and the 3-D geometry of the building surface.

Therefore, the authors clarified four variables related to the previous studies from above. The list of variables is as follows:

1) Open space ratio (OSR) is calculated as the percentage of open space in the building's square footage, with two radii of 100 m and 50 m,

2) Road width (RW),

3) The average building height surrounding the station (BH), and

4) The 3-D geometry of building surface and tree models was created in GIS by the Bangkok Metropolitan Administration using field surveys and satellite images.

The above variables were statistically analyzed. However, the 3-D geometry of the building surface and vegetation objects were used for CFD simulations.

Correlation Analysis Between the Wind Velocity and Urban Physical Variables

First, the authors calculated the average WV from 9:00 to 17:30 with a 10-minute interval from the field measurement data. Second, the meteorological WD is the direction from which the wind blows. WD increases clockwise; that is, a northerly wind is 0°, an easterly wind is 90°, a southerly wind is 180°, and a westerly wind is 270°. For the WD analysis, the authors transferred the direction into a range of 0 to 16, where 0 (0°–11.25°) and 16 (348.75°–360°) are north. While 8 is south (168.75°–191.25°), each interval included 22.5°. Next, the authors selected the highest frequency of direction to represent each interval time. To analyze in SPSS, the authors divided WV data into four periods—all day, 9:00–12:00, 12:00–15:00, and 15:00–17:30. Finally, Pearson's correlation coefficients were calculated.

5.3.4 CFD Simulations and 3D Modeling

Numerical calculations using CFD simulations were performed to understand the overall ventilation of both CBDs. The CFD simulations section is divided into three steps. First, the authors created 3-D models—buildings, land surfaces, trees, and shadow volume—with GIS in ArcGIS Pro. Second, the authors transferred those models of each CBD to the simulation program, AKL Flow Designer 2022. This step defined the computational domain for the CFD simulations and created them. Computational conditions are shown in Table 5-1. Reynolds Averaged Navier-Stokes (RANS) equations were used in this software. The ventilation and climate data at 13:00, when the air temperatures, surface temperatures, and WV were high during the day, were used in the calculations.

The air temperature data input was sourced from the Don Muang Station, selected due to its urban surroundings and similarity to the study environment. In contrast, wind data input was obtained from the Suvarnabhumi Airport Station, chosen for its unobstructed wind conditions at 10 meters, making it a suitable representation of the prevailing wind patterns in the region. Additionally, this station is situated at a latitude of approximately 13°44' N, aligning closely with the latitudes of the two CBDs. Both stations are part of the weather observation network managed by the Thai Meteorological Department. For the input surfaced temperature, the average value of the measurement points was calculated for each material surface related to the result in Chapter 4, which are concrete buildings, asphalt roads, concrete pavement, greenery, and water, and these values were used as input data before calculations.

The last step was the CFD modeling validation. To confirm the accuracy of the numerical calculation results, the authors compared the results from CFD simulations and those from field measurements with raster analysis in GIS. Figures 5-4 and 5-5 show the 3-D geometry simulation models of the building surface, tree models, and the area of simulation of both districts. Additionally. the authors included only five field measurement points (W2–W6) in the study area due to the limitation of the simulation area.
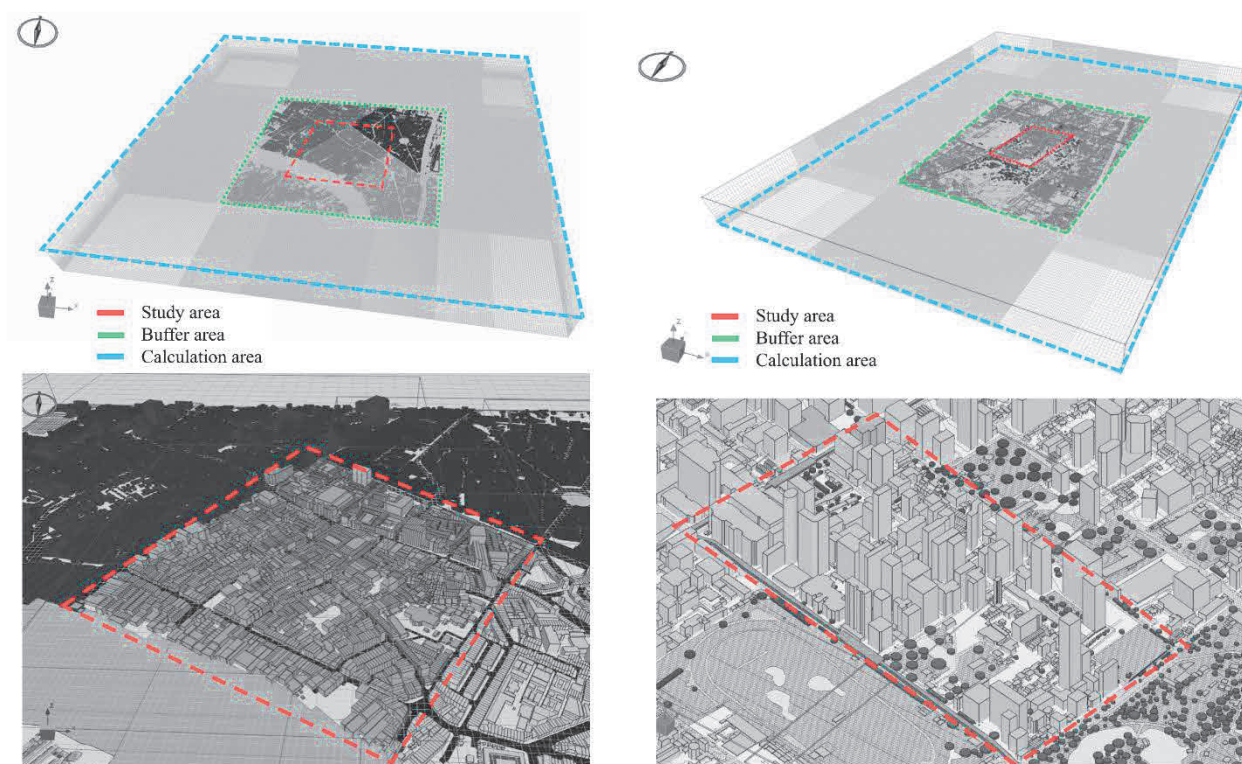
Fig. 5-4 (left) Area of simulation and 3-D models for numerical calculation of Yaowarat

 Fig. 5-5 (right) Area of simulation and 3-D models for numerical calculation of Ratchadamri

Table 5-1 Computational domain for the CFD simulation

Software	AKL FlowDesigner 2022, second revision	
Study area	Yaowarat Area	Ratchadamri Area
Maximum resolution (m): (x × y × z)	Analysis area (m): 2 × 2 × 2 Buffer area (m): 4 × 4 × 4 Calculation area (m): 8 × 8 × 8	
Area of Simulation (m): (x × y × z)	Study area: 900 × 1150 × 268 Buffer area: 1900 × 1596 × 268 Calculation area: 3728 × 3184× 268	Study area: 1100 × 1400 × 416 Buffer area: 2000 × 2600 × 416 Calculation area: 4000 × 5184 × 416
Turbulence model	High Reynolds Number Type, k-ε model	
Analysis conditions	Steady-State Analysis (1-200 times)	
Inflow conditions	Power Measurement Condition: 0.27 Inflow wind: weather station data (h=10m)	
Outflow conditions	Free flow condition	

Input data	Data from the Thai Meteorological Department, Don Muang station (temperature data) and Suvarnabhumi station (wind data), at 13:00 on 20th October 2022 Air Temperature: 32°C, Relative Humidity: 60% WV: 3.60 m/s, WD: East (80°) (h=10m) Surfaced Temperature (ST)[with shade] obtained from field measurement: Building ST: 40–43°C [34°C], Road: 46°C [32°C], Impervious area: 45°C [32°C], Water surface: 30°C, Vegetation area (grass, bush, tree): 35°C [32°C]

5.4 Results and Discussions

The results are divided into four parts:

5.4.1   Ventilation characteristics of old and new CBDs in Bangkok

The prevailing wind rose diagram for Bangkok from TMD (2022) is shown in Figure 5-6. It shows the prevailing wind rose from 2012–2022 (a), and October 2022 (b). In October 2022, WD is mostly between North and East, and the WV is less than 2 m/s. Regarding the field measurement results from the six stations illustrated in Figure 5-7, the surface areas in the figure represent WV, with continuous variables indicated on the left vertical axis, while the dots represent WD, shown with discrete variables on the right. The data reveals that both CBDs exhibited poor WV, closely resembling the prevailing wind patterns. WD data from the six stations exhibited two distinct patterns. One pattern demonstrated a consistent wind direction throughout the day, while the other pattern indicated a shift in wind direction during the afternoon, specifically around 14:00. While the majority of wind directions aligned with the prevailing wind, some stations exhibited different directions, such as South and West (e.g., W3). These WD variations appear to be closely linked to the specific characteristics of each measurement point's surroundings, with road orientation playing a significant role in influencing wind direction.

However, to understand more about both areas, CFD simulations are necessary. Yaowarat and Ratchadamri had similar conditions in the computational domain for the CFD simulation (Table 5-1). Only simulation areas were different, related to the size of each district. The main variables were characteristics of the 3-D geometry of the building and tree surfaces with different surface temperatures depending on the surface material. Figures 5-8 and 5-9 show the WV contours at 1 p.m. (at a 2-meter level) of two CBDs in Bangkok based on the results of CFD simulations. Figure 5-10 illustrates the outcomes of CFD simulations conducted around five designated measurement points. These simulations provide support for the notion that WD downwind (at a distance of 2 meters) within the urban microclimate is intricate and closely tied to several factors, including the approach flow direction, the three-dimensional geometry of buildings, and the overall urban form (as discussed in Oke et al., 2017). The majority of WD within the urban area exhibits complexity and considerable variability. Table 5-2 shows the details of each urban topography. These results supported and showed the ventilation characteristics of each CBD.

5.4.1 Ventilation characteristics of Yaowarat area

Yaowarat was mixed between compact low-rise to compact mid-rise. The average height of the building was 10.2 m, high density of small footprints with 53.3% of building coverage ratio (BCR), and the average road width was 8 m. The prevailing WD of the Yaowarat area was from North and East from the results of W1, which is the location without surrounding obstacles and located parallel to the Chao Phraya River. Nonetheless, it is crucial to acknowledge that the inner urban area can exhibit varying WD, which are influenced by factors such as urban layout, road orientation, and the specific measurement location. As indicated in prior research (Oke et al., 2017), the approach flow around many urban buildings has already been disrupted by upwind structures, resulting in a complex wind pattern. This complexity manifests in several distinctive flow patterns within urban canyons. One case in this area is WD of W3, which is mostly from the south. W3 was behind the building line, which is perpendicular to the approach flow (ENE–E). This created a recirculation vortex and made the WD be the opposite side.

The highest WV among the six stations was observed around the riverside. Based on the field measurement results, W1, representing an open area, exhibited the highest average WV at 1.08 m/s, with the maximum WV occurring in the afternoon at 2.74 m/s. In contrast, both W2 and W3, situated amidst shophouses and buildings characterizing the Yaowarat urban topography, had significantly lower WV values, almost reaching 0 m/s (0.06 and 0.23, respectively). Even though the road is parallel to the wind's direction (W2), the wind cannot pass through the urban area because it is surrounded by compact low-rise buildings. The CFD simulations' results were supported with the field measurement. Figures 5-8 and 5-11 show almost 80% of all open space areas in Yaowarat had WV less than 1 m/s. It had only four spots above the middle of the wide road (15–18 m), which had a WV higher than 2 m/s, however, the WV above the Chao Phraya River could rise to 6.5 m/s. Moreover, both methodologies' results confirmed that the urban area with a high density of small footprints and similar-height buildings (compact low-rise to compact mid-rise) will have stable and poor ventilation and need to improve WV related to its urban topography.

The combination of WD and WV patterns in the Yaowarat area (Figures 5-7 and 5-12-a) shows the potential to increase WV in the afternoon in the urban area. Related to previous research that showed in the afternoon, surrounding buildings accumulated heat and after that, it increased air circulation in the urban area, WV also increased (Oke et al., 2017). Furthermore, the advantage of the riverside area, characterized by its high WV, could be enhanced if more open spaces were created adjacent to the riverside areas, allowing the river's winds to flow through the inner urban region via wider roads. This improvement in ventilation would significantly benefit Yaowarat. However, the primary challenge in developing this area lies in the constraints of limited available land and the presence of numerous small streets and alleys, which are difficult to eliminate due to potential social concerns.

Ventilation characteristics of Ratchadamri area

Ratchadamri was mixed between compact midrise high-rises and open high-rises. The average height of the building was 21.4 m with 33% BCR and an average wider road (13.8 m) (Table 5-2). Although this area had parks and open spaces, the field survey could not measure those locations because it was private land. However, to understand Ratchadamri ventilation, the CFD simulations were necessary.

In the Ratchadamri area, W5 has the highest WV on both days, and W4 has the lowest WV. Only Ratchadamri has WV patterns between W4, W5, and W6 from both days but WD from three points seemed that it does not match with Bangkok's prevailing wind, the WD of the Ratchadamri area was mostly from North and West. Similar reasons as Yaowarat and other urban areas, WD was complicated. The CFD simulations showed that Ratchadamri had a wide range of WV from 0–7 m/s. The private open spaces in the southern part had high WV (5–7 m/s). However, the northern area with compact high-rise buildings had low WV (0.5–1.5 m/s). Moreover, the street canyon in the center had a higher WV (3.5 m/s). This area can trap the upwind air at ground level, thus, almost 30% of the open space had WV higher than 2 m/s (Figure 5-10).

Based on the results of field measurements and spatial analysis, W1 and W4 both represent open space areas. However, it raises a curious question as to why W4 exhibits a high OSR, but a lower WV compared to W1, despite having a similar environmental context. Regarding W4, despite its lack of immediate building surroundings, its proximity to a 4-meter-high linear stretch of bushes (Figure 5-3) is a notable micro-level factor impacting its WV. Interestingly, simulations in Figure 5-10 show that the area around W4 initially experiences high WV before encountering the tall bush boundary. According to Table 5-3, W5 has more OSR and is situated on a wider road.

In addition, Lang Suan Road, where this location is situated, is flanked on both sides by high-rise buildings (Figure 5-9). This creates a "street canyon" that traps up-wind from the air layer above to the ground below, giving W5 a relatively constant and high WV throughout the day. W6 was located near the open space among the compact high-rise buildings, however, its average velocity was about 0.45 m/s (Figures 5-9 and 5-11). Figure 5-10 shows that the surrounding tree model was one of the variables. Although trees had increased the shaded area to mitigate the urban heat, it would affect the WV at the pedestrian level.

The ventilation characteristics of Ratchadamri are contingent on its location and surroundings. In densely populated high-rise areas, WV tends to be low to medium, with WD varying significantly. However, it's worth noting that introducing tall buildings aligned parallel to the prevailing wind and wider roads in this area could potentially boost WV, particularly in the afternoon. Conversely, other open spaces within this region experience high WV, contributing to superior urban ventilation capabilities, which play a vital role in mitigating UHI effects and reducing air pollution.

Both methodologies employed indicate that Yaowarat exhibits poorer ventilation compared to Ratchadamri. When focusing on WV within the urban areas of both CBDs, specifically stations W2, W3, W5, and W6, it becomes apparent that W5 boasts the highest average WV. Furthermore, Ratchadamri consistently demonstrates higher WV values than Yaowarat, with specific figures of 0.06, 0.23, 0.8, and 0.45, respectively. Despite W1 displaying the highest average WV, it doesn't necessarily equate to better ventilation within the inner area due to geographical constraints. These findings underscore the distinct urban ventilation characteristics of Yaowarat and Ratchadamri, even though they share a similar latitudinal position.

Both areas require targeted efforts to enhance and incentivize WV to improve ventilation. Urban climatology emerges as a valuable process for analyzing these characteristics and aiding stakeholders in understanding their respective areas. Ultimately, this knowledge can pave the way for sustainable urban planning within the Bangkok metropolitan area.

Table 5-2 Comparison of urban topography and WV characteristics of two CBDs

Study area		Yaowarat	Ratchadamri
Urban Topography	Area (sqm.)	419,960	679,351
	BCR (%)	53.3%	33%
	Avg. BH (m)	10.2	21.4
	Avg. RW (m)	8.6	13.8
	H/W ratio	1.183	1.54
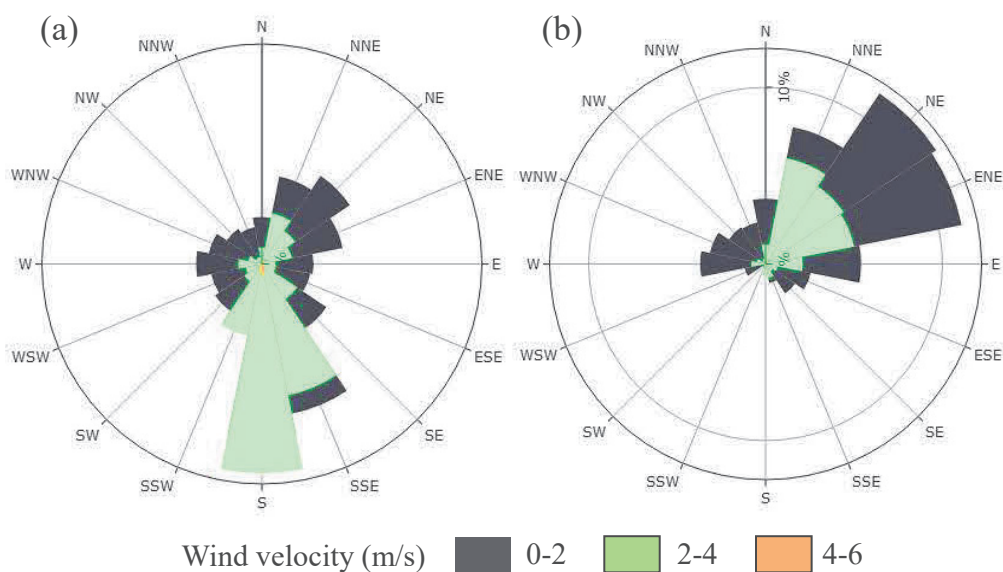
Fig. 5-6 Wind rose diagram for Bangkok: (a) prevailing winds from 2012–2022, (b) October 2022
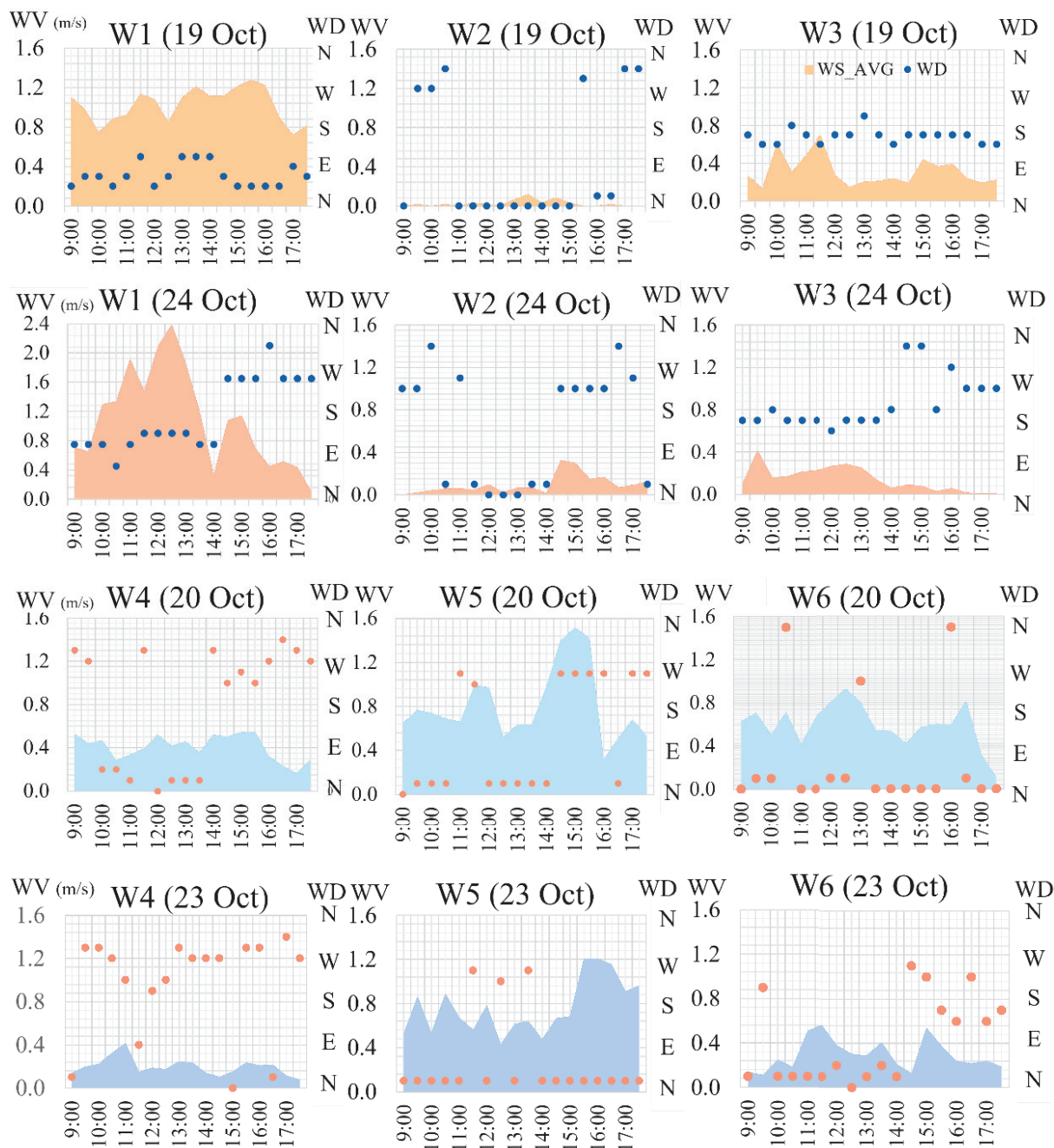
Fig. 5-7 WV and WD data from six fixed stations in four days of actual measurement
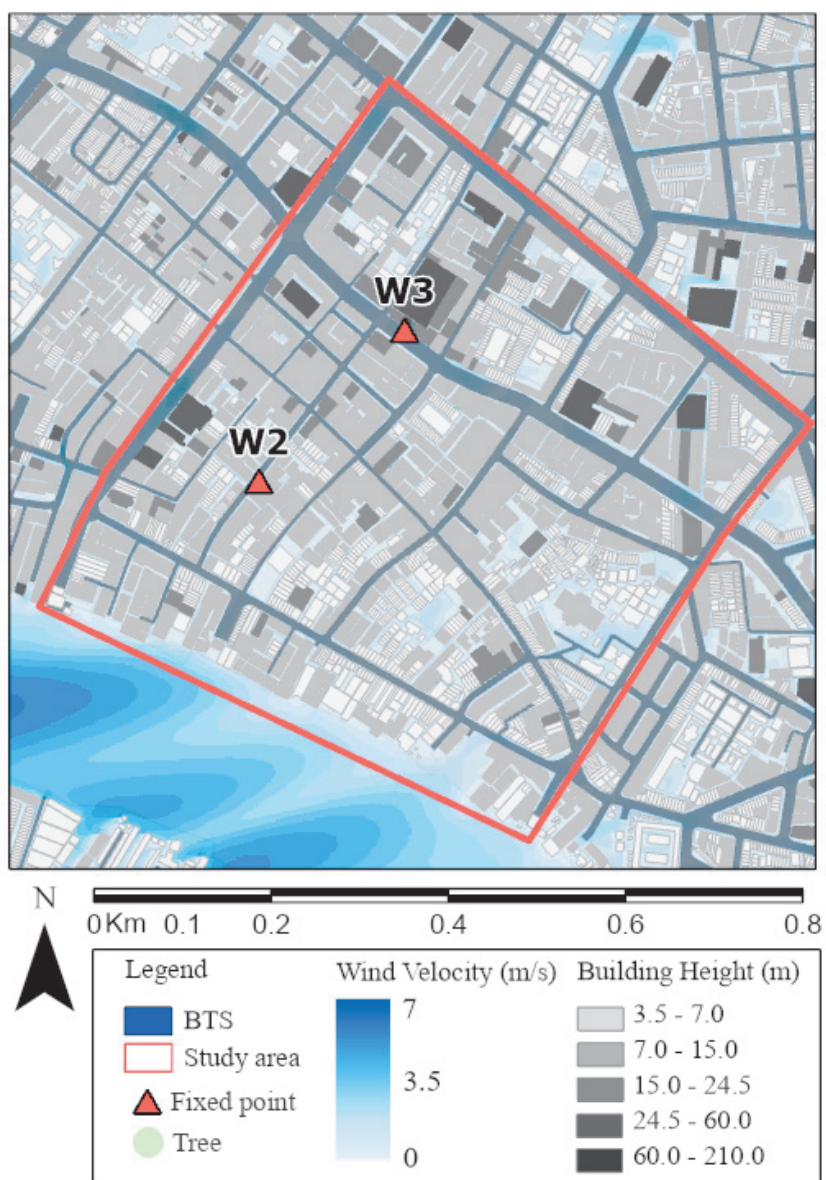
Fig. 5-8 Velocity contours of the Yaowarat area at 1 p.m.

Fig. 5-9 Velocity contours of the Ratchadamri area at 1 p.m.
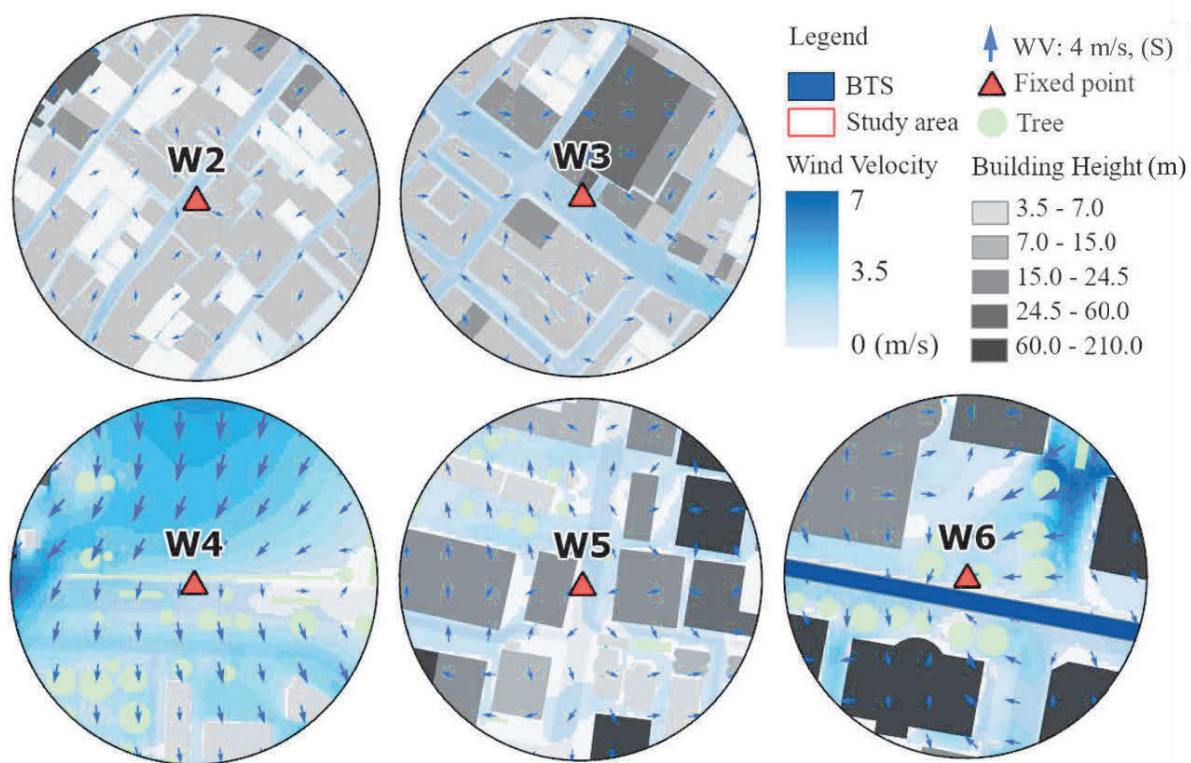
Fig. 5-10 Velocity contour areas at 1 p.m. of five fixed stations in the field measurement
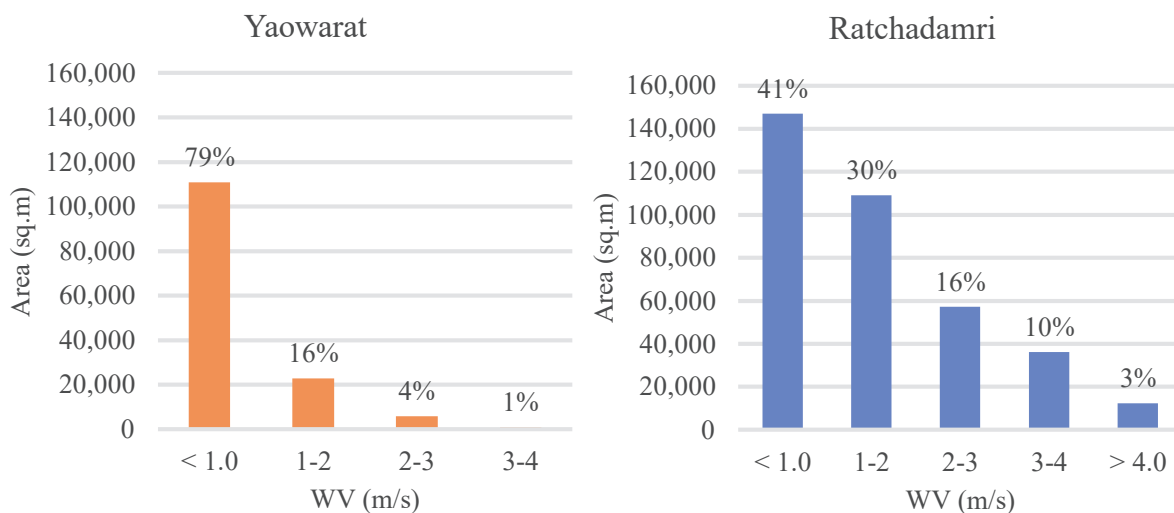
Fig. 5-11 WV range of each CBD from the CFD simulations

5.4.2   Relationship between WV and urban physical variables

In the "Classification of the Physical Variables" section, Table 5-3 presents the characteristics of three variables. Based on the results derived from field measurements and spatial analysis, Figure 5-12(a) illustrates the correlation between WV and different periods using data from six stations, revealing three primary WV patterns. The first pattern, denoted as W1, exhibits the highest WV between 11:00 and 13:30, with a decrease in WV during the late afternoon. The second pattern encompasses W2 and W5, both displaying peak WV values from 14:30 to 16:00 and 14:00 to 16:00, respectively. These patterns highlight the relationship between WV and specific periods. The third pattern involves W3, W4, and W6, which demonstrate a consistent distribution of WV and appear to be less dependent on periods. Subsequently, correlations were computed between WV during different periods and three physical variables. Table 5-4 presents the overall results, consisting of 104 samples per station, all exhibiting similar characteristics in terms of OSR50, OSR100, RW, BH50, and BH100.

The following three segments summarize the relationship in this section. First, OSR is positively correlated with WV across all periods. The correlation was highest between 12:00 and 15:00 and decreased between 15:00 and 17:30. Between the OSR within 100 m and 50 m, OSR100 had a higher correlation coefficient than OSR50. This result was shown by scatter plots in Figures 5-12(b) and 5-12(c). Second, only BH within 50 m of the WV had a low correlation (all-day period). However, only the standard BH of 100 m-radius is positively correlated with the all-day and late afternoon periods. In the third segment, it's worth noting that RW doesn't exhibit a significant correlation with WV, despite the CFD simulations highlighting the presence of four areas with higher WV on the wide roads in the Yaowarat area. In the realm of urban climatology, it's crucial to consider not only the impact of RW but also the ratio between RW and the building height of the area, as this ratio shows correlations with WV.

Finally, this result proves that the measured WV is related to the urban topography. Only three urban physical variables were used, limiting the spatial statistical analysis in this study. Further study could analyze other variables to define more key factors for the ventilation characteristics of CBDs in Bangkok. Although previous studies have shown that the type of land coverage directly affects urban climate (Chapter 2, Matsuo and Tanaka, 2012; Srivanit and Kazunori, 2011), due to research limitations, field measurement points are only in the urban area, which is almost impervious. Furthermore, urban elements such as trees, bushes, signs, or canopies can influence WV, particularly in the cases of W4 and W6. This underscores the need for their consideration in architecture, landscape, and urban planning.

Table 5-3 The physical variables of the fixed station

Fixed station	OSR100 (%)	OSR50 (%)	RW (m)	BH100 (m)	BH50 (m)
W1	75.3	65.4	15.0	3.0	3.0
W2	31.5	34.2	8.0	9.9	9.6
W3	39.7	38.7	20.0	12.4	14.9
W4	72.2	100.0	16.0	3.5	0.0
W5	43.1	62.4	12.0	22.6	11.8
W6	42.7	88.4	23.0	51.3	36.2

Table 5-4 Correlation coefficients analysis from the field measurement

WV	OSR100	OSR50	RW	BH100	BH50
9:00–17:30	**0.420**[**]	**0.181**[**]	0.022	-0.023	**-0.117**[**]
9:00–12:00	**0.474**[**]	**0.195**[**]	0.098	-0.042	-0.119
12:00–15:00	**0.477**[**]	**0.189**[**]	0.018	-0.056	-0.139[*]
15:00–17:30	**0.276**[**]	0.152[*]	-0.069	0.053	-0.078
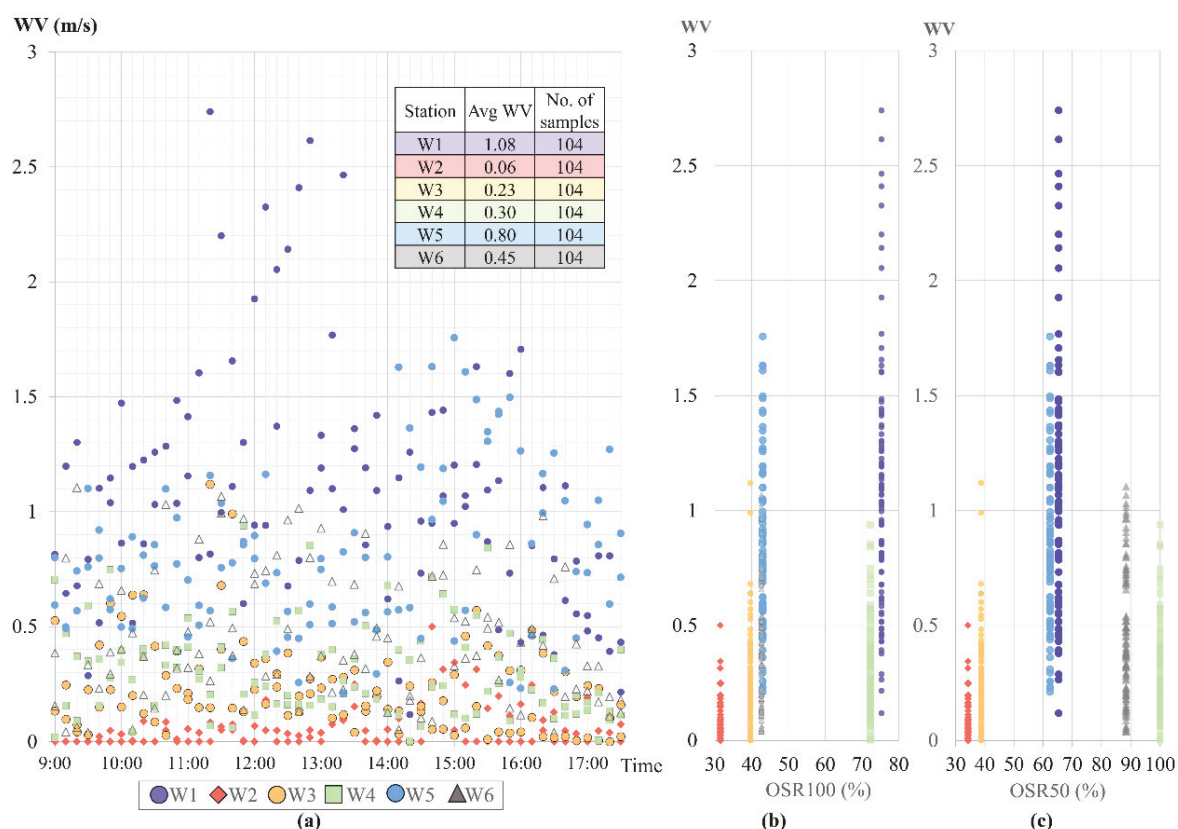
Fig. 5-12 The relationships of WV across W1 to W6 and various times (a),
WV and OSR100 (b), and WV and OSR50 (c)

5.4.3 Data usage and methodology

The methodologies employed in this study draw support from various insights obtained through prior research. This study specifically addresses a gap in the field of urban microclimate studies in tropical countries. Field measurements serve as a primary approach, offering the distinct advantage of capturing the authentic complexity inherent in the studied problem. Additionally, they play a crucial role in validating the accuracy of simulations. However, it's important to acknowledge certain limitations, notably the lack of full controllability due to the inherently variable meteorological conditions. Furthermore, field measurements are not feasible during the design stage of urban areas, presenting a challenge in terms of their temporal applicability (Blocken, 2015). Conversely, numerical modeling using CFD stands out as a potent alternative, offering the advantage of circumventing certain limitations associated with field measurements. CFD has the capability to furnish detailed information regarding pertinent flow variables throughout the entire computational domain under tightly controlled conditions, eliminating the need for similarity constraints.

In addition, it is imperative to subject CFD simulations to thorough assessment through solution verification and validation processes. A comprehensive survey of research in the realm of CFD analysis for urban microclimates indicates a growing prevalence in the field (Toparlar et al., 2017; Yang et al., 2023). As highlighted in Toparlar's study (2017), a significant portion of CFD-based urban microclimate investigations, specifically 105 out of 183 studies, was undertaken without proper validation. The predominant reason for this absence of validation appears to stem from the scarcity of pertinent and well-documented measurement data for comparison with the simulation outcomes. While acknowledging that the validation of CFD simulations demands substantial-high-quality experimental data and entails additional resources in terms of time and cost, our study addresses this limitation by conducting on-site field measurements in Bangkok. This dual approach in our study is designed to mitigate the drawbacks inherent in each method.

In urban studies modeling, Liu et al. (2017) conducted a comparison between wind distributions computed by a full-scale model and a micro-scale local model. Despite the longer time required for constructing a geometrical model, they recommended a full-scale model for predicting wind distribution in urban areas. Additionally, Ricci et al. (2022) suggested incorporating a "buffer zone" around the area of interest in real urban modeling, aligning with the approach employed in this study.

A similar methodology to our study's CFD simulation of urban microclimate is evident in the work conducted in Nicosia, Cyprus, by Tian et al. (2023). However, challenges were noted in accurately simulating urban velocity in locations within narrow streets and close to downwind regions of buildings. The CFD results tended to overpredict wind velocity (WV) due to the absence of obstacles like trees, cars, and detailed building geometries in the model. Addressing this issue was emphasized in our simulation modeling, aiming to enhance the precision of the simulation results.

This study identified cars as a noteworthy obstacle to urban ventilation, considering Bangkok's status as the second most traffic-congested city globally (Traffic Index, TomTom, 2016). Exploring the impact of traffic congestion on urban ventilation could be a crucial factor for future investigations. A study in Dalian City, China (Shi et al., 2022), focused on constructing urban ventilation corridors to introduce fresh air into the urban interior while mitigating the Urban Heat Island (UHI) effect. Although employing a different methodology, this approach could be considered for future research. Similarly, in Nanjing megacity, China (Antonion et al., 2019), urban ventilation shaped the canopy of UHIs and heat waves, demonstrating the potential of urban planners to mitigate the UHI phenomenon through strategic urban ventilation planning.

This research represents a preliminary exploration of urban microclimates in the CBDs of Bangkok. The utilization of numerical calculations via CFD simulations has enhanced our overall understanding of urban ventilation characteristics, complementing the analysis of field measurement data from specific points. Furthermore, the potential of extending CFD simulations to correlate mesh values with urban environmental variables is highlighted. CFD emerges not only as one of the most popular numerical simulation techniques but also as a vital methodology in urban physics, contributing to an applied multidisciplinary approach. This underscores its importance in comprehending and addressing the significant challenges associated with increasing urbanization. Building on the findings of several prior studies (Toparlar et al., 2015; Blocken, 2014; Blocken, 2015), the current study reinforces the potential of CFD in accurately predicting urban microclimates.

In conclusion, to attain a comprehensive understanding of ventilation characteristics in both CBDs, this study emphasizes the importance of combining computational simulations and field measurements. The results strongly advocate for integrating both approaches in future research within the domains of urban climatology and urban design planning.

5.4.4 CFD simulations validation

The computational modeling for CFD simulation at the 2-meter level required developing and inputting more details of 3-D geometry — related to the wind flow — for better accuracy compared with that of the field measurements. In this case, the authors revised the ventilation simulation three times. Each model had the differentiation of urban components as follows:

Model 1: building models and land coverage surfaces.

Model 2: building models, land coverage surfaces, building-shaded surfaces, and trees

Model 3: building models, land coverage surfaces, floated trees (4m aboveground), bushes, floated rail structure (10m aboveground) of Bangkok sky train systems (BTS), and shaded surfaces (13:00 UTC+7, October 2022)

Table 5-5 shows the comparison of the results from CFD simulations and the five points of the field measurement. The average values for ten minutes from 12:50 to 13:00 were used for the actual survey data (13:00), and the average values for the mesh overlapping the 2-meter radius around each measurement point were used for the numerical calculation results. Scatter plots of WV from three models are also shown in Figure 5-12. From the scatter plots, the distribution trend of the numerical calculation results was generally representative of the actual situation with a high correlation coefficient ($R^2 = 0.8664$). The results of the simulations were comparable.

The correlation coefficient between both WV from Model 1, Model 2, and Model 3, were gradually higher ($R^2 = 0.54, 0.58, 0.87$, respectively). These showed that detailed simulation modeling could effectively the accuracy of WV in urban microclimates. However, WD from the simulation is not exactly matched. WDs were different between 22.5–67.5 degrees. The results from field measurement and simulation of W2, W4, W5, and W6, were correlated with the prevailing wind (N–E).

However, the results at W3 were different. WD was between SSW and SSE because W3 was behind the building line, which is perpendicular to the approach flow (ENE–E). This created a recirculation vortex and made the WD be the opposite side. Further study could have considered more variables and adapted the simulation setting and modeling related to these issues. The numerical results from Model 3 were used to analyze each CBD's ventilation characteristics in this research.

Table 5-5 Comparison of measured survey results and numerical results (Model 3)

Measured Points	WV (m/s)		WD	
	Field Measure Results	Numerical Results	Field Measure Results	Numerical Results
W2	0.02	0.37	N	ENE
W3	0.27	0.57	SSW	SSE
W4	0.85	0.87	NNE	N
W5	0.60	0.56	NE	E
W6	0.80	0.83	N	ENE
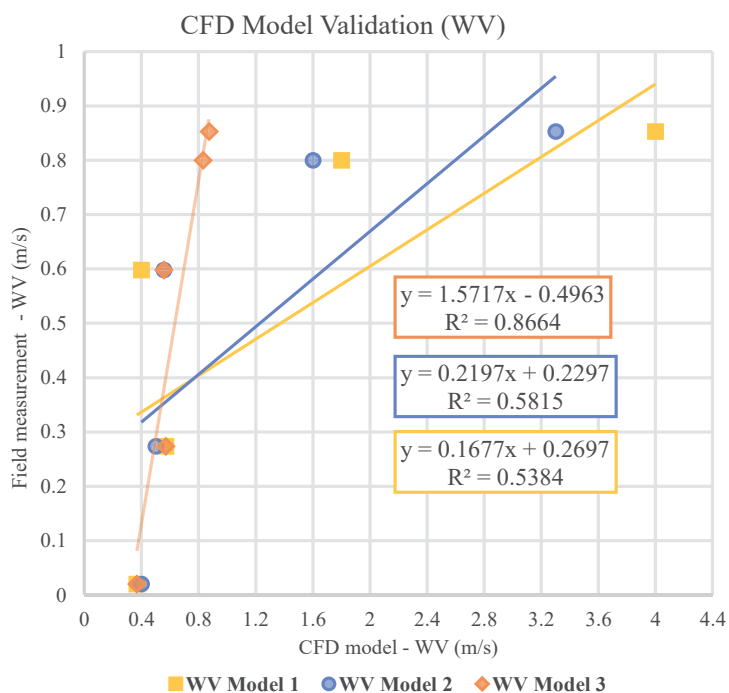
Fig. 5-13 Scatter plots of CFD simulation validation

5.5 Conclusion and Proposals

This study is preliminary research on urban microclimate in the CBDs of Bangkok: a case study in the district of Yaowarat and Ratchadamri districts. Field measurements and numerical calculations using CFD simulations have increased the overall understanding of urban ventilation characteristics, in addition to analyzing the relationship between physical variables and urban ventilation, particularly WV from field measurement data. From the correlation results, within 100 m, WV and OSR were highly correlated. The period of the day had affected WV for the urban area, which had a road orientation similar to the approach flow direction.

Moreover, this study demonstrated the numerical calculation with CFD simulations and combined it with field measurement results to understand the ventilation characteristics of each CBD. Yaowarat, which is a compact low-rise and mid-rise with narrow streets, had poorer ventilation than Ratchadamri. The average velocity at 1 p.m. (at a 2-meter level) in this area was less than 1 m/s. The wind could not pass through this urban topography, while the riverside area without obstacles had the highest average WV (2.78 m/s). It showed the potential to develop the Yaowarat area to better ventilation if it had more open space next to the Chaophraya River.

However, Ratchadamri is compact high-rises, and open high-rises with several open spaces. It had a wide range of WV. The open spaces in this area had high WV (4–7 m/s) and it made better ventilation. Ratchadamri's average WV was 1–2 m/s. Furthermore, the street canyon in the center had a higher WV (approximately 3.5 m/s) than the area with compact high-rise buildings (0.5–1.5 m/s). This urban characteristic can trap the upwind air at ground level and increase the WV for better ventilation. If the urban planners could adapt the urban ventilation, it would mitigate the UHI.

In addition, the WV validation from CFD simulations had high correlation coefficients with the results from field surveys (R^2 = 0.8664). Variables affecting the accuracy of the urban ventilation simulations in the numerical calculation results are the building model, the floated trees model, bushes, the floated BTS structure model, land coverage surfaces, and total components shaded surfaces. These showed that detailed simulation modeling could effectively the accuracy of WV in urban microclimates. However, the results of WD were different between 22.5 and 67.5 degrees due to the complexity of urban variables.

This study shows the old and new CBDs of Bangkok, which are located at similar latitudes, and similar mesoscale climate zoning, have different microclimate ventilation characteristics related to their urban topography and spatial variables. This study confirms the importance of an urban microclimate study, which can lead to understanding the current climate of Bangkok and mitigate the UHI related to WV, as a response to sustainable urban development.

5.6   Limitations and Further Study

The study found obstacles and weaknesses that could provide improvements for future studies. The limitations of this study and topics for further study are as follows:

The validation of the CFD model primarily focused on correlating the mean WV between field measurement data and simulation data at 1 p.m. However, it's essential to note that the field measurements were conducted in October, during Thailand's hot and humid season, which may not fully represent the region's year-round characteristics. Future studies could consider measurements during other periods, such as the hot-dry period (February to April) or cool-dry period (November to February), or explore different seasons using the CFD model. Furthermore, the availability of weather input data from two stations of the Thai Meteorology Department, measured at 2m-level for air temperature and 10m-level for wind data, may not provide comprehensive coverage. Enhanced accuracy could be achieved if additional higher-level wind data were accessible for central Bangkok.

This study used the 3D steady RANS equation with the standard k–ε model in CFD analysis owing to the limits of time and cost. However, steady RANS is associated with important limitations in terms of modeling the important features of fully turbulent flow around bluff bodies in urban physics (Blocken, 2015). It is still by far the most widely used approach in most urban physics focus areas, as it has been developed over the past 15 years. Further studies could expand and use unsteady RANS, Large Eddy Simulation, or other hybrid simulations.

A faster numerical simulation method was developed for large urban or regional scales. A few studies (Wang et al., 2021; Xu et al., 2023) mentioned other methods with less detailed modeling, such as the Porous Media Model, Fast Fluid Dynamics, and outdoor Multizone Model, and these methods reduced computational costs. In the case of Bangkok, which consists of uneven groups of buildings and complex buildings, these methods encounter difficulties. Further study could be considered.

References

Antoniou, N., H. Montazeri, M. Neophytou, & B. Blocken (2019). CFD simulation of urban microclimate: Validation using high-resolution field measurements. *Science of the Total Environment 695,* 133743. https://doi.org/10.1016/j.scitotenv.2019.133743.

Arnfield, A.J. (2006). Micro- and mesoclimatology. *Prog Phys Geogr, 30*, 677-689. https://doi.org/10.1177/030913330607115.

Blocken, B. (2014). 50 Years of Computational Wind Engineering: past, present, and future. *Wind Eng Ind Aerodyn, 129*, 69-102. https://doi.org/10.1016/j.jweia.2014.03.008.

Blocken, B. (2015). Computational Fluid Dynamics for urban physics: importance, scales, possibilities, limitations and ten tips and tricks towards accurate and reliable simulations. *Build Environ, 91*, 219-245. https://doi.org/10.1016/j.buildenv.2015.02.015.

Heshani, A.L.S., & E. Winijkul (2022). Numerical simulations of the effects of green infrastructure on PM2.5 dispersion in an urban park in Bangkok, Thailand, *Heliyon, 8(9),* e10475. https://doi.org/10.1016/j.heliyon.2022.e10475.

Howard, L. (1820). The Climate of London. Volume II, London: W. Phillips.

Kamma, J., K. Manomaiphiboon, N. Aman, T. Thongkamdee, S. Chuangchote, & S. Bonnet (2020). Urban heat island analysis for Bangkok: multi-scale temporal variation, associated factors, directional dependence, and cool island condition. *Science Asia, 46*, 213-223. http://dx.doi.org/10.2306/scienceasia1513-1874.2020.024.

Khamchiangta, D., & S. Dhakal (2020). Time series analysis of land use and land cover changes related to urban heat island intensity: Case of Bangkok Metropolitan Area in Thailand. *Journal of Urban Management, 9(4)*, 1-12. https://doi.org/10.1016/j.jum.2020.09.001.

Liu, S., W. Pan, H. Zhang, X. Cheng, Z. Long, & Q. Chen (2017). CFD simulations of wind distribution in an urban community with a full-scale geometrical model. *Building and Environment, 117*, 11-23. https://doi.org/10.1016/j.buildenv.2017.02.021.

Matsuo K., & T. Tanaka (2019). Analysis of spatial and temporal distribution patterns of temperature in urban and rural areas: Making urban environmental climate maps for supporting urban environmental planning and management in Hiroshima. *Sustainable Cities and Society, 47*, 1-22. https://doi.org/10.1016/j.scs.2019.01.004.

Mill, G. (2014). Urban Climatology: history, status and prospects. *Urban Climate, 10,* 479-89. https://doi.org/10.1016/j.uclim.2014.06.004.

Moonen, P., T. Defraeye, V. Dorer, B. Blocken, & J. Carmeliet (2012). Urban Physics: effect of the micro-climate on comfort, health and energy demand. *Front Archit Res, 1,* 197-228. https://doi.org/10.1016/j.foar.2012.05.002.

Oke, T.R., G. Mills, A. Christen, & J.A. Voogt (2017). Urban Climates. 1st edition, Cambridge, United Kingdom: Cambridge University Press.

Pakarnseree, R., K. Chumkao, & S. Bualert (2018). Physical characteristics of Bangkok and its urban heat island phenomenon. *Building and Environment, 143*, 561-569. https://doi.org/10.1016/j.buildenv.2018.07.042.

Ricci, A., M. Burlano, M.P. Repetto, & B. Blocken (2022). Static downscaling of mesoscale wind condition into an urban canopy layer by a CFD microscale model. *Building and Environment, 225,* 109626. https://doi.org/10.1016/j.buildenv.2022.109626.

Rizwan, A.M., Y.C. L. Dennis, & C. Liu (2008). A review on the generation, determination, and mitigation of urban heat island. *Environ Sci, 20*, 120-128. https://doi.org/10.1016/S1001-0742(08)60019-4.

Santamouris, M. (2007). Heat Island research in Europe: the state of the art. *Adv Build Energy Res, 1*, 123-150. https://doi.org/10.1080/17512549.2007.9687272.

Schwarz, N., U. Schlink, U. Franck, & K. Gromann (2012). Relationship of land surface and air temperature and its implications for quantifying urban heat island indicators-An application for the city of Leipzig. *Ecological Indicators, 18*, 693-704. (in German)

Shi, Z., J. Yang, Y. Zhang, X. Xiao, & J.C. Xia (2022). Urban ventilation corridors and spatiotemporal divergence patterns of urban heat island intensity: a local climate zone perspelusctive. *Environmental Science and Pollution Research 29,* 74394-74406. https://doi.org/10.1007/s11356-022-21037-9.

Souch, C., & S. Grimmond (2006). Applied climatology: urban climate. *Prog Phys Geogr, 30*, 270-279. https://doi.org/10.1191/0309133306pp484pr.

Srivanit, M., & H. Kazunori (2011). The influence of urban morphology indicators on summer diurnal range of urban climate in Bangkok metropolitan area, Thailand. *International Journal of Civil & Engineering, 11(05),* 34-46.

Sundborg, A. (1950). Local climatological studies of the temperature conditions in an urban area. *Tellus*, 2, 222-232. https://doi.org/10.3402/tellusa.v2i3.8544

Takkanon, P. (2017). Urban Geometry and Wind Simulation Studies for Comfort in Bangkok Street Canyon. *World Sustainable Built Environment Conference 2017,* Hong Kong. https://wsbe17hongkong.hk/_bin/ckfinder/userfiles/files/Paper/P_1061-1067%20Urban%20Geometry%20and%20Wind%20Simulation%20Studies.pdf.

Tian, W., Y. Yang, L. Wang, L. Zong, Y. Zhang, & D. Liu (2023). Role of local climate zones and urban ventilation in canopy urban heat island-heatwave interaction in Nanjing megacity, China. *Urban Climate, 449*, 101474. https://doi.org/10.1016/j.uclim.2023.101474.

Toparlar, Y., B. Blocken, P. Vos, G.J.F. van Heist, W.D. Janssen, T. Hooff, H. Montazeri, & H.J.P. Timmermans (2015). CFD simulation and validation of urban microclimate: A case study for Bergpolder Zuid, Rotterdam. *Building and Environment, 83,* 79-90. https://doi.org/10.1016/j.buildenv.2014.08.004.

Toparlar, Y., B. Blocken, B. Maiheu, & G.J.F. van Heijst (2017). A review on the CFD analysis of urban microclimate. *Renewable and Sustainable Energy Reviews, 80*, 1613-1640. https://doi.org/10.1016/j.rser.2017.05.248.

Thai Meteorological Department (TMD) (2023). Average Wind Rose of Bangkok. http://www.aws-observation.tmd.go.th/aws/awsWindRose., last accessed 2023/10/10.

Tom Tom's Traffic Index of 2016, Tom Tom Homepage, https://www.tomtom.com/traffic-index/bangkok-traffic/., last accessed 2022/05/10.

Unsakul, S., C. Sranpat, P. Chaisiriroj, & T. Leephakpreeda (2017). CFD-Based Performance Analysis and Experimental Investigation of Design Factors of Vertical Axia Wind Turbines under Low Wind Speed Conditions in Thailand. *Journal of Flow Control, Measurement & Visualization*, *5*, 86-98. https://doi.org/10.4236/jfcmv.2017.54007.

Wang, H., C. Peng, W. Li, C. Ding, T. Ming, & N. Zhou (2021). Porous media: A faster numerical simulation method applicable to real urban communities. *Urban Climate, 38,* 100865. https://doi.org/10.1016/j.uclim.2021.100865.

Xu, X., Z. Gao, & M. Zhang (2023). A review of simplified numerical approaches for fast urban airflow simulation. *Building and Environment, 234,* 110200. https://doi.org/10.1016/j.buildenv.2023.110200.

Yang, S., L.L. Wang, T. Stathopoulos, & A.M. Marey (2023). Urban microclimate and its impact on built environment – A review. *Building and Environment, 238,* 110334. https://doi.org/10.1016/j.buildenv.2023.110334.

Chapter 6
Guidelines for Urban Land Use Planning in the Central Business District of Bangkok from the viewpoint of Urban Heat Island Mitigation:
Case Study of the Ratchadamri Area

Contents

6.1   Introductions

The preceding chapter underscored the significance of two urban climate study methodologies applied in the central business districts (CBDs) of Bangkok, findings substantiated by prior research (Rizwan et al., 2008; Santamouris, 2007; Blocken, 2014; Blocken, 2015). However, to enhance the understanding and mitigation of the Urban Heat Island (UHI) effect, elucidating its relationship with urban spatial structures becomes imperative (Pakarnseree et al., 2018; Kamma et al., 2020; Khamchiangta and Dhakal, 2020). Comprehending the urban climate is inherently challenging due to multifaceted factors and intricate relationships. Computational fluid dynamics (CFD) simulations are frequently employed to assess urban microclimates. CFD has recently evolved into a predictive tool crucial for translating urban microclimate knowledge into engineering and design practices for urban planning (Toparlar et al., 2017). Its application spans various scales, from the meteorological mesoscale to the microscale, building scale, and indoor environment (Moonen et al., 2012). Importantly, the field measurement data presented in Chapter 4 serves as a validation for CFD simulations, distinguishing this research, as Toparlar et al. (2017) noted a paucity of studies validating field measurement data in tropical climates, particularly in Bangkok, Thailand.

Chapters 4 and 5 focused on the Yaowarat and Ratchadamri areas. This chapter centers on Ratchadamri, the ongoing CBD of Bangkok for compelling economic reasons. Following an examination of the climate characteristics of both CBDs at 1 pm through field measurements and CFD simulations, this chapter delineates the local climate zoning of Ratchadamri based on CFD simulations and the relationship between physical variables and climate outcomes. Additionally, three climate distributions—air temperature, wind speed and direction, and wet-bulb globe temperature (WBGT)—are analyzed across five periods aligned with field measurements (9 am, 11 am, 1 pm, 3 pm, and 5 pm). The 3D modeling process mirrors that of Chapter 5, differing in shade modeling and input weather data for each period. Subsequently, CFD simulation raster data is analyzed for its physical variables and classified to delineate open space areas based on unique climate characteristics.

One key discovery of this study lies in the creation of an urban environmental climate zoning map on a district scale. Coupled with a primary recommendation plan, this map serves as the cornerstone for developing a guideline aimed at mitigating urban heat. Consequently, this chapter is structured into four sections: objectives, methodologies and materials, results and discussions, and finally, conclusions.

6.2   Objectives

1. Analyze the local microclimate of the Ratchadamri area by using the combination of field observation and numerical modeling

2. Clarify the critical area with the severe microclimate of the Ratchadamri area and create the proposal design related to the relevant variables from the viewpoint of urban heat island mitigation adaptation
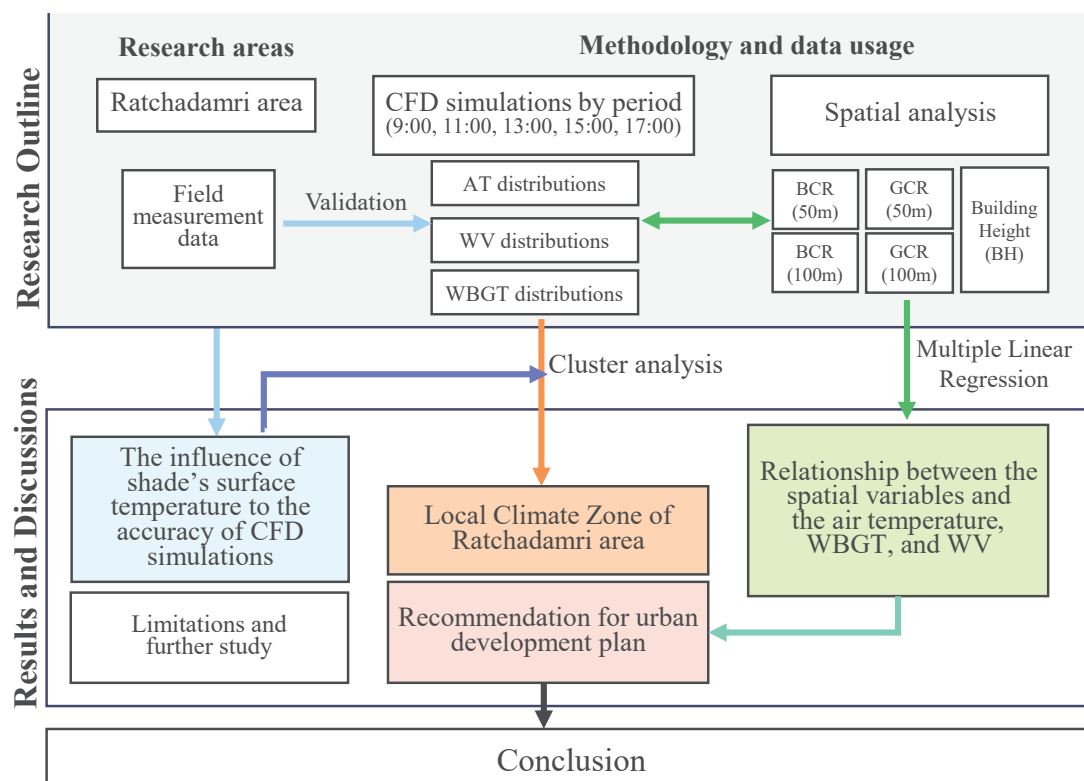
Figure 6-1 Study framework of Chapter 6

6.3   Methodology and Materials

Building upon the methods employed in the previous chapter, this section utilizes CFD simulations to analyze the Ratchadamri area across multiple periods. In addition, to formulate comprehensive guidelines for land use planning and urban heat countermeasure policies specific to this locale, spatial analysis, multiple linear regression analysis, and cluster analysis were undertaken in this chapter.

6.3.1   CFD Simulations and Validation

The CFD simulations were structured into four integral components. The initial phase involved the 3D modeling of buildings, trees, and other urban elements, mirroring the model employed in Chapter 5. Subsequently, the second phase encompassed input data (surface temperature was obtained from the result of Chapter 4), consisting of variables such as wind direction, wind speed (m/s), humidity (%), average temperature (°C), and surface temperature for each model (refer to Tables 6-1 and 6-2)(TMD, 2023). The third phase involved the differentiation of shadow volume footprints across various periods and locations, calculated through 3D spatial analysis in ArcGIS (GMT +7). The final phase encompassed the validation of CFD simulation results against field measurement data. Figure 6-2 illustrates the 3D modeling with a shadow surface at 11 am, presented as the yellow surface, as part of the 3D modeling and CFD simulation process.

Figure 6-2 3D modeling of the CFD simulations in AKL Flow Designer

Table 6-1 The CFD simulation modeling details

Software	AKL FlowDesigner 2022, second revision
Study area	**Ratchadamri Districts**
Maximum resolution (m): (x × y × z)	Analysis area (m): 2 × 2 × 2 Buffer area (m): 4 × 4 × 4 Calculation area (m): 8 × 8 × 8
Area of Simulation (m): (x × y × z)	Study area: 1100 × 1400 × 416 Buffer area: 2000 × 2600 × 416 Calculation area: 4000 × 5184 × 416
Turbulence model	High Reynolds Number Type, k-ε model
Analysis conditions	Steady-State Analysis (1-200 times)
Inflow conditions	Power Measurement Condition: 0.27 Inflow wind: weather station data (h=10m)
Outflow conditions	Free flow condition

Table 6-2 The CFD simulation's input data

Resources		Thai Meteorological Department, Don Muang station (temperature data) and Suvarnabhumi station (wind data), on 20th October 2022.				
Periods		**9:00**	**11:00**	**13:00**	**15:00**	**17:00**
Input data	Air temperature	28	30.3	32	32.8	34
	Relative Humidity	61%	50%	41.00%	39.00%	41.00%
	Surfaced temperature — Building	31.5 [28.1]	35 [32.5]	43 [40]	35 [30]	33 [30]
	Surfaced temperature — Pave	33	41.3	45	46.5 [43]	39.6 [35]
	Surfaced temperature — Road	34	42	50	45.5	39
	Surfaced temperature — Water	28	29.3	30	30.5	30.2
	Surfaced temperature — Vegetation	27.5	31	35 [30]	34 [30]	32 [30]
	Wind speed (m/s)	2.1	3.1	3.6	3.6	2.06
	Wind direction	80°	75°	80°	80°	80°

6.3.2   Spatial Analysis

This chapter, concentrating on the Ratchadamri area, encompassed three facets of spatial analysis. The initial segment involved the classification of the building coverage ratio (BCR) and green coverage ratio (GCR) concerning their surroundings. These variables are of significant influence, correlating with wind speed and temperature in the urban area. Calculations for both BCR and GCR were derived from land coverage raster data obtained from the Bangkok Metropolitan Administrator, utilizing focal statistics within radii of 50 and 100 meters (denoted as BCR50, BCR100, GCR50, and GCR100, respectively). Additionally, the average building height (BH) was computed using similar resources, with a raster resolution of 2 meters for all three variables.

Subsequently, the second phase entailed a correlation analysis between these variables and the climate outcomes derived from CFD simulations. This encompassed binary correlation and multiple linear regression analyses. Finally, the third phase involved a cluster analysis of two variables—wind speed (WS) and wet-bulb globe temperature (WBGT)—during the afternoon in October.

6.4   Results and Discussions

The results and discussions section of this chapter is segmented into four components. It commences with an exploration of the impact of the shading model in CFD simulations, followed by an examination of the relationship between environmental physical variables and climate data derived from CFD simulations in the Ratchadamri area. The third part unveils the local urban environmental climate zoning map of the Ratchadamri area and the associated guidelines for urban land use planning. The final segment delves into the limitations of the study and potential avenues for further research.

6.4.1   The Influence of the Shade Model in CFD Simulations

In alignment with the outcomes presented in Chapter 5, this section entails the computation of temperature and wind distribution data from the CFD simulation using AKL Flow Designer 2022. The simulation, characterized by its steadiness, incorporated input data detailed in Tables 6-1 and 6-2. Figures 6-5 and 6-6 depict the air temperature results for each period, with variations attributed solely to the shade model. The wind distribution is illustrated in Figure 6-7. Furthermore, figure 6-8 and Table 6-3 showcase the results of CFD simulation validation against field measurement data.

The examination of the shading model's influence on CFD simulation results involves a comparative analysis of two models across five periods for air temperature distributions. Figure 6-8 and Table 6-3 reveal three key findings. Firstly, simulations incorporating the shading model consistently exhibited a higher correlation with field measurements. Secondly, the correlation between period, shade influence, and field measurement data was evident. Around noon (11 am and 1 pm), with a lower proportion of shade and ground area, the two models demonstrated close correlation coefficients (0.63 and 0.65, 0.63 and 0.71, respectively). Conversely, during morning and late afternoon periods, the shading model enhanced the simulation results' correlation coefficients. However, the results of Model 2 on 9 A.M. and 5 P.M. were negatively correlation because of the influence of shade. Both period models were covered with the large, shaded model with lower surfaced temperatures than non-shaded areas, but the mobile survey was air temperature data that the shade had less influence therefore the spots located in shade will have high temperatures while the simulation had low temperatures and the area without shade, the air temperature had lower temperature than the simulation. The third finding indicates that, although the shading model significantly influenced simulation outcomes, the correlation coefficients across the five periods varied from low to high.

To analyze the climate zone of the Ratchadamri area, two periods (1 pm and 3 pm) with high correlation (R-square values are 0.5 and 0.58, respectively), were selected. Consequently, the following section focuses on the average data from these two periods.

Figure 6-3 GCR within 50 m in the Ratchadamri area
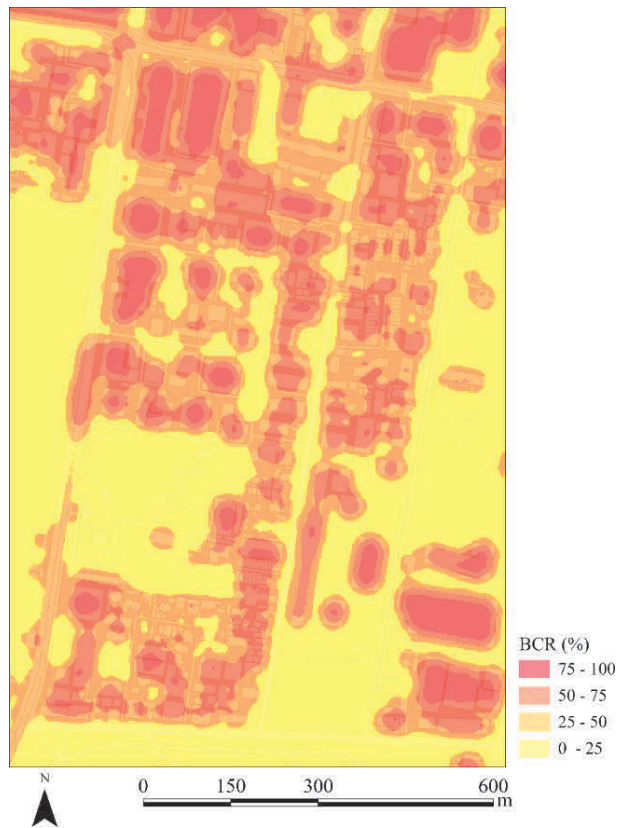
Figure 6-4 BCR within 50 m in the Ratchadamri area

9:00   **11:00**   **13:00**

15:00   **17:00**

Legend
Air Temperature

0.001 - 28		33.501 - 34
28.001 - 29		34.001 - 34.5
29.001 - 30		34.501 - 35
30.001 - 30.5		35.001 - 35.5
30.501 - 31		35.501 - 36
31.001 - 31.5		36.001 - 37
31.501 - 32		37.001 - 38
32.001 - 32.5		38.001 - 40
32.501 - 33		40.001 - 42.3
33.001 - 33.5		
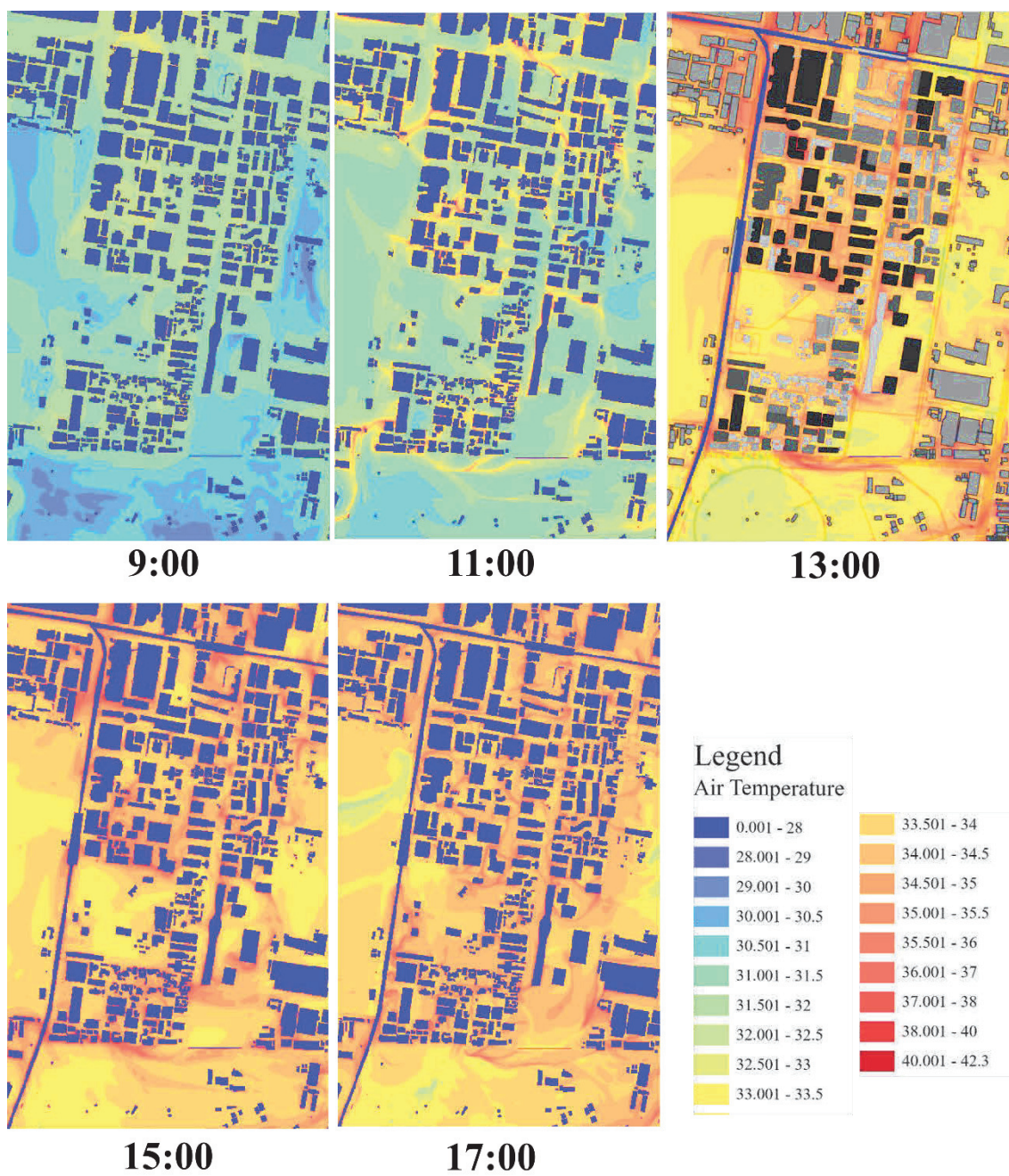
Figure 6-5 Air temperature distribution of the Ratchadamri area (without shaded model)

9:00　　　　　　　**11:00**　　　　　　　**13:00**

15:00　　　　　　　**17:00**

Legend
Air Temperature

0.001 - 28	33.501 - 34
28.001 - 29	34.001 - 34.5
29.001 - 30	34.501 - 35
30.001 - 30.5	35.001 - 35.5
30.501 - 31	35.501 - 36
31.001 - 31.5	36.001 - 37
31.501 - 32	37.001 - 38
32.001 - 32.5	38.001 - 40
32.501 - 33	40.001 - 42.3
33.001 - 33.5	
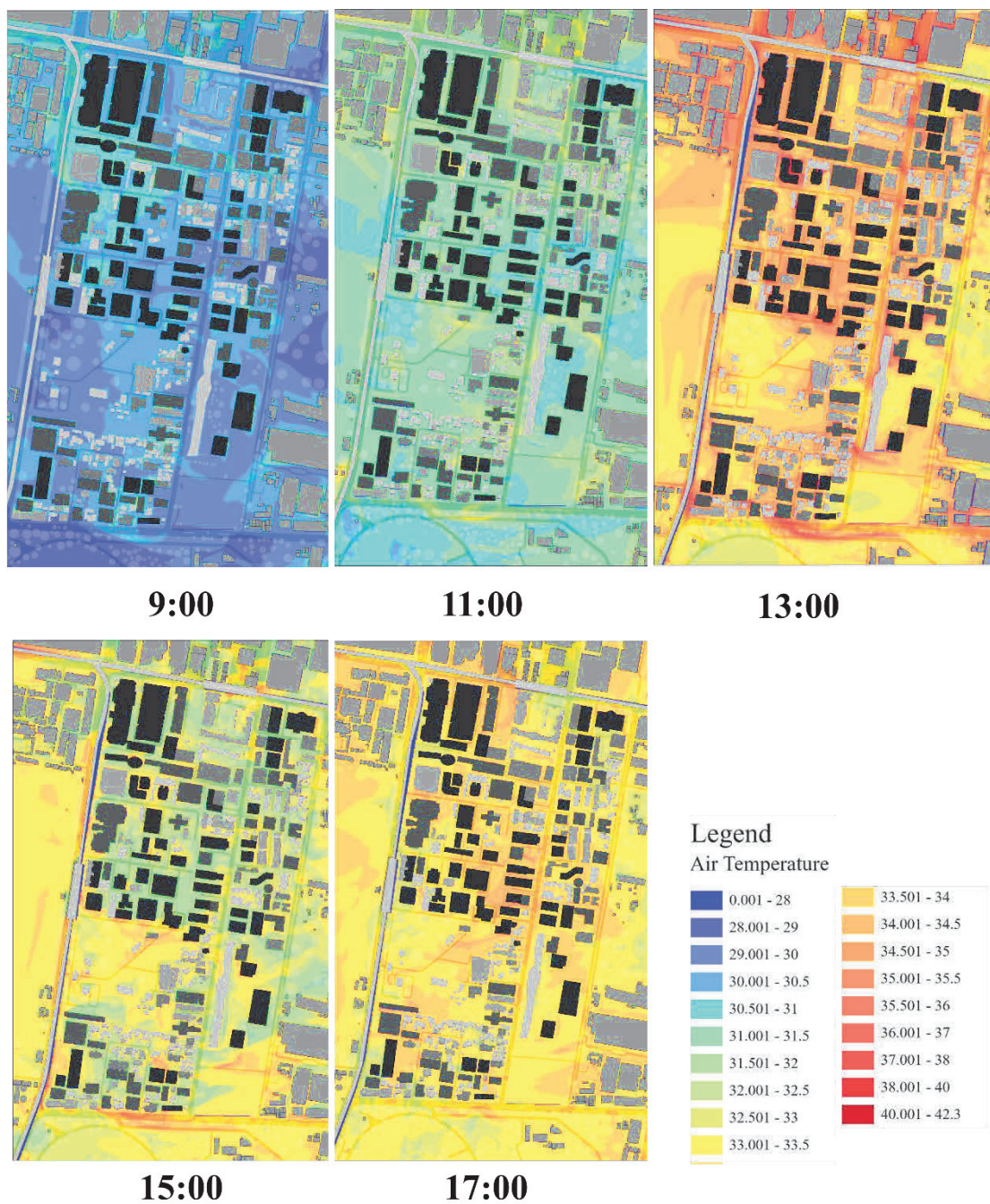
Figure 6-6 Air temperature distribution of the Ratchadamri area (with shaded model)
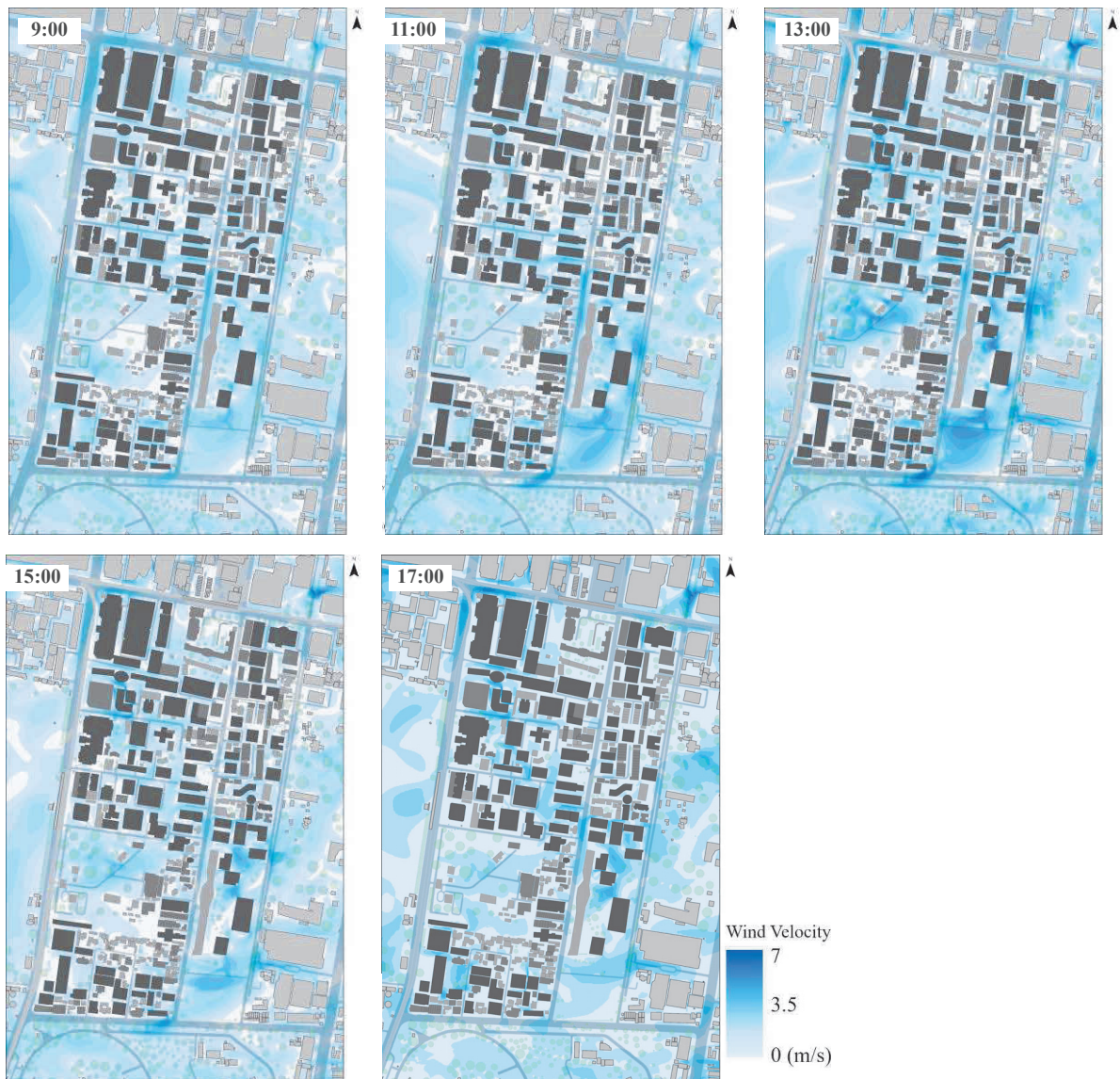
Figure 6-7 Wind velocity distribution of the Ratchadamri area

Table 6-3 Correlation analysis between CFD simulation results and field measurement data

Correlation coefficient	9 am	11 am	1 pm	3 pm	5 pm
Model 1 (Without shade)	-0.4	0.63	0.63	0.37	0.14
Model 2 (Shade model)	-0.591	0.65	**0.71**	**0.76**	-0.52
R-square	0.35	0.42	**0.50**	**0.58**	0.27
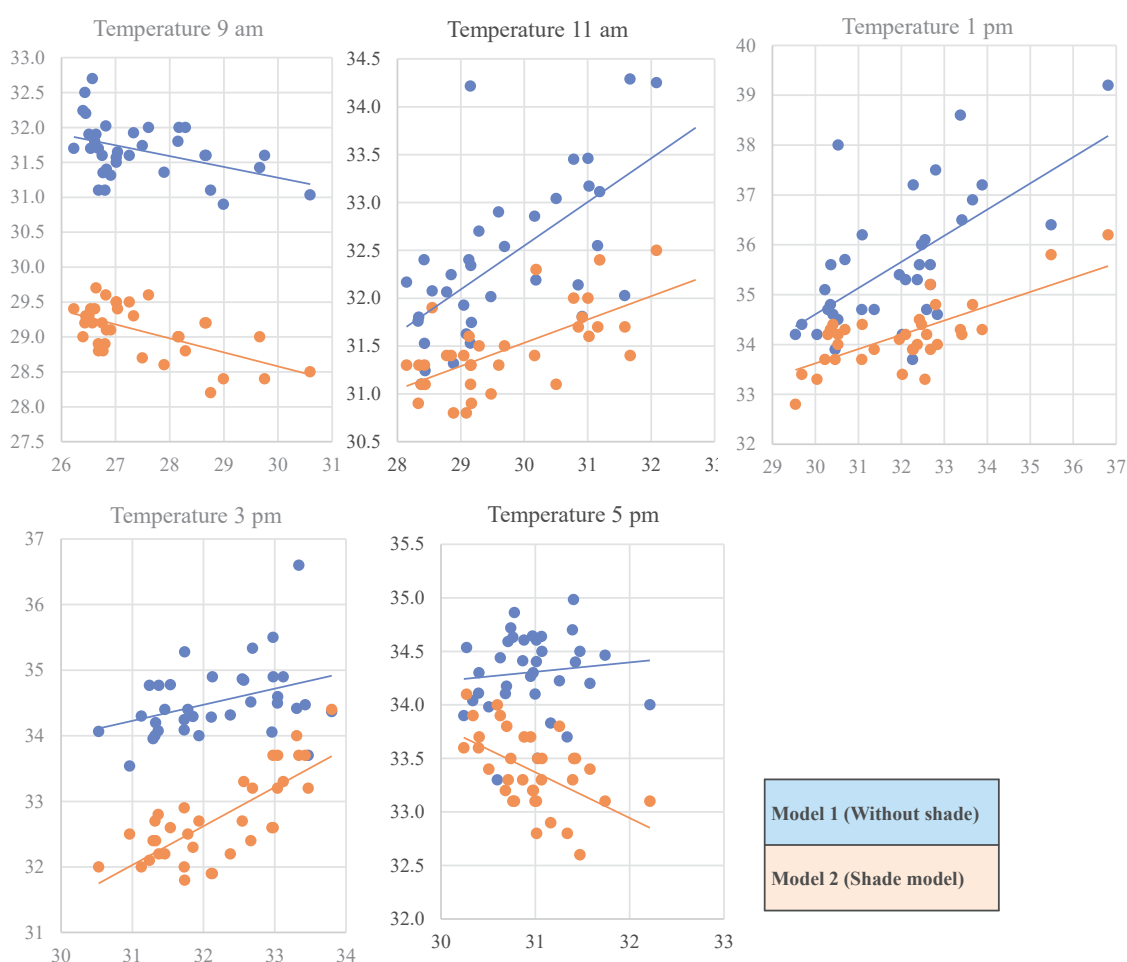
Figure 6-8 Scatter plot of 5-period temperature comparison between two different models.

6.4.2   The Relationship and Influence of Urban Variables in the Ratchadamri Area

Following the spatial data analysis results, the Pearson correlation was initially computed. Table 6-4 presents correlation coefficients between physical variables, wind speed (WS), and temperature. Firstly, WS and BCR exhibit a negative correlation, with BCR50m showing a higher correlation than BCR100m (-0.591 and -0.505, respectively). Secondly, WBGT is predominantly correlated with GCR50m. Thirdly, BH demonstrates a stronger correlation with air temperature (1 pm) than with WBGT. Subsequently, multiple linear regression was conducted. Table 6-5 indicates that WBGT exhibited a high correlation with BCR50m, urban wind speed (WS), and BH (Model 3), with an R-value of 0.525. Furthermore, Table 6-6 highlights a substantial correlation between WS, BCR50m, and BH (0.595). Both tables underscore the significant influence of variables on urban climate, directly impacting human experiences. Areas with high BCR and limited greenery in the inner urban region are deemed most critical. The potential to enhance land cover by increasing green spaces and reducing building footprints, thereby creating more open space in the CBD, promises an improved urban living experience and mitigated urban heat in Bangkok's district. Consequently, the subsequent section utilizes WBGT and WS distribution in the afternoon to formulate the urban zoning map.

Table 6-4 Coefficient correlation between physical variables, WS, and temperature

Variables		BCR 50m	BCR 100m	GCR 50m	GCR 100m	BH 2m	WS
WS	Pearson Correlation	-.591**	-.505**	.377**	.388**	-.194**	
WBGT		.442**	.441**	-.463**	-.454**	.211**	-.379**
AT13		-.365**	-.260**	.193**	.181**	-.414**	.274**
AT15		-.365**	-.279**	.211**	.204**	-.398**	.275**

**. Correlation is significant at the 0.01 level (2-tailed).

Table 6-5 Multiple linear regression of WBGT variable

Model Summary[e]

Model	R	R Square	Adjusted R Square	Std. Error of the Estimate
1	.463[a]	0.214	0.214	0.53485
2	.513[b]	0.263	0.263	0.51801
3	**.525**[c]	0.275	0.275	0.51365

a. Predictors: (Constant), GCR50m

b. Predictors: (Constant), GCR50m, WS

c. Predictors: (Constant), GCR50m, WS, BH2m

d. Dependent Variable: **WBGT**

Table 6-6 Multiple linear regression of WS variable

Model Summary[e]

Model	R	R Square	Adjusted R Square	Std. Error of the Estimate
1	.591[a]	0.350	0.350	0.78806
2	**.595**[c]	0.354	0.354	0.78568

a. Predictors: (Constant), BCR50m

b. Predictors: (Constant), BCR50m, BH2m

c. Dependent Variable: **WS**

6.4.3   Local Environmental Climate Zoning Map of the Ratchadamri Area and Guidelines of Urban Land Use Planning and Countermeasure Policies for the Ratchadamri Area

This section undertakes zoning for the Ratchadamri area, Bangkok's CBD, with a mesh resolution of 2 meters, utilizing data derived from the average WBGT and WS in the afternoon (averaged for 1 pm and 3 pm), as revealed in Figures 6-9 and 6-10. The cluster analysis employed Ward's method, classification was executed using Euclidean distance, and variables were standardized to deviation values. Consequently, the 2m-mesh was classified into six clusters, with details provided in Tables 6-7 and 6-8. Figure 6-11 depicts scatter plots for the six clusters, where the Y-axis represents WS values (m/s) and the X-axis represents WBGT (°C), with a total of 167,153 meshes constituting the open space within this area.

Figure 6-12 illustrates the distribution of each zone mesh in conjunction with the building footprint (depicted in white), while Figure 6-14 illustrates the proportion of each zone. The total area of the study region is 1,105,000 sq.m, with the open space, representing the cumulative area of all six zones, totaling 668,612 sq.m. Notably, the largest proportion of samples is found in clusters 2 (27%), 5 (25%), and 1 (21%). Clusters 4 and 6 exhibit similar samples (11%), while the smallest proportion is observed in cluster 3 (5%). Regarding WBGT characteristics, there is an almost even distribution between clusters with low WBGT and those with medium to high WBGT (48% and 52%, respectively). Clusters 1 and 2, characterized by low WBGT and high wind speed, are considered favorable conditions.

In terms of countermeasure policies, they were formulated based on the climate characteristics of each zone, particularly focusing on ventilation and human temperature comfort. The specific characteristics and guidelines for urban land use planning in each zone are outlined below.

Zone 1: The Low Temperature and High Wind Speed Area (Blue Zone)

Comprising a substantial portion of the Ratchadamri area (21%), Zone 1 stands out as a significant volume characterized by low temperatures and high wind speeds, identified by its distinctive blue coloration. Predominantly constituted by green spaces interwoven with grass, bushes, and water bodies, this zone encompasses four distinct private areas. These include The Royal Bangkok Sports Club and Golf Driving Club to the west, the private land of The Crown Property Bureau, the diplomatic precinct residence the embassies of the Netherlands and the United States to the east, and the renowned Lumpini Park to the south. Notably, a considerable portion of this zone is designated as private space. The abundance of green open areas contributes to cooler temperatures within Zone 1, registering at 28.56°C, coupled with a notable high average wind speed of 2.62 m/s. Consequently, Zone 1 exhibits favorable conditions for urban life and, as of the existing year (2022), is excluded from urban land use planning initiatives.

Zone 2: The Low Temperature and Moderate Wind Speed Area (Light Blue Zone)

Sharing similarities with Zone 1 due to its proximity, Zone 2 also encompasses an extensive open space within the Ratchadamri area, distinguishing itself with a light blue coloration. As the largest open space area in the vicinity, Zone 2 bears a resemblance to Zone 1 but with a notable difference—the wind speed in Zone 2 is slightly lower. Positioned in the periphery or at the edge of the open space, Zone 2 is influenced by the prevalent practice in Bangkok and Thailand of enclosing land with walls or parallel bushes, typically measuring 3-4 meters in height. This landscape characteristic induces variations in wind speed, aligning with insights from the previous chapter that highlighted wind speed reductions in the vicinity of walls. Despite featuring a moderate wind speed, approximately 1.5 m/s, Zone 2 maintains a low-temperature profile, average recorded at 28.76°C. Consequently, Zone 2 enjoys favorable conditions for urban life, and as of the current year (2022), it is not incorporated into urban land use planning initiatives.

Zone 3: The Moderate Temperature and Strong Wind Speed Area (Green Zone)

Comprising the smallest area within Ratchadamri (5%), Zone 3 is predominantly characterized by greenery, specifically grass, situated in the vicinity of the mega project on Langsuan Road. This area is enveloped by Zone 3 and features a mixed-use landscape, incorporating high-rise buildings (luxury hotels and condominiums) alongside low-rise commercial structures. Zone 3 exhibits a moderate temperature profile, recorded at 29.02°C, distinguishing itself with the highest wind speed among the zones, reaching 4.24 m/s. The elevated wind speed in Zone 3 is attributed to its land coverage and distinctive urban characteristics, characterized by a spacious open area among high-rise buildings, devoid of obstacles such as trees or walls. While this zone could be favorable conditions, the exceptionally strong wind speed poses a potential challenge, necessitating focused land use planning aimed at mitigating wind speed for human comfort. As established in previous sections, wind speed correlates with BCR, implying that future development projects in this zone should strategically consider mitigating wind speed by introducing additional trees or vegetation. This not only addresses the wind speed concern but also contributes to temperature reduction and enhanced shading in the afternoon.

Zone 4: The High Temperature and Moderate Wind Speed Area (Yellow Zone)

Zone 4 predominantly constitutes an impervious open space, primarily comprising concrete parking lots associated with commercial buildings and Lumpini Park. This composition results in elevated daytime temperatures, recording at 29.65°C, coupled with a moderate wind speed of 2.05 m/s attributed to the expansive nature of the area. To address the challenge of high thermal conditions in Zone 4, mitigation strategies could involve increasing shading elements, such as awnings with reflective materials. Additionally, integrating greenery into the existing infrastructure could prove beneficial. For instance, altering the material of parking lots from concrete to hollowed concrete, allowing for water absorption and facilitating the growth of grass, would contribute to mitigating surface temperatures. Furthermore, incorporating more trees into the parking lot design would contribute to temperature reduction and enhance the overall environmental quality of the area.

Zone 5: The Moderate Temperature and Low Wind Speed Area (Orange Zone)

Zone 5 encompasses a substantial area within Ratchadamri, primarily characterized by narrow impervious spaces or narrow roads between densely constructed buildings. This spatial arrangement contributes to a low wind speed of 0.73 m/s. Despite the limited wind speed, the narrow spaces between high-rise buildings create shaded areas, resulting in a moderate temperature of 29.27°C. A comparative analysis with Zone 4 highlights that, despite similar materials, the proportion of wide spaces and the height of surrounding buildings significantly influence temperature and wind speed. While Zone 5 benefits from sufficient shading, enhancing urban heat mitigation requires the incorporation of more open spaces and pocket greenery wherever feasible.

Zone 6: The High Temperature and Low Wind Speed Area (Red Zone)

Zone 6 represents a critical area within Ratchadamri, covering 11% of the open space with the highest temperature recorded at 30.15°C and the lowest wind speed of 0.74 m/s. Situated north of Langsuan Road, this zone is surrounded by buildings of varying heights, creating a dense environment that obstructs wind flow from all directions. Given the constraints related to the existing road layout, potential interventions include the development of the roadside and pedestrian areas. The narrow and underdeveloped pedestrian pathway along Langsuan Road suggests a need for improvements to enhance pedestrian comfort. Recommendations for the local governing authorities include improving the quality of the pathway and introducing additional pocket green spaces along the road to provide shade for pedestrians during morning and afternoon break times. To increase wind speed, future urban planning should consider the height of parallel buildings, potentially incorporating a group of high-rise buildings akin to the middle section of Langsuan Road. This strategic urban design could create a more favorable urban street canyon that directs upper-level airflow toward the pedestrian level.

As delineated above, the Ratchadamri area has been stratified into six zones. Figure 6-14 presents the thermal environment, ventilation, and urban characteristics zoning map, encapsulating the distinctive features, evaluations, and recommended countermeasures for each zone. Notably, the focus for targeted interventions is on Zones 3 to 6, characterized by high temperatures and limited urban ventilation.
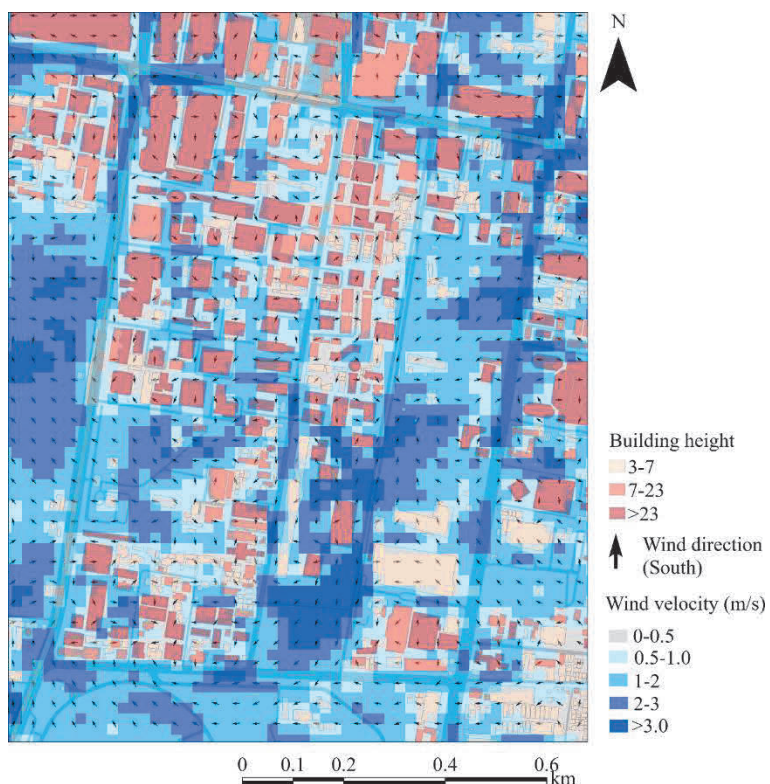
Figure 6-9 Wind velocity distribution result from the average of 1 pm and 3 pm of the CFD simulations
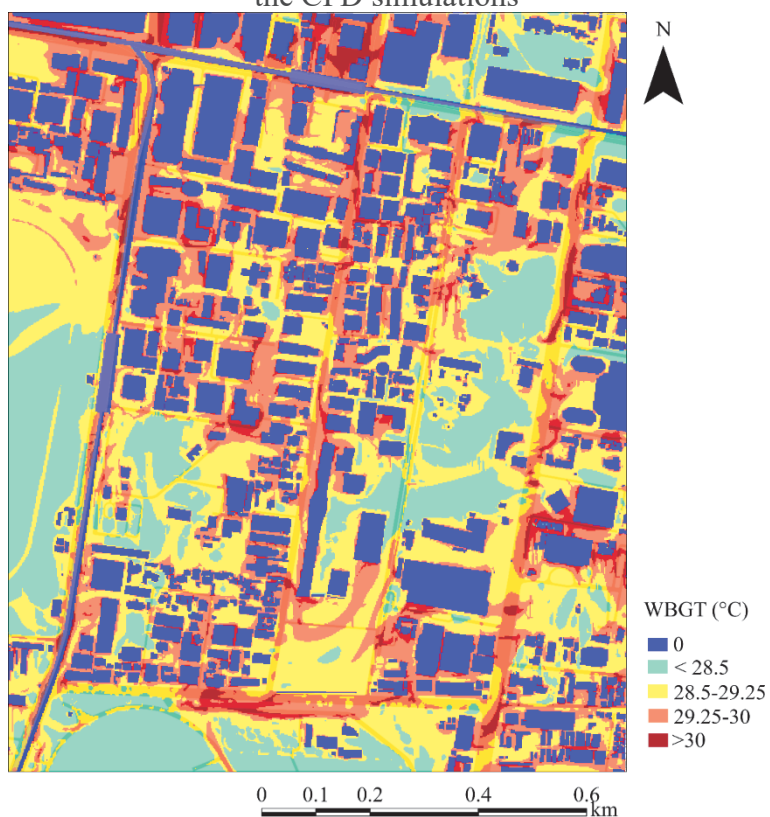
Figure 6-10 The average result of WBGT distribution of the Ratchadamri area in the afternoon

Table 6-7 Detail of the cluster analysis

Variables	Cluster Zone					
	1	2	3	4	5	6
WS (Avg)	2.62	1.48	4.24	2.08	0.73	0.74
WS (Max)	3.62	2.08	6.05	3.63	1.41	2.04
WS (Min)	1.91	0.43	3.23	1.36	0.01	0.01
WBGT (Avg)	28.56	28.76	29.02	29.65	29.27	30.15
WBGT (Max)	29.4	29.4	30.7	32.3	29.7	32.5
WBGT (Min)	27.9	27.9	28	29	28.1	29.8
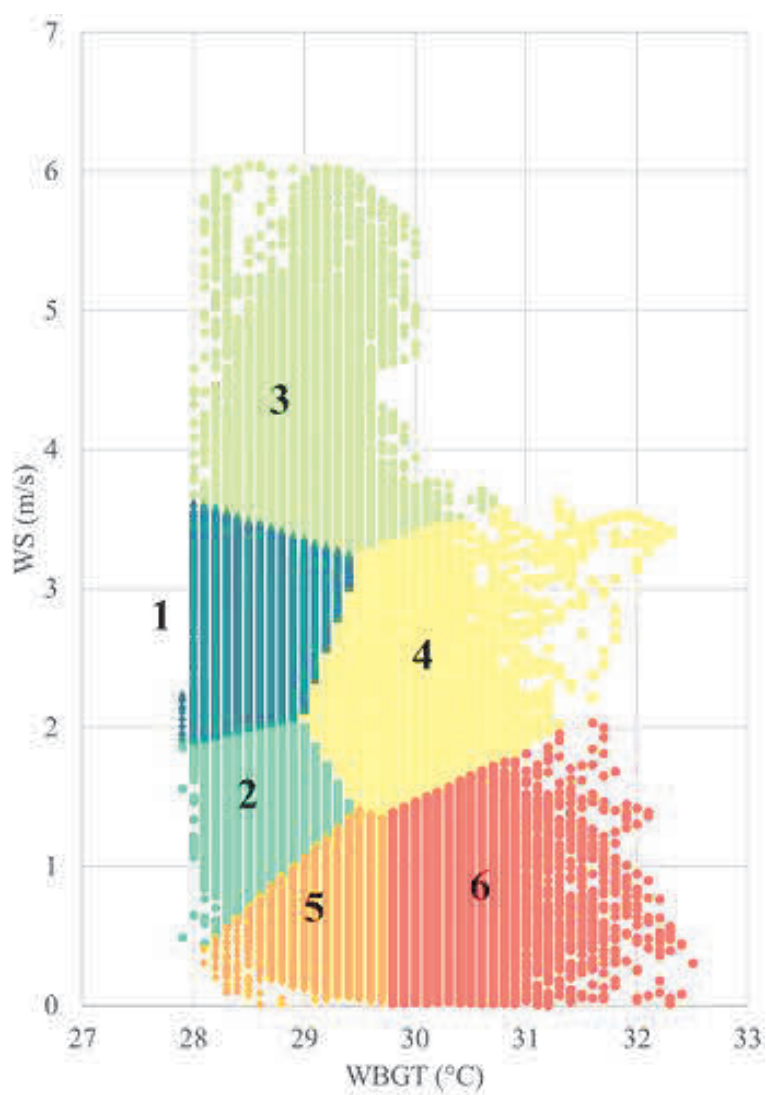
Figure 6-11 Scatter plots of each cluster's variables detail

Figure 6-12 Six typical zones of the Ratchadamri area

Table 6-8 Zonal characteristics and variables in the Ratchadamri area

Zone	Climate characteristics	Urban characteristics	Variables			
			WBGT	WS	GCR	BCR
1	Low temperature and high wind speed area	Open space (water and vegetation)	Low	High	High	Low
2	Low temperature and moderate wind speed area	Green area (park, trees)	Low	Medium	High	Low
3	Moderate temperature and strong wind speed area	Open green space (low vegetation)	Medium	High	High	Low
4	High temperature and moderate wind speed area	Wide open space (impervious)	High	Medium	Medium	Medium
5	Moderate temperature and low wind speed area	Narrow open space (impervious)	Medium	Low	Low	Medium
6	High temperature and low wind speed area	Road, narrow space in high urban density area	High	Low	Low	High
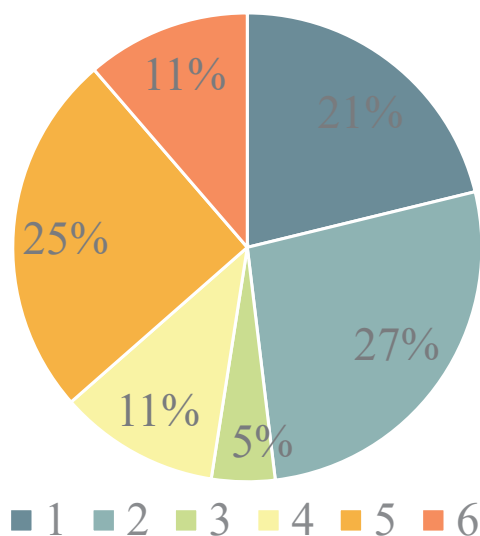
Figure 6-13 Pie chart of the area ratio of each zone in the Ratchadamri area

Local Climate Zoning Map: Ratchadamri area

Location: Pathumwan District, Bangkok   Total area: 1,105,000 sq.m

N

0   150   300   600 m

Zone	Climate characteristics	Recommendation plan		
		Increase open space	Increase shading area	Increase green area /waterbody
1	Low temperature and high wind speed area			
2	Low temperature and moderate wind speed area			
3	Moderate temperature and strong wind speed area		O	
4	High temperature and moderate wind speed area		O	O
5	Moderate temperature and low wind speed area	O		O
6	High temperature and low wind speed area	O	O	O

Figure 6-14 Urban micro-climate zoning map and recommendation plan

6.4.4   Limitations and Further Research

Owing to constraints associated with field measurements and the study period, the guidelines formulated for urban land use planning in the Ratchadamri area rely solely on scientific data and statistical analyses. A more comprehensive exploration of this subject demands the creation of advisory maps, incorporating schematic design plans for individual zones. Additionally, organizing community planning workshops involving urban planners, local government representatives, residents, and stakeholders is imperative. Such forums foster discussions on the plan, design, and implementation processes, ensuring long-term viability. Comparable case studies, such as those conducted by Tanaka et al. (2007), Ng et al. (2012), Kitao et al. (2012), and Matsuo et al. (2023), underscore the efficacy of incorporating specialist workshops in developing urban policies. Furthermore, the conclusive deliberations should elucidate the specifications regarding the types and characteristics of green spaces, open areas, etc., to render the perspectives on future urban planning accessible to non-experts.

The current findings present a local climate zoning map for the Ratchadamri area based on diurnal data derived from CFD simulations, validated through field measurements data. However, a notable gap exists in the investigation of nocturnal climate characteristics within this locale, necessitating further study. Previous research on Urban Heat Island (UHI) effects has predominantly focused on the nocturnal heat island phenomenon in urban residential areas (Giridharan et al., 2005; Takahashi et al., 2011; Zheng et al., 2023). To advance understanding, a future study on the nocturnal UHI specific to Bangkok could be undertaken to elucidate heat distribution during nighttime hours, thereby informing urban land use planning strategies tailored to mitigate nocturnal heat impacts.

6.5   Conclusions

In conclusion, this chapter undertakes a comprehensive analysis of the urban climate in the Ratchadamri area, employing advanced methodologies including CFD simulations and spatial analysis. The result is the identification of six distinct climate zones characterized by nuanced details encompassing temperature, wind speed, and specific urban features. These findings respond to the objectives which aim to clarify the critical climate area. Moreover, it not only contributes to the existing urban climate knowledge but also provides valuable insights for targeted urban planning and countermeasure policies. The creation of an urban environmental climate zoning map, accompanied by guidelines for urban heat mitigation, constitutes a substantial contribution to both academic discourse and practical urban development considerations.

In terms of a practical framework for non-experts in Bangkok, severe urban climate to comprehend and utilize the map when creating proposals, fostering broader considerations of urban climate factors in planning efforts. This research underscores the complexity of urban climate dynamics, emphasizing the need for tailored approaches in mitigating the impacts of urban heat islands. The map aids stakeholders in understanding district weather data related to human comfort and heat stress indices, serving as a primary tool for projects in Bangkok, Thailand, and other similar countries in tropical regions.

References

Blocken, B. (2014). 50 Years of Computational Wind Engineering: past, present, and future. *Wind Eng Ind Aerodyn, 129*, 69-102. https://doi.org/10.1016/j.jweia.2014.03.008.

Blocken, B. (2015). Computational Fluid Dynamics for urban physics: importance, scales, possibilities, limitations and ten tips and tricks towards accurate and reliable simulations. *Build Environ, 91*, 219-245. https://doi.org/10.1016/j.buildenv.2015.02.015.

Giridharan, R., S.S.Y. Lau, & S. Ganesan (2005) Nocturnal heat island effect in urban residential developments of Hong Kong. Energy and Buildings, 37 (9), 964-971. https://doi.org/10.1016/j.enbuild.2004.12.005.

Kamma, J., K. Manomaiphiboon, N. Aman, T. Thongkamdee, S. Chuangchote, & S. Bonnet (2020). Urban heat island analysis for Bangkok: multi-scale temporal variation, associated factors, directional dependence, and cool island condition. *Science Asia, 46*, 213-223. http://dx.doi.org/10.2306/scienceasia1513-1874.2020.024.

Khamchiangta, D., & S. Dhakal (2020). Time series analysis of land use and land cover changes related to urban heat island intensity: Case of Bangkok Metropolitan Area in Thailand. *Journal of Urban Management, 9(4)*, 1-12. https://doi.org/10.1016/j.jum.2020.09.001.

Kitao, N., M. Moriyama, H. Takebayashi, & T. Tanaka (2012). A study on making method of climate atlas in Osaka region. *AIJ Journal of Technology and Design, 18(38)*, 255-258. https://doi.org/10.3130/aija.18.255. (Japanese)

Matsuo, K., K. Inoue, M. Yokoyama, T. Tanaka, & T. Yoshihara (2023). Advice Map For Effective Support Of Urban Thermal Environmental Design: Practice of collaborative workshops by experts in the central area of Hiroshima. *J. Archit. Plann., AIJ, 88 (814)*, 3295-3305. https://doi.org/10.3130/aija.88.3295. (Japanese)

Moonen, P., T. Defraeye, V. Dorer, B. Blocken, & J. Carmeliet (2012). Urban Physics: effect of the micro-climate on comfort, health and energy demand. *Front Archit Res, 1,* 197-228. https://doi.org/10.1016/j.foar.2012.05.002.

Ng, E. (2012). Towards Planning and Practical Understanding of the Need for Meteorological and Climatic Information in the Design of High-density Cities: A Case-based Study of Hong Kong, *International Journal of Climatology, 32 (4),* 582-598.

OpenAI. (2023). ChatGPT [Large language model]. https://chat.openai.com

Pakarnseree, R., K. Chumkao, & S. Bualert (2018). Physical characteristics of Bangkok and its urban heat island phenomenon. *Building and Environment, 143*, 561-569. https://doi.org/10.1016/j.buildenv.2018.07.042.

Rizwan, A.M., Y.C. L. Dennis, & C. Liu (2008). A review on the generation, determination, and mitigation of urban heat island. *Environ Sci, 20*, 120-128. https://doi.org/10.1016/S1001-0742(08)60019-4.

Santamouris, M. (2007). Heat Island research in Europe: the state of the art. *Adv Build Energy Res, 1*, 123-150. https://doi.org/10.1080/17512549.2007.9687272.

Takahashi, K., T. Mikami, & H. Takahashi (2011). Influence of the Urban Heat Island Phenomenon in Tokyo on the Local Wind System at Nighttime in Summer. *Journal of Geography, 120(2),* 341-358. https://doi.org/10.1016/j.enbuild.2004.12.005.

Tanaka, T., T. Yamashita, H. Takebayashi, & M. Moriyama (2007). Urban Environmental Climate Map for Community Planning. J.Environ Eng., AIJ, 511, 91-98. https://doi.org/10.3130/aije.72.91_1. (Japanese)

Thai Meteorological Department (TMD) (2022). Climate data of Bangkok. http://www.aws-observation.tmd.go.th., last accessed 2023/05/10.

Toparlar, Y., B. Blocken, B. Maiheu, & G.J.F. van Heijst (2017). A review on the CFD analysis of urban microclimate. *Renewable and Sustainable Energy Reviews, 80*, 1613-1640. https://doi.org/10.1016/j.rser.2017.05.248.

Zheng, Y., C. Ren, Y. Shi, S. H.L. Yim, D. Y.F. Lai, Y. Xu, C. Fang, & W. Li (2023) Mapping the spatial distribution of nocturnal urban heat island based on Local Climate Zone framework. *Building and Environment, 234,* 110197. https://doi.org/10.1016/j.buildenv.2023.110197.

Chapter 7
Conclusion and the Direction of Future Study

Contents
_____

7.1   Conclusion

The chapter was described in three sections. The first section is the conclusion where the information of each chapter is summarized individually. The second section is Urban Climate and the Proposals for Urban Design from the Viewpoint of a Tropical Region: A Case Study of Bangkok. The third section is the direction of the future study.

Chapter 1

This chapter reviewed the background of the study which are two related research topics: Urban Heat Islands Phenomenon and Urban Climate Study. Related to the research background, there are necessary to apply several methodologies within the multiscale urban climate related to the data-scarce environment of the tropical regions. Subsequently, summarized the target study area and constructed the dissertation framework, where two methodologies from the urban climate study were adapted into each chapter—the field observations in Chapters 2 and 4, and the numerical models in Chapters 3, 5, and 6. Moreover, the significance and originality of the dissertation were emphasized in the last section of this chapter.

Chapter 2

This chapter used 68 weather observation data from the Thai government and the spatial analysis of its surroundings within 300 m to analyze the relationship between air temperature, wind distributions, and spatial environmental factors. Then used the highly correlated variables—GCR, BCR, and DCDS—and synthesized the UECM of the Bangkok Metropolitan Region. The significant findings showed that GCR is the highest influencer to mitigate the nocturnal temperature while DCDS and BCR have a high influence on the diurnal temperature. Moreover, the UECM of BMR separated BMR into nine zones to facilitate a comprehensive investigation of urban climate characteristics. Each zone had distinct geographical attributes and exhibited varying ratios of vegetation to urban areas, which directly influenced air temperature and ventilation patterns.

The outcomes of this study empower local government authorities in each province to gain a comprehensive understanding of the local climate, thereby enabling the extension of this knowledge to other regions across Thailand. This dissemination of information catalyzes creating awareness regarding urban development that aligns with environmental considerations. By sharing insights derived from this study, the aim is to promote informed decision-making and encourage sustainable urban development practices that are harmonious with the unique climatic characteristics of each region.

Chapter 3

This chapter advances the understanding of BMA's urban climate characteristics during the summer, focusing on temperature and wind distribution. Utilizing numerical calculations with the WRF model and cluster analysis, this study synthesizes scientific data and statistics to create temperature and ventilation zoning maps. The integration of these maps, along with insights from the preceding chapter, culminates in the creation of the UECM for BMA. The UECM of BMA provides six characteristics of temperature pattern overlaying with the low wind speed zone and high-density building area. These findings confirmed the importance of UECM as a crucial tool for urban planners, providing a nuanced understanding of temperature variations, ventilation challenges, and high-density urban areas.

This chapter contributes significantly to the comprehension of the BMA urban climate characteristics during the summer, with a specific focus on temperature and wind distribution. Employing numerical calculations through the Weather Research and Forecasting (WRF) model and cluster analysis, the study integrates scientific data and statistics to generate temperature and ventilation zoning maps. Building upon insights from the preceding chapter, these maps collectively form the basis for the development of UECM tailored to the BMA. The UECM for BMA delineates six characteristics related to temperature patterns, incorporating overlays of low wind speed zones and high-density building areas.

These findings underscore the advantage of numerical calculation to understand the overall climate characteristics in a data-scarce environment of tropical regions. Moreover, the comparison between the findings from different urban methodologies emphasized the significance of these developed research methodologies.

Chapter 4

The primary methodology employed in this chapter involved field measurements, with a focus on collecting air temperature, black globe temperature, surface temperature, and wind data in Bangkok during October 2022. The target areas of the microscale of BMA were possibly picked up from the advantage of numerical models from Chapter 3 and combined with weather conditions of the field observation period and plan. This collection of data which was obtained from two CBDs of Bangkok namely Yaowarat and Ratchadamri, constitute the main findings of this chapter. The planning of field measurements, including the establishment of mobile survey routes and fixed station locations, played a crucial role in enhancing data collection efficiency, guided by specific criteria for selecting observation spots.

The microclimate data from the two CBDs exhibited similar patterns, characterized by high temperatures in the high-density urban areas during the afternoon and low wind speeds. Notably, the Ratchadamri area demonstrated a slightly more favorable situation than the Yaowarat area, considering both temperature and wind distribution. These findings were subsequently analyzed and utilized in the validation process of CFD simulations discussed in Chapters 5 and 6.

Chapter 5

Chapter 5 focused on a comparative analysis of the urban ventilation of both CBDs which was measured by the microclimate data from Chapter 4. The CFD simulations were the main methodology of this chapter while the field observation data from Chapters 2 and 4 were the input data and were used to validate the numerical calculation results. Both methodologies increased the overall understanding of urban ventilation characteristics, in addition to analyzing the relationship between physical variables and urban ventilation, particularly wind speed. The correlation results, within 100 m, showed wind speed and open space ratio were highly correlated. The period of the day affects the wind speed and in the afternoon wind speed tends to increase. However, The CFD simulation confirmed that Ratchadamri had wider range of wind speed compared to Yaowarat whose wind speed was 0–2 m/s. The urban topography was one of the significant variables in this scale, Ratchadamri has compact high-rises, and open high-rises with several open spaces while Yaowarat has compact low to midrise buildings with several narrow streets.

In conclusion, to attain a comprehensive understanding of ventilation characteristics in both CBDs, this study emphasizes the importance of combining computational simulations and field measurements. The results strongly advocate for integrating both approaches in future research.

Chapter 6

In Chapter 6, the primary methodology involved CFD simulation, akin to Chapter 5, but with a specific focus on the Ratchadamri area. The simulation was conducted five times throughout the day, yet only two afternoon periods were utilized for classifying the local climate zone in this area due to the simulations' high accuracy and validation. The micro UECM of Ratchadamri, with a mesh resolution of 2 meters, utilized data derived from the average WBGT and wind speed in the afternoon (averaged for 1 p.m. and 3 p.m.). The field observation data from Chapters 2 and 4 were the input data and were used to validate the numerical calculation results.

The Ratchadamri area was stratified into six distinct zones based on climate characteristics, with particular attention directed towards Zones 3 to 6, characterized by elevated temperatures and restricted urban ventilation. This finding clarified the critical area of Bangkok's microclimate and established a framework designed for non-experts in urban climate studies to comprehend and utilize the map effectively when formulating proposals. The aim is to foster a more comprehensive consideration of urban climate factors in planning efforts, providing a tool to address temperature variations and ventilation challenges in the targeted zones of the Ratchadamri area.
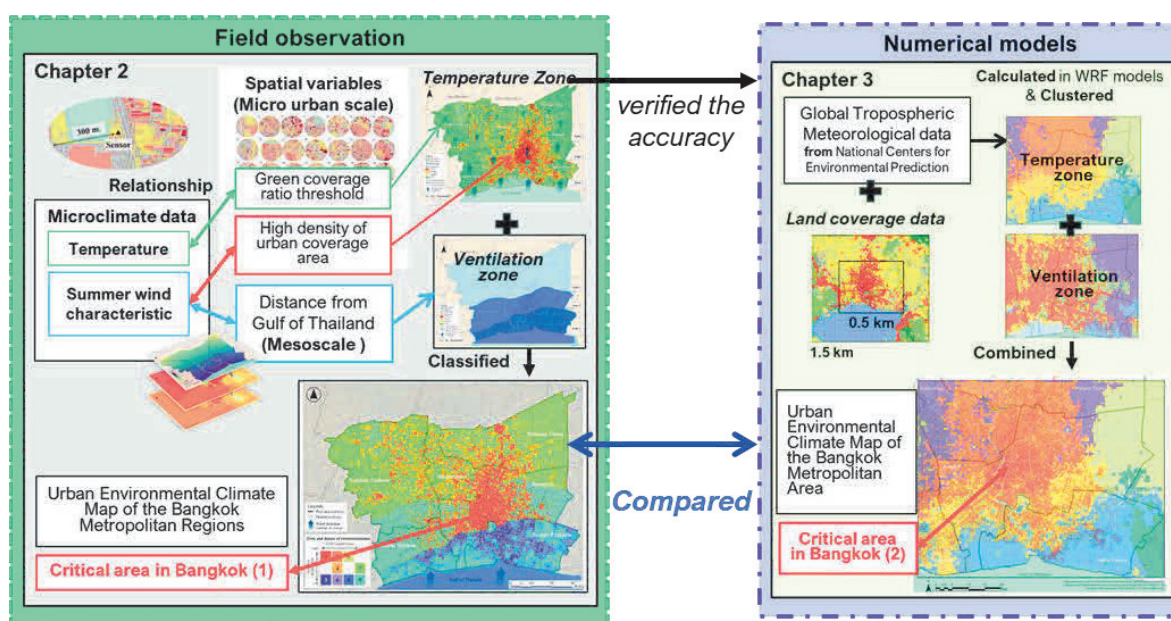

Figure 7-1 The summary of the mesoscale study.

7.2 Urban Climate and the Proposals for Urban Design from the Viewpoint of a Tropical Region: A Case Study of Bangkok

From the viewpoint of tropical regions, in a case study of Bangkok, the climate is divided into dry and wet seasons and has warm temperatures throughout the year influenced by two monsoons and affected by the direction of the prevailing wind. The prevailing wind in the hot period (8 months—March to October) came from the southwest and south direction all period. Bangkok is located in the plain basin, and the wind direction in summer is only influenced by the monsoon and has a low influence from the land breeze. Therefore, the nocturnal temperature of urban areas in the in-land was higher temperature than the coastal area (southern part). In this case, this critical area could develop its land use by increasing the green area to mitigate the nocturnal temperature. Regarding the nocturnal wind, the area with continuous sufficient open space from the direction of north-south had a high wind speed from the influence of monsoon direction while the high density of urban areas near the coast had low wind speeds (Figure 3-17). This result influenced the building direction layout and the development of land use planning in the direction of prevailing wind.

Even though the significant variables are common spatial variables, the detail of each variable is related to the tropical regions such as the greenery classification with tropical plants. Tropical is mostly greenery all year and has unique tropical plants/forests such as the mangrove forests. Mangroves are trees that live along tropical coastlines, rooted in salty sediments, often underwater, and it is the coastal green areas and water areas of Bangkok (Figures 3-4 and 3-5).

This study's unique strength lies in combining microscale field observations with mesoscale numerical models, leading to precise insights into Bangkok Metropolitan Region's (BMR) wind distribution. Findings reveal persistently poor urban ventilation across the four constituent provinces. Figure 7-2 demonstrates how the high-density urban area in Samut Prakan negatively impacts Bangkok's ventilation, while Bangkok's own dense areas likewise affect Nonthaburi and Pathum Thani. Consequently, the regional analysis suggests creating a continuous north-south open space to improve ventilation throughout the BMR, leveraging both the Southwest monsoon's and sea breeze's influence. This has inspired a Master Plan proposal for enhancing urban ventilation, incorporating these winds' daytime and nighttime effects.

Moreover, Bangkok's extensive water network, a legacy of historical agriculture and transportation (comprising 1,161 canals), emerges as a significant factor. Chapters 4 and 5 underscore the water surfaces' role as open spaces with low diurnal temperatures and high wind speeds. This underscores the potential of canals and rivers as humid urban ventilation corridors. Future studies could explore this potential in relation to waterside land use and design planning, canal width, and the connection of open spaces surrounding canals.

At the district scale, the design proposal to mitigate urban air circulation and ventilation (Figure 7-4) involves:

- Adapting vernacular architectural characteristics to enhance ventilation.
- Creating horizontal open public spaces connected to existing open areas for improved airflow and heat mitigation.
- Establishing shaded open spaces beneath building footprints, compatible with tropical activities and livelihoods. This could be particularly relevant in new districts or high-rise buildings commonly featuring high-ceiling open spaces as ground-floor lobbies, often lacking passive ventilation.

To incentivize building cooperation in mitigating environmental problems, additional bonuses could be offered, such as increased Floor Area Ratio (FAR) and additional height allowances from local authorities. This would encourage the private sector to collaborate in addressing these critical challenges.
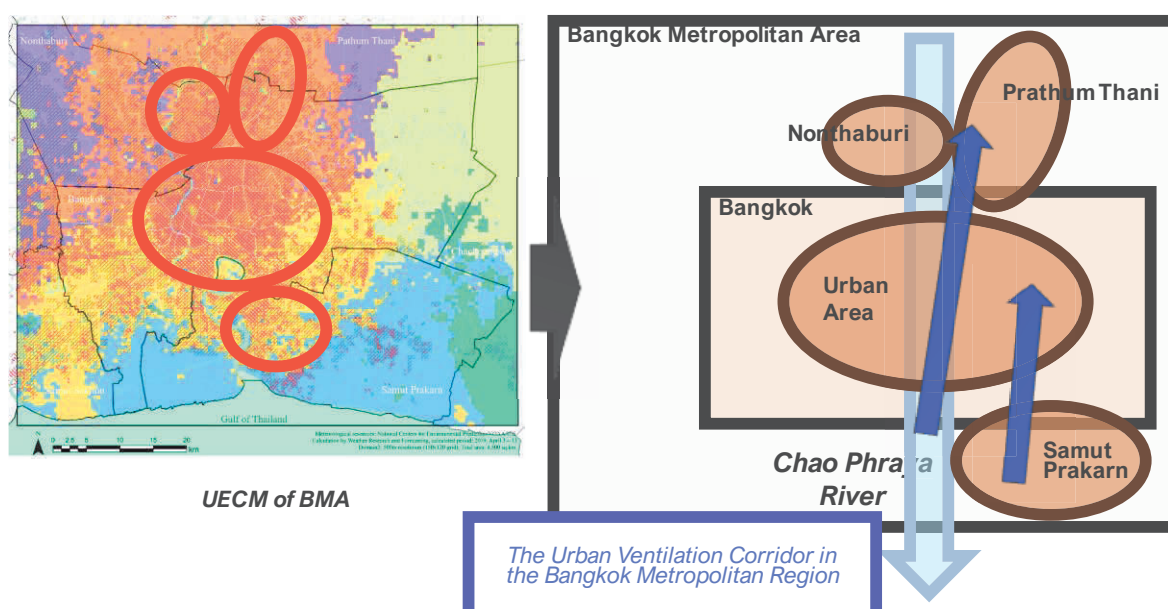
Figure 7-2 The influence of urban area of provincial scale to the regional scale on the urban ventilation crisis.
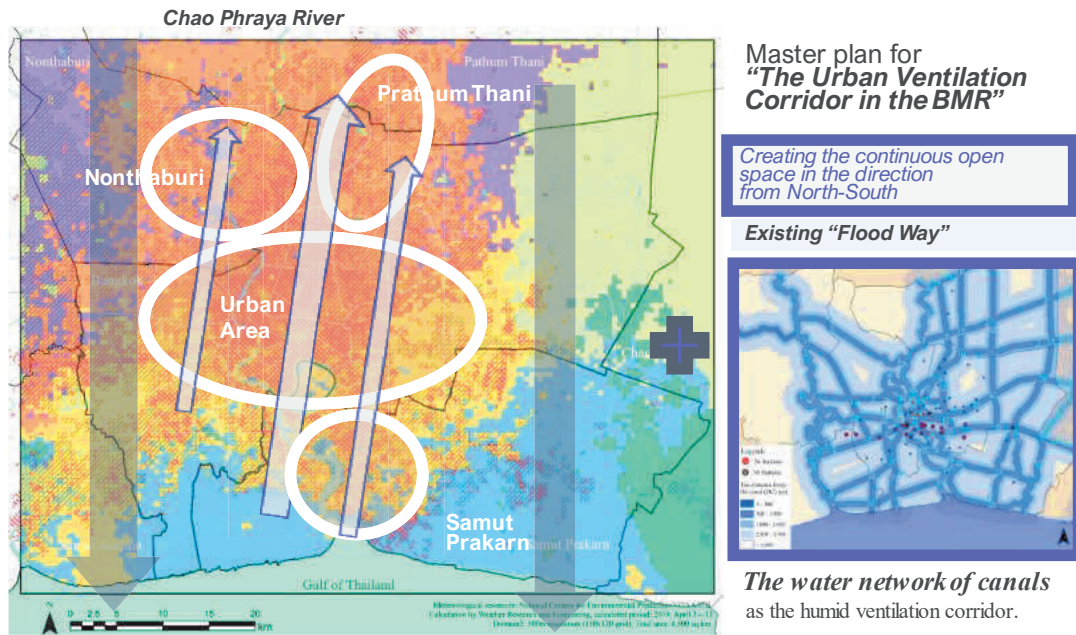
Figure 7-3 Design proposals to mitigate the regional urban ventilation in BMR.

Create or develop an architectural geometry related to the contemporary Vernacular Architecture to *creating the continuous open space in the direction from North-South* including the influence of Southwest monsoon in this region and sea breeze, which possible to affected though out of the day.

Figure 7-4 Design proposals to mitigate the district urban ventilation issue.

7.3 Direction of Future Study

This study's findings pave the way for promising avenues of future research and development in several key areas:

1. Enhanced Urban Climate Maps (UECMs):

Integrating diverse methodologies: Future research should explore combining various methodologies in each urban study, leading to more precise UECMs. These maps would serve as valuable scientific evidence and communication tools for stakeholders, facilitating informed decisions in urban planning, architecture, and environmental policies.

Tailoring UECMs to stakeholder needs: Investigating diverse UECM variations, including differences in measurement scales and zoning, can align these tools with specific stakeholder requirements.

Establishing a national UECM for Thailand: This forward-looking strategy would seamlessly integrate scientific insights and policy formulations to create a superior urban environment. The study's findings, if integrated into regional policies and planning efforts, could elevate the importance of urban topography by exploring the relationship between physical variables and climate distribution within Thailand's BMR.
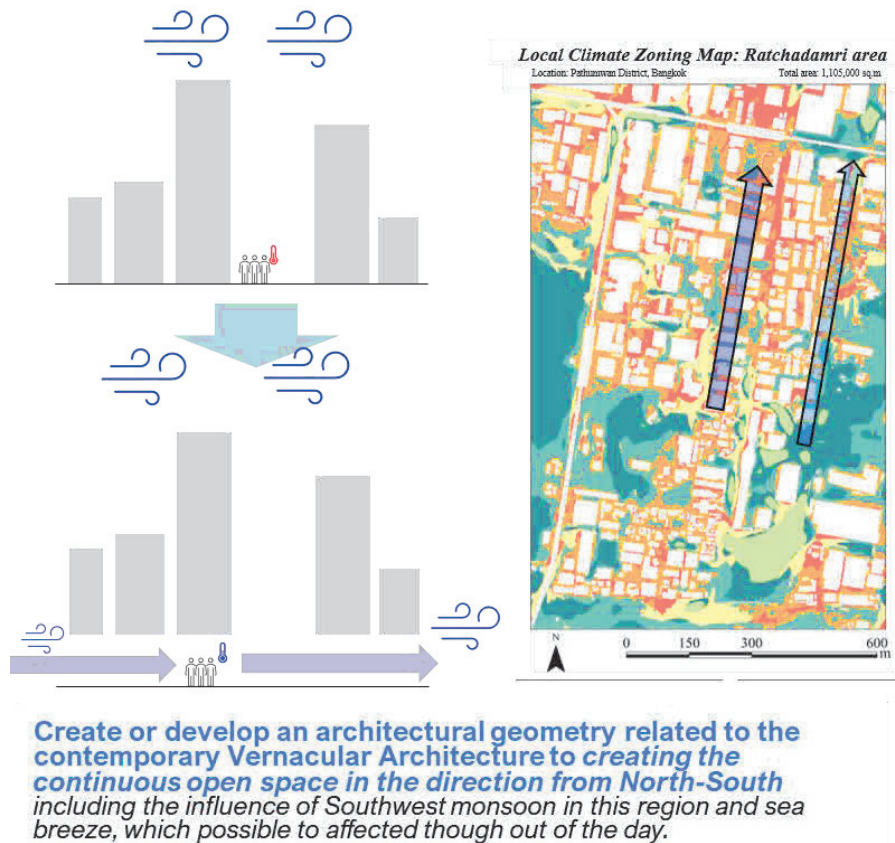
2. Community Engagement and Refinement:

Recommendation maps and schematic designs: Both mesoscale and microscale UECMs would benefit from more comprehensive exploration, including recommendation maps with schematic design plans for individual zones.

Community planning workshops: Organizing workshops involving urban planners, local government representatives, residents, and stakeholders is crucial. These forums can foster discussions on plan, design, and implementation, ensuring long-term viability. Case studies suggest the effectiveness of incorporating such workshops in developing urban policies.

Accessible communication: Ensuring the conclusive deliberations clearly specify the types and characteristics of green spaces, open areas, etc., would make them accessible to non-experts and enhance their value as communication tools for future urban planning in tropical regions.

3. Applicability beyond Summer Climate:

Addressing air pollution: While this study focused on summer, the methodologies employed have the potential to address other environmental challenges. The insights gained could serve as a foundation for developing effective countermeasures to combat air pollution, such as PM 2.5, which emerges in Bangkok during late winter. This adaptability underscores the broader significance of the study's methodologies, extending their utility beyond the specific context of summer climate analysis to encompass broader environmental issues and seasonal variations.

Finalization and Impact: The study's findings, including refined UECMs based on community engagement, aim to contribute to the ongoing revision of Bangkok's land use planning. This alignment with a crucial planning phase underscores the potential to influence and shape accurate city planning practices, ultimately promoting sustainable development in Thailand by ensuring urban policies and strategies are informed by scientific evidence and tailored to address contemporary environmental challenges.

Appendix

Contents

Appendix A: Details of the observation stations

Table A-1 Spatial data of 68 stations from the Thai government

| No. | Name | Agency | Distance from natural water surface | | | LC within 300-m radius | | | | |
			DCDS (m)	DR (m)	DC (m)	UCR (%)	GCR (%)	WCR (%)	OSR (%)	BCR (%)
1	Bang Bon	BMA	15,684.7	11,509.1	5209.0	59.28	31.15	9.57	59.50	40.50
2	Bang Kapi	BMA	25,600.0	11,950.0	117.1	79.03	17.15	3.82	39.65	60.35
3	Bang	BMA	21,910.0	9,059.1	451.7	72.34	26.39	1.27	45.14	54.86
4	Bang Khen	BMA	37,000.0	10,728.7	840.8	61.72	29.42	8.86	63.51	36.49
5	Bang Kho Laem	BMA	19,912.3	526.8	487.6	93.57	6.16	0.27	23.15	76.85
6	Bang Khun Thian	BMA	17,702.3	7,438.4	362.8	76.77	22.41	0.82	57.83	42.17
7	Bang Na	BMA	14,582.5	5,458.3	4074.5	96.63	2.11	1.26	33.68	66.32
8	Bang Phlat	BMA	29,260.0	750.0	562.4	63.80	33.99	2.21	47.68	52.32
9	Bang Rak	BMA	21,900.0	1,070.0	564.3	96.98	1.82	1.20	15.62	84.38
10	Bang Sue	BMA	30,348.8	2,264.8	40.4	72.08	23.51	4.41	34.80	65.20
11	Bangkok Noi	BMA	26,798.9	665.5	591.5	89.27	2.22	8.51	27.40	72.60
12	Bangkok Yai	BMA	24,323.2	2,466.8	738.4	92.36	7.54	0.10	27.72	72.28
13	Bueng Kum	BMA	27,951.6	13,612.2	707.5	49.04	32.47	18.49	72.99	27.01
14	Chatuchak	BMA	33,318.2	7,089.9	1546.2	76.26	16.55	7.19	49.02	50.98
15	Chom Thong	BMA	18,785.6	1,801.6	1707.4	53.47	42.97	3.56	56.48	43.52
16	Din Daeng	BMA	25,104.8	5,224.2	326.9	94.44	4.76	0.80	36.80	63.20
17	Don Mueang	BMA	41,500.0	7,740.2	38.9	91.34	6.57	2.09	43.72	56.28
18	Dusit	BMA	27,119.0	1,835.4	36.1	72.48	22.33	5.19	41.73	58.27
19	Huai Khwang	BMA	26,306.8	7,358.3	1383.4	87.41	11.61	0.98	25.67	74.33
20	Khan Na Yao	BMA	29,832.4	15,614.0	1326.4	55.25	34.84	9.91	104.63	-4.63
21	Khlong Sam Wa	BMA	36,897.8	21,080.1	2639.2	61.30	37.34	1.36	62.06	37.94
22	Khlong San	BMA	21,653.9	400.4	244.8	91.38	2.30	6.32	29.46	70.54
23	Khlong Toei	BMA	18,801.1	1,047.2	475.5	85.76	12.27	1.97	38.04	61.96
24	Lak Si	BMA	38,508.3	8,577.2	191.1	88.64	7.32	4.04	29.38	70.62
25	Lat Krabang	BMA	25,241.4	21,698.8	238.2	79.51	18.71	1.78	25.31	74.69
26	Lat Phrao	BMA	29,300.0	9,908.3	1902.0	83.23	16.29	0.48	38.43	61.57
27	Min Buri	BMA	32,946.2	20,788.3	89.8	59.79	31.33	8.88	62.67	37.33
28	Nong Chok	BMA	40,777.1	35,201.4	222.3	63.29	31.48	5.23	50.54	49.46
29	Nong Khaem	BMA	23,036.1	8,652.5	2589.0	68.60	29.98	1.42	45.49	54.51
30	Pathum Wan	BMA	22,348.6	1,981.5	603.9	89.15	10.65	0.20	40.88	59.12
31	Phasi Charoen	BMA	23,693.2	4,792.1	146.4	77.77	17.78	4.45	34.24	65.76
32	Phaya Thai	BMA	27,574.6	2,722.3	923.9	91.33	7.00	1.67	36.13	63.87
33	Phra Nakhon	BMA	26,486.4	600.5	194.4	95.72	1.17	3.11	16.76	83.24
34	Pom Prap Sattru Phai	BMA	25,300.2	2,238.7	124.2	91.77	4.14	4.09	30.89	69.11
35	Prawet	BMA	17,789.0	6,337.6	2328.4	97.31	2.69	0.00	31.05	68.95
36	Ratchathewi	BMA	24,914.7	3,825.7	922.1	94.53	5.47	0.00	20.67	79.33
37	Sai Mai	BMA	39,802.8	14,980.6	3702.6	68.63	29.93	1.44	49.05	50.95
38	Saphan Sung	BMA	26,666.3	13,852.8	1701.5	62.50	33.89	3.61	58.88	41.12
39	Sathon	BMA	19,732.7	1,846.8	962.6	95.86	4.14	0.00	19.69	80.31
40	Suan Luang	BMA	21,789.2	8,556.3	1394.3	62.96	27.97	9.07	50.64	49.36
41	Taling Chan	BMA	30,808.4	7,092.5	2986.1	70.15	27.44	2.41	55.68	44.32
42	Thawi Watthana	BMA	27,624.1	7,844.8	139.5	55.07	38.18	6.75	58.28	41.72
43	Thon Buri	BMA	21,386.2	1,056.5	983.0	94.30	3.57	2.13	30.03	69.97
44	Thung Khru	BMA	15,681.8	3,770.9	3939.2	82.12	15.36	2.52	31.89	68.11

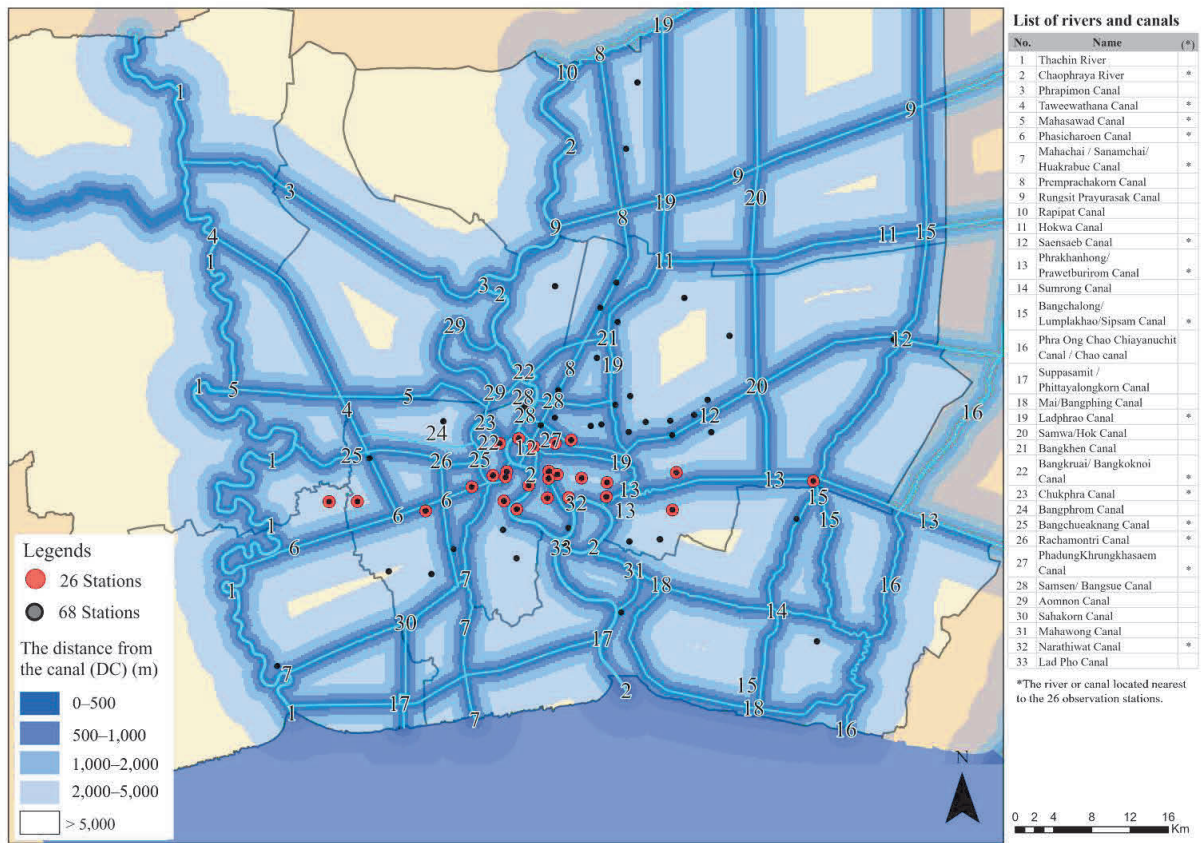| No.	Name	Agency	Distance from natural water surface			LC within 300-m radius				
			DCDS (m)	DR (m)	DC (m)	UCR (%)	GCR (%)	WCR (%)	OSR (%)	BCR (%)
45	Wang Thonglang	BMA	26,518.9	10,116.6	1735.0	89.63	10.37	0.00	24.23	75.77
46	Watthana	BMA	20,300.2	2,581.7	1633.7	95.37	4.63	0.00	22.62	77.38
47	Yan Nawa	BMA	16,129.8	282.9	330.5	79.81	16.77	3.42	33.99	66.01
48	03t bangkhun tien	PCD	15,456.4	10,713.0	2499.5	62.72	34.07	3.21	57.93	42.07
49	50t CU	PCD	21,876.9	2,805.4	856.5	90.29	9.71	0.00	39.36	60.64
50	52t Thonburi	PCD	23,259.4	1,938.4	196.9	81.70	12.21	6.09	26.81	73.19
51	02t Somdej	PCD	23,881.4	1,047.2	137.0	87.09	3.62	9.29	19.79	80.21
52	53t Chokchai4	PCD	28,400.0	8,227.9	318.6	95.15	4.79	0.06	23.89	76.11
53	05t Bang Na	TMD	14,300.0	2,435.7	2297.5	55.74	38.30	5.96	67.78	32.22
54	10t Chong Chan	PCD	27,014.8	11,589.2	1558.5	92.30	7.70	0.00	36.04	63.96
55	11t HK stadium	PCD	26,169.1	6,300.4	2129.4	99.05	0.95	0.00	21.33	78.67
56	12t Nontree	PCD	19,144.2	1,000.9	833.1	78.59	20.46	0.95	41.72	58.28
57	61t Bodin	PCD	25,500.0	8,705.7	859.2	79.58	18.82	1.60	35.66	64.34
58	SKT	TMD	20,875.3	1,981.7	2170.5	70.59	12.96	16.45	53.74	46.26
59	22t Nontraburi	BMA	41,182.5	4,132.5	4118.4	59.64	34.38	5.98	51.88	48.12
60	PTN MET	TMD	63,901.3	8,169.9	2282.4	51.22	41.40	7.38	67.37	32.63
61	20t PTN	BMA	55,100.0	5,405.1	1218.5	45.66	50.09	4.25	63.34	36.66
62	SVB	TMD	20,748.3	19,250.5	313.1	11.35	78.91	9.74	100.02	-0.02
63	08t	BMA	14,579.8	283.1	347.8	53.53	31.72	14.75	51.75	48.25
64	18t	BMA	6,700.0	400.4	397.7	66.19	9.18	24.63	43.53	56.47
65	19t	BMA	8,500.0	20,859.4	2464.2	31.26	61.00	7.74	75.94	24.06
66	14t	BMA	22,276.7	6,247.9	3431.0	80.70	19.30	0.00	31.74	68.26
67	27t	BMA	5,263.1	1,000.9	1058.2	68.19	30.68	1.13	44.87	55.13
68	NKT MET	TMD	65,000.0	19,860.3	1479.4	36.65	62.00	1.35	79.91	20.09

Appendix B: Canal data in Bangkok

Fig. B-1 Map of rivers and canals for calculating the distance from canals

The legend and table within the figure read:

Legends
- 26 Stations
- 68 Stations

The distance from the canal (DC) (m)
- 0–500
- 500–1,000
- 1,000–2,000
- 2,000–5,000
- > 5,000

List of rivers and canals

No.	Name	(*)
1	Thachin River	
2	Chaophraya River	*
3	Phrapimon Canal	
4	Taweewathana Canal	*
5	Mahasawad Canal	*
6	Phasicharoen Canal	*
7	Mahachai / Sanamchai/ Huakrabue Canal	*
8	Premprachakorn Canal	
9	Rungsit Prayurasak Canal	
10	Rapipat Canal	
11	Hokwa Canal	
12	Saensaeb Canal	*
13	Phrakhanhong/ Prawetburirom Canal	*
14	Sumrong Canal	
15	Bangchalong/ Lumplakhao/Sipsam Canal	*
16	Phra Ong Chao Chiayanuchit Canal / Chao canal	
17	Suppasamit / Phittayalongkorn Canal	
18	Mai/Bangphing Canal	
19	Ladphrao Canal	*
20	Samwa/Hok Canal	
21	Bangkhen Canal	
22	Bangkruai/ Bangkoknoi Canal	*
23	Chukphra Canal	*
24	Bangphrom Canal	
25	Bangchueaknang Canal	*
26	Rachamontri Canal	*
27	PhadungKhrungkhasaem Canal	*
28	Samsen/ Bangsue Canal	
29	Aomnon Canal	
30	Sahakorn Canal	
31	Mahawong Canal	
32	Narathiwat Canal	*
33	Lad Pho Canal	

*The river or canal located nearest to the 26 observation stations.

Table B-1 List of canals used to calculate the distance from canals

No.	Name	*	Width (m)	Avg width
1	Thachin River		46–500	273.0
2	Chaophraya River	*	200–1,200	700.0
3	Phrapimon Canal		30–40	35.0
4	Taweewathana Canal	*	6–35	20.5
5	Mahasawad Canal	*	6–40	23.0
6	Phasicharoen Canal	*	15–30	22.5
7	Mahachai / Sanamchai/ Huakrabue Canal	*	8–50	29.0
8	Premprachakorn Canal		12–30	21.0
9	Rungsit Prayurasak Canal		16–24	20.0
10	Rapipat Canal		16–20	18.0
11	Hokwa Canal		21–24	22.5
12	Saensaeb Canal	*	20–35	27.5
13	Phrakhanhong/ Prawetburirom Canal	*	20–44	32.0
14	Sumrong Canal		10–50	30.0
15	Bangchalong/ Lumplakhao/Sipsam Canal	*	20–40	30.0
16	Phra Ong Chao Chiayanuchit Canal / Chao canal		40–60	50.0
17	Suppasamit / Phittayalongkorn Canal		16	16.0
18	Mai/Bangphing Canal		10–20	15.0
19	Ladphrao Canal	*	12–30	21.0
20	Samwa/Hok Canal		14–25	19.5
21	Bangkhen Canal		11–20	15.5
22	Bangkruai/ Bangkoknoi Canal	*	10–40	25.0
23	Chukphra Canal	*	5–25	15.0
24	Bangphrom Canal		6–35	20.5
25	Bangchueaknang Canal	*	15–20	17.5
26	Rachamontri Canal	*	5–37	21.0
27	PhadungKhrungkhasaem Canal	*	20–24	22.0
28	Samsen/ Bangsue Canal		10–25	17.5
29	Aomnon Canal		12–18	15.0
30	Sahakorn Canal		6–38	22.0
31	Mahawong Canal		12–18	15.0
32	Narathiwat Canal	*	15–17	16.0
33	Lad Pho Canal		15	15.0

Note: * The river or canal located nearest to the 26 observation stations